

Understanding Stellar Evolution

Henny J.G.L.M. Lamers
Visiting Professor, University of Amsterdam, NL
Email: h.j.g.l.m.lamers@uu.nl
Tel: 206-543-4858

Preface

These are the lecture notes of my graduate class “Understanding Stellar Evolution” (AST531) that I have been giving at the University of Washington in Seattle in the spring quarter of almost every other year since 2004.

These notes have developed over the years due to comments and suggestions by students and requests by the staff. (I am sure they will keep evolving).

They are written as “lecture notes” rather than in the form of a book. I have chosen for this form because I find it more easy to teach from them, and I think it is easier for the students to quickly see the important points in explanations and descriptions.

I have avoided (long) purely mathematical explanations. Although these may be appealing, straight forward and physically correct, they often obscure the physical processes behind them. So, where possible, I explain concepts in simple (?) or intuitive physical terms, giving the reference where the more rigorous explanations and derivations can be found. My goal is to give the students a “feeling” and “understanding” of stellar evolution. From the reactions of the students, I sense that this is appreciated.

I am grateful for my Utrecht colleague Onno Pols, for his lecture notes on “Stellar structure and evolution” and the more recent one on “Binary evolution”. They often formed the skeleton of my lectures. I also thank Maurizio Salaris for providing me with the pictures from his book “Evolution of stars and stellar populations”.

The first version of these lecture notes in Word were typed by Rachel Beck. (The first versions were handwritten). Thanks Rachel for deciphering my scribbles with its many equations. You did an excellent job. I am also grateful to Chris Suberlak, for painstakingly finding all the errors and typos in the last version. I hope you found them all!

Most thanks go to the many graduate students who followed this course. I thank them for their many discussions, comments and suggestions about this class, the notes and the exercises.

--- I learned a lot from your constant questioning during the lectures ---

Henny Lamers, Seattle, June 11 2014

h.j.g.l.m.lamers@uu.nl

Literature

0. Henny Lamers, 2014
“Understanding Stellar Structure and Evolution”
These lecture notes
1. Onno Pols, Utrecht, 2014 (OP) (recommended: similar but more extended)
“Stellar Structure and Evolution”
http://www.astro.ru.nl/~onnop/education/stev_utrecht_notes/
2. Dina Prialnik, 1999 (DP) (recommended: very basic)
“An Introduction to the Theory of Stellar Structure and Evolution”, (2nd ed)
Cambridge University Press, ISBN 0-521-65937-X
3. A. Maeder, 2009 (M)
(recommended if you work in stellar modelling and evolution: very thorough)
“Physics, Formation and Evolution of Rotating Stars”
Springer Verlag, ISBN 978-3-540-76948
4. Salaris and Cassisi, 2005 (SC)
(recommended: late evolution stages and observations and theory of clusters)
“Evolution of Stars and Stellar Populations”,
Wiley, ISBN 978-0-470-09219-4
5. Onno Pols, Nijmegen 2014 (OP 2014) (recommended for binary evolution)
“Binary evolution”
http://www.astro.ru.nl/~onnop/education/binaries_utrecht_notes/
This is the second half of a course on “Binaries” (Verbunt and Pols)
6. Hansen and Kawaler, 1999 (HK)
“Stellar Interiors: Physical Principles, Structure and Evolution”,
Springer, ISBN 0-387-94138-A
7. Carroll and Ostlie, 1996 (CO)
“An introduction to Modern Astrophysics”
Addison-Wesley, ISBN 0-201-54730-9

Questions:

Throughout the course I ask many questions to the students.
These are indicated by “Q “ in this syllabus.

Understanding Stellar Evolution

Table of Contents

1: Introduction	10-13
1.1 What is a star?	10
1.2 What can we learn from observation?	10
1.3 How can we measure stellar parameters?	10
1.4 Mass Luminosity Relation	10
1.5 Hertzsprung-Russell Diagrams	11
1.6 Summary of Stellar Characteristics	13
2: Hydrostatic Equilibrium	14-18
2.1 Conservation of Mass	14
2.2 Hydrostatic Equilibrium	14
2.3 The Virial Theorem: consequences of HE <i>Homework 2.1</i>	16 15
3: Gas Physics	18-19
3.1 Definitions	18
<i>Homework 3.1, 3.2</i>	19
4: Stellar Timescales	20-21
4.1 Dynamical Timescale	20
4.2 Thermal Timescale = Kelvin-Helmholtz Timescale	21
4.3 Nuclear Timescale	21
4.4 Comparison of Timescales <i>Homework 4.1</i>	21
5: The Equation of State	22-32
5.1 Gas Pressure	22
5.2 Ideal Gas	23
5.3 Degeneracy	24
5.4 Radiation Pressure	27
5.5 Limits of the equation of state	28
5.6 Polytropic Gas	30
5.7 Proof that a fully convective star is a polytrope	31
5.8 The polytrope index of partially ionized gas <i>Homework 5.1, 5.2</i>	32 29
<i>Homework 5.3</i>	31
6: Opacities in Stars	33-37
6.1 Electron Scattering	33
6.2 Free-free Absorption	33
6.3 Bound-free Absorption	34

6.4	Bound-bound Absorption	34
6.5	Total Opacity	34
6.6	Opacity in stellar atmospheres	35
6.7	Rosseland-mean Opacities	35
6.8	Mean-free Path of Photons	36
	<i>Homework 6.1, 6.2</i>	<i>37</i>
7:	Radiative Energy Transfer: Transport Inside a Star	38-39
7.1	Eddington's equation for radiative equilibrium	38
8:	The mass -luminosity relation and the Eddington limit	40-43
8.1	Thermal equilibrium	40
8.2	The mass luminosity relation	40
8.3	The Eddington limit	42
	<i>Homework 8.1</i>	<i>41</i>
	<i>Homework 8.2</i>	<i>43</i>
9:	Convective Energy Transfer	44-54
9.1	Stability against convection	44
9.2	Schwarzschild criterium	44
9.3	Convection in a layer with a μ -gradient: Ledoux criterium	46
9.4	The mixing length	47
9.5	Efficiency of convective energy transport	48
9.6	Convective velocity	49
9.7	Typical values of convective velocity and timescale	51
9.8	Superadiabatic T-gradient	51
9.9	Convection: where and why?	52
9.10	Convective overshooting	53
9.11	Chemical mixing by convection	54
	<i>Homework 9.1</i>	<i>45</i>
	<i>Homework 9.2, 9.3</i>	<i>50</i>
	<i>Homework 9.4</i>	<i>51</i>
	<i>Homework 9.5</i>	<i>53</i>
	<i>Homework 9.6, 9.7</i>	<i>54</i>
10:	Nuclear Fusion	55-70
10.1	Reaction rates and energy production	55
10.2	Thermonuclear reactions rates and the Gamov peak	57
10.3	Abundance changes	58
10.4	H-fusion	59
10.5	He-fusion	62
10.6	C and O-fusion	62
10.7	Si-fusion and photo-disintegration	63
10.8	Summary of major reactions	63
10.9	Formation of heavy elements : s- and r-process	63
10.10	Consequences of fusion reactions for stellar evolution	65
10.11	Minimum core mass for ignition	67
	<i>Homework 10.1</i>	<i>56</i>
	<i>Homework 10.2</i>	<i>66</i>
	<i>Homework 10.3</i>	<i>69</i>

11: Calculating Stellar Structure and Evolution	70-75
11.1 Assumptions	70
11.2 Equations of Stellar Structure	71
11.3 Boundary conditions	72
11.4 Solving the structure equations	73
11.5 Structure of polytropic stars	74
<i>Homework 11.1</i>	70
<i>Homework 11.2</i>	75
12: Star formation	76-87
12.1 The ISM	76
12.2 The Jeans mass	76
12.3 The collapse of molecular clouds	78
12.4 The end of the free-fall phase	79
12.5 Contraction of convective proto-star: Hayashi track	81
12.6 Contraction of radiative pre-main sequence star	82
12.7 The destruction of Lithium and Deuterium	85
12.8 Brown dwarfs	85
12.9 Summary of star formation	86
12.10 The stellar initial mass function (IMF)	87
<i>Homework 12.1</i>	77
<i>Homework 12.2, 12.3</i>	85
<i>Homework 12.4</i>	87
13: The Zero-Age Main Sequence (ZAMS)	88-97
13.1 Homology relations for Main sequence stars	88
13.2 The Mass-Luminosity Relation for ZAMS stars	88
13.3 The Mass-Radius Relation for ZAMS stars	90
13.4 The Mass-T _{eff} Relation for the ZAMS	90
<i>Homework 13.1</i>	92
14: Evolution During the Main Sequence Phase	93-97
14.1 Nuclear Fusion as a Thermostat	93
14.2 Changes in L and R	93
14.3 Changes in the Chemical Profile	94
14.4 The MS evolution of the Sun	95
14.5 Convective Overshooting in the MS Phase	96
14.6 The End of the MS Phase: core contraction	97
<i>Homework 14.1</i>	94
15: Principles of Post-Main Sequence Evolution	98-109
15.1 Definitions of Zones and Regions	98
15.2 The Evolution of the Core	98
15.3 Isothermal Cores	101
15.4 The Mirror Principle of Shell Burning	104
15.5 The Hayashi-line of Fully Convective Stars	106
<i>Homework 15.1, 15.2</i>	103
16: Stellar Winds and Mass Loss	110-125

16.1 Coronal Winds	110
16.2 Dust-driven Winds of Pulsating Stars	114
16.3 Line-driven Winds of Hot Stars	118
16.4 Mass Loss Formulae of Stellar Evolution	123
<i>Homework 16.1, 16.2</i>	<i>125</i>
17. Mass ranges of Post-MS evolution	126
18. H-Shell Fusion and the Red Giant Branch	127-134
18.1 The start of H-shell fusion	127
18.2 H-Shell fusion phase of a star of $1 M_{\text{sun}}$	127
18.3 H-shell fusion phase of stars of $1-2 M_{\text{sun}}$	131
18.4 H-shell fusion phase of stars of $2-8 M_{\text{sun}}$	131
18.5 The core mass -luminosity relation for RGB stars	133
18.6 Metallicity dependence of the RGB	133
18.7 Mass loss on the RGB	134
19. Ignition of He-fusion: from RGB to HB	135-136
19.1 The He-flash in degenerate cores of stars of $M < 2 M_{\text{sun}}$	135
19.2 The start of the He core fusion in stars of $M > 2 M_{\text{sun}}$	136
20. Helium Fusion in the Core: The Horizontal Branch	137-141
20.1 The evolution on the Horizontal Branch	138
20.2 Observed HB in Globular Clusters	139
<i>Homework 20.1, 20.2</i>	<i>138</i>
21. The Asymptotic Giant Branch for stars of $2 < M < 8 M_{\text{sun}}$	142-153
21.1 The Core Mass-Luminosity Relation of AGB Stars	143
21.2 The second dredge-up at the early AGB phase	144
21.3 Thermal Pulses and the third dredge-up on the AGB	145
21.4 Summary of the dredge-up phases	149
21.6 The evolution speed during the AGB phase	150
21.7 Mass Loss and the end of the AGB Evolution	151
<i>Homework 21.1</i>	<i>153</i>
22. Post-AGB Evolution and Planetary Nebulae	154-158
22.1 The Post-AGB Phase	154
22.2 Born-again AGB Stars	156
22.3 Planetary Nebulae	156
23. White Dwarfs	159-161
23.1 The evolution of White Dwarfs	159
23.2 The Chandrasekhar Mass-Limit for White Dwarfs	160
24. Stellar Pulsation	162-167
24.1 The instability strip in the HRD	162
24.2 The Kappa Mechanism	162
24.3 Pulsating Stars in the HRD	164
24.4 Radial pulsations	165

24.5 Non-radial pulsations	167
25. The Evolution of Massive Stars	168-178
25.1 Main characteristics of massive star evolution	168
25.2 The effect of mass loss during the MS phase	170
25.3 The photospheric Eddington limit and the HD limit	171
25.4 Luminous Blue Variables (LBVs)	173
25.5 Wolf-Rayet Stars (WR)	175
25.6 Evolution of a 60 M _{sun} star with mass loss	176
25.7 Evolution lifetimes of massive stars	177
25.8 Summary: the Conti scenario	178
26. The Effect of Rotation On Stars	179-182
26.1 The Von Zeipel effect	179
26.2 Meridional circulation	181
26.3 Non-spherical mass loss of rotation stars	182
27. Late Evolution Stages of Massive stars	183-186
27.1 Fusion phases	183
27.2 Pre-Supernovae	185
28. Supernovae	187-190
28.1 Core collapse	187
28.2 The SN explosion	187
28.3 Energetics of supernovae	188
28.4 Types of supernovae	189
28.5 Remnants of stellar evolution	189
29. Stellar Yields	191-192
30. Binary evolution	193-199
30.1 Potential surfaces of binaries	193
30.2 Contact phases	193
30.3 Changes in periods and separation during mass transfer	195
30.4 Stable and run-away mass transfer	195
30.5 Case A transfer and Algols	196
30.6 Case B transfer and massive interacting binaries	197
30.7 Case C: unstable mass loss	198
30.8 The formation of high mass X-binaries	198
30.9 The formation of low mass X-binaries	199
31. The End	200

Appendices

- Appendix A: Physical Constants
- Appendix B: Stellar Data
- Appendix C1: Properties of ZAMS: external and internal
- Appendix C2: Properties of ZAMS: internal, external, lifetimes
- Appendix D: A model for the present Sun

- Appendix E: Evolution tracks for $0.8 < M_i < 120 M_\odot$; $Z = 0.02$ and $Z = 0.001$
Appendix F: Properties of AGB Stars of $1 < M_i < 5 M_\odot$

Homework exercises

2.1	15
3.1 , 3.2	19
4.1	21
5.1, 5.2	29
5.3	31
6.1, 6.2	37
8.1	41
8.2	43
9.1	45
9.2, 9.3	50
9.4	51
9.5	53
9.6, 9.7	54
10.1	56
10.2	66
10.3	69
11.1	70
11.2	75
12.1	77
12.2, 12.3	85
12.4	87
13.1	92
14.1	94
15.1, 15.2	103
16.1, 16.2	125
20.1, 20.2	138
21.1	153

There are few homework exercises after chapter 21.

That is the time (late May-early June) that the students are busy studying for their final exam.

Chapter 1. Introduction and Observations

This section contains a recapitulation of the information about stars and stellar evolution from introductory courses. It is meant to refresh your memory by giving topics and suggestions for reading.

1.1 What is a star? (OP 1, DP 1.1) : read this

1.2 What can we learn from observations?

(OP1, DP 1.2): read this

1.3 How can we measure stellar parameters?

- a. Distance
- b. Mass
- c. Radius
- d. Surface Temperature
- e. Luminosity
- f. Composition
- g. Surface Gravity
- h. Rotation Velocity
- i. Surface Magnetic Field

1.4 Mass Luminosity Relation (OP 1.2.2, DP 1.4)

- Valid for main sequence stars, massive giants ($M > 20 M_{\text{sun}}$)
- Not valid for:
red giants, horizontal branch stars, AGB stars, white dwarfs, neutron stars.

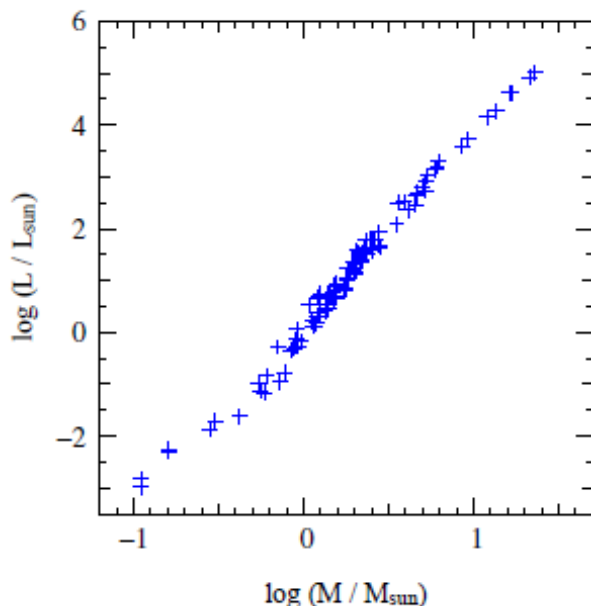


*Fig 1.1
The mass-luminosity relation
from double-lined spectroscopic
binaries
(Pols, Fig 1.3)*

The mean slope in the mass range of $0.8 < M < 30 M_{\text{sun}}$ is 3.8. $L \sim M^{3.8}$

For masses above $M > 30 M_{\text{sun}}$ the M-L relation is less steep, because of the increasing role of the radiation pressure, as we will see later.

For masses below $M < 0.8 M_{\text{sun}}$ the mass luminosity relation is less steep because of the increasing role of convection throughout the star and the different opacity.

1.5 Hertzsprung-Russell Diagrams (OP 1.2.1, DP 1.4)

Young Open Clusters

Old Globular Clusters

Field stars

- magnitude limited samples
- distance limited samples

Q? What do they represent, why are they different?

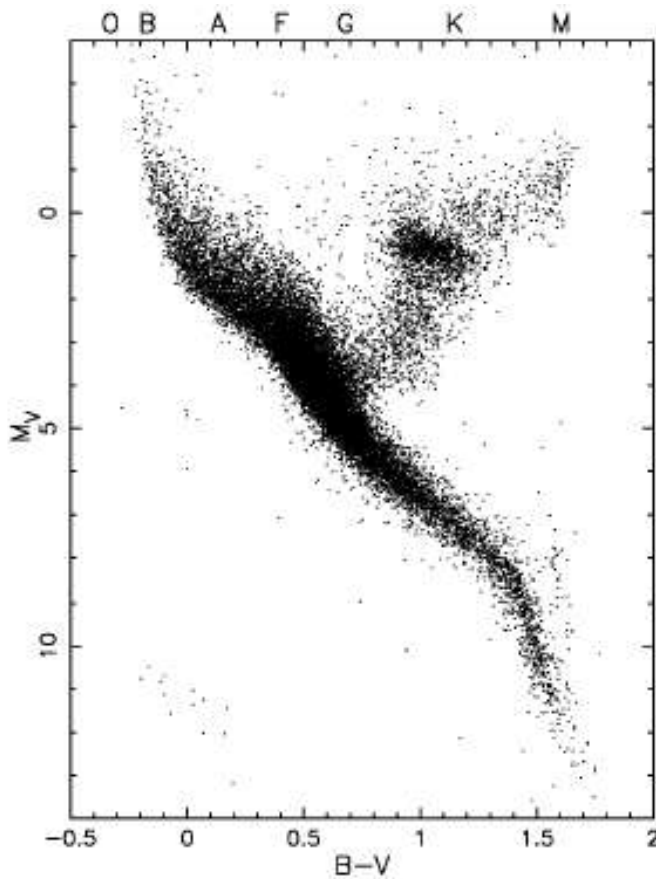


Fig 1.2

The H-R diagram of stars in the solar neighbourhood measured by the Hipparcos satellite.

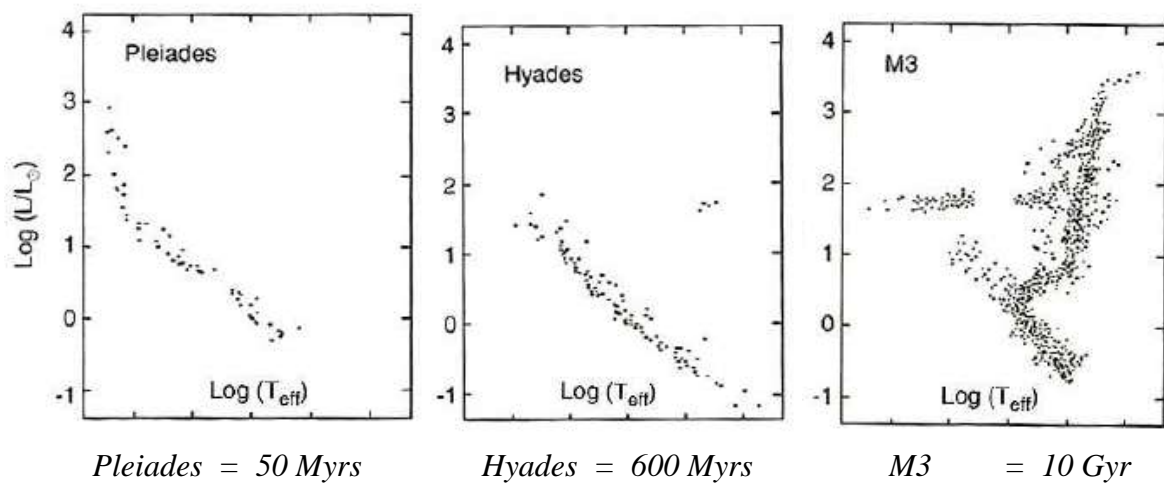


Fig 1.3 H-R diagrams of clusters with different ages (DP Fig 1.5)

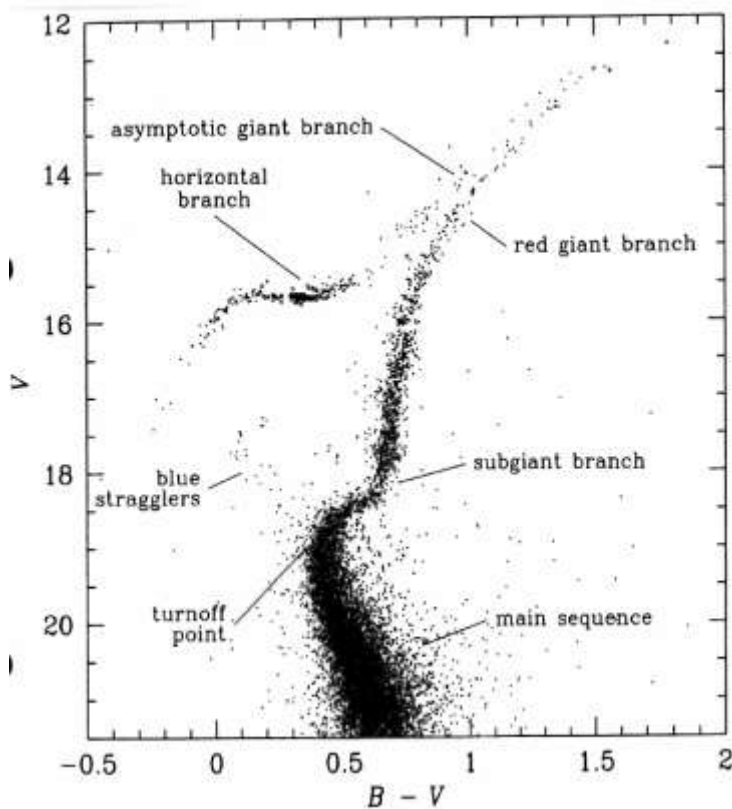


Fig 1.4 Nomenclature of the various regions in the H-R diagram

- Main sequence
- Turnoff point
- Subgiant branch
- Red giant branch
- Asymptotic giant branch
- Horizontal branch
- Blue stragglers

1.6 Summary of Stellar Characteristics

Assumptions

1. Star is spherically symmetric

- Physical quantities vary only in radial direction: $P(r)$, $\rho(r)$, $T(r)$, etc.
- Ignore effects of rotation and B-fields? When is this allowed?

Q?

2. Star is in hydrostatic equilibrium

- When is this assumption justified, timescale?

Q?

3. Energy sources are

- Gravitational energy
- Thermonuclear reactions
- Internal (thermal) energy (important for white dwarfs)

4. Energy transport mechanisms

- Radiation
- Convection
- Conduction (white dwarfs)

5. Chemical composition

- Newly formed stars have homogeneous composition
- Assume initial composition (from surface spectrum)

X = Mass fraction of H

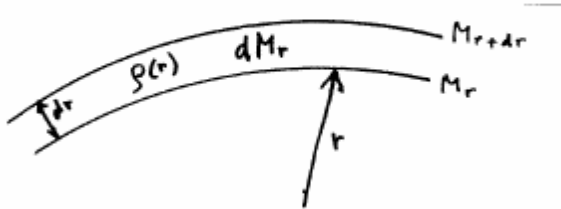
Y = Mass fraction of He

Z = Rest, mainly C, N, O

- Follow composition changes throughout the star during evolution

Chapter 2. Hydrostatic Equilibrium

2.1 Conservation of Mass (mass continuity equation)



Spherical shell of thickness dr :
$$\frac{dM_r}{dr} = 4\pi r^2 \rho(r)$$

2.2 Hydrostatic Equilibrium

Equation of motion of one cm³ gas, density ρ in shell dr (Newton f = m. a)

$$\rho \frac{d^2r}{dt^2} = -\frac{GM_r}{r^2} \rho - \frac{dP}{dr}$$

in H.E. $\frac{d^2r}{dt^2}=0$, so

$$\frac{dP}{dr} = -\rho \frac{GM_r}{r^2} = -\rho \cdot g_r \quad \text{with mass continuity } \rho = \frac{1}{4\pi r^2} dM_r/dr$$

↓

$$\frac{dP}{dM_r} = -\frac{GM_r}{4\pi r^2}$$

Consequence:

$$P(M_*) - P(M=0) = \int_0^{M_*} \frac{GM_r dM_r}{4\pi r^2} > \int_0^{M_*} \frac{GM_r dM_r}{4\pi R_*^4}$$

so

$$P_c > \frac{GM^2}{8\pi R_*^4} \quad \text{with } M_* \equiv M(R) \equiv M$$

This is a very safe lower limit because $r \ll R$ near center. Better estimate:

$$\frac{dP}{dr} = \frac{-GM_r}{r^2} \rho \rightarrow \frac{P(R_*) - P(0)}{R_*} \quad \text{with } P(R_*) = 0 \text{ so} \quad P_c \simeq \frac{GM_*}{R_*} \bar{\rho} \sim \frac{GM_*^2}{R_*^4}$$

The proportionality factor depends on density concentration.

Estimate for the Sun: P_c

$$P_c^\odot \simeq \frac{7 \times 10^{-8} (2 \cdot 10^{33})^2}{(7 \times 10^{10})^4} \simeq 1 \cdot 10^{16} \text{ dyne.cm}^2 \simeq 10^{10} \text{ atm!!}$$

Actually: $P_c^\odot \simeq 10^{17} \text{ dyne/cm}^2$ because $\rho_c \gg \bar{\rho}$

- Q?** Could you have “guessed” that $P_c \sim GM^2/R^4$ based on simple physical insight?
Hint: consider weight of a column from $r = 0 \rightarrow R$

Estimate of central T_c (if $P_{\text{gas}} \gg P_{\text{rad}}$)

$$\text{Ideal gas law: } P \sim \frac{\rho}{\mu m_H} \cdot kT$$

$$\text{In center: } P_c \sim GM^2/R^4 \sim \frac{\rho k T_c}{\mu m_H} \rightarrow \frac{GM}{R} \sim \frac{k T_c}{\mu m_H}$$

$$T_c \simeq \frac{\mu m_H}{k} \cdot \frac{GM}{R}$$

$$\text{Estimate for the Sun: } T_c^\odot \simeq \frac{0.5 \times 1.7 \cdot 10^{-24}}{1.4 \cdot 10^{16}} \times \frac{7 \cdot 10^{-8} \times 2 \cdot 10^{33}}{7 \cdot 10^{10}} \simeq 2 \cdot 10^7 K$$

the actual value: $T_c^\odot = 1.4 \cdot 10^7 K$

- Q?** Why is this estimate of T_c better than the one of P_c ?

H2.1 Homework***Improved estimates of central T_c and P_c***

Assume that $\rho \simeq \rho_c \left\{ 1 - \left(\frac{r}{R_*} \right)^2 \right\}$ (not a bad approximation)

- Calculate the mean density in the star
- Calculate central pressure (using the proper HE equation)
- Estimate the central temperature (using ideal gas law)
- Apply this to:

Sun: $1M_\odot, 1R_\odot$

Massive O5V star: $50M_\odot, 20R_\odot$

- Compare the values with those of structure models and comment on the results of this comparison. (e.g Appendix C1)

2.3 The Virial Theorem: consequence of HE

The virial theorem links the gravitational potential energy to the internal (kinetic) energy of star as whole.

H.E.

$$\frac{dP}{dr} = \frac{-GMr}{r^2} \rho$$

multiply by $4\pi r^3 dr$ and integrate from $0 \rightarrow R_*$

$$\int_0^{R_*} 4\pi r^3 dP = - \int_0^{R_*} \frac{GMr}{r} \rho \cdot 4\pi r^2 dr$$

a) $- \int_0^{R_*} \left(\frac{GMr}{r} \right) \rho \cdot 4\pi r^2 dr = E_{\text{pot}} = \underline{\text{total pot. energy of star}}$ (also called Ω)

b) $\int_0^{R_*} 4\pi r^3 dP$ define $u = 4\pi r^3$ and $v = P \rightarrow dP = dv$, $du = 3 \times 4\pi r^2 dr$

remember $\int_a^b d(uv) = uv \Big|_a^b = \int_a^b u dv + \int_a^b v du$
(integrate in parts)

$$\int_0^{R_*} 4\pi r^3 dP = \underbrace{4\pi r^3 P \Big|_0^{R_*}} - \int_0^{R_*} P \cdot 3 \times 4\pi r^2 dr = -3 \int_0^{R_*} P \cdot 4\pi r^2 dr$$

0 because $r = 0$ and $P(R_*) = 0$

We can link P to the internal energy.

Ideal gas: $P = nkT$ ($n = \text{nr of particles per cm}^3$)
 $u = 3/2 kTn$ = internal energy per cm^3

So $P = 2/3 \cdot u$

$$\text{So } \int_0^R 4\pi r^3 dP = -3 \int_0^R P 4\pi r^2 dr = -2 \int_0^R u 4\pi r^2 dr = -2E_{\text{kin}}$$

E_{kin} or $U = \underline{\text{total kinetic energy of star!}}$

From a)=b)

$-E_{\text{pot}} = 2E_{\text{kin}}$	<u>Only for star as a whole (not for each layer individually !)</u>
-------------------------------------	---

$E_{\text{kin}} = - \left(\frac{1}{2} \right) E_{\text{pot}}$
--

$$E_{\text{tot}} = E_{\text{pot}} + E_{\text{kin}} = -\left(\frac{1}{2}\right) E_{\text{pot}} < 0$$

The total energy of a star is negative.

This also applies to star clusters or clusters of galaxies in H.E.
That is how dark matter was discovered.

- Q?** The easiest way to derive Kepler's 3rd law is by using this virial equation.
Show this.

Consequences for contracting stars

When a star contracts and decreases its potential energy, (E_{pot} becomes more negative). The virial equilibrium requires

$$d E_{\text{kin}} / dt = -0.5 d E_{\text{pot}} / dt$$

1. So only half of the released energy goes into thermal energy for heating of the star, the other half must be radiated.
2. When a star is out of nuclear energy and it compensates its radiative energy loss by contraction, it needs twice as much because half of it is used for heating the star!

- Q?** Does the Virial Theorem apply to degenerate stars?
hints: a. Did we use the ideal gas law in deriving it?
b. How did we use it?
c. For degenerate gas $P = 1/3u$
- If degenerate stars obey some Virial Theorem, what is it? What is the consequence?

Chapter 3. Gas Physics inside Stars

3.1 Definitions

Mean kin energy per particle	$\frac{3}{2} kT$	for ions and electrons
Gas pressure for ideal gas (fully ionized gas, no molecules)	$P = nkT$	$n = \text{nr particles per cm}^3$
Mass fractions	X_i	e.g. $X_H, X_{He}, X_c \dots$ etc ($X = X_H, Y = X_{He}, Z = \text{rest}$)
Atomic mass	$A_i m_H$	e.g. $A_C = 12$
Nr free electrons	q_i	of element i (q_i depends on r) eg. $q_C = 1$ at solar photosphere $q_C = 6$ in solar core

Nr of atoms or ions per gram: $\Sigma_i X_i / A_i m_H = 1 / \langle m_i \rangle = 1 / \mu_i m_H$

Nr of free electrons per gram: $\Sigma_i (X_i / A_i m_H) \cdot q_i$

Define

$$\text{mean mass per ion} \equiv \mu_i m_H = 1 / \Sigma_i (X_i / A_i m_H) \rightarrow \mu_i = \{ \Sigma_i X_i / A_i \}^{-1}$$

$$\text{mean mass per electron} \equiv \mu_e m_H = 1 / \Sigma_i (X_i q_i / A_i m_H) \rightarrow \mu_e = \{ \Sigma_i q_i X_i / A_i \}^{-1}$$

$$\text{mean mass per particle (electron or ions)} \equiv \mu m_H$$

$$\mu m_H = \frac{1}{\Sigma_i (X_i / A_i m_H) + \Sigma_i (q_i X_i / A_i m_H)} \rightarrow \mu = \{ \Sigma_i (X_i / A_i) (1 + q_i) \}^{-1}$$

Fully ionized gas:

$$q_H = 1, q_{He} = 2, q_i = 0.5 A; \quad (\text{for } i > 2)$$

H3.1 Homework

- a. Derive a simple expression (in terms of X , Y , Z) for μ , μ_b , μ_e
- b. Show that for fully ionized gas: Nr of electrons per gram is $(1+X) / 2m_H$ and $\mu_e = 2/(1+X)$
(This factor plays a role in calculating the electron scattering coefficient)

H3.2 Homework

- a. Calculate for a massive star the time it takes for a $60 M_\odot$ star to increase its mean internal temperature by a factor 5 (e.g. to go from H-burning at $T_c \sim 2 \cdot 10^7$ K to He- burning at $T_c \sim 10^8$ K) if the luminosity remains constant.
(Use M , R and L from Appendix C)
 - b. Compare this with the Main Sequence lifetime.
-

Chapter 4. Stellar Timescales

4.1 Dynamical Timescale

1. Free-fall timescale: suppose pressure vanished suddenly
(restoring force = gravity)

$$\left. \begin{array}{l} \Delta r \sim gt^2 \rightarrow t^2 \sim \Delta r/g \\ \Delta r \sim R \\ g \sim GM/R^2 \end{array} \right\} t_{\text{ff}} \simeq \sqrt{\frac{R}{GM/R^2}} \sim \sqrt{\frac{R^3}{GM}} \rightarrow \boxed{t_{\text{ff}} \simeq \frac{1}{\sqrt{G\rho}}}$$

2. Sound speed crossing time: suppose star is out of pressure equilibrium
(restoring force = gas pressure)

$$\left. \begin{array}{l} t_{\text{sound}} \sim R/c_s \\ c_s^2 \sim kT/m \end{array} \right\} t_{\text{sound}} \sim \frac{R}{\sqrt{GM/R}} \sim \sqrt{\frac{R^3}{GM}} \sim \sqrt{\frac{1}{g\rho}} \rightarrow \boxed{t_{\text{sound}} \simeq \frac{1}{\sqrt{G\rho}}}$$

Q?

Notice: free fall time \simeq sound speed crossing time!! Why??

Together they are called:

Dynamical time scale $\boxed{\tau_{\text{dyn}} = \frac{1}{\sqrt{G\rho}}}$

This proportionality also applies to pulsating stars!

Q?

Estimate the dynamical timescale of the Sun.

4.2

Thermal Timescale = Kelvin-Helmholtz Timescale

How long can a star keep up its radiation if nuclear fusion stops and thermal energy is the only energy source left?

$$\left. \begin{array}{l} \tau_{KH} \simeq E_{th}/L \\ \text{Virial } E_{th} = -\frac{1}{2}E_{\text{pot}} \end{array} \right\} \tau_{KH} \simeq -\frac{E_{\text{pot}}}{L} \simeq \frac{GM^2}{R}/L$$

Kelvin-Helmholtz timescale $\boxed{\tau_{KH} = \frac{GM^2}{RL}}$

Also called: thermal – timescale

Q?

What is τ_{KH} for stars like the sun?

4.3 Nuclear Timescale

$$\tau_{\text{nucl}} \sim \frac{E_{\text{nucl}}}{L} \sim f_M M c^2 \epsilon_n / L$$

ϵ_n = efficiency = fraction of mass that is converted into energy $\epsilon_n = \frac{\Delta m}{m}$

H-fusion: $\epsilon_H = 0.007$

He-fusion: $\epsilon_{He} = 0.0007$

f_M = fraction of stellar mass that takes part in nuclear fusion

Sun: $f_M \sim 0.10$

For MS stars: $f_M \cdot \epsilon_H \simeq 10^{-3}$

Nuclear timescale:

$\tau_{\text{nucl}} \sim 10^{-3} M c^2 / L$	H-fusion
$\tau_{\text{nucl}} \sim 10^{-4} M c^2 / L$	He-fusion

For Sun:

$$\left. \begin{aligned} M &= 2.10^{33} \text{ gr}, \quad L = 3.6^{33} \text{ erg/s} \\ f_M \times \epsilon_M &= 0.10 \times 0.007 = 7 \times 10^{14} \end{aligned} \right\} \rightarrow \tau_{\text{nucl}}^{\odot} \simeq 3 \times 10^{17} \text{ sec} = 10^{10} \text{ yr}$$

Q?

The actual MS phase of massive stars ($M > 30 M_{\text{sun}}$) is longer than $10^{10} (M/M_{\text{sun}})/(L/L_{\text{sun}})$ yrs , by factor ~ 3 to 5.

Can you think of a reason ?

4.4 Comparison of timescales

$$\tau_{\text{dyn}} \ll \tau_{KH} \ll \tau_{\text{nucl}}$$

Sun: 1 hr << 3.10^7 yr << 10^{10} yr

So:

- except for explosive phases, stars are always in quasi-hydrostatic equilibrium!
- contraction phases last about 1% of nuclear phases

H4.1 Homework

Calculate dynamical, thermal, nuclear timescales and their ratios of

- MS star of $1 M_{\text{sun}}$
- MS star of $50 M_{\text{sun}}$
- Red supergiant $20 M_{\text{sun}}$
- AGB star
- White dwarfs

and comment on the consequences of these results.

(For data of AGB stars: see Appendix F)

Chapter 5. The Equation of State

5.1 Gas Pressure

The equation of state (EOS) describes the relation between P, T, ρ

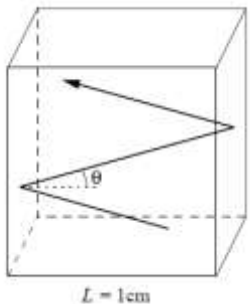


Fig 5.1 Consider particles in box 1x1x1 cm³

Calculate the force on one side (1cm²) by the collisions (momentum exchange) of all particles per second. (OP Fig 3.1)

Simplified : assume all particles have the same speed v

time between collisions on same side:

$$\Delta t = 2l/v \cos \theta = 2/v \cos \theta \quad (l = 1 \text{ for } 1\text{cm}^3)$$

momentum transfer per collision

Q?	$\Delta p = 2p \cos \theta$	Why 2?
----	-----------------------------	--------

momentum transfer per particle per second =

$$\frac{1}{\Delta t} \cdot \Delta p = v \cdot p \cdot \cos^2 \theta$$

integrate over all possible angles for an isotropic velocity distribution

$$\int_0^{\pi/2} \sin \theta \cdot d\theta \cdot \cos^2 \theta = \frac{1}{3} \cos^3 \theta \Big|_0^{\pi/2} = \frac{1}{3}$$

multiply by total nr of particles (n= particle density)

$$P = 1/3 v \cdot p \cdot n$$

Better: general distribution of velocities and momenta

$$P = 1/3 \int_0^\infty v \cdot p \cdot n(p) \cdot dp$$

1/3 from integration over all possible angles: isotropic

Total pressure:

$$P = P_{\text{ion}} + P_{\text{electr}} + P_{\text{rad}} = P_{\text{gas}} + P_{\text{rad}}$$

This is also expressed as:

$$\begin{aligned} P_{\text{gas}} &= \beta P & \text{with } 0 < \beta < 1 & \beta = 0 : P_{\text{rad}} \text{ dominates} \\ P_{\text{rad}} &= (1 - \beta)P & & \beta = 1 : P_{\text{gas}} \text{ dominates} \end{aligned}$$

Almost all stars are dominated by gas pressure. Only in the most massive ones ($M > 30M_{\odot}$) is radiation pressure in the center important.

5.2 Ideal Gas (OP 3.3.2)

$$\left. \begin{aligned} n(p)dp &= n_{\text{tot}} \frac{4\pi p^2 dp}{(2\pi m k T)^{3/2}} \cdot e^{-p^2/2mkT} \\ &= \text{Maxwell distribution} \\ v &= p/m \end{aligned} \right\} P = \frac{1}{3} \int v \cdot p \cdot n(p) dp = n_{\text{tot}} \frac{kT}{m}$$

Ion Pressure of Ideal Gas

$$\begin{aligned} P_i &= n_i k T \text{ with } n_i = \rho / \mu_i m_H \text{ with } \frac{1}{\mu_i} \simeq X + \frac{Y}{4} + \frac{Z}{20} \\ P_i &= \frac{\mathfrak{R} \rho T}{\mu_i} \quad (\mathfrak{R} = \frac{k}{m_H} = 8.31 \times 10^7 \text{ erg/K.mole} = \text{gas constant}) \end{aligned}$$

Electron Pressure of Ideal Gas

$$P_e = n_e k T = \frac{\mathfrak{R} \rho T}{\mu_e} \quad \text{with } 1/\mu_e \simeq \frac{1}{2}(1+X) \text{ only in stellar interior}$$

Gas Pressure of Ideal Gas

$$P_{\text{gas}} = n_{\text{tot}} k T = \frac{\mathfrak{R} \rho T}{\mu}$$

$$\text{with } 1/\mu = 1/\mu_e + 1/\mu_i$$

5.3 Degeneracy (OP 3.3.5)

At very high densities, or very low temperatures, the quantum mechanical effects become important. This changes the relation between P, T and ρ , i.e. the equation of state.

a. Heisenberg uncertainty principle:

$$\Delta x \Delta p > h \text{ in 1-dimension } [h] = \text{erg.s} = [g \text{ cm}^2/\text{s}]$$

$$\Delta \text{Vol} \Delta^3 p > h^3 \text{ in 3-dimensional phase-space}$$

h^3 is the unit of phase-space volume

b. Pauli exclusion principle:

No two identical particles (same quantum-state) can exist at same time at same place, i.e. in same phase-space volume $h^3 \rightarrow$ at most 2 electrons (spin up and spin down.)

Simple 1-D demonstration:

What happens if you squeeze more and more particles in a volume?

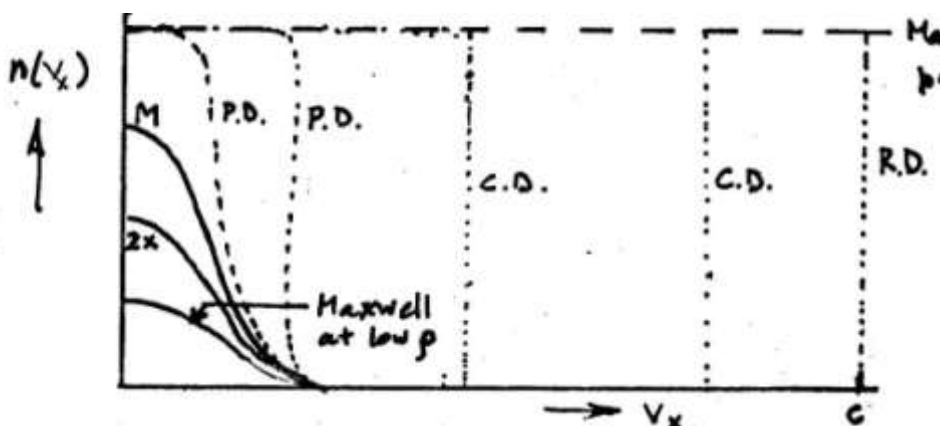


Fig. 5.2 1 dimensional velocity distributions at increasing density

- Maxwellian
- particle degeneracy = P.D. = still Maxwell tail
- complete degeneracy = C.D. = rectangular distribution
- relativistic = R.D. = most particles have $v \sim c \rightarrow p.v = p.c$

Q?

What is the role of temperature in the transition from Maxwellian to degenerate distribution?

What is the role of the particle mass?

5.3.1 Partial Degeneracy in 3-D distribution: (O.P. Fig 3.2)

Fig. 5.3 Electron momentum distributions

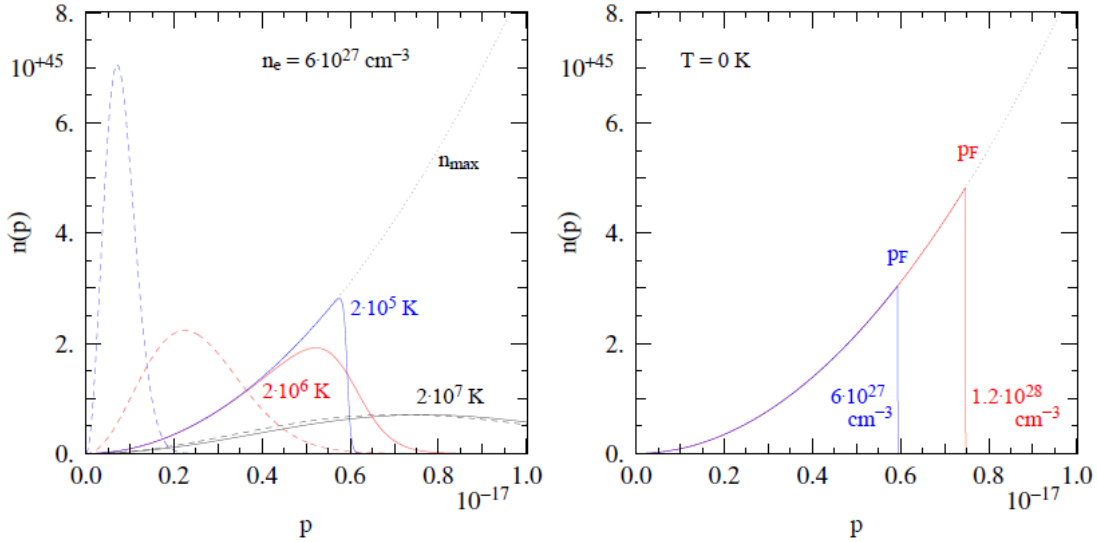


Figure 3.2. *Left:* Electron momentum distributions $n(p)$ for an electron density of $n_e = 6 \times 10^{27} \text{ cm}^{-3}$ (corresponding to $\rho = 2 \times 10^4 \text{ g/cm}^3$ if $\mu_e = 2$), and for three different temperatures: $T = 2 \times 10^5 \text{ K}$ (black lines), $2 \times 10^6 \text{ K}$ (red lines) and $2 \times 10^7 \text{ K}$ (blue lines). The actual distributions, governed by quantum mechanics, are shown as solid lines while the Maxwell-Boltzmann distributions for the same n_e and T values are shown as dashed lines. The dotted line n_{\max} is the maximum possible number distribution if all quantum states with momentum p are occupied. *Right:* Distributions in the limit $T = 0$, when all lowest available momenta are fully occupied. The blue line is for the same density as in the left panel, while the red line is for a density two times as high.

5.3.2 Complete Degeneracy:

$n(p)$ distribution is rectangular in nr per ($\text{cm}^3 \text{ g. cm/s}$)

$$\begin{aligned} \text{Electrons: } n_e(p) d^3p &= \frac{2}{\Delta Vol_l} = \frac{2}{h^3} (4\pi p^2 dp) && \text{if } p < p_F \text{ (F= Fermi)} \\ n_e(p) d^3p &= 0 && \text{if } p \geq p_F \end{aligned}$$

Derive p_F :

$$\text{Electron density: } n_e = \int_0^{p_F} n_e(p) \cdot d^3p = \int_0^{p_F} \frac{2}{h^3} \cdot 4\pi p^2 dp = \frac{8\pi}{3h^3} \cdot p_F^3$$

$$\text{So } p_F = \left(\frac{3h^3 \cdot n_e}{8\pi} \right)^{1/3}$$

Now we can find P_e , with $v = p/m_e$

$$P_e = \frac{1}{3} \int p \cdot v \cdot n_e(p) \cdot dp = \frac{1}{3} \int_0^{p_F} \frac{p^2}{m_e} \cdot \frac{2}{h^3} \cdot 4\pi p^2 dp = \frac{8\pi}{15h^3} p_F^5 \quad \text{with } p_F \sim n_e^{1/3}$$

So: $P_e (C.D) \sim n_e^{5/3}$ independent of T !

$$P_e(CD) = K'_1(\rho/\mu_e)^{5/3}$$

$$K_1 = 1.00 \times 10^{13} \frac{\text{dyne.cm}^{-2}}{(\text{g.cm}^{-3})^{5/3}} \quad \text{if } \mu_e = 2 \text{ i.e. if } X_H = 0$$

5.3.3 Extreme Relativistic Degeneracy:

most electrons have $\mathbf{v} \approx \mathbf{c}$ and $\mathbf{v.p} = \mathbf{c.p}$

$$P_c = \frac{1}{3} \int p \cdot v \cdot n_e(p) \cdot 4\pi p^2 dp = \frac{c}{3} \int p \cdot n_e(p) \cdot 4\pi p^2 dp$$

$$= \frac{2c}{3h^3} \int_0^{p_F} 4\pi p^3 \cdot dp = \frac{2c}{3h^3} \cdot \pi p_F^4 \quad \text{with } p_F \sim n_e^{1/3}$$

So: $P_e(R.D) \sim n_e^{4/3}$ independent of T .

$$P_e(R.D) = K'_2(\rho/\mu_e)^{4/3}$$

$$\text{with } K'_2 = 1.24 \times 10^{15} \frac{\text{dyne/cm}^2}{(\text{g.cm}^{-3})^{4/3}}$$

5.3.4 Partial Degeneracy (Not derived, just for completeness) (See Maeder 7.7 for the derivation)

n(p) is not a rectangular profile but has a Maxwell tail

$$P_e(P.D) = \frac{8\pi}{3h^3} (2m_e kT)^{3/2} \cdot kT \cdot F_{3/2}(\psi)$$

$$\text{where } F_{3/2}(\psi) \equiv \int_0^\infty \frac{x^{3/2}}{e^{r-\psi} + 1} dx$$

All of this was for electron degeneracy.

- Q?** Do baryons also become degenerate? (in particular He-nuclei or neutrons)
If so, at the same density as electrons?

Hints:

1. Energy exchange $\langle m_e v_e^2 \rangle = \frac{3}{2} kT = \langle m_n v_n^2 \rangle$
2. Degeneracy occurs when $d^3 p \sim h^3 / \Delta \text{Vol}$ $\Delta \text{Vol} \sim \frac{1}{n_n}$
i.e. when p reaches some value that depends on the density

5.3.5 The equation of state: completely degenerate electron gas

Fig 5.4: the transition in the EOS for completely degenerate electron gas (O.P. Fig. 3.3). The transition occurs at $\rho \approx 10^6 \mu_e \text{ g cm}^{-3}$.

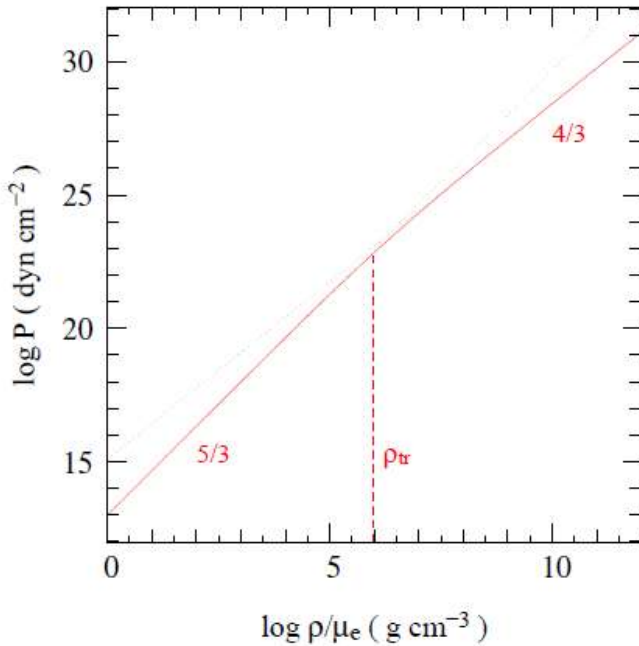


Figure 3.3. The equation of state for completely degenerate electrons. The slope of the $\log P$ - $\log \rho$ relation changes from $5/3$ at relatively low densities, where the electrons are non-relativistic, to $4/3$ at high density when the electrons are extremely relativistic. The transition is smooth, but takes place at densities around $\rho_{\text{tr}} \approx 10^6 \mu_e \text{ g cm}^{-3}$.

5.4 Radiation Pressure

Momentum of a photon: $p = h\nu/c \rightarrow n(p)dp = n(v)dv$
velocity = c

$$P_{\text{rad}} = \frac{1}{3} \int p \cdot v \cdot n(p) \cdot d^3p$$

$$n(v)dv = \frac{8\pi v^2}{c^3} \frac{dv}{e^{hv/kT}-1} \quad \text{Blackbody law = Planck function}$$

so

$$n(p)dp = \frac{8\pi v^2}{c^3} \frac{dv}{e^{hv/kT}-1} \cdot \frac{c}{h} dp \quad \text{with} \quad \left(\frac{c}{h} dp = dv \right)$$

$$\text{So } P_{\text{rad}} = \frac{1}{3} \int_0^\infty \frac{hv}{c} \cdot c \cdot n(v)dv$$

$P_{\text{rad}} = \frac{1}{3} a T^4$

$$a = \frac{4\sigma}{c} = \frac{8\pi^5 k^4}{15 c^3 h^3} = 7.56 \cdot 10^{-15} \text{ erg cm}^{-3} \text{ K}^{-4}$$

5.5 Limits of the equations of state

Fig 5.5: the regimes of the various equations of state in a ρ , T diagram. (O.P. Fig 3.4)

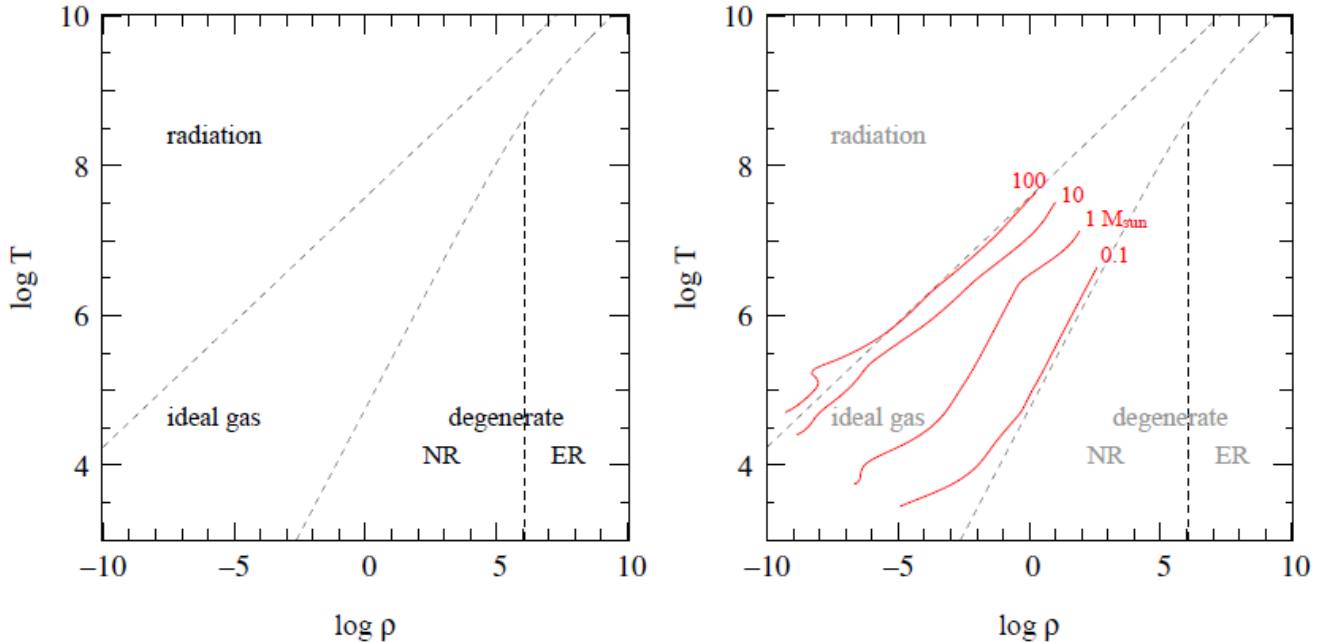


Figure 3.4. *Left:* The equation of state for a gas of free particles in the $\log T$, $\log \rho$ plane. The dashed lines are approximate boundaries between regions where radiation pressure, ideal gas pressure, non-relativistic electron degeneracy and extremely relativistic electron degeneracy dominate, for a composition $X = 0.7$ and $Z = 0.02$. *Right:* Detailed structure models for homogeneous main-sequence stars of $0.1\dots 100 M_{\odot}$ have been added (solid lines). The $1 M_{\odot}$ model is well within the ideal-gas region of the equation of state. In the $0.1 M_{\odot}$ star electron degeneracy pressure is important, except in the outer layers (at low ρ and T). In stars more massive than $10 M_{\odot}$, radiation pressure becomes important, and it dominates in the surface layers of the $100 M_{\odot}$ model.

H5.1 Homework

Equation of State

- *Derive the limits/boundaries between the 4 types of the equations of state (P_{rad} , ideal gas, Complete Degeneracy, Relative Degeneracy) by considering where in the (ρ, T) diagram the pressures are equal ($P_a = P_b$)*
- *How do these boundaries change if we go from a star consisting of H to one consisting of He?*
- *Explain in words (physics!) why these boundaries are (in)dependent of T .*
- *The figure above shows the limits of the EoS regions, together with the T - ρ structure of several stars. Consider the consequences, in terms of the conditions of the gas, the density and the radius of the stars.*

H5.2 Homework

Radiation Pressure

- *Use the models of Appendix C1 and C2 to calculate the ratio P_{rad}/P_{gas} in the center of main sequence stars of $0.8 < M < 120M_\odot$. At what masses is radiation pressure significant ($P_{rad}/P_{gas} > 0.5$)?*
-

5.6 Polytropic Gas

$$P = \rho^\gamma$$

γ = polytrope index

The structure of polytropic stars is easy, because there is no T-dependence. So HE $\rightarrow P(r)$ and $\rho(r)$!

Historical importance: Eddington “guessed” that stars behave as polytropes; he calculated the first model for the solar interior using the polytrope approximation $P \sim \rho^{4/3}$ and found approximately the correct M, R and even L.

Which stars behave as polytrope?

- a. Complete electron degenerate stars: because $P \sim \rho^{5/3} \sim n^{5/3}$
- b. Relativistic degenerate stars: because $P \sim \rho^{4/3} \sim n^{4/3}$
- c. Stars dominated by radiation pressure $P_{\text{rad}} \sim T^4$
ideal gas $P \sim \rho$
 $T \sim P/\rho$ } $P \simeq P_{\text{rad}} \rightarrow P \sim \rho^{4/3}$
- d. Stars with a constant ratio $\beta = P_{\text{gas}}/P_{\text{tot}}$ (this is what Eddington assumed)
 $P_{\text{rad}} = (1 - \beta)P \rightarrow P \sim P_{\text{rad}} \rightarrow P \sim \rho^{4/3}$ (as above)
- e. Fully convective stars $P \sim \rho^{5/3}$ (we will proof this below)

In all these cases:

$$\left. \begin{array}{l} \text{- if gas behaves as polytrope } P \sim \rho^\gamma \\ \text{- and gas behaves ideal } P \sim \rho T \end{array} \right\} \rightarrow \begin{array}{l} T \sim \rho^{\gamma-1} \\ T \sim P^{(\gamma-1)/\gamma} \end{array}$$

If a star is a polytrope then:

H.E. defines the $P(r)$ and $\rho(r)$. If the star is not degenerate then $T(r) = \frac{\mu}{k} \cdot \frac{P(r)}{\rho(r)}$ is also known, but $T(r)$ defines the energy flow by radiation.

So: **luminosity is known !!** (We will show this later)

H5.3 Homework

- The location of a modern solar model in the T, ρ diagram is shown in the figure 5.5 and listed in the Appendix D. Can you estimate the best value of γ ? (Ignore the outer layers of the star.)
- In the first model of the Sun by Eddington (1928) he assumed that the ratio $P_{rad}/P_{gas} = \text{constant}$. Compare the value of γ that he adopted with the one that you derive from the model. Comment on the result.
Show from the Solar model in App D how good/bad Eddington's assumption was.
- What is the best value of γ for a MS star of $0.1M_{\odot}$ and $100 M_{\odot}$? (derive from fig 5.5). Explain why these values could have been guessed.

5.7 Proof that a fully convective adiabatic star is a polytrope

Assume that convection is adiabatic: convective cells have no energy loss or gain

$$\left. \begin{array}{l} \text{First law of Thermodynamics: } du + PdV = dQ \\ \text{Adiabatic condition: } dQ = 0 \end{array} \right\} du = -PdV$$

u = specific internal energy (in ergs/gram)

$$\text{ideal gas: } u = (3/2) NkT \quad N = \text{nr particles per gram} \quad N = nV$$

$$P = nkT \quad n = \text{nr particles per cm}^3 \quad n = N/V \rightarrow P \cdot V = NkT$$

$$V = \text{volume of one gram of gas} = 1/\rho$$

$$\begin{aligned} du = -PdV &\rightarrow d\left(\frac{3}{2}PV\right) = -PdV \rightarrow \frac{3}{2}PdV + \frac{3}{2}VdP = -PdV \\ &\rightarrow \frac{5}{2}PdV = -\frac{3}{2}VdP \rightarrow \frac{dP}{P} = -\frac{5}{3}\frac{dV}{V} \end{aligned}$$

So

$$P \sim V^{-5/3} \rightarrow [P \sim \rho^{+5/3}]$$

$$\text{for ideal gas } P \sim \rho T$$

$$[T \sim \rho^{2/3}]$$

Q? Can a fully convective star be completely adiabatic?

5.8 The polytrope index of partially ionized gas

If gas is partially ionized, then $u \neq (3/2)NkT$ because part of energy goes into ionization of atoms or dissociation of molecules!

Convective zones are often partially ionized (see later).

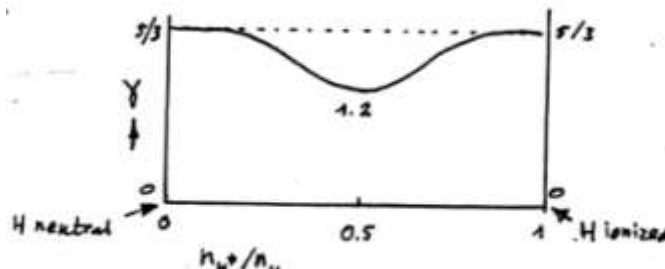


Fig 5.5 The polytrope index of partially ionized H-gas.

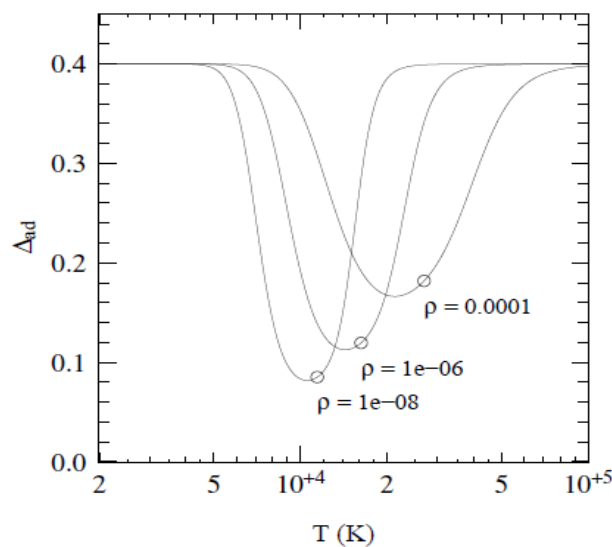
Partially ionized gas reaches a minimum value of $\gamma = 1.19$ close to half-ionization. (For the derivation see Pol: section 3.5)

Fig 5.6 The polytrope index of partially ionized H-gas for various densities (OP Fig 3.5)

The polytropic index γ is expressed in terms of the adiabatic temperature gradient $\Delta = d \ln T / d \ln P$ and $\gamma = d \ln P / d \ln \rho$

$$\Delta_{ad} = \frac{\gamma-1}{\gamma} \quad \text{so} \quad \gamma = \frac{1}{1-\Delta_{ad}}$$

$\Delta_{ad}=0.4$ corresponds to $\gamma = 5/3$ and $\Delta_{ad}=0.25$ corresponds to $\gamma = 4/3$



Q? Explain why $\Delta_{ad}=0.4$ at both the high and low temperature end.

Q? Why does the dip shift to higher T if the density increases?

Q? What is the physical reason that γ drops in a partially ionized region?

Chapter 6. Opacities in Stars

For understanding and calculating stellar structure, in particular the energy transport by radiation, we have to know the absorption coefficient of the gas as a function of density, temperature and composition. The absorption coefficients for radiation depend on wavelength. However, for solving the equation of radiative transfer inside a star we can use a wavelength-independent mean value, which is called the **Roseland-mean opacity**. Its definition is derived below in section 6.7.

6.1 Electron Scattering : σ_e in cm^2/g

σ_e is the scattering coefficient per gram of gas. **Q?** Why is it in cm^2/g ? Deep inside stars gas is fully ionized and electron scattering is the dominant opacity

$$\sigma_e = \sigma_T \cdot n_e$$

$$\sigma_T = 6.65 \cdot 10^{-25} \text{ cm}^2/\text{elec}$$

σ_T = Thomson cross-section for electrons

$$n_e = \text{nr of electrons per gram}$$

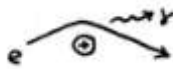
$$\mu_e m_H = \text{mean particle mass per electron}$$

$$\boxed{\sigma_e = \frac{\sigma_T}{m_H} \cdot \frac{1}{\mu_e} = \frac{0.40}{\mu_e} \approx 0.40 \frac{1+X}{2} \approx 0.2(1+X) \text{ cm}^2/\text{g}}$$

6.2 Free-free absorption: κ_{ff} in cm^2/g

Free-free absorption of a photon by an electron that briefly interacts with an ion (= inverse of Bremstrahlung)

$$\begin{aligned} Z &= \text{charge of ions} \\ n_i &= \text{ion density in nr/cm}^3 \\ n_e &= \text{electr dens in nr/cm}^3 \end{aligned}$$



$$\kappa_{ff} \text{ per cm}^3 \sim Z^2 \cdot n_i n_e \cdot T^{-7/2}$$

Q? Why is $\kappa_{ff} \sim n_i \cdot n_e$

$$\text{with } n_i = \rho / \mu_i m_H$$

$$n_e = \rho / \mu_e n_e$$

$$\kappa_{ff} \text{ per cm}^3 \sim Z^2 \rho^2 T^{-7/2} / \mu_i \mu_e$$

So κ_{ff} in cm^2/g is

$$\boxed{\kappa_{ff} = 7.5 \cdot 10^{22} \left(\frac{1+X}{2}\right) \langle \frac{Z^2}{A} \rangle \rho T^{-7/2} \text{ cm}^2/\text{g}}$$

6.3 Bound-free absorption : κ_{bf} in cm^2/g

The Kramers bound-free opacity law is calculated by summing all possible bound-free transitions (i.e. photo-ionizations) of many ions



$$\kappa_{bf} = 4.3 \times 10^{25} (1+X) \cdot Z \cdot \rho \cdot T^{-7/2} \text{ cm}^2/\text{g}$$

Q?

Notice that it is much larger than the free-free absorption.

Why is $\kappa_{bf} \sim \rho^2$ if it is defined per gram.

6.4 Bound-bound absorption: κ_{bb} in cm^2/g

Very difficult to calculate (!) due to numerous possible transitions, especially of highly ionized Fe-group elements. The Fe group elements give a peak in the opacity at around 10^5 to 10^6 K, depending on the density (see below).

6.5 Total opacity: $\kappa_{\text{Rosseland}}$ in cm^2/g

Tables of stellar opacities in stars and stellar atmospheres can be found on the web at

<http://www-phys.llnl.gov/Research/OPAL/index.html>

<http://www.osc.edu/hpc/opacities/>

<http://webs.wichita.edu/physics/opacity/>

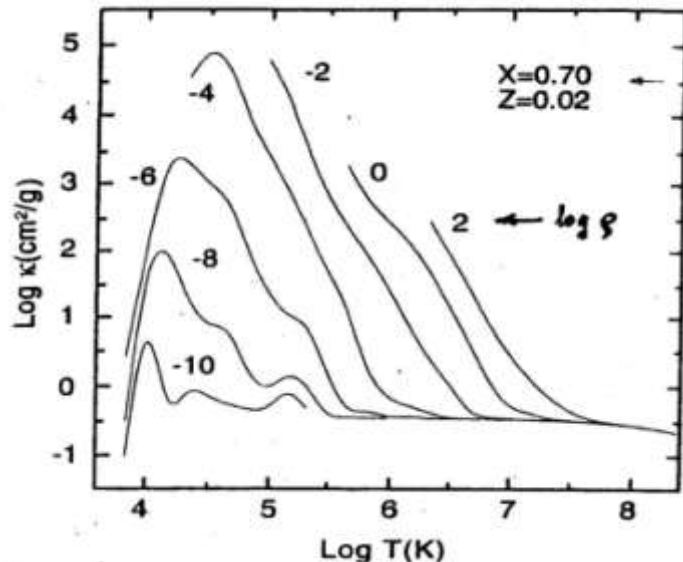


Fig 6.1
The total
Rosseland-mean
opacity for solar
composition as a
function of T and ρ
(OPAL data)

Notice

1. At high T and low density all matter is ionized so $\kappa = \sigma_e \simeq 0.3 \text{ cm}^2/\text{g}$
2. As T decreases bound-free and free-free absorption gets important with $\kappa \sim \rho \cdot T^{-7/2}$. This explains the downslope to higher T.
3. At intermediate temperatures (depending on ρ) the gas is partly ionized \rightarrow many more possible electron transitions \rightarrow huge opacities. This produces the peaks around 10^5 K for densities 10^{-6} to 10^{-4} g/cm^3 , i.e. inside the stars.
4. The peak at $10^4 < T < 10^5 \text{ K}$ at very low density, 10^{-10} to 10^{-8} g/cm^3 is due to H and is responsible for convection in the outer layers of cool stars!
5. The Fe-opacity peak around 10^5 to 10^6 K is important for Cepheids and Wolf-Rayet stars.
6. At very low $T < 10^4 \text{ K}$, the opacity (due to H) decreases steeply to very low values, as $\kappa \sim T^9$. This explains the steep slope at low T. This is important for stars on the Hayashi track, AGB-stars and red supergiants. It explains why the effective temperatures of stars cannot drop below about 2000 K (as we will see later).

Q? Why does the peak shift to higher temperatures when the density increases?

6.6 Opacity in stellar atmospheres

There are other absorption/scattering processes in stellar atmospheres:

- H⁻ absorption (H with 2 electrons) in the solar photosphere and cool stars.
- Bound-bound transitions = abs/emission lines (blanketing of atmospheres)
- Dust absorption and scattering (AGB stars, OH/IR stars)
- etc.

We will not discuss these in the context of stellar structure. They will later be discussed in the context of stellar winds.

6.7 Rosseland-mean Opacities

All opacities mentioned in this section are independent of frequency. In reality, the absorption coefficients depend on frequency. For instance free-free absorption is proportional to $\kappa \sim \lambda^2$.

For the calculation of the stellar structure, the frequency-dependent absorption coefficients have been averaged over frequency in a particular way, i.e. by using a weighting function of $dB/\nu dT$.

The resulting frequency-averaged absorption coefficients, mentioned above, are called **Rosseland-mean opacities**. They are defined as

$$\frac{1}{\kappa_R} \equiv \int_0^\infty \frac{1}{\kappa_\nu} \frac{dB\nu}{dT} \cdot d\nu / \int_0^\infty \frac{dB\nu}{dT} \cdot d\nu$$

Simple derivation of Rosseland-mean opacity

We will show later that the flux $F_\nu \sim \frac{-1}{\kappa_\nu} \frac{dB\nu}{dr}$

Define $F = \int_0^\infty F_\nu d\nu$

then $F = \int -\frac{1}{\kappa_\nu} \frac{dB\nu}{dT} \cdot d\nu \times \frac{dT}{dr}$

For calculating stellar evolution we want to write this as $F \sim \frac{-1}{\kappa_R} \frac{dB}{dr}$

So $\frac{1}{\kappa_R} \frac{dB}{dT} \cdot \frac{dT}{dr} = \int_0^\infty F_\nu d\nu = \int \frac{1}{\kappa_\nu} \frac{dB\nu}{dT} \cdot d\nu \times \frac{dT}{dr} \rightarrow \frac{1}{\kappa_R} = \int \frac{1}{\kappa_\nu} \frac{dB\nu}{dT} \cdot d\nu / \frac{dB}{dT}$

6.8 Mean-free Path of Photons : ℓ

$$l \simeq \frac{1}{\kappa\rho} \quad \left[\frac{\text{cm}^2}{\text{g}} \right]^{-1} \cdot \left[\frac{\text{g}}{\text{cm}^3} \right]^{-1} = [\text{cm}]$$

$$\text{Inside a star: } \left. \begin{array}{l} \rho \approx 1 \text{ g/cm}^3 \\ \kappa \sim 1 \text{ cm}^2/\text{g} \end{array} \right\} \quad l \approx 1 \text{ cm}$$

After 1cm a photon is absorbed and reemitted or scattered

→ photons quickly lose information on direction

→ radiation must be (almost) isotropic!

Q? If radiation inside a star is isotropic, how can there be a radiative outward flux?

Q? For a Brownian-motion the average radial distance traveled by a photon is $r \sim \ell\sqrt{N}$

(N = nr of random steps, ℓ = step length)

Use: $v = c$, $r = R_{\text{sun}}$ to calculate the total length L and the time it takes $\tau_L = L/c$ for a photon to move from center to outside of sun.

- Q?**
 - Is it still the same photon? (same λ , ν)?
 - Does it mean that, if the sun's nuclear fusion would stop suddenly, it would take us τ_L seconds before we noticed?
 - If not, how long would it take approximately before we noticed it?

H6.1 Homework

- a. Estimate the fraction of the radiation that is non-isotropic in the sun at $r = 0.5 R_\odot$?
- b. Could the same method be applied to derive the non-isotropic fraction of the radiation at $r = 0.9 R_\odot$? Why or why not?
- c. If you would apply the same method as in a. would you over or underestimate the non-isotropic fraction?

Hint

Consider this radiation density at some point (the length of the arrows is proportional to the radiative intensity in that direction)



H6.2 Homework

Identify in the figure of the total opacity (Sect 6.5) the region where electron scattering dominates and where $ff + bf$ dominate.

Check the dependence on ρ and T in these regions.

Chapter 7. Radiative Energy Transport

7.1 Eddington's Equation for radiative equilibrium

$$\frac{dT}{dr} = -\frac{3}{4} \cdot \frac{1}{ac} \cdot \frac{\kappa\rho}{T^3} \cdot \frac{L_r}{4\pi r^2}$$

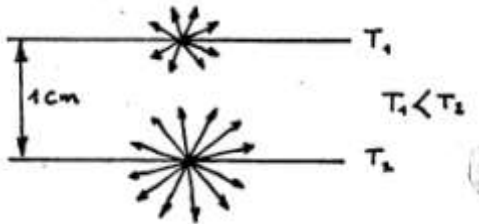
Eddington's equation for optically thick case

a = radiation density constant = $4\sigma/c$

σ = Stefan-Boltzmann constant

$$= 5.7 \times 10^{-5} \frac{\text{ergs}}{\text{cm}^3 \cdot \text{s} K}$$

Intuitive derivation: (easy to remember)



Consider a cm^3 in a layer of 1 cm thickness

Flux from below: $\sim \sigma T_2^4$

Flux from above: $\sim \sigma T_1^4$

F= Net flux $\sim \sigma(T_2^4 - T_1^4)$

a. $F \sim -\frac{d}{dr}(\sigma T^4)$

b. $F \sim \text{"transparency of layer"} \sim 1/\text{abs coeff per cm} \sim 1/\kappa$

c. $F \simeq L_r / 4\pi r^2$

Combine these three conditions:

$$\frac{L_r}{4\pi r^2} \sim \frac{-1}{\kappa\rho} \cdot \frac{d}{dr} \sigma T^4 = -\frac{1}{\kappa\rho} \cdot \frac{1}{4} \cdot ac \cdot 4T^3 \frac{dT}{dr} \quad \text{with } ac/4 \equiv \sigma$$

So from this simple intuitive derivation we expect

$$\frac{dT}{dr} \sim \frac{-1}{ac} \cdot \frac{\kappa\rho}{T^3} \cdot \frac{L_r}{4\pi r^2}$$

This is very similar to the real Eddington equation for energy transport by radiation. The difference of a factor 3/4 comes from proper integration of the radiation intensity over all angles.

For me, the simplest way to remember Eddington's equation is

$$\frac{L_r}{4\pi r^2} = -\frac{4}{3} \cdot \frac{1}{\kappa\rho} \cdot \frac{d\sigma T^4}{dr}$$

Comments:

- OP 4.4.2 gives the full derivation in terms of radiative diffusion.
- In several textbooks the Eddington equation is derived by using the radiation pressure. But this is confusing, because radiative transfer is not related to the pressure balance but to the diffusion of energy.

Q? Free-free absorption and bound-free absorptions are real absorptions: photons disappear. But electron scattering does not “absorb” photons, it just sends them into another direction (with very small mean free path).
So: why does electron scattering play a role at all in radiative transfer and in the structure of stars?

NB. **Radiative equilibrium means that the energy is transported by radiation. It does NOT mean that the gravity is balanced by radiation pressure !**

Chapter 8. The Mass-Luminosity Relation and the Eddington Limit

8.1 Thermal Equilibrium

We have seen that (almost) all stars are in **Hydrostatic Equilibrium (H.E.)**. Stars must also be in **Thermal Equilibrium (T.E.)**, i.e. all energy generated in a star per second by nuclear fusion or contraction, must be transported outwards and emitted from the surface. If a star is not in T.E. it quickly heats or cools inside. The transport of energy outwards can be by convection or radiation. The layers are then in **Convective Equilibrium (C.E.)** or in **Radiative Equilibrium (R.E.)**.

8.2 The Mass-Luminosity relation for stars in H.E. and R.E.

Stars in H.E. that transport energy by radiation obey a strict mass-luminosity relation. This can be derived rigorously for stars with a constant ratio $P_{\text{rad}}/P_{\text{gas}}$ (i.e. for polytropic stars with $\gamma = 4/3$ in R.E.) but we will derive it intuitively.

We have seen that for stars in H.E.

$$T_c \simeq \frac{\mu}{R} \cdot \frac{GM}{R}$$

We have also seen that for stars in R.E.

$$\frac{L_r}{4\pi r^2} = -\frac{4}{3} \cdot \frac{1}{\kappa\rho} \cdot \frac{d\sigma T^4}{dr}$$

Approximate

$$-\frac{dT^4}{dr} \simeq \frac{T_c^4}{R}, \quad \rho \simeq (4\pi/3)M/R^3, \quad L_r/4\pi r^2 \simeq L/4\pi R^2$$

This yields

$$L \simeq +\frac{4\sigma}{3\kappa} \cdot 4\pi R^2 \cdot \frac{4\pi R^3}{3M} \cdot \frac{1}{R} \cdot \frac{\mu^4}{R^4} \frac{G^4 M^4}{R^4} \sim \frac{\mu^4}{\kappa} \cdot M^3 \quad (\text{radius } R \text{ cancels !})$$

So, for stars in H.E. and R.E. we expect the following **Mass-Luminosity relation**

$$L \approx \frac{\mu^4}{\kappa} \cdot M^3 \cdot \text{constant}$$

- Q?**
- a. This relation is not valid for stars that are largely convective, i.e. lower main sequence stars and red (super) giants, and for degenerate stars. Why?
 - b. Considering the simplicity of our derivation, it fits surprisingly well the observed M-L relation for massive main sequence stars of $0.8 < M < 30 M_{\odot}$.
 $M_{\odot} : L \sim M^x$ with $x \approx 3.8$ and so $t_{nucl(MS)} \sim M/L \sim M^{2.8}$.
 - c. The most surprising result is that we made **no assumption about the energy production process** (type of fusion or contraction). This shows that a star can only be in H.E. and R.E if it has some fixed luminosity: independent of the luminosity source! The energy generation process has to adjust itself to the required value, otherwise the star is not in equilibrium!
 - d. The dominant opacity in massive stars is electron scattering
 $\kappa = \sigma_e \approx 0.20(1+X) \text{ cm}^2/\text{g}$. The values of κ and μ are
 $\kappa = 0.34$ and $\mu = 0.61$ if $X = 0.70$ and $Y = 0.30$ and
 $\kappa = 0.20$ and $\mu = 1.33$ if $X=0$ and $Y=1$.
So a He star of $1M_{\odot}$ will be about 30x more luminous than a star of $1M_{\odot}$ with normal composition. This explains why **hot horizontal branch stars** are so much more luminous than the MS stars at the turn-off point, although they have about the same mass. (See Fig 1.4)
 - e. The M-L relation explains why stars of $M > 1 M_{\odot}$ on the M.S. get brighter during their H-fusion.
 - f. It also explains why the evolution tracks of massive stars are approximately horizontal, except in RSG phase when the star is largely convective.
-

H8.1 Homework

1. Calculate the expected increase in luminosity when a star of $2M_{\odot}$ has converted all its H in the core into He and the core contains 10% of the stellar mass.
 2. Compare the result with the stellar evolution tracks in Appendix E.
 3. Calculate the expected value of the “constant” in the M-L relation.
Compare the predicted luminosity of a $10 M_{\odot}$ main-sequence star with the value from evolutionary models. Which approximation that we made in the derivation is mainly responsible for the difference?
 4. Explain in words why stars in H.E. and R.E. obey a M-L relation that is independent of the energy source. (What is the basic physics behind it?)
 5. Consider three stars with the same mass. Star A is in radiative equilibrium. Star B has a convective core that contains 30% of its mass. Star C has a convective core that extends to 30% of its volume. Which one of the stars, B or C will have a luminosity closest to that of star A. Explain this.
-

8.3 The Maximum Stellar Mass and Luminosity: the Eddington Limit

For a star with strong radiation pressure, the inward force due to gravity should be larger than the outward force by radiation pressure because H.E. requires

$$\left| \frac{dP_{rad}}{dr} \right| < \left| \frac{dP_{rad}}{dr} \right| + \left| \frac{dP_{gas}}{dr} \right| = \frac{GM(r)}{r^2} \cdot \rho \quad \text{with } P_{rad} = \frac{a}{3} T^4$$

Radiative Equilibrium requires

$$\frac{dP_{rad}}{dr} = \frac{d}{dr} \left(\frac{aT^4}{3} \right) = \frac{-3}{4} \cdot \frac{\kappa \rho_r}{c} \cdot \frac{L(r)}{4\pi r^2}$$

Combining these two equilibrium conditions gives (with r^2 and ρ_r cancelling)

$$L(r) < \frac{4\pi c GM(r)}{\kappa(r)}$$

This must apply at all radii, also at R_* .

In massive stars electron scattering is the dominant opacity and it is about constant throughout the star. This gives an upper limit for the luminosity of massive stars

$$L_* < 4\pi c GM / \kappa = L_{\text{Eddington}}$$

Eddington Luminosity

If a star would be brighter than L_E it would be blown-up by its radiation pressure! The electron scattering coefficient $\sigma_e = 0.20 (1+X) \text{ cm}^2/\text{g}$.

Filling in the constants gives

$$\frac{L_E}{L_\odot} = \frac{1.3 \times 10^4}{\sigma_c} \frac{M}{M_\odot} \simeq 3.8 \times 10^4 \frac{M}{M_\odot} \quad \text{if } X = 0.70$$

The influence of the radiation pressure is often expressed in terms of the **Eddington factor**

$$\Gamma_E \equiv \frac{L}{L_E} = \frac{\kappa L}{4\pi c GM} \quad \text{with } \Gamma_E < 1 \text{ for stable stars.}$$

The empirically derived maximum stellar mass is $M_{max} \simeq 160 - 300 M_\odot$ and $L_{max} \simeq 3 \cdot 10^6 L_\odot$ in the cluster NGC6303 in the LMC (Crowther et al. 2010 MNRAS 408, 731).

H8.2 Homework

- a. Derive the Mass-Luminosity relation for massive MS stars from the tables in Appendix C2. Extrapolate this relation to higher masses by assuming $L/L_\odot = A(M/M_\odot)^\alpha$ and derive A and α . Compare this with the expression for the Eddington luminosity and derive the maximum mass and maximum luminosity of stars.

 - b. Now consider what happens deep inside a massive main-sequence star. The luminosity of a massive star is generated in a small region, where $\frac{L(r)}{4\pi r^2} \gg L_*/4\pi R_*^2$ and $M(r) < M_*$
 - i. How can this region be stable against radiation pressure?
 - ii. What would happen if a region deep inside a star has $L > L_{\text{Edd}}$?
 - iii. The maximum stable models that have been calculated have $M \simeq 125 M_\odot$ and the maximum observed initial mass is $300 M_\odot$. What is the reason for the difference between these values and your result in (a)?
-

Chapter 9. Convective Energy Transport

9.1 The convection criterium: is the star stable against convection?

Qualitative picture (K. Schwarzschild 1906)

Idea: Assume that a blob of gas inside a star, accidentally starts moving upwards. If it keeps rising, that layer is obviously unstable for rising blobs = convection! If it falls back immediately, that layer is stable.

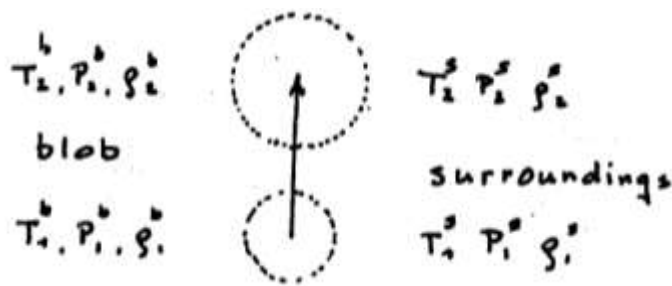


Fig 9.1
Schematic
representation
of convective
blobs.

It is easy to show that the blob will keep rising (due to the Archimedes force) if $\left| \frac{dT}{dr} \right|_b < \left| \frac{dT}{dr} \right|_s$

Q? Show this, by considering a blob rising from r_1 to r_2 , with $r_2 > r_1$.
Hint: blob is always in pressure equilibrium with its surroundings.

Q: What is the reason for the absolute signs?

9.2 The Schwarzschild criterium for convection

Idea: assume that the star is in radiative equilibrium. $\rightarrow (dT/dr)_s = (dT/dr)_{\text{rad}}$ (s for “surroundings”). What would happen to a blob of gas if it was accidentally displaced upwards? If the layer is convective, the temperature gradient will be adiabatic.

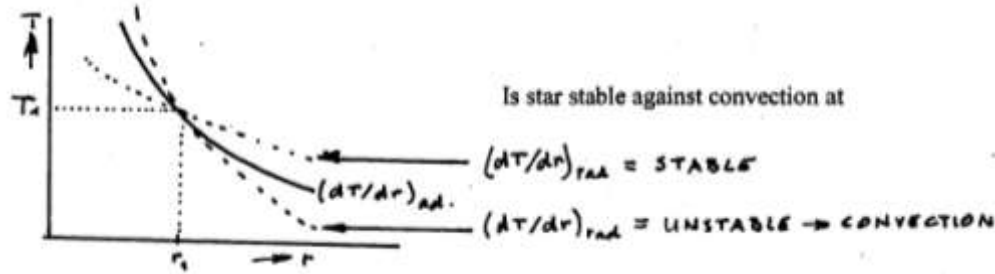
A layer will be convective if

$$\boxed{\left| \frac{dT}{dr} \right|_{\text{ad}} < \left| \frac{dT}{dr} \right|_{\text{rad}}} \quad = \text{Schwarzschild criterium}$$

or (easy to remember) : “the star always adopts the less steep temperature gradient.”

We will show below that the mean temperature gradient in a convective zone is *very close* to the adiabatic gradient

Fig. 9.2 The Schwarzschild-criterium in a picture



H9.1 Homework

Show that the condition $|dT/dr|_{ad} < |dT/dr|_{surrounding}$ that leads to the rising of hot bubbles, also leads to the descent of cool bubbles.

9.2.1 The Schwarzschild criterion in terms of the polytrope index

We can also express the Schwarzschild criterium for convection in terms of the local adiabatic polytrope index $\gamma \equiv d\ln P/d\ln \rho$

Schwarzschild criterium: convection if

$$\left(\frac{dT}{dr}\right)_{ad} > \left(\frac{dT}{dr}\right)_{rad} \rightarrow \left(\frac{d\ln T}{dr}\right)_{ad} > \left(\frac{d\ln T}{dr}\right)_{rad}$$

$$\left. \begin{array}{l} \text{For ideal gas} \\ \text{Polytrope index} \end{array} \right\} \quad \begin{array}{l} T \sim P/\rho \\ P \sim \rho^\gamma \end{array} \quad \left. \begin{array}{l} \frac{d\ln T}{dr} = \left(1 - \frac{1}{\gamma}\right) \frac{d\ln P}{dr} \\ \text{with } \frac{d\ln P}{dr} \text{ from H.E.} \end{array} \right.$$

$$\text{So: convection occurs if } \left(1 - \frac{1}{\gamma_{ad}}\right) \frac{d\ln P}{dr} > \left(1 - \frac{1}{\gamma_{rad}}\right) \frac{d\ln P}{dr} \rightarrow \boxed{\gamma_{ad} < \gamma_{rad}}$$

$$\boxed{\left|\frac{dT}{dr}\right|_{rad} < \left(\frac{\gamma_{ad}-1}{\gamma_{ad}}\right) \cdot \frac{T}{P} \cdot \left|\frac{dP}{dr}\right|} \quad \text{with } 1.2 < \gamma_{ad} < 5/3 \quad (\text{Section 5.5})$$

9.3 Convection in a layer with a μ -gradient

The **Ledoux-criterium** for convection

We have derived the Schwarzschild criterium for convection by considering the rise of bubbles in a medium of constant chemical composition. We now consider the case of a chemically stratified star with the mean particle mass μ decreasing outward.

Q?

Why “decreasing”?

If a bubble (b) rises adiabatically and the surrounding (s) is in radiative equilibrium, then the condition for convection to occur is:

$$\left| \frac{d\rho}{dr} \right|_{\text{ad}} > \left| \frac{d\rho}{dr} \right|_s \quad \text{or} \quad \left| \frac{d\ln\rho}{dr} \right|_{\text{ad}} > \left| \frac{d\ln\rho}{dr} \right|_s$$

With $P = \mathfrak{R}\rho T/\mu$ and $\rho = \mu P/\mathfrak{R}T$ (\mathfrak{R} = gas constant)
we find that convection occurs if

$$\left(\frac{d\ln P}{dr} \right)_b + \left(\frac{d\ln\mu}{dr} \right)_b - \left(\frac{d\ln T}{dr} \right)_b > \left(\frac{d\ln P}{dr} \right)_s + \left(\frac{d\ln\mu}{dr} \right)_s - \left(\frac{d\ln T}{dr} \right)_s$$

Since the bubble will remain in pressure equilibrium with its surrounding, and since the composition inside the bubble will not change when it rises, we find the condition for convection:

$$-\left(\frac{d\ln T}{dr} \right)_b > -\left(\frac{d\ln T}{dr} \right)_s + \left(\frac{d\ln\mu}{dr} \right)_s$$

So, if convective cells rise adiabatically in a medium that is in radiative equilibrium and has a μ -gradient, the condition for convection is

$$\left| \frac{d\ln T}{dr} \right|_{\text{rad}} > \left| \frac{d\ln T}{dr} \right|_{\text{ad}} + \left| \frac{d\ln\mu}{dr} \right|$$

Ledoux-criterium

Notice:

1. The Ledoux-criterium in a homogeneous layer is the same as the Schwarzschild criterium.
2. For given adiabatic and radiative temperature gradients, **a chemically stratified zone in a star is more stable against convection than a chemically homogeneous zone.**
3. Convection is very efficient in chemical mixing. So the chemical stratification disappears in a convective zone and the zone will adopt the “mass-mean” average of μ .

9.4 The mixing length:

How far does a convective cell rise before it dissolves in its surroundings?

A rising convective cell will dissolve into its surroundings, i.e. loose its identity, when the temperature of the gas inside the cell gradually adjusts to the temperature of its surrounding by the loss of radiation or heat at its boundary. The distance a hot cell rises or a cold cell descends is called the “**mixing length**”: ℓ_m . The proper calculation of this mixing length is complicated, because it involves the proper 3-D (magneto-) hydrodynamical calculations of convective flows.

As a reasonable guess, we can assume that it will be of the order of the “*pressure scaleheight*” inside the star. We make a rough estimate of the pressure scaleheight.

H.E. requires

$$\frac{dP}{dr} = -\rho \frac{GM_r}{r^2} \quad \text{with} \quad \rho = \frac{P\mu}{RT} \rightarrow \frac{1}{P} \frac{dP}{dr} = -\frac{GM_r}{r^2} \cdot \frac{\mu}{RT}$$

$$\frac{d\ln P}{dr} = -\frac{GM_r}{r^2} \cdot \frac{\mu}{RT}$$

Now if T and M_r do not vary too strongly with distance and have mean values of \bar{T} and \bar{M}_r at distance r , we can approximate

$$P(r_0 + h) \simeq P(r_0) e^{-h/\ell_P}$$

We see that the **pressure scaleheight** is approximately $\boxed{\ell_P \simeq \frac{RT}{\mu} \cdot \frac{r^2}{GM_r} \simeq \frac{RT}{\mu g}}$

The **mixing length for convection** is usually written as $\ell_m = \alpha \ell_P$ with $\alpha \simeq 1$.

N.B. The assumption of near-constant T is a rather bad one, because there certainly is a temperature –gradient. The proper value of the pressure scaleheight can only be derived when the structure of the star has been calculated.

However, for our purpose of estimating and for “getting a feeling” of the properties of the convection, the approximation is good enough.

The expression above also applies to stellar and planetary atmospheres, where it is usually written as $H_p = RT/\mu g$.

This expression also applies to the earth atmosphere.

- Q?** Do you need extra oxygen when you climb Mount Everest (~10 km)?

9.5 The Efficiency of Convective Energy Transport

The convective flow has to transport the stellar luminosity.
We will make a simple estimate to get a “feeling” for the physical process.

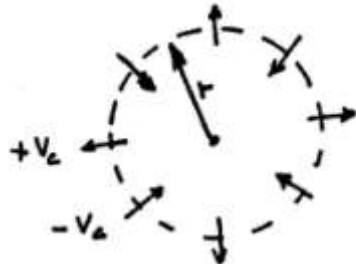


Fig. 9.3 The transport of energy by convection with velocity v_c through a sphere with radius r inside the star.

Suppose:

- half the matter moves up, the other half down
- upward velocity = v_c , downward velocity = $-v_c$ ($v_c = v_{\text{convection}}$)
- the difference is temperature between up and downward moving cells is $T_{\text{up}} - T_{\text{down}} = \Delta T$

Then:

the difference in thermal energy content per cm^3 is $(3/2)nk\Delta T$

Consider transport through a sphere at distance r from the stellar center

The amount of gas per sec through sphere r = flow $\uparrow - \downarrow$

Mass transport: $4\pi r^2(\rho v_c) - 4\pi r^2(\rho v_c) = 0 \rightarrow$ No net transport of gas

Energy transport through the shell by convection:

$$4\pi r^2 v_c \frac{3}{2} nk T_{\text{up}} - 4\pi r^2 v_c \frac{3}{2} nk T_{\text{down}} = 4\pi r^2 \cdot nk \Delta T \cdot v_c = \\ 4\pi r^2 \frac{\rho}{\mu m_H} \cdot k \cdot (\Delta T \cdot v_c) = \frac{4\pi r^2 \rho \mathcal{R}}{\mu} \cdot (\Delta T \cdot v_c) = L_r$$

So $\boxed{\Delta T \cdot v_c \simeq (L_r / 4\pi r^2) \cdot \rho \cdot \mathcal{R} / \mu}$

Estimate this for a “typical” star = Sun

$$r \simeq 0.5 R_\odot = 3.5 \times 10^{10} \text{ cm}$$

$$\rho \simeq 1 \text{ g/cm}^3$$

$$\mu \simeq 0.5$$

$$\Delta T \cdot v_c \simeq 10^4 \frac{\text{cm}}{\text{s}} \cdot K \quad \text{extremely small!}$$

$$\mathcal{R} = 8.3 \times 10^7 \text{ erg/K.mole}$$

$$L_\odot = 4 \times 10^{33} \text{ erg/s}$$

We show that $\Delta T \cdot v_c$ is extremely small.

If $\Delta T \simeq 0.1\bar{T} \simeq 10^5 K \rightarrow v_c \simeq 0.1 \text{ cm/s} \ll v_{\text{sound}} \simeq 10^7 \text{ cm/s}!$

If $v_c \simeq v_{\text{sound}} \simeq 10^7 \text{ cm/s} \rightarrow \Delta T \simeq 10^{-3} K \ll T \simeq 10^6 K!$

So either : convection speed is very slow

or: T-difference between up and down is very small

or: both (This is what happens in reality, as we will see below).

Q? What is the physical reason that $\Delta T v_c$ so very small??

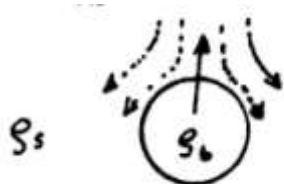
Hint: think in terms of gas-energy content.

9.6 The convective velocity

We can estimate the convection velocity by considering a convective cell as a balloon.

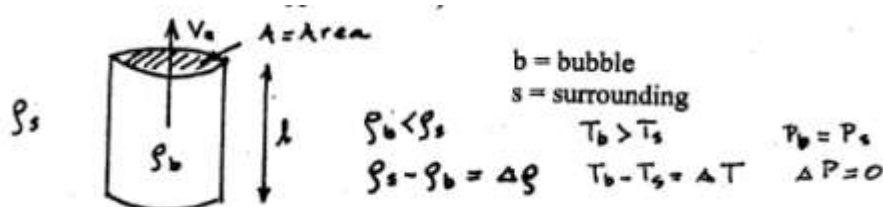
Fig 9.4 Balloon analogy of convection for estimating convection velocity

Balloon : b = balloon , s = surrounding



Upward force = Archimedes force
Downward force = drag

Convective cell : cylinder approximation



Up: $F \uparrow = \text{Archimedes force} = \underbrace{\text{Volume} \times \text{density difference} \times \text{gravity}}_{\text{Weight difference}}$

$$F \uparrow = A \cdot \ell \cdot \Delta \rho \cdot \frac{GM(r)}{r^2} \quad [\text{cm}^2] \cdot [\text{cm}] \cdot [\text{g/cm}^3] \cdot [\text{cm/s}^2] = [\text{g cm/s}^2]$$

Down: Momentum transfer of gas that is pushed away at top = ram-force

$$F \downarrow = \underbrace{\rho_s v_c}_{\text{mom}} \times \underbrace{v_c A}_{\text{volume of displaced gas per sec}} = \rho_s v_c^2 A \quad [\text{g/cm}^3] \cdot [\text{cm/s}]^2 \cdot [\text{cm}^2] = [\text{g cm/s}^2]$$

The bubble (or balloon) reaches a constant upward velocity when $F\uparrow = F\downarrow$:
 $\rho_s v_c^2 A = A \cdot \ell \cdot \Delta\rho \cdot g(r)$. So the speed of the convective cell is approximately

$$v_c^2 = g(r) \cdot \ell \cdot (\Delta\rho / \rho_s)$$

where $\ell \sim$ length of the rising bubble (cylinder)

We can assume $|\Delta\rho_s / \rho_s| = |\Delta T / T|$ because of pressure equilibrium between inside and outside cell.

So

$$\frac{v_c^2}{\Delta T} \sim \frac{g(r) \cdot \ell}{T}$$

This equation, in combination with the one derived above from the energy transport

$$\Delta T \cdot v_c \simeq (L_r / 4\pi r^2) \cdot \rho \cdot \mathcal{R} / \mu$$

provides expressions for both the convective velocity, v_c , and the temperature difference between the rising convective cells and the surroundings.

The values that follow from this exercise are derived in Homework H9.2

H9.2 Homework

- a. Calculate the thermal energy content of a cm^3 of gas in the sun at $r = 0.9 R_\odot$
- b. Calculate the speed of sound at that location.
- c. Assume that the temperature difference between the ascending and descending bubbles is δ_T of the mean local value, and that the velocity of the bubbles is δ_v of the local sound speed.
Calculate the luminosity that would be transported by convection in this case.
- d. Compare this with the true luminosity, L_r , at $0.9 R_\odot$.
Derive the values of δ_v and δ_T , and of ΔT and v_c .

H 9.3 Homework

- a. Sketch a diagram of outward decreasing μ as function of r .
Adopt some lower limit and some upper limit for a zone that would be convective according to the Schwarzschild criterium.
- b. Show schematically where the convection zone would be according to the Ledoux criterium for convection in a medium with a μ -gradient.
- c. Show how the μ -profile would be changed by convection in these 2 cases.

H9.4 Homework

- a. Estimate the pressure scaleheight in the Sun at $r = 0.9 R_{\odot}$, using the expression derived above.
- b. Compare it with the real pressure scaleheight of a solar model.
- c. Comment on the differences

9.7 Typical values of convective velocity and timescale

Estimate for the Sun

(at $r=0.5 R_{\odot}$, although the Sun is not convective there)

$$\left. \begin{aligned} g(0.5R_{\odot}) &\simeq 10^5 \text{ cm/s}^2 \\ \ell_p &\sim 0.1R_{\odot} = 7 \times 10^9 \text{ cm} \\ T &\sim 2.10^6 K \end{aligned} \right\} \frac{v_c^2}{\Delta T} \simeq 3.5 \times 10^8 \text{ cm}^2/\text{s}^2 \text{ K}$$

We have derived before

$$\left. \begin{aligned} \Delta T \cdot v_c &\simeq 10^4 \text{ cm.K/s} \\ v_c^2 / \Delta T &\simeq 3.5 \times 10^8 \text{ cm}^2 \end{aligned} \right\} v_c^3 \simeq 3.10^{12} \frac{\text{cm}^3}{\text{s}^3} \rightarrow \boxed{v_c \simeq 10^4 \frac{\text{cm}}{\text{s}}} \lll v_{\text{sound}} 10^7 \frac{\text{cm}}{\text{s}}$$

Now find ΔT

$$\frac{\Delta T}{v_c} = 10^4 \text{ cm.K/s} \rightarrow \boxed{\Delta T \simeq 1K} \rightarrow \Delta T/T \simeq 10^{-6} \quad (\text{very small!})$$

Rise time of convective cells

$$t_{\text{rise}} \simeq \ell_p/v_c \simeq \frac{7 \times 10^9 \text{ cm}}{10^4 \text{ cm/s}} \simeq 7 \times 10^5 \text{ s} \rightarrow \boxed{t_{\text{rise}} \sim \text{week}}$$

9.8 The superadiabatic T-gradient

The mean T-gradient of the surroundings must be steeper than $(dT/dr)_{\text{ad}}$ of the convective cells, otherwise the convection would stop.

$$\text{So } \left| \frac{dT}{dr} \right|_{\text{actual}} > \left| \frac{dT}{dr} \right|_{\text{ad}} \quad \text{define: } \left| \frac{dT}{dr} \right|_{\text{actual}} = \left| \frac{dT}{dr} \right|_{\text{ad}} + \left| \frac{dT}{dr} \right|_{\text{superadiabatic}}$$

We have seen that the superadiabatic T-gradient produces a difference of only $\simeq 1K$ over a distance of a pressure scaleheight.

$$\text{So } \left| \frac{dT}{dr} \right|_{\text{superadiabatic}} \ll \left| \frac{dT}{dr} \right|_{\text{ad}}$$

So the real temperature gradient in a convection zone is

$$\left| \frac{dT}{dr} \right| = \left| \frac{dT}{dr} \right|_{\text{ad}} (1 + \epsilon) \quad \text{with} \quad \epsilon \ll 1$$

So we can safely adopt $|dT/dr| = |dT/dr|_{\text{ad}}$ in a convection zone!

9.9 Convection: Where and Why?

The Schwarzschild criterium for convection is $\left| \frac{dT}{dr} \right|_{\text{rad}} > \left| \frac{dT}{dr} \right|_{\text{ad}}$

$$\text{With } \left| \frac{dT}{dr} \right|_{\text{rad}} \sim (\kappa/T^3) \cdot (L_r/4\pi r^2)$$

From this we can see that there are **two reasons for convection:**

1. Layers where κ is very large = layers where H is partly ionized (remember Fig 6.1)
This occurs in outer layers of cool stars:
 - MS stars cooler than about F0
 - at type G0: a thin outer convection layer,
 - at type M : almost fully convective
 - Red giants and supergiants : almost fully convective (except core)
2. Layers where $L_r/4\pi r^2$ is very large = center of massive stars .
These stars have a high luminosity, created in small core.
 - MS stars of $M \gtrsim 1.4M_\odot$, because the CNO-cycle has a strong T-dependence.

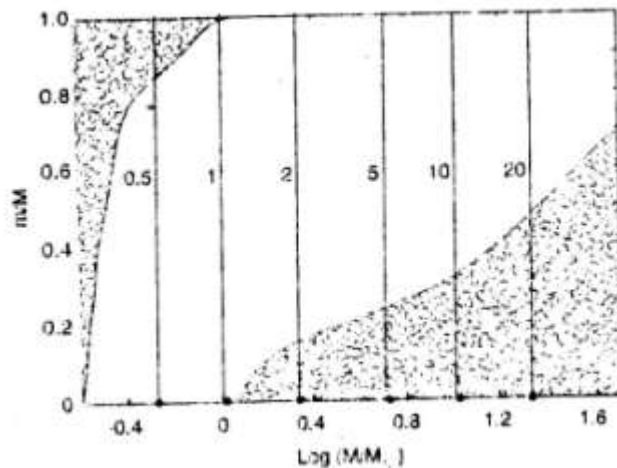


Fig. 8.4 Schematic picture of occurrence of convection for MS stars (KW p. 213, fig 22.7)
Shaded area = convective. Vertical lines indicate stellar masses.

H9.5 Homework

Massive stars burn H via the CNO-cycle (to be discussed later).

This is very sensitive to T.

Explain why this gives massive MS stars convective cores.

9.10 Convective Overshooting

The Schwarzschild criterium is derived from the condition that the Archimedes force provides an upward force.

At the top and the bottom of the convection zone there is no up/down ward force, but the moving cells do not suddenly halt there. They will **overshoot** the convection boundaries.

First observational indications ~1985:

nuclear products appear at surface of massive stars (especially He and N) before mass loss has peeled the outer layers down to the mass of the old convective core.

So: there must have been some mixing to layers higher than the convective core boundary.

From several comparisons between observations \leftrightarrow theory:

overshooting is about 1 pressure scaleheight !

(see Maeder and Meynet 1987 AA)

Difference between convection and overshooting:

Convection \rightarrow energy transport and mixing

Overshooting \rightarrow only mixing (but the temperature gradient is radiative)

9.11 Chemical Mixing by Convection

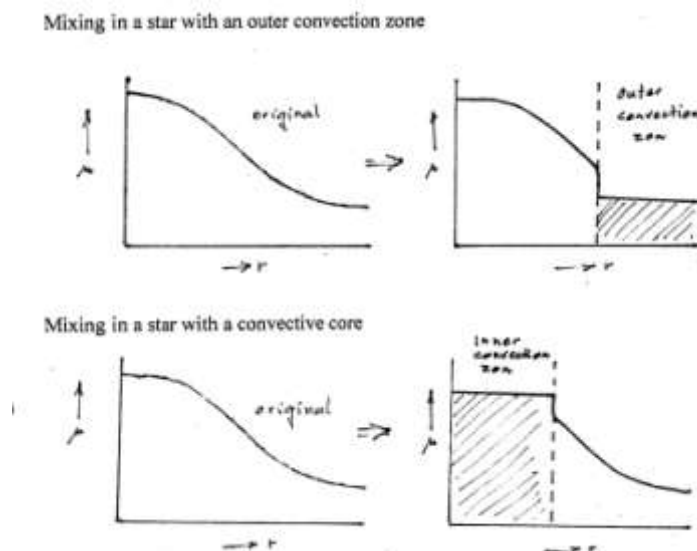


Fig. 8.5 Mixing in stars with inner or outer convection zones

Consequence of mixing by convection and overshooting:

Massive stars on the main sequence have convective cores. Although the nuclear fusion happens in the very center, the nuclear products are mixed throughout the convective core. One of the immediate consequences is that H is brought into the center from all over the convective core. This results in an increase of the mass fraction of the star that takes part in H-fusion (f_M in the estimate of the nuclear timescale in Sect 4) from about $f_M \approx 0.14$ for solar type stars to $f_M \approx 0.75$ for stars with $M > 60M_\odot$. This extends the expected MS lifetimes of massive stars considerably.

H9.6 Homework

Use the data shown in Appendix C2 (convective cores) to estimate as accurately as possible the MS lifetimes of stars of 1, 5, 20, 85 M_\odot and compare it with results of evolution models. What could be the reason for the systematic difference?

H9.7 Homework

- a. *Massive stars in the H-burning phase have a convective core. The mass fraction of the convective core decreases during the main sequence. Can you think of a reason why?*
- b. *How does this affect the He-abundance distribution in the star as a function of age during the MS phase. Explain this with a sketch.*

Chapter 10. Nuclear Fusion (OP 6)

During nuclear fusion two particles (i and j) react, which results in one or two other particles (k and l). The particles involved have a charge Z and a mass A .

So the reaction is $i + j \rightarrow k + l$

$$\begin{aligned} \text{nuclear charge conservation: } & Z_i + Z_j = Z_k + Z_l \\ \text{baryon number conservation: } & A_i + A_j = A_k + A_l \end{aligned}$$

10.1 Reaction rates and energy production

The **reaction rate** is expressed as r_{ijkl} (in nr per sec per gram)

The **energy generation rate** by nuclear fusion per gram per second is
 $\epsilon_{ijkl} = r_{ijkl} \cdot Q_{ijkl}$ Q usually in MeV (1MeV = $1.602 \cdot 10^{-6}$ ergs)

where

$$Q_{ijkl} = (m_i + m_j - m_k - m_l)c^2$$

is the amount of energy produced by one reaction.

The term in brackets is the **mass-defect** of the reaction, i.e. the mass that has been converted into energy. Q corresponds to the difference in binding energy of the nuclei involved in this reaction.

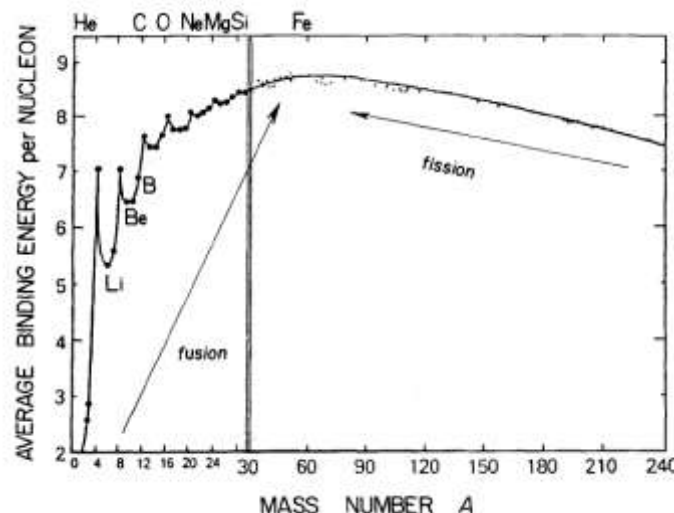


Fig 10.1
The average binding energy in MeV per nucleon (proton or neutron) as a function of atomic mass.
(Fig OP6.1)

In the rising part of the curve, fusion produces energy. In the descending part of the curve fusion requires energy but fission produces energy.

Q?

Explain in why the cosmic abundance of Li, Be etc. is low.

The mass defect can conveniently be expressed as a fraction of the mass that goes into the fusion process. This is the the **mass defect fraction**: $\Delta m/m$

For instance, for $H \rightarrow He$ fusion : $\Delta m/m = 0.00712$

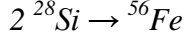
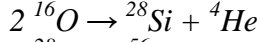
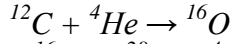
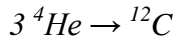
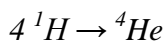
For $He \rightarrow C$ fusion : $\Delta m/m = 0.00065$

The table below gives the masses of isotopes involved in the most important nuclear fusion reactions in stars (OP tbl 6.1)

element	<i>Z</i>	<i>A</i>	<i>M/m_u</i>	element	<i>Z</i>	<i>A</i>	<i>M/m_u</i>	element	<i>Z</i>	<i>A</i>	<i>M/m_u</i>
n	0	1	1.008665	C	6	12	12.000000	Ne	10	20	19.992441
H	1	1	1.007825		6	13	13.003354	Mg	12	24	23.985043
	1	2	2.014101	N	7	13	13.005738	Si	14	28	27.976930
He	2	3	3.016029		7	14	14.003074	Fe	26	56	55.934940
	2	4	4.002603		7	15	15.000108	Ni	28	56	55.942139
Li	3	6	6.015124	O	8	15	15.003070				
	3	7	7.016003		8	16	15.994915				
Be	4	7	7.016928		8	17	16.999133				
	4	8	8.005308		8	18	17.999160				

H10.1 Homework

a. Calculate the mass defect fractions of the following relations



b. Notice the trend and discuss what this trend implies for stellar evolution.

10.2 Thermonuclear reaction rates and the Gamov peak

Ions have a positive charge, so they will repulse one another by electric Coulomb-forces. To enable fusion, the particles have to overcome this Coulomb barrier.

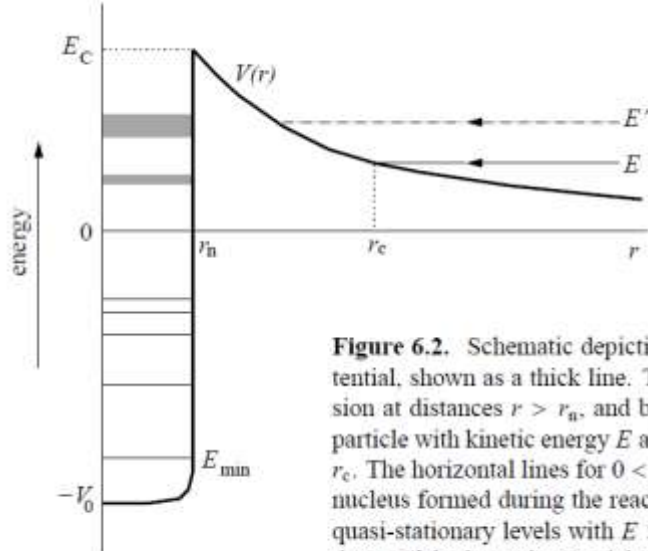


Figure 6.2. Schematic depiction of the combined nuclear and Coulomb potential, shown as a thick line. The potential is dominated by Coulomb repulsion at distances $r > r_n$, and by nuclear attraction for $r < r_n$. An incoming particle with kinetic energy E at infinity can classically approach to a distance r_c . The horizontal lines for $0 < r < r_n$ indicate energy levels in the compound nucleus formed during the reaction. The ground state is at energy $-E_{\min}$; the quasi-stationary levels with $E > 0$ are broadened due to their very short lifetimes. If the incoming particles have energy E' corresponding to such a level they can find a resonance in the compound nucleus (see text).

Fig 10.2 The tunneling effect through the Coulomb barrier (OP Fig 6.2)

The velocity of the particles follows the Maxwell distribution. Only the fastest particles have a probability of overcoming the Coulomb barrier. But their number decreases rapidly with velocity v or energy E as

$$N(E) \sim \exp(-E/kT)$$

The quantum mechanical **tunneling effect** allows particles whose energy is smaller than the Coulomb barrier to overcome this barrier. If it was not for this effect, the fusion process in stars would require a much higher T than in reality. The tunneling probability P_t increases with energy as

$$P_t(E) \sim \exp\left(-\frac{b}{\sqrt{E}}\right)$$

where b is a constant that depends on the reaction. The net result is that the reaction rate scales with the product of the two functions, and shows a peak, called the **Gamov-peak**

$$R(E) \sim N(E) \cdot P_t(E) \sim \exp\left(-\frac{E}{kT} - \frac{b}{\sqrt{E}}\right)$$

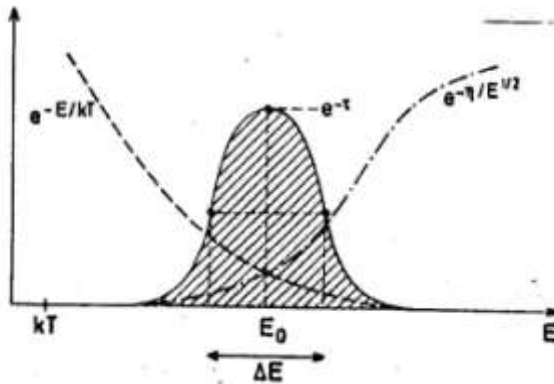


Fig 10.3
The Gamov peak is the result of the product of two functions: the number of particles with energy E , which decreases with E , and the probability for tunneling, which increases with E .

Because of the strong dependence of the Coulomb barrier on the charge of the fusing ions and on the combination of the Maxwell energy distribution and the tunneling effect, the reaction rates of the fusion reactions depend very strongly on temperature. For instance

$H \rightarrow He$	(p-p chain)	$T \approx 1 \cdot 10^7$	$\varepsilon \sim T^4$
$H \rightarrow He$	(CNO-cycle)	$T \approx 2 \cdot 10^7$	$\varepsilon \sim T^{12}$
$He \rightarrow C$	(3α-process)	$T \approx 1 \cdot 10^8$	$\varepsilon \sim T^{40}$

NB: The reaction rates are not really power laws of T , but can be approximated by partial power laws. The exponents of the T -dependence given above are the exponents near the T -range of the fusion reactions in stars.

10.3 Abundance changes

The **change in abundance** per second of element i due to this reaction can be expressed as

$$\boxed{dX_i/dt = -r_{ijkl} \cdot A_i m_u}$$

where $m_u = m_c/12$ is the standard atomic mass unit (amu).

If element i is involved in more fusion reactions, some of which destroy and others create i , then the change in abundance should be written as the sum of all possible destruction reactions (- sign) and all formation reaction (+ sign).

$$\frac{dX_i}{dt} = A_i m_u \left\{ \sum_x -r_{i \rightarrow x} + \sum_y +r_{y \rightarrow i} \right\}$$

10.4 H→He fusion

There are two major routes for converting H into He in stars :

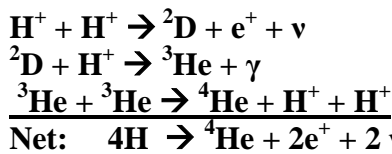
- **the proton-proton chain** (pp-chain)

- **the CNO cycle** (there are actually two main cycles)

Although the net reactions of these two routes are the same, they have very different effect on the abundance evolution of the stars.

10.4.1 The proton-proton chain

At $5 < T < 15$ MK, H is predominantly fused via the proton-proton chain



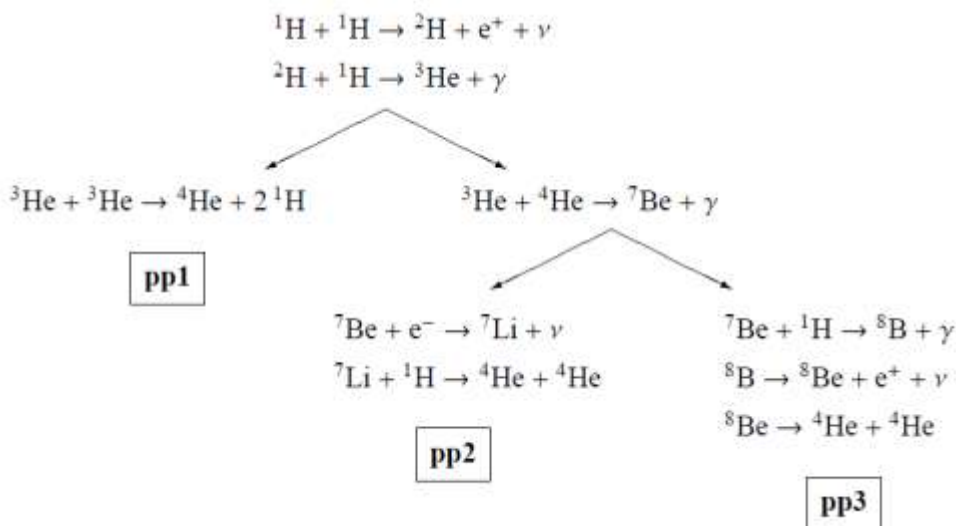
The positrons annihilate with free electrons to give $\text{e}^+ + \text{e}^- \rightarrow 2\gamma$

The energy production rate is : $\epsilon_{pp} \sim X^2 \cdot \rho \cdot T^4$ erg/g.sec.

The neutrinos carry off about 1% of the energy

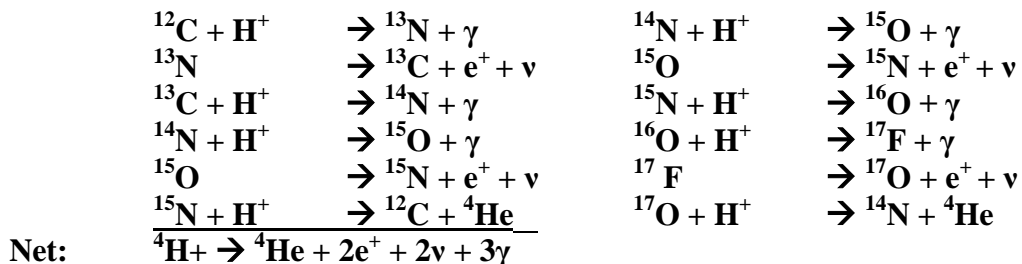
Q? Why is $\epsilon_{pp} \sim \rho^1$?? Why is $\epsilon_{pp} \sim X^2$??

There are actually 3 variations of the pp-chain, but pp1 is the most important one for stellar evolution. The net effect of all 3 reactions is the same.

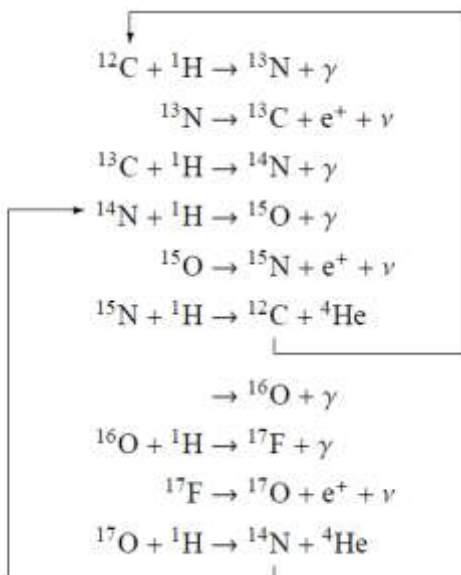


10.4.2 The CNO- cycles

At $T > 15$ MK, H is predominantly fused in CNO-cycles (or bi-cycle)



The positrons annihilate with free electrons to give $\text{e}^+ + \text{e}^- \rightarrow 2\gamma$
Q? What is the net reaction of these two cycles?



The energy production rate of the CNO-cycle is $\epsilon_{\text{CNO}} \sim X_{14} \cdot \rho \cdot T^{18}$ where X_{14} is the mass fraction of ${}^{14}\text{N}$.

Fig 10.4 shows production rates of the pp-chain and the CNO-cycle.

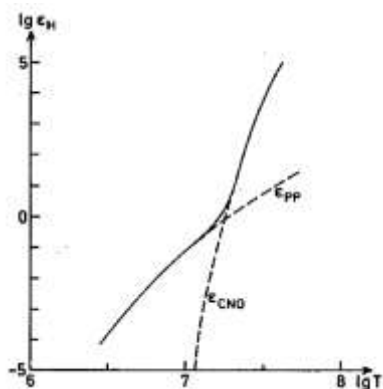


Fig 10.4 (Op Fig 6.5)
The energy production at density 1 g/cm^3 and composition $X=1.0$ and $X_{\text{CNO}}=0.01$. At $T \approx 1.5 \times 10^7 \text{ K}$ the contributions of the CNO-cycle and the pp-chain are about equal. In the Sun, at $T_c \approx 1.4 \times 10^7 \text{ K}$, pp $\sim 90\%$ and CNO $\sim 10\%$ of energy production.

In massive stars with $M \gtrsim 2 M_\odot$ the H-fusion goes mainly via the CNO-cycles.

- Q?** The energy production by the CNO-cycle has a much steeper dependence on T than the p-p-chain.
What does that imply for the extent and the mass of the region where H-fusion occurs in massive stars?

10.4.3 Equilibrium Abundances of the CNO-cycle

The CNO=cycle is a cyclic process that quickly reaches equilibrium.
This has two important consequences:

1. **The total number of C+N+O ions is conserved (CNO is just catalyst)**
2. **In equilibrium: all steps have to proceed at the same reaction rate (nr of reactions per gram per second).**

The rate , $r_{i \rightarrow j} \sim n_i \times \sigma_{i \rightarrow j}$, is the same for all steps.

However, some steps have smaller cross-section, so a higher number of those ions are needed to keep the rate the same as for other steps.

- Q?** Can you think of some consequences in terms of surface abundances of stars?

Define the **lifetime of a nucleus** in this process as

$$\tau(i) \equiv n_i / |dn_i/dt| = n_i / r_{ij} \quad \text{with } n_i \text{ in nr/gram}$$

and the reaction rate r_{ij} in nr/gram.s

All reaction rates are equal so $n_i/n_j = \tau_i/\tau_j$ etc.

At $T \simeq 2 \times 10^7$ K, the equilibrium of the reaction cycle implies

$$\begin{array}{ccccccc} \tau(^{15}N) & \ll & \tau(^{13}C) & < & \tau(^{12}C) & \ll & \tau(^{14}N) \\ 35 \text{ yr} & & 1600 \text{ yr} & & 6600 \text{ yr} & & 9 \times 10^5 \text{ yr} \\ & & & & & & \text{longest} \end{array} \ll \tau_{nuc} \quad \sim 10^9 \text{ yr}$$

In equilibrium: $n_i(^{14}N) / n_i(^{12}C) \simeq 140$

The initial ‘cosmic’ composition is $n(^{14}N) / n(^{12}C) \simeq 0.27$

So the $^{14}\text{N} / ^{12}\text{C}$ ratio increases drastically inside the star due to CNO-cycle.

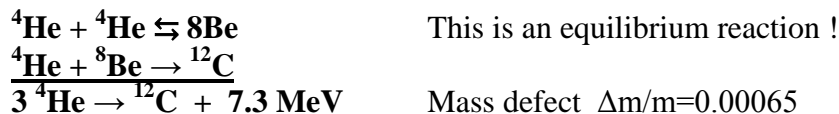
- Q?** How long does it take this cycle to reach equilibrium?

The two main abundance effects of $\text{H} \rightarrow \text{He}$ via CNO-cycle:

- H decreases and He increases
- ^{12}C decreases and ^{14}N increases

- Q?** Which one is faster?

10.5 He-fusion = Triple α reaction: at $T > 10^8$ K



The first reaction is an equilibrium reaction that results a very small fraction of Be ions. The mean lifetime of ${}^8\text{Be}$ ions is only 3×10^{-16} sec!

The second reaction is possible at $T \approx 10^8$ K because of a resonance in the He + Be reaction: the cross section as function of energy shows a peak.

This was predicted by Fred Hoyle in 1954 based on the cosmic abundance of C!

The energy production rate of 3α proces : $\epsilon_{3\alpha} \sim Y^3 \rho^2 T^{40}$!

- Q?** Why is $\epsilon_{3\alpha} \sim \rho^2$? Why is $\epsilon_{3\alpha} \sim Y^3$?
 What would the dependence be if $\text{He} + \text{He} \rightarrow \text{Be}$ was not an equilibrium reaction.
 Argue on the basis of Fig 10.3 and the table of isotopes that this is an equilibrium reaction.
- Q?** What is the consequence of the very high T-dependence of the energy production?
 What does it imply for the mass of the Helium-burning core compared to that of the H-burning core of a star with a given initial mass?
- Q?** Would you exist if the ${}^{12}\text{C}$ nucleus did not have a resonant energy level around 8 MeV? Explain.

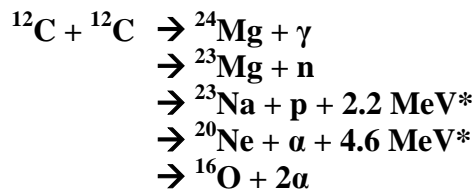
Towards the end of the He-fusion phase, when there is enough ${}^{12}\text{C}$, the following reaction occurs:



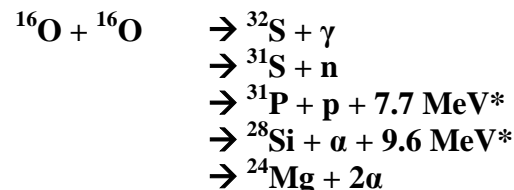
10.6 C and O-fusion

The C+C fusion and the O+O fusion process has several branches:

at $T > 6 \times 10^8$ K



at $T > 1 \times 10^9$ K



* These are the most probable reactions that are the major source of energy.

10.7 Si-fusion and photo-disintegration

Above $T \gtrsim 1.5 \times 10^9$ K heavy nuclei can be destroyed by photons. The average λ of photons (Wien's law) $\lambda \approx 0.4/T$ cm) is $\lambda \approx 3 \times 10^{-10}$ cm. The average energy of photons is : $hc/\lambda \approx 10^{-8}$ erg ≈ 0.4 MeV

This destruction of heavy nuclei creates mixture of massive nuclei, such as Mg, Si, P, S, plus p, n, α .

The net reaction is $^{28}\text{Si} + ^{28}\text{Si} \rightarrow ^{56}\text{Fe}$, but it goes in many steps, creating also many other elements and isotopes. Most of the energy in these reactions is lost in the form of neutrinos that leave the star.

The resulting equilibrium gives rise to the formation of Fe-group elements with stable nuclei: ^{56}Fe , ^{59}Co , ^{58}Ni
via e.g. $^{28}\text{Si}(\alpha,\gamma)$ $^{32}\text{S}(\alpha,\gamma)$ $^{36}\text{Ar}(\alpha,\gamma)$ $^{40}\text{Ca}(\alpha,\gamma)$ $^{44}\text{Ti}(\alpha,\gamma)$... ^{56}Ni

10.8 Summary of major reactions

Nuclear Fuel	Process	$T_{\text{threshold}}$ 10^6 K	Products	Energy per Nucleon (MeV)
H	$p-p$	~4	He	6.55
H	CNO	15	He	6.25
He	3α	100	C, O	0.61
C	C + C	600	O, Ne, Na, Mg	0.54
O	O + O	1000	Mg, S, P, Si	~0.3
Si	Nuc. eq.	3000	Co, Fe, Ni	<0.18

The reaction rates and energy production for stellar nucleosynthesis have been compiled by the Lawrence Livermore National Laboratory and can be found at <http://www-physics.llnl.gov/Research/RRSN>

10.9 Formation of Heavy Elements: slow (s) and rapid (r) neutron capture

The photo-disintegration in the Si-fusion phase creates a mixture of neutrons, ions (protons, He-ions, C-ions etc.) and massive ions (Fe, Co, Ni).

Because neutrons have no charge, they can penetrate (be captured by) ions, thus creating neutron-rich isotopes. The isotopes resulting from the bombardment by neutrons can be either stable or unstable isotopes. The net result depends on the neutron-flux, i.e. on the time between successive neutron captures by an ion.

10.9.1 Slow neutron capture in low mass stars (s-process)

If the neutron capture rate is relatively “slow”, a particle can capture neutrons until it forms an unstable isotope. This isotope will then suffer beta-decay ($n \rightarrow p + e^+$) until it reaches a stable isotope .

This process is shown in the figure below for a series of neutron captures, starting with a ^{56}Fe nucleus. The isotope ^{59}Fe is unstable and will decay to ^{59}Co . This ion can then start capturing neutrons again, until another unstable isotope is formed.

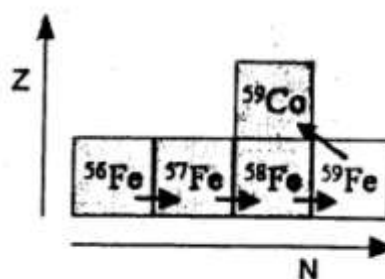


*Fig 10.5
The formation
of ^{59}Co by
slow neutron capture.*

In this way, a whole series of stable isotopes of heavy elements can be formed, depending on the stable isotope of the element that started the process.

**Typical elements formed by the s-process are: Zr, Sr, Ba, Pb.
Their enhanced abundance in stellar photospheres of certain AGB stars shows that these stars must have gone through a phase that produced a large neutron flux.**

10.9.2 Rapid neutron capture in Supernova (r-process)

If the neutron density is very high and the capture rate of the neutron is so high that the time between successive neutron captures is smaller than the typical decay time of unstable ions, the unstable isotopes have no time for beta-decay but keep capturing neutrons. In this way super-neutron-rich isotopes will be formed. When the neutron flux stops, e.g. because the matter is expelled in a supernova explosion, these neutron-rich isotopes will suffer a series of beta-decays, until a stable isotope is reached. These final stable isotopes are called r-process elements.

**Typical r-process elements are: Eu, Au, Xe, Pt.
They can only be formed in supernova explosions.**

Both processes are shown schematically in an isotope-diagram, which shows on the vertical axis the charge (Z) and on the horizontal axis the number of neutrons (N) of the isotopes.

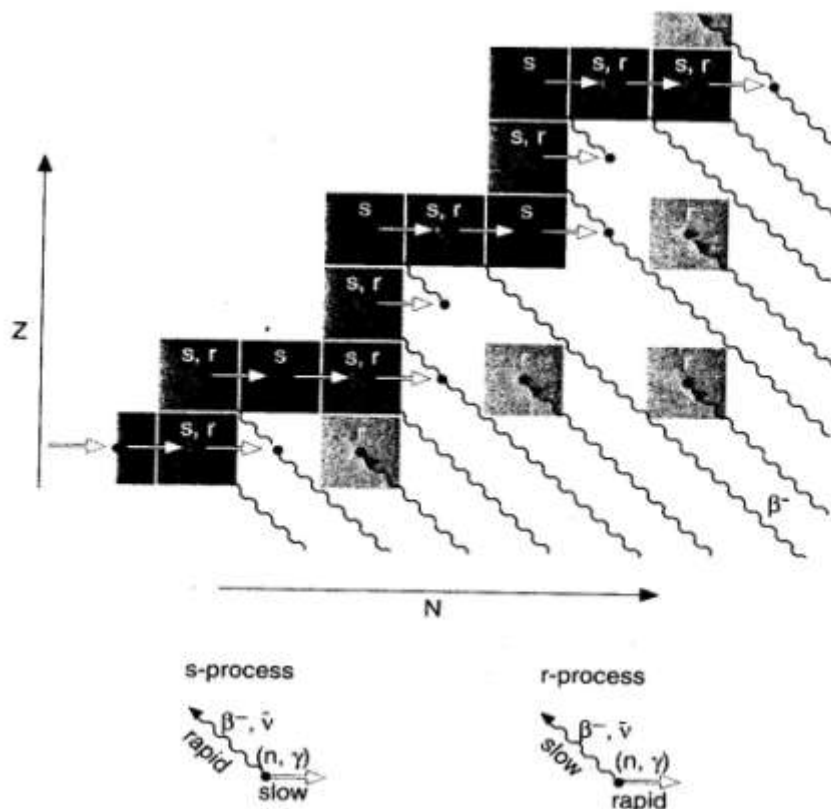


Fig 10.6 Schematic representation of the s and r process of neutron capture and the formation of neutron rich isotopes. The grey squares contain isotopes that can only be formed by the r-process.

Depending on the location of an isotope in this diagram, actually depending on the stability of its neighbours, stable isotope can be formed via the r-process, the s-process or both.

10.10 Consequences of fusion reactions for stellar evolution

1. Each successive reaction has a higher Coulomb barrier, due to a higher charge of the nuclei. So a higher T_c is needed → the core has to contract.

2. Each successive reaction has a steeper T-dependence. This implies that it will occur more concentrated in the core of the star, i.e. in a region that has less mass.
3. Each successive reaction has a smaller $\Delta m/m$, i.e. it produces less energy. So the reaction rate has to be higher and the fusion faster (more reactions per sec. gr) to provide luminosity L.
4. At $T > 10^9$ K the neutrinos carry away a larger and larger fraction of the energy. This also reduces the net energy production for the star and speeds up the evolution.

All these effects result in two significant factors concerning stellar evolution:

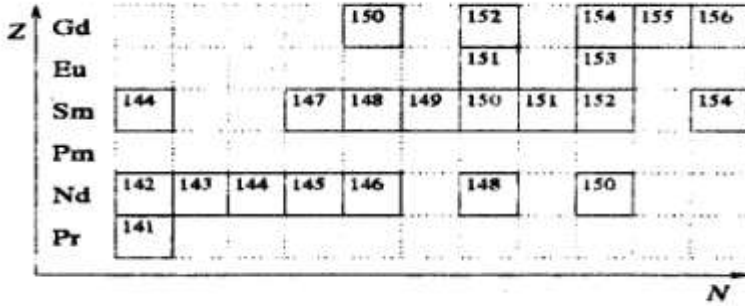
- A. Because the mass taking part in each successive fusion process is smaller than in the one before, the chemical evolution of the star will develop into an “onion-skin model”, with the most massive products (the latest) in the center surrounded by concentric layers of less massive elements.
 - B. The lifetime of the successive evolution phases will be shorter and shorter.
-

H10.2. Homework

The figure below shows a fraction of the isotope diagram of Pr (= Praesodymium) until Gd (= Gadolinium).

Stable isotopes are indicated by enclosed squares.

- a. Show the path of slow-neutron capture, starting at ^{141}Pr
- b. Show a number of paths of rapid neutron capture, starting at the same isotope.
- c. Which isotopes in this diagram can only be made by the r-process?
Give element and mass of isotopes.
- d. Which isotopes can be made only by the s-process?
- e. Which isotopes in this diagram can be made by both the r- and s-process?
- f. Which isotopes in this diagram cannot be made by either r- or s-process?



10.11 Minimum Core Mass for Ignition

Each reaction requires a minimum temperature to be ignited (see Table in 10.8).

The central temperature of a star can rise if the star (or rather “the core”) contracts. We have derived before (from HE and ideal gas law) that we can estimate the central temperature of a star as

$$T_c \simeq \frac{m_H \mu}{k} \cdot \frac{GM}{R}$$

In the case of a contracting core, that we are considering here, (e.g. after H-fusion) most of the central pressure is due to the mass of the core, as the layers outside the core have a much lower density and contribute little to the pressure. Therefore we can estimate the central temperature in this case as

$$T_c \simeq \frac{m_H \mu_c}{k} \cdot \frac{GM_c}{R_c} \quad \text{with} \quad R_c \simeq \left(\frac{M_c}{\rho_c} \right)^{1/3} \rightarrow T_c \approx \frac{m_H \mu_c}{k} \cdot GM_c^{2/3} \cdot \rho_c^{1/3}$$

$$\text{so } T_c \sim M_c^{2/3} \cdot \rho_c^{1/3}$$

So, when the core of a star with mass M_c contracts, its central temperature will increase with its central density as $T_c \sim \rho_c^{1/3}$

This might suggest that a star can create any high T_c by contracting to small enough radius. However this is not the case, because the star may become degenerate before it reaches the required ignition temperature T_i and then the contraction stops. (Degenerate stars do not contract, unless mass is added).

So: to reach the ignition temperature of the next fusion reaction, the star must avoid degeneracy.

The temperature limit for electron degeneracy depends on density: as $T \sim \rho_e^{2/3}$ (Sec. 5.5 : Fig 5.5 and Homework 5.1)

Degeneracy is prevented if $P_{\text{ideal gas}} > P_{\text{el. degen.}}$

$$\frac{\mathcal{R}}{\mu_c} \rho_c T_c > K'_1 \left(\frac{\rho_c}{\mu_e} \right)^{5/3} \rightarrow \boxed{T_c > \frac{K'_1}{\mathcal{R}} \left(\frac{\mu_c}{\mu_e} \right) \left(\frac{\rho_c}{\mu_e} \right)^{2/3}}$$

Q? Why does this equation contain both μ_c and μ_e ?

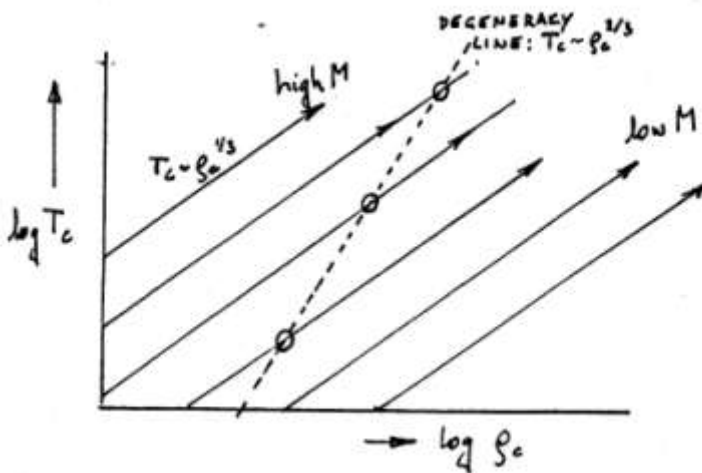


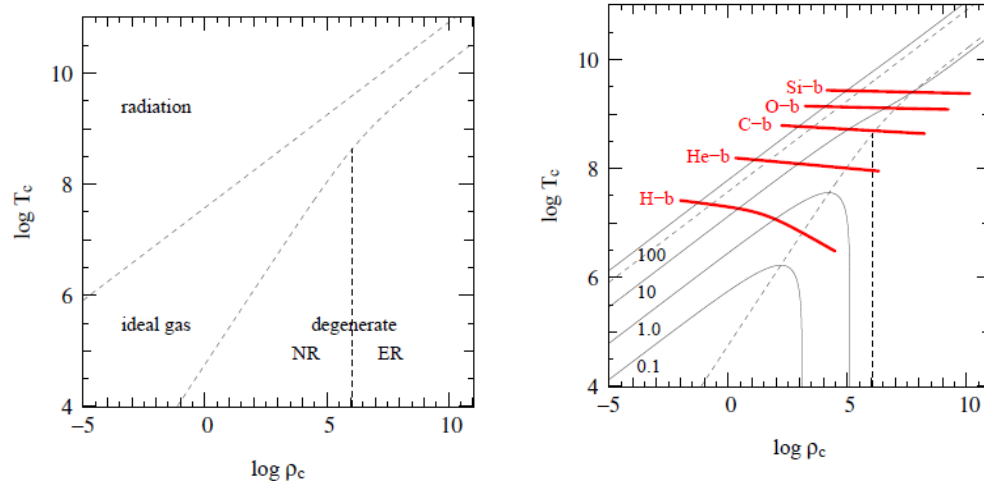
Fig 10.7
Schematic evolution of the central T_c and ρ_c of contracting cores of various masses. The contraction stops when the core becomes degenerate. This point is indicated by circles.

So: to avoid degeneracy before T_{ign} is reached, the star must have a **minimum mass**, (or rather a minimum mass of the contracting core).

Combining these equations, we find that the mass of a contracting core that reaches a temperature T_{ign} and avoid degeneracy must be higher than

$$\boxed{M_{\text{core}} > M_{\text{crit}} \approx \left\{ \frac{\mathfrak{R} K'_1}{\mu_c \mu_e^{5/3} G^2} \right\}^{3/4} \cdot T_{\text{ign}}^{3/4}}$$

Fig. 10.7. The systematic evolution tracks of stars of different mass in the $(\log \rho_c, \log T_c)$ -diagram. The left figure shows the regions of the different equations of state. The tilted thin lines in the right figure represent the evolution of the central parameters for stars of 0.1 to $100 M_\odot$. The thick nearly horizontal lines indicate the temperature and density range of the central fusion processes. (OP fig. 7.3)



Notice that stars of $0.1 M_\odot$ do not reach H-fusion, Stars of $1 M_\odot$ barely reach He-fusion. Stars of $M \geq 8 M_\odot$ reach all fusion phases.

Once the center of a star becomes degenerate, it can no longer contract, so the density reaches its upperlimit. Its density can increase a little bit, when the degenerate core becomes more massive due to fusion in the shell surrounding the degenerate core, as we will see later. (Degenerate stars decrease in size and increase in density when their mass increases.)

H 10.3 Homework

Suppose that the He-fusion requires a minimum core mass of about $0.3 M_{\text{sun}}$. What would be the minimum core mass for the next fusion phases ? (see Sec 10.8)

11. Calculating Stellar Structure and Evolution

11.1 Assumptions

- 1. Star is spherically symmetric**
 - Physical quantities vary only in radial direction: $P(r)$, $\rho(r)$, $T(r)$, etc.
 - Ignore effects of rotation and \vec{B} fields? When is this allowed?
- 2. Star is in hydrostatic equilibrium**
 - When is this assumption justified, timescale?
- 3. Energy sources are**
 - Gravitational energy
 - Thermonuclear energy
 - Internal (thermal) energy (important for white dwarfs)
- 4. Energy transport mechanisms**
 - Radiation
 - Convection
 - Conduction (white dwarfs)
- 5. Chemical composition**
 - Newly formed stars have homogenous composition
 - Assume initial composition (from surface spectrum)
 - X = Mass fraction of H
 - Y = Mass fraction of He
 - Z = Rest, mainly C, N, O
 - Follow composition changes through the star as function of time

H11.1. Homework

Stellar Rotation

- Calculate the rotation speed of a star for which the centrifugal force would reduce gravity at equator by 30% and 80%
- Compare these values with the observed mean rotation velocities
- Do this for the following stars:
 - a. Mainsequence star like sun
 - b. AGB Star
 - c. Mainsequence O-star
 - d. White dwarf

11.2 Equations of Stellar Structure (OP 6)

	in r Euler coordinates	in m = M(r) Lagrange coordinates
Mass continuity	$\frac{dm}{dr} = 4\pi r^2 \rho$	$\frac{dr}{dm} = \frac{1}{4\pi r^2 \rho}$
Hydrost equilibrium	$\frac{dP}{dr} = -\frac{Gm\rho}{r^2}$	$\frac{dP}{dm} = -\frac{Gm}{4\pi r^4}$
Energy generation*	$\frac{dL}{dr} = 4\pi r^2 \rho (\epsilon - \epsilon_v - \frac{Tds}{dt})$	$\frac{dL}{dm} = \epsilon - \epsilon_v - \frac{Tds}{dt}$
Energy transport by radiation or by convection	$\frac{dT}{dr} = -\frac{3}{4ac} \cdot \frac{\kappa \rho}{T^3} \frac{L}{4\pi r^2}$ $\frac{dT}{dr} = \frac{\gamma_{ad}-1}{\gamma_{ad}} \cdot \frac{T}{P} \cdot \frac{dP}{dr}$	$\frac{dT}{dm} = -\frac{3}{4ac} \cdot \frac{\kappa}{T^3} \frac{L}{(4\pi r^2)^2}$ $\frac{dT}{dm} = \frac{\gamma_{ad}-1}{\gamma_{ad}} \cdot \frac{T}{P} \cdot \frac{dP}{dm}$

Equation of state	$P = P_{\text{gas}} + P_{\text{rad}} = P_{\text{rad}} + P_e + P_i$	
	$P_{\text{rad}} = \frac{a}{3} T^4$	
	$P_e = \rho \mathcal{R} T / \mu_e$	or $K_1' (\rho / \mu_e)^{5/3}$ (electr. degen.)
	$P_i = \rho \mathcal{R} T / \mu_i$	
Absorption coefficient	$\kappa = \kappa_{\text{ff}} + \kappa_{\text{bf}} + \kappa_e$	$\kappa_{\text{ff}} + \kappa_{\text{bf}} \sim \rho T^{-7/2}$
		$\kappa_e \sim \rho / \mu_e \sim 1 + X$
Nuclear energy production	$\epsilon \sim \epsilon_0 \rho^m T^n$ ϵ_0, m, n depend on the reaction The term $-\epsilon_v$ in the energy generation describes the loss of energy by escaping neutrinos	
Composition	$X(m), Y(m), Z(m)$ or $X_i(m)$ with $i = 1 \dots$ all isotopes	

* The entropy term $-Tds/dt$ expresses the energy generated by contraction ($-Tds/dt > 0$) or lost by expansion ($-Tds/dt < 0$) with $Tds \equiv du - \frac{P}{\rho} d\rho$.

If $Tds/dt = 0$, the star is in **thermal equilibrium**.

Remarks and questions

These structure equations describe either
 T, P, L, ρ, m as function of r (Euler)
 or
 T, P, L, m, r as function of m (Lagrange)

The Lagrangian equations can be derived from the Euler equations by using
 $\frac{dx}{dm} = \frac{dx}{dr} \cdot \frac{dr}{dm}$ with $\frac{dr}{dm} = \frac{1}{4\pi\rho r^2}$

- Q?** Why is it more practical to use m as the free parameter than r ?
- Q?** How do we know which one of the two energy transport equations to use?
- The term $-T \frac{ds}{dt}$ in the equation of energy generation allows for the gain or loss of energy when a layer respectively contracts or expands on a Kelvin-Helmholtz timescale.
- Q?** How can we calculate this term, considering that we are calculating models in hydrostatic equilibrium?
- The calculation of an evolutionary track consists of the calculation of a series of subsequent hydrostatic equilibrium (!) models, each with the chemical structure, calculated by using the reaction rates of the previous model and extrapolating it a certain time-step.
- Q?** Which timesteps would you use?

11.3 Boundary Conditions

Four boundary conditions are needed for the 4 differential equations as $f(m)$.

$$r(m=0) = 0$$

$$L(m=0) = 0$$

$$P(m=M_*) = 0 \rightarrow \text{actually, this defines } R_* (!)$$

$$T(m=M_*) = \{L(M_*)/4\pi\sigma r^2(m=M_*)\}^{1/4}$$

or a better approximation if you fit an atmospheric model for the outer layers.

The problem is:

There are two boundary conditions at $r=0$ and two conditions at $r=R_*$
 So you cannot simply start integrating from the inside out or outside in.

11.4 Solving the structure equations

The Henyey method: (see SC 3.2, p. 90-97)

Introduce the general parameter y^i with $i=1$ to 4, and define the parameters $y^1 = r$, $y^2 = P$, $y^3 = L$, $y^4 = T$

Divide the star in a large number (N) of spherical shells with radii r_j with $j=1$ to N . Each parameter is at any radius is described by y^i_j

For each shell with radius between r_j and r_{j+1} the differential equations that describe the stellar structure in Lagrangian coordinates can be written as

$$\frac{dy^i}{dm_j} = \frac{y^i_{j+1} - y^i_j}{m_{j+1} - m_j} = f(y^1_{j+0.5}, y^2_{j+0.5}, y^3_{j+0.5}, y^4_{j+0.5})$$

where f describes the dependence of the derivatives on the local parameters at mass $j+1/2$. This results in a set of equations of the type

$$E_j^i \equiv \frac{y^i_{j+1} - y^i_j}{m_{j+1} - m_j} - f(y^1_{j+0.5}, y^2_{j+0.5}, y^3_{j+0.5}, y^4_{j+0.5}) = 0$$

Suppose that a good first order model is available, then the equations of the next step can be written as a small correction to the first model. For instance in Lagrange coordinates (with parameters r , P , L and T as function of m) the value of T in the next iteration ($T_2 = T_1 + \Delta T$) at a given value of m can be written as a correction

$$\Delta T = (dT/dr)\Delta r + (dT/dP)\Delta P + (dT/dL)\Delta L$$

with all the terms dT/dP etc. given by the partial derivatives of the right hand side of the structure equations. For instance, $dT/dP = \mu m_H / k\rho$, if radiation pressure can be ignored. The equation can also be written as

$$\Delta T - (dT/dr)\Delta r + (dT/dP)\Delta P + (dT/dL)\Delta L = 0$$

and similar expressions for the other parameters. A model agrees with the four structure differential equations at all values of m if **all** differences Δ are zero, i.e. at all values of m (=throughout the star) and for all parameters (r, P, L, T). This set of linear equations can therefore be written as a large matrix that can be solved with standard mathematical techniques.

The solution of these equations then give the values of y^i_j , which are the radii, temperature, pressure and luminosity as function of m . With these values, calculate the nuclear processes in each layer per second of time. Take a time step Δt and predict the abundances in each layer at time $t+\Delta t$. These new abundances result in changes of the value of the function f at each layer, that contain e.g. the opacity and reaction rates. Start the process over again and calculate an equilibrium model at the next time step. Etc. Etc.

Q? What time steps would you use?

11.5 Structure of Polytropic Stars : $P = K\rho^\gamma$

In this case, the temperature does not enter at all into the equations and there are analytical solutions for certain values of γ .

HE:

$$\left. \begin{aligned} \frac{r^2}{\rho} \frac{dP}{dr} &= -Gm \rightarrow \frac{d}{dr} \left(\frac{r^2}{\rho} \frac{dP}{dr} \right) = -G \cdot \frac{dm}{dr} \\ \frac{dm}{dr} &= 4\pi r^2 \rho \end{aligned} \right\} \frac{1}{r^2} \frac{d}{dr} \left(\frac{r^2}{\rho} \frac{dP}{dr} \right) = -4\pi G \rho$$

(NB: $m = M(r)$ here)

Now use polytrope relation $P = K\rho^\gamma \rightarrow dP/dr = K\gamma\rho^{\gamma-1}d\rho/dr$ which gives

$$\frac{1}{r^2} \frac{d}{dr} \left(r^2 K \gamma \rho^{\gamma-2} \frac{d\rho}{dr} \right) = -4\pi G \rho \rightarrow \frac{K\gamma}{4\pi G} \cdot \frac{1}{r^2} \frac{d}{dr} \left(r^2 \rho^{\gamma-2} \frac{d\rho}{dr} \right) = -\rho$$

Two practical substitutions:

- a. $\gamma = 1 + 1/n \rightarrow n = 1/(\gamma - 1)$
- b. $\rho = \rho_c \theta^n$ θ is dimensionless

Gives

$$\boxed{\left[\frac{(n+1)K}{4\pi G \rho_c^{(n-1)/n}} \right] \frac{1}{r^2} \frac{d}{dr} \left(r^2 \frac{d\theta}{dr} \right) = -\theta^n} \rightarrow \theta(r)$$

The term in square brackets = $\alpha^2 = \text{constant}$ α in cm!!

Q? Although θ is dimensionless, can you think of what it may describe in physical terms?
 Hint: $\rho \sim \theta^n \rightarrow \theta \sim \rho^{1/n}$

Q? What does an $n = 0 \rightarrow \gamma = \infty$ model describe (in physical terms)?
 $n = \infty \rightarrow \gamma = 1$

Q? What is the range of θ ?

For mathematical reasons (to make the equation look nicer), define $r = \alpha\xi$ with ξ = dimensionless, α in cm

$$\text{Then } \boxed{\frac{1}{\xi^2} \cdot \frac{d}{d\xi} \left(\xi^2 \frac{d\theta}{d\xi} \right) = -\theta^n} \rightarrow \theta = f(n, \xi)$$

This is the **Lane-Emden equation** that describes the structure of polytropic stars.

This equation describes the run of density, $\rho(r)$ in a dimensionless form, with only one parameter: $n = 1/(\gamma - 1)$. There are analytical solutions for $n = 0, n = 1$. For any other value of n the equation can easily be solved by numerically by computer.

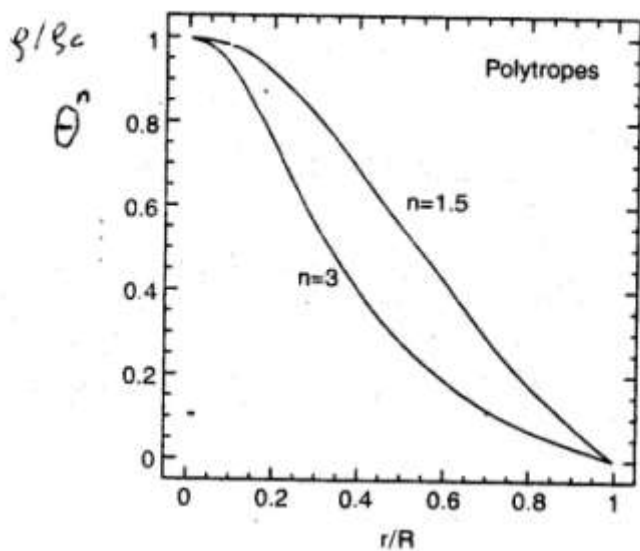


*Fig 11.1
The density structure
of two polytrope
models.
 $n=3 \rightarrow \gamma = 4/3$
and
 $n=1.5 \rightarrow \gamma = 5/3$.*

Polytropic models were historically important because they could be calculated (by hand and analytically) before the age of computers. Eddington (~1929) calculated the first polytropic model, assuming $\gamma = 4/3$, for the Sun and obtained the Mass-Luminosity relation for stars: $L \sim \frac{\mu^4}{K} \cdot M^3$

H11.2 Homework

- a. Explain to what types of stars do the polytrope models of $n=1.5$ and $n=3$ correspond to?
- b. Explain in simple physical terms why a star with $\gamma = 4/3$ has a more concentrated density structure than a star with $\gamma = 5/3$.

12 Star formation

12.1 The ISM

The interstellar medium consists of gas in different phases.

Component	T(K)	n (cm ⁻³)	nT
Molecular clouds	10 – 20	10 ³ - 10 ⁶	10 ⁴ - 10 ⁷
Cold neutral gas	50 – 100	20 – 50	10 ³ - 10 ⁴
Warm neutral gas	10 ³ - 10 ⁴	0.2 - 0.5	10 ³
Warm ionized gas	10 ⁴	0.1 – 1	10 ³ - 10 ⁴
Hot gas	10 ⁶ – 10 ⁷	10 ⁻² - 10 ⁻⁴	10 ³ - 10 ⁴

The mean value of the pressure factor (nT) in the galactic disk is
 $nT \approx 3 \cdot 10^3 \text{ K.nr/cm}^3$

In most cases these components are in pressure equilibrium.

- Q? Give examples of cases where the ISM is not in pressure equilibrium and explain why that is.

12.2 The Jeans mass for gravitational contraction

Let us consider a spherical homogeneous cloud of mass M and radius R with temperature T and density ρ .

If the cloud is in hydrostatic equilibrium, i.e. neither expanding nor contracting, the virial theorem applies : $E_{\text{kin}} = -1/2 E_{\text{pot}}$ with

$$E_{\text{kin}} = (3/2) kT (M / \mu m_H)$$

and

$$E_{\text{pot}} = - \int_0^M \frac{Gm_r}{r} dm_r = - \frac{3}{5} \frac{GM^2}{R}$$

where we used $r = (m_r/M)^{1/3}$ for a constant density medium. Check this! If $-1/2 E_{\text{pot}} > E_{\text{kin}}$ then gravity wins from the gas pressure and the cloud will contract. This is the case if

$$M > M_J \equiv \frac{5kT}{\mu m_H} \cdot \frac{R}{G}$$

where M_J is the **Jeans mass**

Substitution of

$$R = \left(\frac{3}{4\pi\mu m_H} \right)^{1/3} \left(\frac{M}{n} \right)^{1/3}$$

yields

$$M_J = \left(\frac{3}{4\pi} \right)^{1/2} \left(\frac{5k}{G m_H^{4/3}} \right)^{3/2} \left(\frac{T^3}{\mu^4 n} \right)^{1/2}$$

So

$$M_J \approx 100 \left(\frac{T^3}{\mu^4 n} \right)^{1/2} M_\odot$$

The higher the temperature, the larger M_J , so the more massive a cloud should be in order to collapse. That is why the clouds that contracted in the early Universe must have been very massive. These formed the proto-globular clusters.

- Q?** What is the typical Jeans mass of a cloud of neutral hydrogen with a density of $n = 1 \text{ cm}^{-3}$ and $T = 10^3 \text{ K}$?

H12.1 Homework

- a. Assume that the different components of the ISM are in pressure equilibrium. What would be the Jeans mass of clouds forming out of
 - 1. cold neutral gas
 - 2. warm neutral gas
 - 3. warm ionized gas
- b. How is it possible that molecular clouds are not in pressure equilibrium with their surroundings?
- c. Giant molecular clouds have masses of order $10^5 M_\odot$. Show that they are forming stars.

12.3 The collapse of molecular clouds

When a cloud has a mass higher than the Jeans mass it will collapse. This will occur approximately on a free-fall timescale.

$$t_{ff} \approx (G\rho)^{-\frac{1}{2}} \approx 1.10^8 (\mu n)^{-\frac{1}{2}} \text{ yr}$$

If clouds did not have a cooling mechanism, they would contract adiabatically with temperature increasing as $T \sim \rho^{2/3}$. Because the Jeans mass is $M_J \sim (T^3/\rho)^{1/2}$, its value would increase as the density increases. At some point the Jeans mass would reach the cloud mass: i.e. the cloud would be in virial equilibrium. At this moment the cloud would be in hydrostatic equilibrium and the contraction would stop.

Fortunately, however, clouds do have a cooling mechanism. (If not: star formation would be extremely inefficient and we would not exist!)

Clouds cool by radiative losses. For this to be effective it has to emit IR photons, because the clouds are optically thick for UV and visual photons. The main cooling agents in molecular clouds are: emission by molecules and emission by dust.

Cooling by molecules

Collisions between molecules in high density gas results in collisional excitation to higher rotation or vibration levels. An excited molecule can fall back to a lower rotation or vibration level by emission of a photon (photo de-excitation). The dominant transitions are in the IR or sub-mm range, and these photons can leave the clouds because the cloud is optically thin at IR wavelengths. So the net effect is: kinetic energy of molecules is transferred into excitation which results via photo de-excitation in IR and sub-mm photons which escape. This is a cooling mechanism.

Cooling by dust

If the density in a cloud is high and the kinetic temperature is low enough ($T < 1200$ K) dust may form. Collisions with molecules and dust absorption of trapped photons (UV, optical or near-IR) heat dust grains. Dust grains emit almost like blackbodies with a radiation temperature less than ~ 1000 K. This results in a large IR flux that leaves the cloud. Therefore molecular clouds are very strong IR emitters. So the net effect is: kinetic energy of molecules and optical radiation is converted into IR radiation that leaves the cloud. This is a cooling mechanism.

These cooling mechanisms prevent the adiabatic heating of a cloud when it collapses. The potential energy gained by the contractions is immediately emitted, and so the collapse proceeds approximately isothermally. The increasing density of isothermal clouds implies that the Jeans mass decreases, and substructures of the cloud can start to contract. This results in a **fragmentation of the original cloud** that splits up into fragments that may split up again. This fragmentation continues on a faster and faster timescale, because the free-fall timescale decreases as $\sim n^{-1/2}$ as the fragments get denser. Eventually the density in the clumps will become so high that they become optically thick for IR radiation. When that happens, the cooling mechanism is switched off and the collapse continues adiabatically. This results in a *T*-rise and subsequent increase of the Jeans mass to the actual mass of the clump. At this point the fragment reaches hydrostatic equilibrium. Observers call these fragments **clumps**.

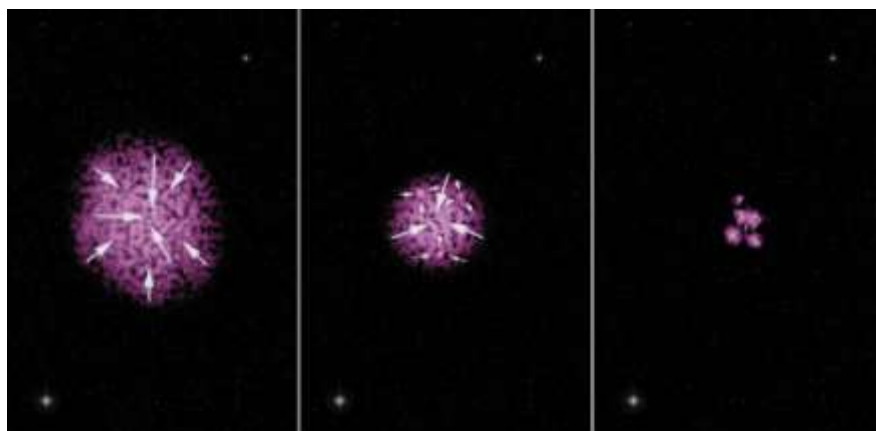


Fig. 12.1 Schematic figure of the fragmentation of a collapsing molecular cloud. As the cloud contracts almost isothermally, the Jeans mass decreases and fragments of the cloud start to contract, giving rise to a clumpy structure of the cloud. The clumps evolve into stars.

The mass distribution of the clumps sets the initial mass function (IMF) of the resulting stars. Observations show that the IMF of the clumps has the same shape as the IMF of the stars except from a constant ratio. So not all the mass of a clump ends up in the star. (The stellar IMF will be discussed in Sect. 12.8)

12.4 The end of the free-fall phase.

At the end of the free-fall collapse, the center of a clump reaches equilibrium first, while the surrounding gas keeps falling onto the core. From now on it is a proto-star. Up to this point the temperature is so low and the density so high that hydrogen is in H₂ molecules. The energy gained by the contraction is used for the dissociation and later the ionization of H and He. So the proto-star still has a cooling mechanism, which accelerates the contraction.

We can estimate the size of the clump when all H_2 is dissociated, and H and He are both ionized by comparing the energy gained in the contraction with that needed for the dissociation and ionization.

The energy needed for dissociation of an H_2 molecule is $x_{\text{H}_2} = 4.5 \text{ eV}$, and the ionization energy of an H atom is $x_H = 13.6 \text{ eV}$, with $1 \text{ eV} = 1.602 \cdot 10^{-12} \text{ ergs}$. The total energy needed for dissociation and ionization of a cloud consisting of H_2 molecules with composition $X = 0.7$ and $Y = 0.30$ is

$$E_{\text{dis}} = \frac{M}{m_H} \left\{ \frac{X}{2} x_{\text{H}_2} + X x_H \right\} = 1.3 \cdot 10^{58} \left(\frac{M}{M_\odot} \right) \text{ eV} \approx 2 \cdot 10^{46} \frac{M}{M_\odot} \text{ ergs}$$

This energy is provided by the contraction in the form of potential energy

$$\Delta E_{\text{pot}} \approx A G M^2 \left\{ \frac{1}{R_{\text{end}}} - \frac{1}{R_{\text{begin}}} \right\} \approx A \frac{G M^2}{R_{\text{end}}} \approx 4 \cdot 10^{48} A \frac{(M/M_\odot)^2}{R_{\text{end}}/R_\odot}$$

The constant $A = 3/5$ for a constant density cloud (see Sect 12.2). During the collapse the proto-star will become centrally concentrated. So the factor $A=3/5$ is a lower limit. Let us assume for simplicity that it is about a factor ≈ 3 larger, so $A \approx 2$.

Although the collapsing cloud loses most of the gained energy in the form of far-IR photons, a fraction f of ΔE_{pot} is used for dissociation and ionization. Detailed calculations show that $f \approx 1/3$.

Equating the energy needed for dissociation and ionization E_{dis} with $f \Delta E_{\text{pot}}$ we find that the proto-star is ionized when it reaches a radius of order

$$R/R_\odot \approx 100 M/M_\odot$$

We see that a proto-star of $1 M_\odot$ has a radius of $\sim 100 R_\odot$ at the end of the fast contraction and a star of $0.5 M_\odot$ has a radius of $\sim 50 R_\odot$. The effective temperature of the stars is $\sim 3000 \text{ K}$ so the luminosities are $\sim 10^3$ and $\sim 2 \cdot 10^2 L_\odot$ respectively.

We can estimate the mean temperature inside the star by applying the virial theorem (because at the end of the collapse the star reaches H.E.)

$$\frac{3}{2} \frac{M}{\mu m_H} kT = \frac{A}{2} \frac{GM^2}{R} \rightarrow \bar{T} \approx \frac{A}{3} \frac{\mu m_H}{k} \cdot \frac{GM}{R}$$

with $M/R \approx (\frac{1}{100}) M_\odot/R_\odot$ and $\mu \approx 1/2$. This gives $\bar{T} \approx 7 \cdot 10^4 \text{ K}$. So fusion has not started yet.

The mean density of a protostar $1 M_\odot$ and $100 R_\odot$ is $\rho \approx 10^{-6} \text{ g/cm}^3$. At such low T and density, the absorption coefficient is very high. See Fig 6.1. This means that the energy transport by radiation would be very inefficient and would require a high value of $|dT/dr|_{\text{rad}}$ (Sect 7.1). So the star is almost completely convective according to the Schwarzschild criterium.

So at the end of the fast contraction, when the star is ionized, it will be in hydrostatic equilibrium and fully convective.

12.5 The contraction of a convective proto-star: the descent along the Hayashi track

When the dissociation and ionization of the star is complete, the star is in hydrostatic equilibrium. The star does not have nuclear fusion yet, but it has a temperature gradient and so it radiates. The star must contract to cover this energy loss.

At this phase the star is fully convective. We will show later (Section 15.5) that fully convective stars occupy a rather narrow vertical strip in the HRD at $T_{\text{eff}} \approx 3000 \text{ K}$. This is called the **Hayashi-line**. Fully convective stars will evolve almost vertically upward along the Hayashi line if they expand, because $L \sim T_{\text{eff}}^4 R^2$ with $T_{\text{eff}} \approx \text{constant}$, or downward if they contract. Proto-stars are contracting, so their luminosity decreases. This part of their evolution path in the HRD is called the **Hayashi track**.

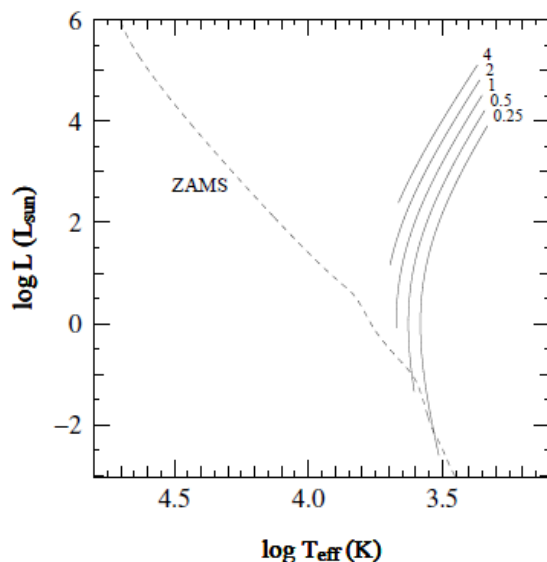


Figure 12.2:
Hayashi tracks for proto-stars of $0.25 < M/M_\odot < 4$ for $X=0.70$, $Y=0.28$ and $Z=0.02$. Notice that the lines are approximately vertical, at $T_{\text{eff}} \approx 3000 \text{ K}$, but not exactly. At $L \gtrsim 10L_\odot$ T_{eff} decreases somewhat towards higher luminosity. (OP Fig 9.3)

As the star contracts, its gas temperature and density increases. This results in a drastic decrease of κ and so the core of the star is no longer convective, but its

energy transport goes by radiation. The star has developed a radiative core and does no longer evolve downward on the Hayashi track.

We can estimate the radius of the proto-star at the end of the Hayashi track by assuming that the mean gas temperature should be of order a few 10^6 K, say $3 \cdot 10^6$ K, to be in the range of $\kappa \approx \sigma_e \approx 0.3 \text{ cm}^2/\text{g}$ (see Fig 6.1). Using the estimate of the mean temperature that we derived above, we see that this happens when the radius of the star has decreased by a factor $\frac{3 \cdot 10^6}{7 \cdot 10^4} \approx 50$. So the radius of a $1 M_\odot$ proto-star has gone down from $\sim 100 R_\odot$ to ~ 2.0 . At this time the luminosity is $L = 4\pi r^2 T_{\text{eff}}^4 \sim 0.5 L_\odot$ for a $1 M_\odot$ proto-star. We can use this value to estimate the duration that the star needed for descending the Hayashi track. Because the star is contracting in hydrostatic equilibrium the timescale for contraction is given by

$$t_{\text{Hayashi}} \approx \frac{-\Delta E_{\text{pot}}}{L} = \frac{AGM^2}{\bar{L}R_{\text{end}}}$$

Because the luminosity decreases drastically during the descent along the Hayashi track, we can take the logarithmic mean luminosity between the top and the bottom of the Hayashi track for \bar{L} , assuming a constant T_{eff} so $L \sim R^2$

$$\bar{L} \equiv 4\pi\sigma T_{\text{eff}}^4 R^2 \cong 15 L_\odot \quad \text{if} \quad R \cong (R_{\text{top}} \cdot R_{\text{bottom}})^{\frac{1}{2}} \approx 15 R_\odot$$

This gives $t_{\text{Hayashi}} \approx 2 \cdot 10^6$ yrs for a $1 M_\odot$ protostar.

So the descent along the Hayashi track of a proto-star of $1 M_\odot$ takes about 2 million years, and $t_{\text{Hayashi}} \sim M^{-1}$.

At the end of the Hayashi phase the star is no longer fully convective, but it is goes into radiative equilibrium.

12.6 The contraction of a radiative pre-main sequence star: from the Hayashi track to the main sequence.

The proto-star in radiative equilibrium has not yet started nuclear fusion yet, so it will keep contracting to cover the loss of energy by radiation. However, because it is mostly in radiative equilibrium and hydrostatic equilibrium, it will roughly obey the mass luminosity relation. This means that the evolution track is now approximately horizontal. The star moves to the main sequence. This phase is called **the pre-main sequence phase**.

During this PMS contraction the convective region shrinks from inside out. At the end of the Hayashi phase it was still mostly convective, but when it reaches

the MS the massive stars have no more outer convection zone, whereas the stars less than about $1 M_{\text{sun}}$ still have an outer convection zone on the MS.

During the pre-main sequence contraction, the star keeps approximately the same luminosity as it had at the end of the Hayashi contraction phase.

We can estimate the duration of this PMS contraction phase because we know the radius that the star has when it reaches the main sequence.

At the end of the contraction phase, when H-fusion starts on the main sequence, the radius is approximately the main sequence radius. We will show later that the radius on the MS is

$$R_{\text{MS}}/R_{\odot} \approx (M/M_{\odot})^{0.7}$$

Substituting this into the expression for t_{PMS} we find

$$t_{\text{PMS}} \approx A \frac{GM_{\odot}^2}{R_{\odot}L_{\odot}} \cdot (M/M_{\odot})^2 (R/R_{\odot})^{-1} (L/L_{\odot})^{-1} \approx 6 \times 10^7 (M/M_{\odot})^{-2.5} \text{ yrs}$$

where we used $A \approx 2$, $L \sim M^{3.8}$ and $R \sim M^{0.7}$.

This results in the following estimates

M_{\odot}	t_{PMS} (estimated)	t_{PMS} (model)
0.2	$3 \cdot 10^9$	$7.3 \cdot 10^8$
0.5	$3 \cdot 10^8$	$2.1 \cdot 10^8$
1	$6 \cdot 10^7$	$6.2 \cdot 10^7$
2	$1 \cdot 10^7$	$2.9 \cdot 10^6$
4	$2 \cdot 10^6$	$0.5 \cdot 10^6$

Notice that the simple estimate gives about the correct time except for the lowest mass PMS. Notice also that these time scales are considerably longer than the duration of the contraction on the Hayashi track.

Q? Why is the phase of the Hayashi track much shorter than the PMS phase?

Q? Which effects could be responsible for the deviation between estimated and calculated lifetimes? (Hint: see Fig 12.3)

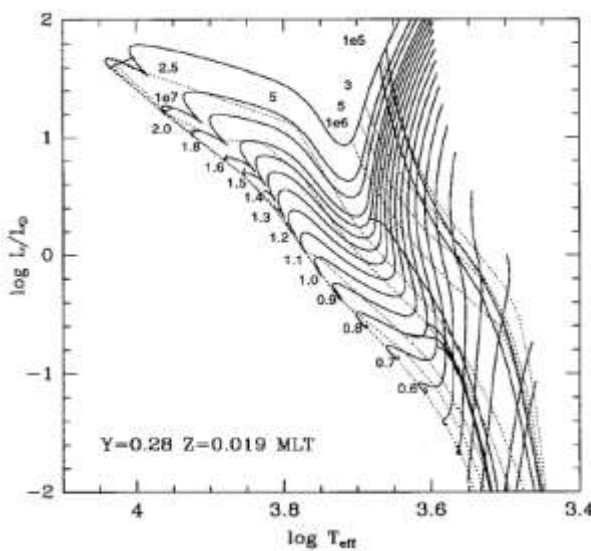


Figure 12.3
Calculated PMS tracks for stars in the range of 0.3 to $2.5 M_{\odot}$. The dotted lines are isochrones of 10^5 , $3 \cdot 10^5$, $5 \cdot 10^5$, 10^6 , $5 \cdot 10^6$ and 10^7 yrs. The vertical lines near the 10^5 yr isochrones indicate the region of the D-destruction. The lines near the 10^6 yr isochrones, indicates the region of Li-destruction. (OP Fig 8.4)

Notice that the PMS lifetime decreases toward increasing mass. This implies that in an HR-diagram or colour-magnitude diagram of a very young cluster, the more massive stars are already on the MS whereas the lower mass stars are still on the PMS contraction tracks.

Low mass stars ($M \leq 2 M_{\odot}$) on the radiative contraction phase are called **T Tauri stars**: pre-main sequence stars of types F,G,K with strong emission lines formed in an accretion disk around these stars.

Higher mass stars ($M \geq 2 M_{\odot}$) on the radiative contraction phase are called **Herbig Ae-Be stars**: pre-main sequence stars of types A and B with strong emission lines formed in an accretion disk around these stars

Figure 12.3 shows that PMS contraction track is not exactly horizontal in the HRD but that L increases, by about a factor 3. Part of this is due to the decrease of κ as the star contracts and gets hotter ($L \sim M^3/\kappa$) and part is due to the continuous increase of the mass via the accretion disk.

The tracks also show that a star that enters the MS and starts H-fusion will adjust its radius, luminosity and T_{eff} slightly. This produces the little curl at the end of the PMS tracks.

Fig 12.4 : Different phases of T Tauri stars (OP fig 9.2, after Maeder)

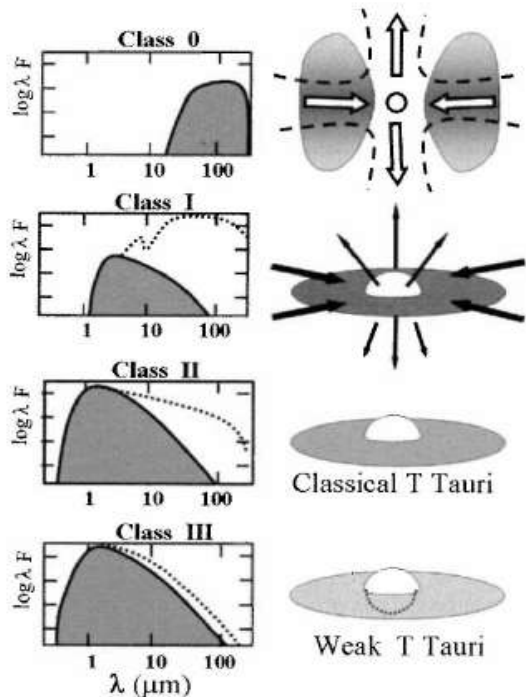
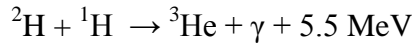


Figure 9.2. Schematic illustration of four stages in the evolution of protostars and their circumstellar disks. On the left, the stellar flux is depicted (shaded area) and the contribution from the disk (dotted line). On the right the corresponding geometry of the object is shown.

Class 0 objects are very young protostars ($\lesssim 10^4$ yrs) with almost spherical accretion at a high rate, emitting in the far-IR and sub-mm range. Class I protostars correspond to an advanced stage of accretion (age $\sim 10^5$ yrs), where the star is still embedded in a massive accretion disk, while jets or bipolar outflows are also observed. In class II the protostar has become visible as a classical T Tauri star on the pre-main sequence (age $\sim 10^6$ yrs), while the accretion disk is still optically thick giving rise to a large IR excess. Class III stars are already close to the main sequence (age $\sim 10^7$ yrs), with an optically thin accretion disk and weak emission lines. Figure from MAEDER.

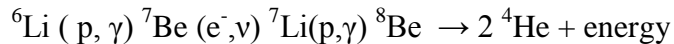
12.7 The destruction of Lithium and Deuterium

At temperature of about 10^6 K, the small fraction of initial Deuterium (formed in the Big Bang) is destroyed by the reaction



This occurs when the stars is approximately on the 10^5 yr isochrone.

Some time later, at a core temperature of about $2.5 \cdot 10^6$ K, i.e. when the star is near the 10^6 yr isochrone, Li is destroyed by the reaction chain



The stellar surface abundance of Li and D provides an important diagnostic tool for studying the formation of low mass stars. This is because Li is only depleted at the stellar surface if the convection was deep enough to include the Li-destruction zone. Figure 12.3 shows that this is only the case in PMS stars of $M < 1.4 M_\odot$! At higher masses, the Li-destruction occurs when the star is no longer on the Hayashi track, so convection does not affect the surface composition of Li.

H12.2 Homework

Estimate the duration of the Hayashi contraction phase and of the pre-main sequence contraction for stars of 0.1, 0.3, 1.0, 3, 10, 30 and 100 M_\odot .

Estimate de radii at the beginning and end of the Hayashi contraction phase and at the beginning and end of the pre-main sequence contraction.

H12.3 Homework

Explain the difference in the Lithium surface abundance of stars on the main sequence that had Lithium destruction during the Hayashi contraction phase or during the pre-main sequence contraction.

12.8 Brown dwarfs

We have seen that the collapse stops when a clump becomes optically thick for IR radiation. This requires a minimum mass of about $0.01 M_\odot$. So this sets the **lower mass limit of stars at $0.01 M_\odot$**

We have also seen that the minimum mass for H-fusion is about $0.1 M_\odot$ (Fig 10.7). Detailed calculations show that the actual mass limit is $0.08 M_\odot$.

Stars in the mass range of $0.08 < M < 0.01 M_\odot$ do not reach H-fusion: these are the brown dwarfs.

12.9 Summary of Star formation

Collapse of cloud = free fall phase $\tau_{\text{ff}} \sim 10^5 - 10^7 \text{ yr}$

Cooling by molecules and dust IR radiation

$\langle T \rangle$ low and about constant

Fragmentation of cloud into clumps

Start: when cloud exceeds Jeans mass

End : when H₂ is dissociated and H ionized

Characteristic: $\langle T \rangle \sim 10^5 \text{ K}$, $R/R_{\text{sun}} \sim 120 \text{ M/M}_{\text{sun}}$

Proto-star = pseudo-hydrostatic contraction $\tau_{\text{KH}} \sim 2 \cdot 10^6 \text{ yr}$

Fully convective because of low $\langle T \rangle$ and high κ

$T_{\text{eff}} \approx 3000 \text{ K} \approx \text{constant}$

Hayashi track : approximately vertical in HRD

Start: when collapsing cloud is dissociated

Characteristic: $R \sim 120 R_{\text{sun}}$, $T_{\text{eff}} \sim 3000 \text{ K}$, $L \sim 10^3 L_{\text{sun}}$

End : when $\langle T \rangle \sim 10^6 \text{ K} \rightarrow$ low $\kappa \rightarrow$ radiative equilibrium

Characteristic: $R \sim 2.5 R_{\text{sun}}$, $T_{\text{eff}} \sim 3000 \text{ K}$, $L \sim 0.5 L_{\text{sun}}$

Pre-main sequence = pseudo-hydrostatic contraction $\tau_{\text{KH}} \sim 7 \cdot 10^6 \text{ yr}$

Radiative equilibrium because of high $\langle T \rangle \rightarrow$ low κ

L about constant

Approximately horizontal track in HRD

Short phases of D-fusion and Li-fusion

Start: when proto star reaches radiative equilibrium ($\langle T \rangle \sim 10^6 \text{ K}$)

Characteristic: $R \sim 2.5 R_{\text{sun}}$, $T_{\text{eff}} \sim 3000 \text{ K}$, $L \sim 0.5 L_{\text{sun}}$

End : when H-fusion starts = on main sequence

Characteristic: $R \sim 1 R_{\text{sun}}$, $T_{\text{eff}} \sim 6000 \text{ K}$, $L \sim 1 L_{\text{sun}}$

NB :

1. The process starts when the mass of a cloud exceeds the Jeans mass
2. The free-fall time of the cloud depends on the initial density as $\tau_{\text{ff}} \sim n^{-1/2}$
3. The timescales and characteristics of the proto-star and pre-main sequence star are given for a $1 M_{\text{sun}}$ object.
They are **shorter for more massive objects.**

12.10 The stellar IMF

The initial mass function of the stars has been derived from observations of star clusters of different ages or field stars. If field stars are used the number of stars in any magnitude limited sample must first be corrected for three effects:

- the distance to which stars are observed, which depends on their absolute magnitude
- the conversion of absolute magnitude to stellar mass
- the evolutionary effect for late stages of evolution, to convert the present mass into the initial mass
- the lifetime effect, to correct the number of stars in a certain evolutionary phase for the duration of that phase.

In this way the observed distribution of the stars as function apparent magnitude, spectral type and evolutionary phase is converted into an initial mass function.

The best known modern IMFs are those of Kroupa (2001) and Chabrier (2003).

$$\begin{aligned} \text{Kroupa-IMF} \quad N(m)dm &= C_1 m^{-2.3} \text{ for } m > 0.5M_{\odot} \\ &N(m)dm = C_2 m^{-1.3} \text{ for } 0.08 < m < 0.5M_{\odot} \\ &N(m)dm = C_3 m^{-0.3} \text{ for } m < 0.08M_{\odot} \end{aligned}$$

$$\begin{aligned} \text{Chabrier-IMF} \quad N(m)dm &= D_1 \frac{1}{m} \exp[-\{\log(m/0.08)^2/0.952\}] \text{ for } m < 1M_{\odot} \\ &N(m)dm \cong D_2 m^{-2.3} \text{ for } m > 1M_{\odot} \end{aligned}$$

with the constants C and D adjusted to match the different mass ranges.

These two mass functions are very similar at $m \gtrsim 0.5M_{\odot}$ but deviate at smaller masses, where the Chabrier-IMF predict more/less stars than the Kroupa-IMF.

H12.4 Homework

- a. Plot the two versions of the IMF (Kroupa and Chabrier) in terms of $\log(N) dm$ versus $\log m$, in the range of 0.01 to $100 M_{\odot}$, both normalized at $M = 1M_{\odot}$.
- b. Which fraction of the mass is in the range of $0.01 - 0.1 M_{\odot}$, $0.1 - 1 M_{\odot}$, $1-10 M_{\odot}$, and $10 - 100 M_{\odot}$ in the two IMFs?
- c. Which fraction of the number of stars is in these ranges?
- d. Which fraction of the luminosity is in these regions?
(assume for simplicity that $L \sim M^3$)
- e. Which fraction of the visual (V-band) luminosity is in these regions?
(adopt one characteristic value of T_{eff} on the MS for each region, App B1)

13. The Zero Age Main Sequence (ZAMS)

13.1 Homology relations for Main Sequence Stars

The properties of stars on the ZAMS can be understood on the basis of *homology considerations*, because they all have the same chemical composition throughout the star. Homologous stars are those that have the same density structure. So two stars are homologous if

$$\left[\frac{\rho}{\rho_c} \left(\frac{r}{R} \right) \right]_1 = \left[\frac{\rho}{\rho_c} \left(\frac{r}{R} \right) \right]_2$$

The values of ρ_c and R can be different for both stars but the structure of ρ/ρ_c as function r/R is the same. Because of hydrostatic equilibrium the same homology applies for T/T_c and P/P_c

$$\left[\frac{P}{P_c} \left(\frac{r}{R} \right) \right]_1 = \left[\frac{P}{P_c} \left(\frac{r}{R} \right) \right]_2 \text{ and } \left[\frac{T}{T_c} \left(\frac{r}{R} \right) \right]_1 = \left[\frac{T}{T_c} \left(\frac{r}{R} \right) \right]_2$$

The stars differ only by their scaling factors ρ_c , T_c , P_c , M , R , L . With homology relations we can predict *trends* in stellar properties. If we know R_* , L_* and T_{eff} for a star of mass M (for instance from a stellar model or from an observed double-lined spectroscopic binary), we can predict R_* , L_* and T_{eff} of other stars with a similar structure but different M .

13.2 The Mass-Luminosity relation for ZAMS stars

We already derived the homology relations for P_c and T_c

$$P_c \sim M^2/R^4 \text{ and } T_c \sim \mu M/R$$

(Remember how this was derived!) So the temperature structure of one ZAMS star will be about the same as that of another star as a function of r/R , except that it will differ by a factor $(\mu M/R)_2 / (\mu M/R)_1$, as long as convection is not important.

Using similar homology arguments we already derived the first approximation for the mass-luminosity relation of stars in **radiative equilibrium**.

$$L \sim \frac{\mu^4 M^3}{\kappa}$$

We now consider this relation more closely for ZAMS stars.

For massive stars, $M > 10 M_\odot$, electron scattering is the dominant opacity. So

$$L \sim \mu^4 M^3 (1 + X)$$

This is independent of the metallicity, Z, but strongly dependent on He. Ignoring the small fraction of Z, we find $(1+X)^{-1} = (2-Y)^{-1}$ and $\mu^4 = (2 - 5Y/4)^{-4}$. Massive stars convert a larger fraction of their H mass into He than low mass stars, because of their convective cores.

This is important for understanding the brightening of stars during the H-fusion phase, when the He content gradually increases.

For ZAMS stars of $1 < M < 10 M_\odot$, the main opacity source is free-free and bound-free absorption, which is described by Kramer's law: $\kappa \sim Z\rho T^{-7/2}$

Using $\rho \sim M/R^3$ and $T \sim \mu M/R$ this gives

$$L \sim \mu^4 M^3 / Z \left(\frac{M}{R^3}\right) \cdot \mu^{-7/2} M^{-7/2} R^{+7/2}, \text{ so}$$

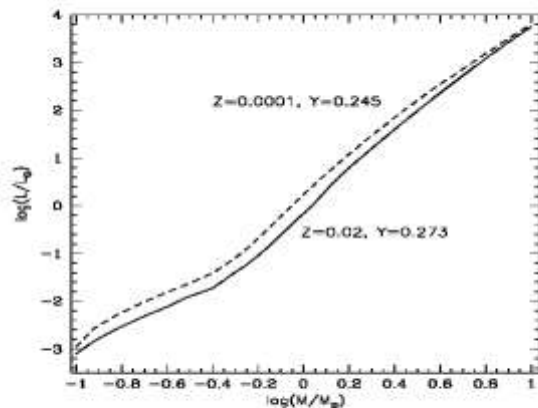
$$L \sim \mu^{7.5} M^{5.5} / Z R^{0.5}$$

We see that for stars with the same μ and Z, the M-L relation predicts $L \sim M^{5.5} / R^{0.5}$. We will see below that $R \sim M^x$ with $x \approx 0.6$ so we predict

$$L \sim \mu^{7.5} M^{5.2} / Z$$

- i. This explains why the M-L relation of ZAMS stars is steeper in the region between 1 and $10 M_\odot$ than for more massive stars.
- ii. It shows that stars with small metallicity, $Z \ll 0.01$, will be **brighter** than solar metallicity stars. This is a direct result of $L \sim 1/\kappa$ and $\kappa \sim Z$
- iii. It explains the brightening during the H-fusion phase when Y increases.

Fig 13.1 The predicted Mass Luminosity relation for ZAMS stars, based on detailed model calculations. The slope is steepest in the region 1 to $10 M_\odot$, and flattens to lower masses where convection plays a role (CS Fig 5.11)



13.3 The Mass-Radius relation for ZAMS stars

We can derive the M-R relation from the M-L relation if we can eliminate L. Since all ZAMS stars have H-fusion we can derive a homology relation based on the nuclear energy production.

The energy production per gram.second is $\epsilon \sim \rho T^\nu$ with $\nu \simeq 4$ for the P-P chain and $\nu \simeq 18$ for the CNO-cycle. The nuclear luminosity is given by

$$L = \int_0^R \epsilon \rho 4\pi r^2 dr \sim \epsilon \rho R^3 \sim \epsilon M$$

with

$$\epsilon \sim \rho T^\nu \sim (M/R^3) \mu^\nu M^\nu / R^\nu \sim \mu^\nu M^{1+\nu} / R^{3+\nu}$$

Comparing the above expression for L with $L \sim \mu^4 M^3 / \kappa$ we get

$$\frac{\mu^\nu M^{2+\nu}}{R^{3+\nu}} \sim \frac{\mu^4 M^3}{\kappa}.$$

This yields an expression for R

$$R \sim \mu^{\frac{\nu-4}{3+\nu}} \cdot M^{\frac{\nu-2}{3+\nu}} \cdot \kappa^{\frac{1}{3+\nu}}$$

For massive ZAMS stars, $M > 10 M_\odot$, where $\kappa \sim 1/(1+X)$ and the H-fusion goes by the CNO-cycle, so $\nu \simeq 18$, and $\kappa = \sigma_e$, so we find

$$R \sim M^{0.81} \cdot \mu^{2/3} \cdot (1+X)^{0.05} \quad \text{for } M \gtrsim 10 M_\odot$$

For $1 < M < 10 M_\odot$ ZAMS stars where H-fusion also goes by the CNO-cycle, so $\nu \simeq 18$, but κ is the Kramers opacity, we find

$$R \sim M^{0.08} \cdot \mu^{-0.54} \cdot Z^{0.13} \quad \text{for } 1 < M \lesssim 10 M_\odot$$

We see that for $M > 10 M_\odot$ ZAMS stars the radius scales with $M^{0.81}$ whereas for lower mass, $1 - 10 M_\odot$ ZAMS stars the radius is almost independent of mass.

13.4 The Mass-T_{eff} relation for ZAMS stars

The most interesting homology relation for ZAMS stars is the relation between M and T_{eff} because that is plotted in HR-diagrams and CMDs. We can find the homology relation for T_{eff} by combining the predicted M-L and R-M relations using $T_{\text{eff}} \sim [L/R^2]^{1/4}$

For massive ZAMS stars, $M > 10M_{\odot}$, where $\kappa = \sigma_e$, we find

$$T_{\text{eff}} \sim M^{0.31} \cdot \mu^{2/3} \cdot (1 + X)^{1/4}$$

For lower mass ZAMS stars, $1 < M < 10 M_{\odot}$, we find

$$T_{\text{eff}} \sim M^{1.26} \cdot \mu^{2.1} \cdot Z^{-0.31}$$

- i. We see that T_{eff} decreases with decreasing mass, (that is why the ZAMS goes to the right and downwards for decreasing mass), and that the decrease is a stronger function of M for stars of $1-10 M_{\odot}$ than for $10-100 M_{\odot}$.
- ii. These relations cannot be applied for stars with $M < 1 M_{\odot}$ because of the influence of convection.
- iii. We see that for massive ZAMS stars T_{eff} is rather insensitive to metallicity (Z), but for intermediate mass ZAMS stars a lower Z implies a higher T_{eff} and a larger L .
- iv. This shows that T_{eff} increases for ZAMS stars of higher He abundance. This is important for understanding the globular clusters whose CMD shows multiple main sequences.

So the ZAMS of low metallicity stars and the ZAMS of stars with higher initial (!) He abundance are to the left and slightly upward compared to the ZAMS for solar metallicity stars.

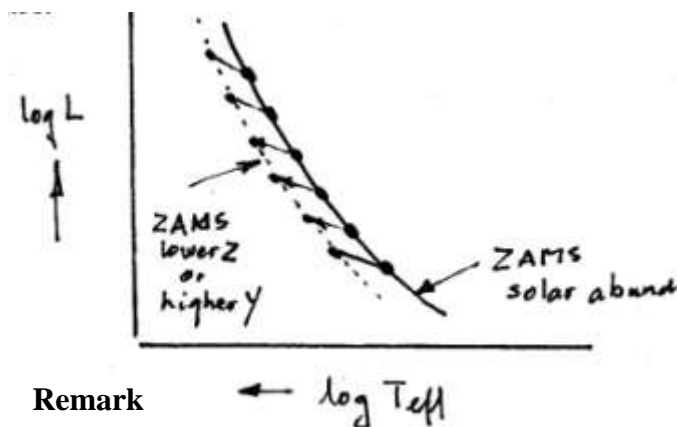


Fig 13.2 Schematic drawing of the effect of higher initial He or metal abundance on the location of the ZAMS in the HRD.

Note:

It is not important that you know the formulae of the homology relations of T_{eff} and R . But it is important that you understand the way in which these were derived, and the consequences for the location of the ZAMS in the HRD as a function of deviations from solar abundances, because this is important for understanding **globular clusters**.

Summary of the homology relations for chemically homogeneous stars (ZAMS), derived from detailed stellar evolution models

Process	R	T_c	ρ_c	$P_c \sim \rho_c T_c / \mu$
pp-chain $v \approx 4$	$M^{+0.43}$	$\mu^{+1} M^{+0.57}$	$M^{-0.3}$	$M^{+0.27}$
CNO-cycle $v \approx 18$	$\mu^{+2/3} M^{+0.81}$	$\mu^{+1/3} M^{+0.21}$	$\mu^{-2} M^{-1.4}$	$\mu^{-8/3} M^{-1.2}$

H13.1 Homework

Calculate the displacement (in terms of $\Delta \log T_{\text{eff}}$ and $\Delta \log R$) of stars 1, 3, 9, 20 and $40 M_\odot$ on the ZAMS if

- i. the Helium abundance changes from $Y = 0.28$ to $Y = 0.38$
 - ii. the metal abundance changes from $Z = 0.02$ to $Z = 0.001$ (which is the mean metallicity of galactic globular clusters)
 - iii. Use the values of M , L , T_{eff} from the models for solar metallicity (from Appendix C2) and plot the three ZAMS, based on stars of 1, 3, 9, 20, 20 M_\odot , for
 - (a) solar abundance : $X, Y, Z = 0.68, 0.30, 0.02$
 - (b) increased Helium abundance: $X, Y, Z = 0.58, 0.40, 0.02$
 - (c) decreased metal abundance : $X, Y, Z = 0.70, 0.30, 0.001$
-

14. Evolution During the Main Sequence Phase

14.1 Nuclear Fusion as a Thermostat

During the MS phase H is converted into He in the core. The temperature in the core can only change very little, because fusion is a strong function of T with $\epsilon \sim T^4$ for P-P chain and $\sim T^{18}$ for the CNO-cycle. Even a small change in T would result in a large change in ϵ and in L, which is not allowed by the HE-requirement. So **nuclear fusion acts like a thermostat** in the center of the star.

14.2 Changes in L and R

If T_c remains constant during the MS-phase but μ_c increases, then $P_c/\rho_c \sim T_c/\mu_c$ must decrease. So either P_c decreases or ρ_c increases as more H is converted into He. It turns out that both effects occur. (Verify this with models; e.g. Schaller et al 1992 AA Supl 96, 269.)

In H.E. the central pressure is set by the weight of the layers above.

So, as the central pressure decreases during the MS phase the outer layers of the star have to expand.

So when μ increases in the center the radius has to increase.

At the same time the luminosity increases (μ -effect).

(NB: The luminosity does not increase as steeply as $L \sim \mu^4$, because that was derived for homogeneous chemical composition, which is not the case when the star is fusing H in the core. In fact L increases less steeply.)

Because R^2 increases more than L, the effective temperature $T_{eff} \sim (L/R^2)^{1/4}$ decreases. **This implies that the stars move up and to the right in the HRD during H-fusion in the core.**

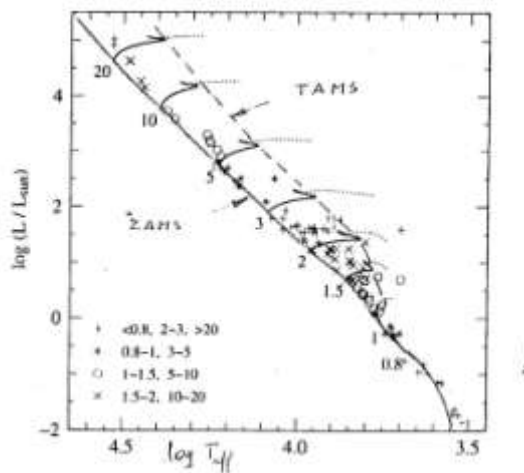


Fig 14.1

Evolution tracks during H-fusion. The locations of the Zero Age Main Sequence (ZAMS) and the Terminal Age of the Main Sequence (TAMS) are indicated. Symbols indicate binary observations. (based on OP Fig 8.9)

14.3 Changes in the chemical profile

Stars with $M \geq 1.2 M_{\odot}$ fuse H via the CNO-cycle, which is very sensitive to T. Therefore the nuclear energy is generated in a very small volume. This means that the energy flux is very high in and around the core of these stars. If that energy was transported by radiation, it would require a steep temperature gradient. So the central regions of these stars become convective.

Core convection has two effects.

- i. Convection brings fresh H into the center from all over the convective region so more H can be fused. This extends the MS lifetime of these stars.
- ii. The chemical profile of MS-stars with $M > 1.2 M_{\odot}$ is flat in the center, whereas it is peaked for lower mass stars. As the H-fraction in the core decreases, the convection zone shrinks in mass.

Q?

Why?

Hint: remember what the effect of a μ -gradient is on the convection criterium.

This implies that the chemical profile is flat in a decreasing fraction of the mass. Both effects result in a chemical profile that evolves like sketched below.

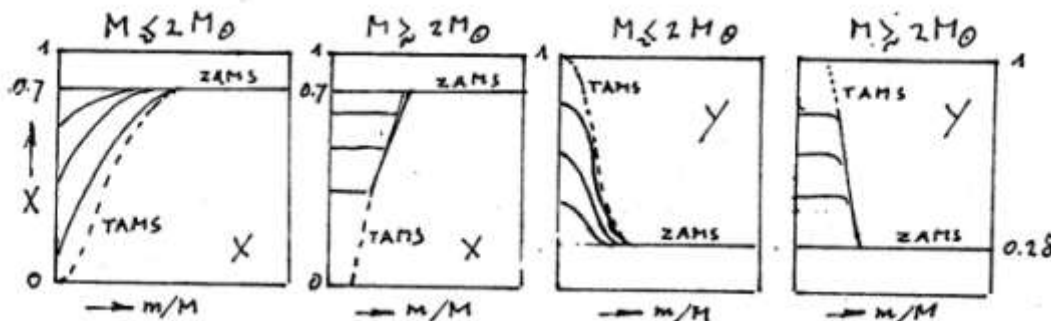


Fig 14.2 Changes in the chemical profile during the MS-phase of stars with and without convective cores. The dashed line is the distribution at the end of the MS phase TAMS.

H14.1. Homework

Verify that the MS lifetimes of stars $M > 1.2 M_{\odot}$ increase in the way we expect for stars with convective cores. Do this for stars with $Z = 0.02$ (solar) and $M = 120, 25, 5, 1$ and $0.8 M_{\odot}$.

Use the tables in Appendix C2 where q_{cc} = mass fraction contained in the convective core at $t = 0$. (Data from Schaller et al. 1992, AA Supl 96, 269)

Compare your result with the data in the lower part of the table, and comment and explain the differences.

14.4 The MS evolution of the Sun

The two figures below show the distributions of abundances as well as the distributions of $r(m)$, $T(m)$, $P(m)$, $\rho(m)$ and $L(m)$ for the solar model now ($t=4.5$ Gyr: Fig 14.3) and at the TAMS ($t=12.3$ Gyr: Fig 14.4).

(Figs from CO)

Study these figures and try to understand the basic features:
in particular the changes in $L(r)$ and abundances (r). ($X_{12} = {}^{12}\text{C}$, $X_{14} = {}^{14}\text{N}$)

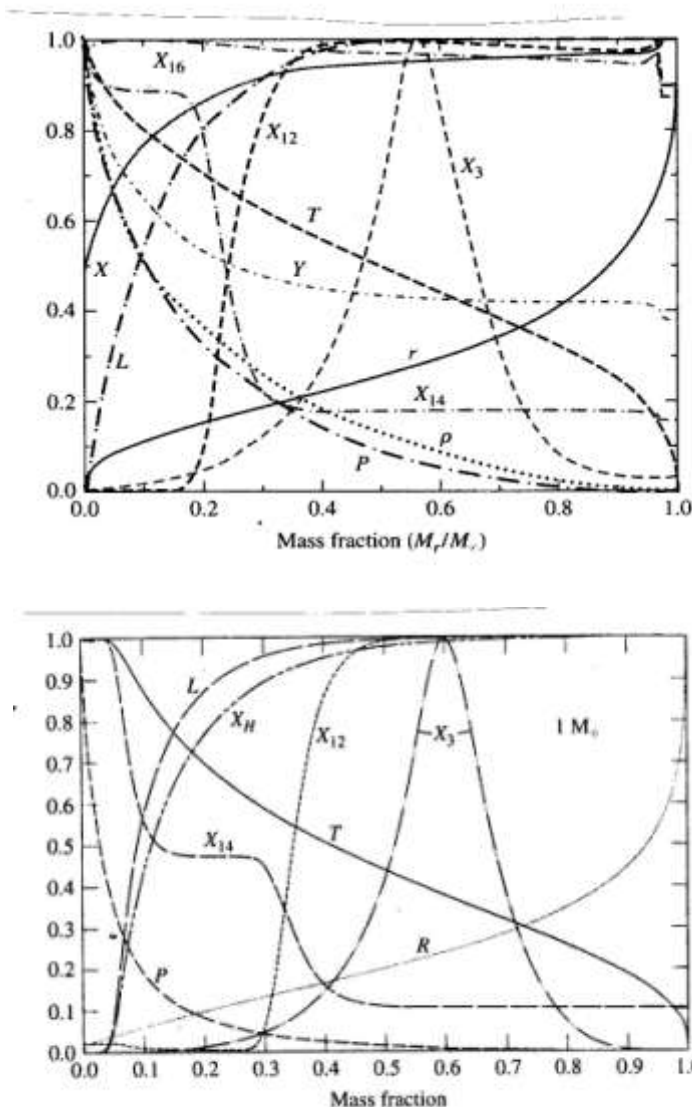


Fig 14.3 and 14.4

*The internal structure of a $1 M_\odot$ star at $t=4.5$ Gyr (= Sun now) (fig 14.3)
and $t=12.3$ Gyr (at the end of the H-fusion phase = TAMS) (fig 14.4).*
(Figs. from CO)

14.5 Convective Overshooting in the MS phase

We have argued before that where-ever there is convection, there may be convective overshooting. This produces chemical mixing over a larger region than predicted by the Schwarzschild or Ledoux criterium.

Overshooting has two effects (similar to normal convection)

- i. It extends the MS lifetime
- ii. It increases L because $\langle\mu\rangle$ increases in a larger region.

The observed colour-magnitude diagrams of star clusters provide evidence for overshooting.

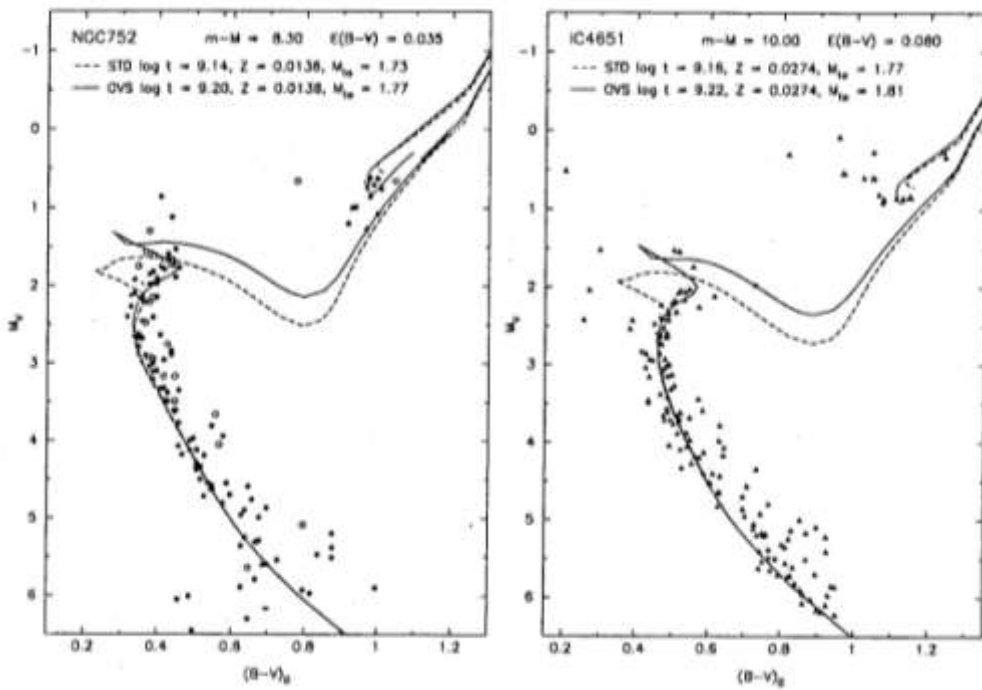


Fig. 14.5 Comparison between the observed CMD of two open clusters NGC752 (left) and IC4651 (right), both ≈ 1.5 Gyr old, with predicted isochrones with overshooting (OVS = full lines) and without (STD = dashed lines). (OP Fig 8.11)

The isochrones calculated with overshooting (full lines) fit the observations better than those without overshooting (dashed lines). From studies like this it is concluded that in the mass range of 1.5 to $8 M_\odot$ the overshooting parameter is $\alpha_{os} = 0.25$ so the overshooting length is $l_{os} = 0.25 \mathcal{H}_p$.

14.6 The end of the MS phase: core contraction

When H-fusion stops in the core, the core has to contract to compensate the radiative losses.

In stars of $M > 1.2 M_{\odot}$ the whole core contracts “suddenly” because H is exhausted in the *whole* core, due to convection. (see the Fig 14.2).

In stars of $M < 1.2 M_{\odot}$ the contraction is *more gradual*, because the chemical profile allows H-fusion to keep going gradually.

As a result of this difference, stars with $M > 1.2 M_{\odot}$ contract as a whole. This reduces the stellar radius, which produces **a small leftward loop in the HRD at the end of the H-fusion phase**. This contraction ends when the region around the He-core has reached a sufficiently high T and density to start H-fusion in a shell around the He-core.

Stars with $M < 1.2 M_{\odot}$ do not contract as a whole because the H-fusion is extinguished more gradually. Meanwhile the core contracts (just like in stars with $M > 1.2 M_{\odot}$) but this slower contraction does not result in a decrease of the outer radius. So these stars do not make a leftward ward loop in the HRD.

Check this with the tracks in Appendix E.

15 . Principles of Post-Main Sequence Evolution

15.1 Definition of zones and regions

For discussing the evolution of stars it is useful to distinguish several regions in the star.

- a. **The core:** is where fusion is going on or has gone on.
- b. **The shell zone:** is where fusion occurs in a shell or in shells around the core.
- c. **The envelope:** is the region between the shell zone and the atmosphere.
- d. **The atmosphere:** is the region where the optical depth for most of the radiation is less than $\tau \lesssim 10$. Radiation can escape from this layer.
- e. **The chromospheres and corona:** is the region above the atmosphere where the temperature rises far above the effective temperature. This is typically for stars with convective envelopes which generate shocks in the upper atmosphere, so only cool stars have chromospheres and coronae.
- f. **The wind:** is the region from which gas escapes with a typical speed of a few times the escape speed. We will discuss wind processes later.
Cool stars (like the Sun) have winds driven by gas pressure due to the high temperature of the coronal gas.
Very cool stars (like AGB-stars) have winds driven by radiation pressure on dust-grains.
Hot stars (O, B, and Wolf-Rayet stars) have winds driven by radiation pressure on ions.

15.2 The evolution of the core

We have shown before (10.11) that during the evolution of a star in radiative and hydrostatic equilibrium , supported by gas pressure, the central temperature and density are related via

$$T_c \simeq \frac{\mu G}{R} \cdot M_c^{2/3} \cdot \rho_c^{1/3}$$

where M_c is the mass of the core that contracts. This is the mass that was enriched by the previous evolution phase.

(Remember the way this expression was derived!)

So the evolution of T_c and ρ_c in the *center* of a star, due to nuclear burning and contraction, proceeds roughly along a line of

$$\log T_c = \text{const} + \log \mu_c + 2/3 \log M_c + 1/3 \log \rho_c$$

In the most massive stars, $M > 50 M_{\odot}$, radiation pressure dominates the gas pressure in supporting the star. In that case

$$T_c^4 \sim P_c \sim \frac{M^2}{R^4} \sim M_c^{2/3} \cdot \rho_c^{4/3} \quad \text{independent of } \mu_c, \text{ so}$$

$$\log T_c = \text{const} + 1/6 \log M_c + 1/3 \log \rho_c$$

We can compare these tracks in the T_c, ρ_c diagram with the location of the fusion zones, and with the regions of the different equations of state, as a function of the initial stellar mass. (The regions for the different EOS were shown in Fig 10.7)

This is shown in the figure below.

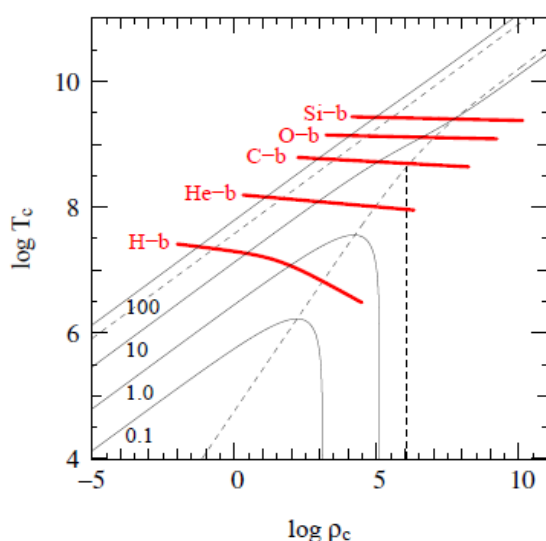


Fig 15.1
Schematic evolution of stars in the (ρ_c, T_c) -diagram with the regions of nuclear fusion in the center indicated.

(Same as fig 10.7,
OP Fig 7.3)

Q?

Check that the temperatures of the fusion phases agree with those in Table in 10.8. If not, what could be the reason?

Q?

Why does the line for H-fusion show a kink?

Caution: the figure describes the evolution of the star in the (ρ_c, T_c) -diagram as a function of the *total mass*. We have seen above that this is not the correct parameter to describe the central evolution, because the relation depends on the mass of the core that contracts and not on the initial total stellar mass.

From the figure we can learn several interesting facts about the evolution of stars of different masses.

- A. Stars with $M \lesssim 0.1 M_{\odot}$ do not reach H-fusion.
 Detailed calculations show that the real limit is $0.08 M_{\odot}$.
- Q?** Can you think of a reason why the simple estimate, based on scaling the solar model to estimate T_c and ρ_c fails?
 (Stars which never reach H-fusion are “brown dwarfs”).
- B. Stars with $0.08 < M \lesssim 0.8 M_{\odot}$ reach H-fusion but not He-fusion.
 They end up as He-rich degenerate white dwarfs.
- C. Stars with $0.8 < M < 2 M_{\odot}$ reach He-fusion and then become C-rich WDs.
- D. The figure suggests that stars with $2 \lesssim M \lesssim 6 M_{\odot}$ would go through C-fusion and then enter the region of Extreme Relativistic WDs. Since ER stars only exist if they have exactly the Chandrasekhar mass, they will collapse.
 However, we will see below that most (or maybe all) stars in this mass range suffer very high mass loss near the end of their life (i.e. in the AGB-phase). This results in a strong reduction of the stellar mass, which prevents the stars from reaching the ER-state.
- E. Stars with $M \gtrsim 6 M_{\odot}$ do not become degenerate and go through all fusion phases.

The picture above gives a reasonably good description and explanation of the internal evolution of stars. However, detailed evolutionary calculations show that a few modifications have to be made.

The most important one is the use of the *total initial stellar mass* to describe the location of the tracks in the (T_c, ρ_c) diagram:

- When a star contracts on a Kelvin-Helmholtz timescale at the end of a fusion phase, not the whole star contracts, but only the central region which took part in the previous fusion phase.
 (For instance, at the end of H-fusion the newly formed He-core contracts.)
 This means that the constant ($\mu M^{2/3}$) of the T_c, ρ_c relation is smaller.
 Therefore the criterium whether or not a star reaches a certain fusion phase is better described by its “core-mass” than by its initial mass.
- Stars may lose a substantial fraction of their mass due to stellar winds.
 For high mass stars of $M > 30 M_{\odot}$ the mass loss is significant during their whole life. For low mass stars it is only important in the later phases, after the H-fusion phase. (We will discuss stellar winds and how it affects the evolution later).

Taking into account these two effects, it turns out that

- **the minimum required core mass for He-fusion is $0.3 M_{\odot}$.**
- **the minimum required core mass for C-fusion is $1.1 M_{\odot}$.**

15.3 Isothermal Cores

At the end of the H-fusion phase the fusion in the core has stopped so the core does not produce energy, which implies $L(r) = 0$ for $r < R_c$ (R_c is the radius of the core and M_c is the mass in that core). If $L(r < R_c) = 0$ then $dT/dr = 0$ in the core. **So the core has become isothermal.**

An isothermal core in hydrostatic equilibrium must have a steep density gradient because for constant temperature $dP/dr \sim Td\rho/dr$. In other words: the density gradient has to provide the pressure gradient without the help of the temperature gradient. **It turns out that an isothermal core can only exist if its mass is smaller than a certain fraction of the total mass of the star.**

We will derive this in a way that shows resemblance to the derivation of the Virial Theorem.

$$\text{Hydrostatic Equilibrium} \quad \frac{dP}{dr} = -\frac{Gm}{r^2} \rho$$

Multiplication by $4\pi r^3$ and integration over the core, i.e. $0 < r < R_c$, gives

$$\int_0^{R_c} 4\pi r^3 dP = - \int_0^{R_c} \frac{Gm}{r} \rho \cdot 4\pi r^2 dr = E_{\text{pot}}^c = -\alpha \frac{GM_c^2}{R_c} \quad \text{with } \alpha \gg 1.$$

Partial integration of the left hand term (as in Virial Theorem derivation) gives

$$\begin{aligned} \int_0^{R_c} 4\pi r^3 dP &= 4\pi r^3 P \Big|_0^{R_c} - 3 \int_0^{R_c} P 4\pi r^2 dr \\ &= 4\pi R_c^3 P(R_c) - \frac{3\mathcal{R}T_c}{\mu} \int_0^{R_c} \rho \cdot 4\pi r^2 dr = 4\pi R_c^3 P(R_c) - \frac{3\mathcal{R}T_c}{\mu_c} \cdot M_c \end{aligned}$$

where we have used the isothermal condition $P = \mathcal{R}\rho T_c / \mu_c$ with $T_c = \text{constant}$. Notice that the first right-hand term is not zero as in the derivation of the Virial Theorem, because here we do not integrate up to R_* , where $P(R_*) = 0$, but up to R_c . Here $P(R_c)$ is the pressure at the outer boundary of the isothermal core.

$$\text{So } 4\pi R_c^3 P(R_c) - \frac{3\mathcal{R}T_c}{\mu_c} M_c = -\alpha \frac{GM_c^2}{R_c}$$

This gives a relation between the pressure at the boundary of the core and its radius, for a given core mass M_c and a given temperature T_c .

$$P(R_c) = \frac{3}{4\pi} \frac{\mathcal{R}T_c}{\mu_c} \frac{M_c}{R_c^3} - \frac{\alpha}{4\pi} \frac{GM_c^2}{R_c^4}$$

This expression is of the type $y = Ax^3 - Bx^4$ if $x = 1/R_c$. It has a maximum at $x = 3A/4B$ where $y_{\text{max}} = 3^3 A^4 / 4^4 B^3$.

Substituting A and B gives the **maximum pressure** that an isothermal core can support.

$$P^{\max}(R_c) = C \cdot \frac{T_c^4}{\mu_c^4 M_c^2}$$

So the “weight” of the envelope on top of the core should be less than this maximum value, otherwise the core cannot be stable. But the higher the core mass, the smaller this pressure!

Q? Explain in physical terms why there is a maximum for $P(R_c)$.

Let us assume that the isothermal core contains only a small fraction of the total stellar mass M , and that the radius of that star is much larger than R_c . Then the pressure at the bottom of the envelope (which is at R_c) can be estimated in the same way as the estimate of the central pressure of any star in H.E.:

$$P^{\text{env}}(R_c) \cong GM^2/R^4.$$

The temperature at the bottom of the envelope is the same as the core temperature T_c with

$$T_c \sim \frac{\mu_{\text{env}}}{R} \cdot \frac{GM}{R} \quad \text{or} \quad \frac{M}{R} \sim \frac{RT_c}{G\mu_{\text{env}}} \quad \text{where } \mu_{\text{env}} \text{ is } \mu \text{ in the envelope.}$$

Substitution of this into the expression $P^{\text{env}}(R_c)$ gives

$$P^{\text{env}}(R_c) \sim \frac{T_c^4}{\mu_{\text{env}}^4 M^2}$$

The isothermal core can only be stable if $P^{\text{env}}(R_c) < P_{\max}^c(R_c)$. This gives

$$\boxed{\frac{M_c}{M} \lesssim C \cdot \left(\frac{\mu_{\text{env}}}{\mu_c}\right)^2} \quad \text{with } C = 0.37$$

This is called the **Schönberg-Chandrasekhar limit for isothermal cores**.

So at the end of H-fusion in the core, the remaining isothermal Helium core, with $\mu_c = 4/3$, can only be stable if its core has an estimated mass of

$$\frac{M_c}{M} < 0.37 \left(\frac{0.60}{1.33}\right)^2 \approx 0.08$$

Here we assumed that the envelope is not chemically enriched at all. In reality the lower part of the envelope has also increased He-abundance, so $\mu_{\text{env}} > 0.6$.

If that is taken into account then the

Schönberg-Chandrasekhar limit for isothermal cores is $M_c/M < 0.10$

If the core is *less massive* than this, then the subsequent H-shell fusion occurs around a stable Helium core. If the core is *more* massive than this, the isothermal Helium core cannot carry the weight of the shell plus envelope, so it will contract during the H-fusion in a shell around it.

Contraction of the He-core will create a temperature gradient that produces extra gas pressure and helps to stabilize the core. So the core is no longer isothermal. The temperature gradient also results in an energy flux from the core. So once the core starts to contract it has to keep doing so until He-fusion starts in the core. This contraction occurs on the Kelvin-Helmholtz timescale of the core.

$$\tau_{\text{KH}} \simeq \frac{GM_c^2}{R_c}/(L - L_{\text{shell}})$$

Q? Why $L - L_{\text{shell}}$ instead of L ?

Q? Estimate the timescale for a post-MS star of $3 M_\odot$ that has a core of $0.45 M_\odot$ and gets 10% of its luminosity from core-contraction. Compare it with the MS-life of this star.

Q? Which one of the stars is more likely to have a *contracting* core during H-shell burning: a star of $10 M_\odot$ or a star of $2 M_\odot$? Why?

H15.1 Homework

Use the model data in the appendix of Schaller et al (1992, AA Supl 96, 269) to determine the initial masses of stars of solar composition that create a stable isothermal He-core at the end of the MS phase, and of those that have a He-core that is larger than the Schönberg-Chandrasekhar limit and has to contract.

Hint: The moment of core contraction can be seen in the HRD by the short leftward motion at the end of the MS phase. In Schaller's models this is characterized by the increase in T_{eff} just before $X=0$ in the center. The mass of the convective core, q_{cc} , at that moment gives the mass of the He core at the end of the MS-phase.

H15.2 Homework

Explain in physical! terms (words) why there is a limit to the pressure of the envelope that an isothermal core can support.

15.4 The mirror principle of stars with shell burning

Whenever a star has a shell burning source, it appears to act like a mirror:

core contraction → envelope expansion

core expansion → envelope contraction

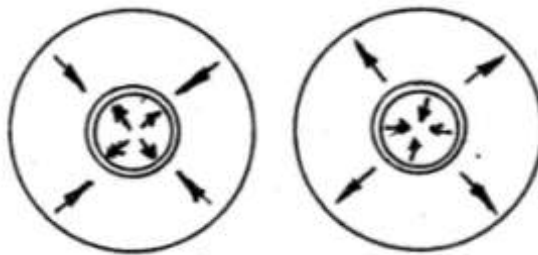


Fig 15.4 The mirror action of shell fusion: if the core contracts the envelope expands and vice-versa.

There are two ways to explain this: by using the virial argument or using the pressure argument. In both arguments the **thermostatic behavior** of a fusion shell plays a key role (see section 14.1).

The Virial argument

The fusion efficiency is very sensitive to T. Therefore, as the core contracts the fusion shell can hardly contract with it, because otherwise it would increase its T and its energy production.

So the shell has to remain at about the same distance and the same T. So the “mean T” of the star will not change very much. If the mean T does not change, then the total kinetic (thermal) energy will not change. The virial theorem then implies that the *total potential energy* should also remain about constant.

So if the core contracts (more negative E_{pot}) then the envelope must expand (less negative E_{pot}), and vice versa.

The pressure argument

For the star to remain in thermal equilibrium, the energy generation by fusion must remain constant. So if the core contracts and the shell follows it, the temperature in the fusion shell will rise. This would imply a higher energy generation rate unless the density in the shell decreases (remember: $\epsilon \sim \rho T^4$). But as the density decreases, at about the constant temperature of the fusion-reaction, the pressure in the shell decreases. This implies that the pressure of the envelope on top of the shell must decrease. So the envelope must expand.

N.B.

The argument for the mirror principle does not apply to stars with degenerate cores. In these stars the shell is right on top of the degenerate core. So if the degenerate core shrinks the shell has to contract with it and reaches a higher P and T. This results in an increasing luminosity.

Q? Why would the degenerate core contract?

We conclude that:

- 1. Fusion shells act like mirrors in the expansion or contraction of the core and the envelope. This is due to the thermostatic action of fusion shells.**
- 2. The contraction of a non-degenerate core surrounded by a fusion shell will result in an expansion of the star.**
- 3. The contraction of a degenerate core surrounded by a fusion shell will result in an increase in luminosity.**

15.5 The Hayashi-Line of Fully Convective Stars

Fully convective stars occupy a narrow, almost vertical line at low temperature, in the HRD diagram if it is plotted as L versus T_{eff} . We have seen that this applies to fully convective pre-MS stars. But it also applies to fully convective Red Giants and AGB stars. They are all on about the same line in the HRD, the **Hayashi line** after the Japanese astronomer who explained this observed effect in the early sixties. It is the result of two effects in stellar structure theory:

- convective stars have extended envelopes and so their T_{eff} is low.
- at low temperatures of $T < 3000$ K the opacity in the photosphere drops steeply towards lower T_{eff} .

We will derive the physical principle of the Hayashi-line by showing what happens if a (nearly isothermal) photosphere is attached on top of the envelope of a fully convective star. The star is supposed to be convective up to the layer where $\tau \approx 1$, i.e. the photosphere. We will call this radius R_1 (which of course is very similar to the stellar radius R).

15.5.1 The pressure at R_1 , derived from the interior, $P(R_1)^{\text{int}}$

A fully convective star obeys the polytropic relation: $P = K \rho^{5/3}$

Since all convective stars are homologous (same P/P_c , T/T_c and ρ/ρ_c if these are expressed in function of r/R_*) we can derive how K depends on the mass or radius of the star by realizing that the central pressure is proportional to

$$\begin{array}{lll} P_c \sim \frac{GM^2}{R^4} & \text{and} & P_c = K \rho_c^{5/3} \\ \text{H.E.} & \text{polytrope} & \text{with} \\ & & \rho_c \sim M/R^3 \\ & & \text{homology} \end{array}$$

So the scaling constant K of the polytropic index depends on the stellar parameters as

$$K = \frac{P_c}{\rho_c^{5/3}} \sim \frac{M^2}{R^4} / \rho_c^{5/3} \sim \frac{M^2}{R^4} / \frac{R^5}{M^{5/3}} \rightarrow K \sim M^{1/3} R$$

The polytrope expression for P is valid at *all* depth, also at the top of the convection zone at R_1 , so

$$P_1^{\text{int}} = K \rho_1^{5/3} \sim M^{1/3} R \rho_1^{5/3}$$

15.5.2 The pressure at R_1 , derived from the atmosphere, $P(R_1)^{\text{phot}}$

Remember that the temperature structure of a simple (grey) photosphere is given by

$$T^4 = \frac{3}{4} T_{\text{eff}}^4 (\tau + \frac{2}{3})$$

This implies that the photosphere is almost isothermal because:
 $0.84 < T / T_{\text{eff}} < 1.06$ if $0 < \tau < 1$. Therefore we adopt for simplicity that the photosphere is isothermal with $T = T_1$.

The pressure then decreases exponentially with height as

$$\frac{dP}{dr} = \frac{\mathcal{R}T_1}{\mu} \frac{dp}{dr} = -\frac{GM}{R^2} \rho \quad \rightarrow \quad \frac{d \ln \rho}{dr} = -\frac{GM}{R^2} \frac{\mu}{\mathcal{R}T_1} = \frac{\mu g}{\mathcal{R}T_1} \equiv \frac{1}{\mathcal{H}}$$

So the density distribution in the isothermal photosphere is $\rho = \rho_1 e^{-\frac{r-R_1}{\mathcal{H}}}$.

The density scale height is $\mathcal{H} \equiv \frac{\mathcal{R}T_1}{\mu g} \sim T_1 R_1^2 / GM$

Using this expression for ρ , we can now find the pressure P_1 at $\tau = 1$, which we want to compare with the pressure P_1 that was derived from the polytropic interior.

The optical depth $\tau = 1$ is defined by

$$\int_{R_1}^{\infty} \kappa \rho dr = 1 \quad \rightarrow \quad \bar{\kappa} \int_{R_1}^{\infty} \rho_1 e^{-\frac{(r-R_1)}{\mathcal{H}}} dr = \bar{\kappa} \rho_1 \mathcal{H} = 1$$

where we used a mean constant value for $\bar{\kappa} \equiv \kappa(\tau = 1)$.

So the density ρ_1 at $\tau = 1$ is $\rho_1 = 1/\mathcal{H}\bar{\kappa} \sim GM/TR^2\kappa$ and the pressure at $R_1 = R$ ($\tau=1$) due to the photosphere is

$$P_1^{\text{phot}} = \sim \rho_1 T_1 \sim \frac{GM}{R^2} \cdot \frac{1}{\kappa}$$

15.5.3 Match the pressure of Interior to Photosphere at $\tau = 1$

We now have two expression for the pressure P_1 , one derived for the top of the polytropic interior, and one derived for the bottom of the photosphere. These two should be equal. The value of P_1^{int} depends on the density at the top of the interior, for which we derived an expression from the photosphere $\rho_1 \sim GM/TR^2\kappa$ (with M , T , R and κ at $\tau=1$).

Substitutions yields

$$P_1^{\text{phot}} = P_1^{\text{int}} \rightarrow MR^{-2}\kappa^{-1} \sim M^2 R^{-7/3} T^{-5/3} \kappa^{-5/3} \rightarrow R \sim M^3 T^{-5} \kappa^{-2}$$

Up to now we have not specified the energy source, nor the luminosity.
(NB: The luminosity does not have to obey the M-L relation that we derived earlier, because that was derived under the assumption that energy transport is by radiation, and in these stars it is by convection!)

The luminosity is set by R_1 and T_1 : $L \sim R^2 T^4$
 This gives the luminosity of fully convective stars:

$$L \sim M^6 T^{-6} \kappa^{-4}$$

15.5.4 The absorption coefficient κ in the photosphere of cool stars

For very cool stars ($T_{\text{eff}} < 6000$) H^- is the dominant atmospheric opacity, with

$$\kappa \simeq \kappa_0 \rho T^9 (Z/0.02) \quad \text{with } \kappa_0 = 2.5 \cdot 10^{-36} \text{ cm}^2/\text{g}$$

if ρ and T are in cgs units.

We can write this as $\kappa = \kappa_0 \rho^a T^b$ with $a \simeq 1$ and $b \simeq 9$
 This opacity is very small: at $T = 3000$ and $\rho = 10^{-10} \text{ g/cm}^3$, which are the
 approximate values in an atmosphere of an AGB star, the opacity is only $5 \cdot 10^{-5}$
 cm^2/g . (Compare this with $\kappa \approx 0.3 \text{ cm}^2/\text{g}$ in the interior of ionized stars).

Substituting this into the expression for L , we find (after long but not difficult algebra)

$$\log L = A \log T_{\text{eff}} + B \log M + \text{constant}$$

with

$$A = \frac{18a+4b+6}{3a-1} \simeq 60$$

$$B = \frac{2a+6}{3a-1} \simeq 4$$

We see that for fully convective stars

$$L \sim T_{\text{eff}}^{60} M^4 \quad \text{or} \quad T_{\text{eff}} \sim L^{0.017} M^{0.07}$$

This means that T_{eff} is “almost” independent of L and M , so Hayashi line is almost vertical in the HRD when the luminosity is plotted versus $\log T_{\text{eff}}$, and lines of constant M are very close together.

N.B.

- i. Detailed evolutionary models show that the Hayashi line bends a little bit to the right (towards cooler temperatures) at $L > 10^2 L_\odot$ (see Figure 12.2)
- ii. In the colour-magnitude diagram the Hayashi line of fully convective stars bends so much stronger to the right, e.g. in B-V colour, because this colour depends very strongly on T_{eff} . For cool stars (see Figure 1.4).

15.5.5 Intuitive Explanation for Hayashi Line

We have derived the location of the Hayashi line from mathematical expressions. Can we also understand the location of the Hayashi line based on simple physical insight?

Consider the two main ingredients:

- i. Fully convective stars are geometrically extended and so: their effective temperature will be small.
- ii. The opacity, or absorption coefficient, at low temperatures is due to H⁻. This opacity is very small (e.g. $\kappa \sim 10^{-4}$ at $T \simeq 3000K$, $\rho \simeq 10^{-10}$) and decreases very steeply with decreasing temperature T^9 .

Suppose a very cool star of constant of constant L would increase its size, then the photospheric T would decrease and the outer layers would become (almost) transparent. So *even* if the star's size would increase, we could look deeper and deeper into the star up to the depth where $\tau = 1$ is reached at **almost constant T_{eff}** .

This is the main reason why the Hayashi line is approximately vertical in HRD.

The argument does not apply to stars which contain dust in their envelope. For such stars (e.g. stars at the tip of the AGB with dense cold winds and class 0 TTauri stars, see Fig 12.4) the main opacity is dust opacity, which is large and has a weak dependence on T. So these stars radiate as black bodies with the temperature of the dust and the radius of the dusty wind.

16. Stellar Winds and Mass Loss

The history of stellar winds, their observations and theories and their effects on the stellar evolution have been described in “**Introduction to Stellar Winds**” (Lamers and Cassinelli 1999, Cambridge University Press, ISBN0-521-59565-7). I will refer to this book as “ISW.”

Mass loss by stellar winds play a key role in the late evolution phases of low mass stars and throughout the whole evolution of massive stars. There are basically four types of stellar winds:

- a. **Coronal winds** are driven by gas pressure due to the high temperatures of stellar coronae. This mechanism is responsible for the winds of cool stars on the main sequence like the Sun and possibly also red giants. (ISW 3 and 5)
- b. **Dust driven winds** are driven by radiation pressure on dust grains. This mechanism also needs stellar pulsations to be efficient. It produces the winds of pulsating red giants and AGB stars. (ISW 7)
- c. **Line driven winds** of hot stars are driven by radiation pressure on highly ionized abundant atoms. This mechanism is responsible for the winds of hot luminous stars: O and B-type main sequence stars, hot giants and hot supergiants, Wolf-Rayet stars and central stars of planetary nebulae. (ISW8)
- d. **Alfvén wave driven winds** are driven by magnetic waves. The magnetic fieldlines are rooted in the photosphere. Horizontal motions of the footpoints (due to convective cells) produce waves of the fieldlines (like a hanging string that is shaken at the top). These waves produce an outward pressure gradient that can accelerate ionized gas. This mechanism is (probably) responsible for the mass loss from red giants. (ISW 10)

Mass loss rates are expressed in units of $1M_{\odot}/\text{yr} = 6.3 \times 10^{25} \text{ g/s}$. A typical mass loss rate of $10^{-6} M_{\odot}/\text{yr}$ corresponds to the loss of about an earth-mass per year.

16.1 Coronal Winds and the critical point

We describe the coronal wind theory for a star that is surrounded by an **isothermal corona of temperature T_c** . We assume that the wind is stationary and spherical and we ignore magnetic effects.

For a stationary wind the mass loss rate is given by the equation of mass conservation

$$\boxed{\dot{M} = 4\pi r^2 \rho(r) v(r)} \quad \text{with } \dot{M} \equiv -dM/dt > 0$$

For a stationary wind the time derivatives are zero, so

$$\frac{dv(r,t)}{dt} = \frac{\delta v(r,t)}{\delta t} + \frac{\delta v(r,t)}{\delta r} \cdot \frac{dr}{dt} = 0 + \frac{dv}{dr} \cdot v = v \cdot \frac{dv}{dr}$$

Newton's law $f = m \cdot a = m \cdot v dv/dr$ with the forces due to the gas pressure gradient and gravity can be written as an equation of motion

$$\rho \cdot v \frac{dv}{dr} = -\frac{GM_*}{r^2} \cdot \rho - \frac{dP}{dr} \quad \text{or} \quad v \frac{dv}{dr} + \frac{GM_*}{r^2} + \frac{1}{\rho} \frac{dP}{dr} = 0$$

where $P = \frac{R\rho T}{\mu}$ is the gas pressure. For an isothermal corona the last term is

$$\frac{1}{\rho} \frac{dP}{dr} = \frac{RT}{\mu} \cdot \frac{1}{\rho} \frac{d\rho}{dr} = \frac{a^2}{\rho} \frac{d\rho}{dr}$$

with the isothermal sound speed $a = (\mathcal{R}T/\mu)^{1/2}$

Using the equation of mass conservation, $\rho \sim v^{-1}r^{-2}$, we can express

$$\frac{1}{\rho} \frac{d\rho}{dr} = -\frac{1}{v} \frac{dv}{dr} - \frac{2}{r}$$

Substitute this into the equation of motion and find

$$v \frac{dv}{dr} + \frac{GM_*}{r^2} + a^2 \left(-\frac{1}{v} \frac{dv}{dr} - \frac{2}{r} \right) = 0$$

$$\text{or } \frac{1}{v} \frac{dv}{dr} = \left(\frac{2a^2}{r} - \frac{GM_*}{r^2} \right) / (v^2 - a^2)$$

This is a critical equation which has a numerator and a denominator that both can go through 0. The numerator is negative close to the star, where $GM_*/r^2 > 2a^2/r$ and increases outwards as GM/r^2 decreases faster than a^2/r . The denominator is also negative close to the star where the wind speed is still very small at the photosphere and increases outwards as the wind accelerates. This means that close to the star the velocity gradient is positive: $v(r)$ increases.

Q: What happens if the denominator reaches 0 when the numerator is still negative?

Q: What happens if the numerator reaches 0 when the denominator is still negative?

The only solution with a velocity gradient that is positive at **all distances** requires that both the numerator and the denominator flip signs at the same distance. This so-called **critical solution** thus requires that

$$v = a \quad \text{where} \quad \frac{2a^2}{r_c} = \frac{GM_*}{r_c^2}$$

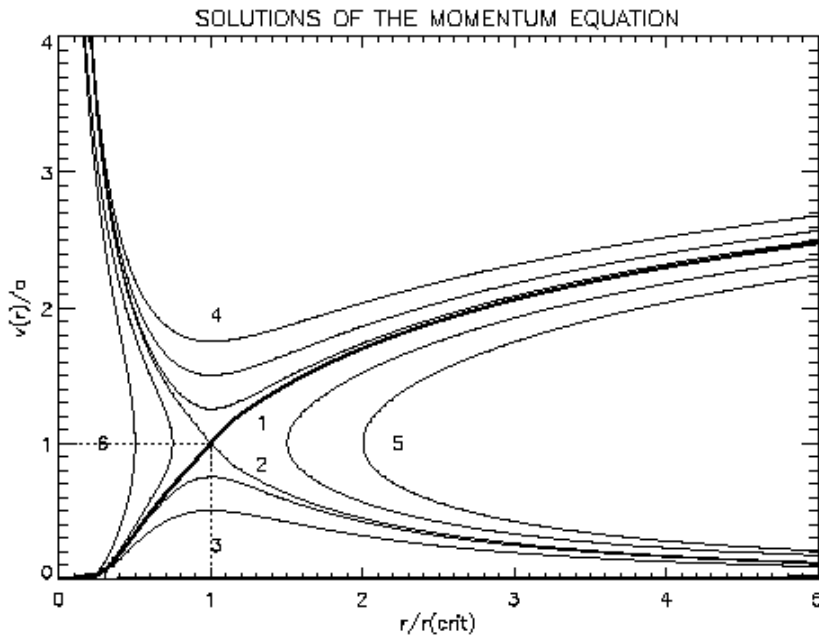


Fig 16.1 The topology of the solutions of the (critical) momentum equation of an isothermal wind. The critical point is $r_{\text{crit}} = r_c = GM_ / 2a^2$, where a is the isothermal sound speed $a^2 = \mathcal{R}T / \mu$. (ISW Fig 3.01)*

This shows that the wind reaches the sound speed at the critical point

$$r_c = GM_* / 2a^2$$

So we know v and r_c at critical point. If we can derive the density there, we know the mass loss rate. It turns out that the density structure in the subsonic region, $v < a$, is almost exactly the same as that of a hydrostatic atmosphere. For a hydrostatic isothermal atmosphere

$$\frac{1}{\rho} \frac{dp}{dr} + \frac{GM_*}{r^2} = 0 \quad \text{or} \quad \frac{r^2}{\rho} \frac{dp}{dr} = -\frac{GM_*}{a^2}$$

The solution of this equation gives the density structure in the subsonic region

$$\rho(r) = \rho_0 \exp \left\{ -\frac{(r-r_0)}{\mathcal{H}_0} \cdot \frac{r_0}{r} \right\} \quad \text{with scale height } \mathcal{H}_0 = \frac{\mathcal{R}T}{\mu g} = \frac{\mathcal{R}T}{\mu} \frac{r_0^2}{GM_*}$$

with r_0 is the bottom of the corona.

This gives an estimate of the density at the critical point r_c . Substituting this in the equation of mass conservation gives mass loss rate of coronal winds of

$$\dot{M} \simeq 4\pi r_c^2 a \rho_0 \exp \left\{ -\frac{(r_c-R_*)}{\mathcal{H}_0} \cdot \frac{R_*}{r_c} \right\} \quad \text{with } r_c = GM_* / 2a^2$$

where we have assumed that the bottom of the corona is at $r_0 = R_*$.

Quantitatively

$$\dot{M}/M_{\odot}/\text{yr} \simeq 1.2 \times 10^{-10} \left(\frac{T_c}{10^6}\right)^{1/2} \left(\frac{\rho_0}{10^{-14}}\right) \left(\frac{R_*}{R_{\odot}}\right)^2 \left(\frac{r_c}{R_*}\right)^2 \exp\left\{-2\left(\frac{r_c}{R_*} - 1\right)\right\}$$

$$\text{with } \frac{r_c}{R_*} = 6.9(M_*/M_{\odot})(R_*/R_{\odot})^{-1}(T_c/10^6)^{-1}$$

Notice that the dominant factor in the expression of \dot{M} is the exponential function. If $r_c \gg R_*$ then the exponent is $\ll 1$ and the mass loss rate is very small.

The table below (ISW Table 3.1) gives the predicted mass loss rates of coronal winds for main sequence stars and giants of 1 and $10 M_{\odot}$ for different coronal temperatures if $\rho_{\odot} = 10^{-14} \text{ g/cm}^3$ at the bottom of the corona.

Table 3.1 *Characteristics of isothermal winds with a density at the lower boundary of $\rho_0 = 10^{-14} \text{ g/cm}^3$.*

M_* (M_{\odot})	R_* (R_{\odot})	v_{esc} (km/s)	T (K)	a (km/s)	H_0 (R_*)	r_c (R_*)	$\frac{r_c - R_*}{H_0}$	\dot{M} (M_{\odot}/yr)
1	1	617.5	1.10^5	37.2	$7.3 \cdot 10^{-3}$	68.7	$9.3 \cdot 10^3$	$1.2 \cdot 10^{-68}$
			3.10^5	64.5	$2.2 \cdot 10^{-2}$	22.9	$1.0 \cdot 10^4$	$1.5 \cdot 10^{-28}$
			1.10^6	117.7	$7.3 \cdot 10^{-2}$	6.9	$8.0 \cdot 10^1$	$1.6 \cdot 10^{-14}$
			3.10^6	203.9	$2.2 \cdot 10^{-1}$	2.3	5.9	$8.2 \cdot 10^{-11}$
			5.10^6	263.2	$3.6 \cdot 10^{-1}$	1.4	1.1	$4.0 \cdot 10^{-10}$
1	100	61.7	3.10^3	6.4	$2.2 \cdot 10^{-2}$	22.9	$1.0 \cdot 10^3$	$1.5 \cdot 10^{-25}$
			1.10^4	11.8	$7.3 \cdot 10^{-2}$	6.9	$8.1 \cdot 10^1$	$1.6 \cdot 10^{-11}$
			3.10^4	20.4	$2.2 \cdot 10^{-1}$	2.3	5.9	$8.2 \cdot 10^{-8}$
			5.10^4	26.3	$3.6 \cdot 10^{-1}$	1.4	1.1	$4.0 \cdot 10^{-7}$
10	10	617.5	1.10^5	37.2	$7.3 \cdot 10^{-3}$	68.7	$9.3 \cdot 10^3$	$1.2 \cdot 10^{-66}$
			3.10^5	64.5	$2.2 \cdot 10^{-2}$	22.9	$1.0 \cdot 10^3$	$1.5 \cdot 10^{-26}$
			1.10^6	117.7	$7.3 \cdot 10^{-2}$	6.9	$8.0 \cdot 10^1$	$1.6 \cdot 10^{-12}$
			3.10^6	203.9	$2.2 \cdot 10^{-1}$	2.3	5.9	$8.2 \cdot 10^{-9}$
			5.10^6	263.2	$3.6 \cdot 10^{-1}$	1.4	1.1	$4.0 \cdot 10^{-8}$
10	1000	61.7	3.10^3	6.4	$2.2 \cdot 10^{-2}$	22.9	$1.0 \cdot 10^3$	$1.5 \cdot 10^{-23}$
			1.10^4	11.8	$7.3 \cdot 10^{-2}$	6.9	$8.1 \cdot 10^1$	$1.6 \cdot 10^{-9}$
			3.10^4	20.4	$2.2 \cdot 10^{-1}$	2.3	5.9	$8.2 \cdot 10^{-6}$
			5.10^4	26.3	$3.6 \cdot 10^{-1}$	1.4	1.1	$4.0 \cdot 10^{-5}$

¹ $M_{\odot}/\text{yr} = 6.303 \cdot 10^{25} \text{ g/s}$, $\mu = 0.60$

Notice that:

- For a star of $1 M_{\odot}$ and $1 R_{\odot}$ and $T_c = 1 \cdot 10^6 \text{ K}$ the coronal mass loss rate is $10^{-14} M_{\odot}/\text{yr}$, in good agreement with the observed rate of $2 \cdot 10^{-14} M_{\odot}/\text{yr}$. This is so small that it does not play a role in the MS evolution of the sun because $M \times t_{\text{ms}} \ll M_{\odot}$.

2. A red giant of $1 M_{\odot}$ and $100 R_{\odot}$ has a coronal mass loss rate of $\sim 10^{-7} M_{\odot}/\text{yr}$ if the coronal temperature is only $3 \times 10^4 \text{ K}$ and it increases strongly with increasing T_c .
3. Appreciable mass loss rates of $M > 10^{-8} M_{\odot}/\text{yr}$ are only obtained for coronal winds which reach their critical point r_c at less than about 10 scale heights above the photosphere.

Q: Why is \dot{M} very strongly dependent on $(r_c - R_*)/H_0$?

16.2 Dust Driven Winds of Pulsating Stars (ISW Chapter 7)

Cool stars can have dust in their outer envelopes. Dust is an efficient absorber of radiation so the absorption of stellar photons by dust grains produces transfer momentum from the photons to the dust grains (= radiation pressure) which are then accelerated outwards. The dust grains collide with the gas atoms and molecules and drag these outward as well, producing a stellar wind.

16.2.1 Dust Opacity and Radiation Pressure (ISW 7.3)

Q: Observations show that the average dust/gas ratio (by mass) is about 0.01.
Why is it so low?

Suppose that the dust grains are spherical with a mean radius a and a mean density ρ_d . For icy particles $\rho_d \approx 1 \text{ g/cm}^3$ and for silicates (sand) $\rho_d \approx 4 \text{ g/gm}^3$. For simplicity we adopt a mean value of $\rho_d \approx 2 \text{ g/cm}^3$. So 1 gram of gas contains $n_d = 3.10^{-2}/4\pi a^3 \rho_d$ dust grains, with a total cross section $n_d \pi a^2$. The total absorption coefficient of one gram of dusty gas

$$\kappa_d = n_d \pi a^2 Q \simeq \frac{3 \times 10^{-2} Q}{4 a \rho_d} \simeq 10 \text{ cm}^2 \text{ per gram of gas}$$

where $Q \approx 10^{-2}$ is the efficiency factor for absorption and scattering and the mean particle radius is $a \approx 0.05 \mu$.

The wind can be driven by dust if the radiation pressure force exceeds gravity

$$\frac{L\kappa}{4\pi r^2 c} > \frac{GM_*}{r^2} \quad \rightarrow \quad L > \frac{4\pi GM_* c}{\kappa} \quad \rightarrow \quad \frac{L}{L_{\odot}} \gtrsim 10^3 \frac{M}{M_{\odot}}$$

This is the case for stars with $M > 10 M_{\odot}$ i.e. for massive Red Giants, and for Red Supergiants and AGB stars.

16.2.2 The Temperature of Dust

The temperature of dust can easily be calculated by radiative equilibrium: the amount of energy absorbed per second = the emitted radiation.

The energy absorbed by a grain per second is $E_{\text{in}} = \pi a^2 Q_{\text{abs}} \frac{L}{4\pi r^2}$ with $L = 4\pi R_*^2 \sigma T_{\text{eff}}^4$ where L is the stellar luminosity and r is the distance of the grain from the star.

The energy radiated per second (black body) is $E_{\text{out}} = 4\pi a^2 Q_{\text{em}} \sigma T_d^4$ Where Q_{em} is the emission efficiency with $Q_{\text{abs}} \approx Q_{\text{em}}$.

Equating these two gives the dust temperature at distance r from the star

$$T_d \simeq T_{\text{eff}} \left(\frac{R_*}{2r} \right)^{1/2}$$

NB:

T_d is independent of the size of the dust grains. So this equation can also be used to estimate the mean temperature of planets (with a small correction for their reflection by clouds or ice).

Q? Check this for the Earth.

Dust sublimates if it gets hotter than the condensation temperature, T_{cond} , which is about 1200 to 1500 K for different types of dust. This means that dust can form only at

$$\frac{r}{R_*} \gtrsim \frac{1}{2} \left(\frac{T_{\text{eff}}}{T_{\text{cond}}} \right)^2$$

For a cool stars of $T_{\text{eff}} = 3000K$ dust can only form at $r \approx 2 R_*$, i.e. about R_* above the surface.

16.2.3 The problem of the scale height and the role of pulsation

We have seen above that all cool stars with $L/L_{\text{sun}} > 10^3 M/M_{\text{sun}}$ could in principle drive a wind by radiation pressure on dust grains. However, we have also seen that dust can only form at $\sim 2R_*$. This creates a serious problem, because if there is no wind the density at a distance of $2R_*$ is so low that dust formation at $2R_*$ would be extremely inefficient: **so if there is no wind, dust cannot form and if dust cannot form there is no wind.**

We can express this problem in terms of photospheric scale height. We have seen in the discussion of the coronal wind that the density decrease in the subsonic structure (where $v < a$ and $f_{\text{rad}} < GM/r^2$) is given by

$$\rho(r) \simeq \rho_0 \exp \left\{ -\frac{(r-R_*)}{H_0} \cdot \frac{R_*}{r} \right\} \quad \text{with} \quad H_0 = \frac{\mathcal{R} T_{\text{eff}}}{\mu g}$$

Apply this to a Red Giant with $M \approx 1M_{\text{sun}}$, $R = 40R_{\text{sun}}$, $L = 100L_{\text{sun}}$, $T_{\text{eff}} = 3000\text{K}$, $g = 20 \text{ cm/s}^2$, $\mu = 1$, $H_0 = 0.18R_{\text{sun}} = 0.004R_*$, and a photospheric density of $\rho_0 \approx 10^{-12} \text{ g/cm}^3$. We see that at a distance of $r = 2R_*$ which is $250 H_0$ above the photosphere, the density is 10^{-54} smaller than the photospheric density!! Even for an AGB star of $1M_{\text{sun}}$ and $R = 300R_{\text{sun}}$ dust can only form at $2R_*$, i.e. $2.5 H_0$ above the photosphere, where $\rho \approx 10^{-6} \rho_0 \approx 10^{-18} \text{ g/cm}^3$ and dust would form very slowly.

The only way in which the density at $2R_*$ could be increased drastically is by increasing the density scale height H_0 in the region between R_* and $2R_*$. Here is where pulsation comes in!

Many RGs and AGB stars are pulsating. Pulsation tosses the outer layers up, giving rise to a slower density decrease than in a hydrostatic atmosphere. This is depicted in Fig. 16.2

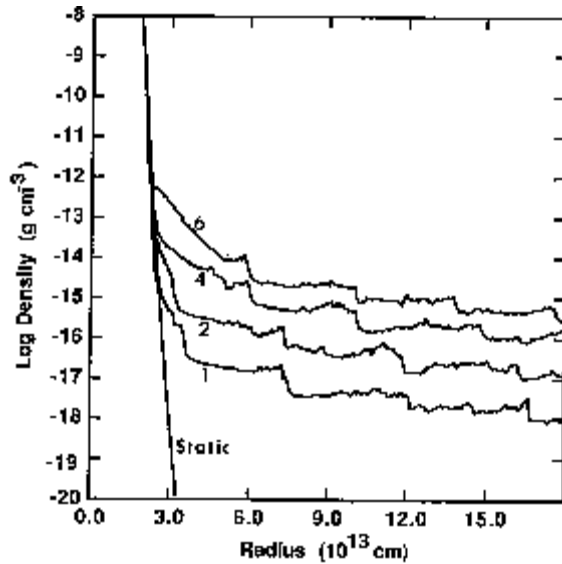


Fig 16.2 The density structure in the atmosphere, $\rho(r)$, of a pulsating AGB star of $R_ = 250R_{\text{sun}}$ for different pulsation amplitudes of 1, 2, 4 and 6 km/s. The structure is ragged because it shows $\rho(r)$ at one particular time in the pulsation cycle. The straight line is the density structure if the star would not pulsate. Notice the much slower decrease in density due to pulsation, which is equivalent to a large increase in the density scaleheight. (Fig ISW 7.6, based on Bowen, 1988)*

The figures below show the motions of the outer layers above the photosphere (at $r > R_* = 2 \times 10^{13} \text{ cm}$) without dust (left) and with dust (right).

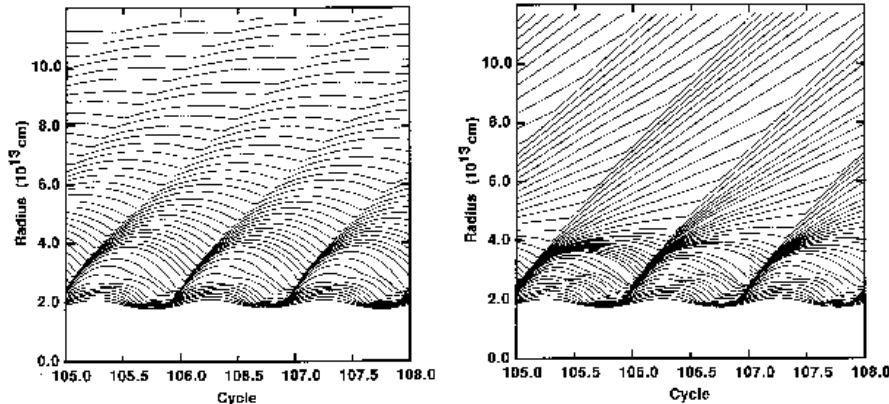


Fig 16.3 The motions of the outer layers above the photosphere (at $r > R_ = 2 \times 10^{13} \text{ cm}$) of a pulsating star without dust (left) and with dust (right). The right figure shows that once the matter has reached a distance of $2R_*$ it is accelerated outward by radiation pressure on dust and moves outward.*
(Fig ISW 7.5, from Bowen 1988)

Fig. 16.4 shows empirical evidence that the mass loss of Mira variables is related to their pulsation.

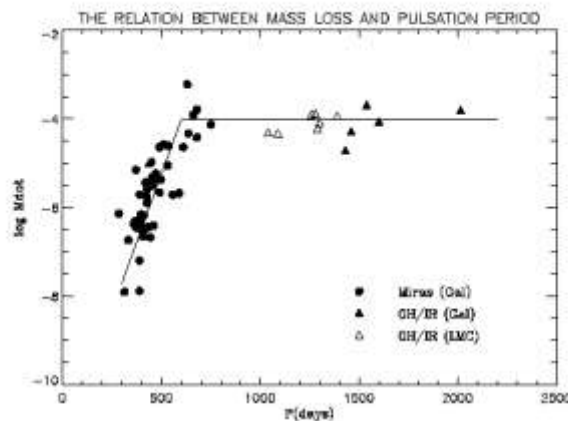


Fig. 16.4 The mass loss rates of Mira variables increases with increasing pulsation periods, until it saturates at a mass loss rate of about $10^{-4} M_{\odot}/\text{yr}$.
(ISW Fig. 2.26, based on Vassiliades and Wood 1993)

16.3 Line-driven winds of hot stars

(ISW Chapter 8)

Line driven winds are due to **the transfer of the momentum of the stellar radiation to the gas above the photosphere.**

Hot stars with $T \gtrsim 30000K$ emit most of their light in the UV. This is also where most of the abundant elements, mainly C, N, O, Si, S, Fe, etc. have their strongest spectral lines, i.e. where the photons are most easily absorbed by electron transitions in the ions. These specific ions are accelerated by the repeated absorption or scattering of photons. Hydrogen does not produce any radiation pressure because it is ionized and has no electron transitions. Helium can add a little bit of the radiation pressure, but He II has few absorption lines and the strongest ones are very far in the UV where the stellar flux is low. So only a small fraction of all ions are accelerated. However, because of the frequent interactions of these ions with protons and electrons (Coulomb interaction of charged particles), all the gas is dragged along.

16.3.1 A few simple estimates: the momentum of the wind

Suppose a particular abundant ion in the wind of an O-star, i.e. a C IV ion, has one very strong absorption line at a wavelength λ_0 that corresponds to the peak of the Planck function for that star. Assume that it is so strong that the line is optically thick and absorbs or scatters all photons at its wavelength. How much mass loss can one absorption line produce?

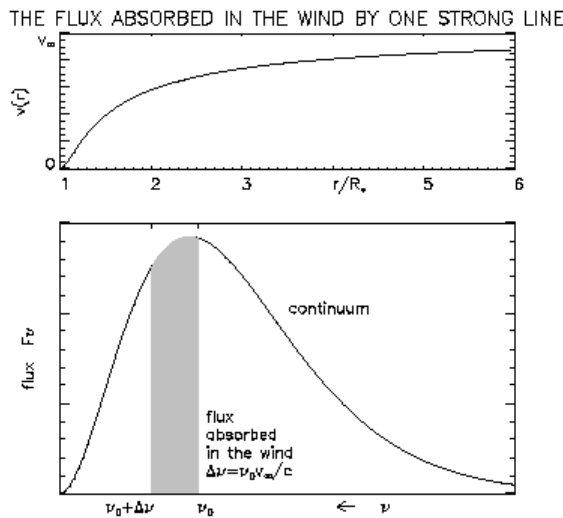


Fig. 16.5. Upper figure: the velocity of a stellar wind increases from 0 at the photosphere to v_∞ at large distance. Lower figure: the flux absorbed by one strong spectral line of rest frequency ν_0 , near the peak of the stellar energy distribution. All photons emitted by the photosphere in the shaded area are absorbed or scattered in the wind. (ISW Fig 8.2)

Suppose that the wind of that star has a velocity loss that increases from $V = 0$ at the photosphere to V_∞ at large distances. Due to the Doppler shift, those ions absorbs all photons in the frequency range ν_0 to $\nu_0(1 + \frac{V_\infty}{c})$. So the total energy absorbed per second is

$$L_{\text{abs}} = \int_{\nu_0}^{\nu_0(1 + \frac{V_\infty}{c})} 4\pi R_*^2 F_\nu d\nu = L_\nu \cdot \Delta\nu \quad \text{with} \quad \Delta\nu = \nu_0 V_\infty / c$$

The momentum of photons is $h\nu/c$ so the **total momentum** transferred from the radiation into the wind per second is L_{abs}/c . The momentum of a gram of gas that leaves the star with a velocity $m v = 1V_\infty$. So the total momentum loss in the wind per second is $\dot{M}V_\infty$.

For a wind that is driven by the transfer of momentum from stellar photons to the gas, $\dot{M}V_\infty$ must be equal to the radiative momentum put into the wind per second, so

$$\dot{M}V_\infty = L_{\text{abs}}/c = L_\nu \cdot \Delta\nu/c = L_\nu \nu_0 V_\infty / c^2$$

At the peak of the Planck function $L_\nu \nu_0 \simeq 0.6L$ and so we find that one strong spectral line can drive mass loss rate of

$$\boxed{\dot{M} \simeq 0.6L/c^2 \simeq L/c^2} \quad \text{per optically thick spectral line.}$$

For a hot star of $L = 10^6 L_\odot$ this corresponds to a mass loss rate of about $7 \times 10^{-8} M_\odot/\text{yr}$. If the spectrum contains N_{eff} optically thick spectral lines, with $N_{\text{eff}} \simeq 10^2$, then the mass loss rate of that star is

$$\dot{M} \simeq N_{\text{eff}} L/c^2 \simeq 10^2 L/c^2 \simeq 7.10^{-6} M_\odot/\text{yr}$$

which is about the mass loss rate of luminous hot stars!

If the spectrum is **completely covered** with optically thick absorption lines then **all** the photons from the star are absorbed or scattered in the wind and the momentum of the wind is equal to the momentum of the radiation. This provides an upper limit for a radiation driven wind of

$$\dot{M}_{\text{max}} V_\infty < L/c \rightarrow \boxed{\dot{M}_{\text{max}} \simeq L/V_\infty c}$$

The wind velocities of hot stars are typically 2 or 3 times the escape velocity at the photosphere: $V_\infty \simeq 3\sqrt{2GM/R}$

For a typical O main sequence star this is about $V_\infty \simeq 2000 \text{ km/s}$. So the maximum radiation driven mass loss of an O-star of $L \simeq 10^5 L_\odot$ is $1.10^{-6} M_\odot/\text{yr}$ and for a star of $10^6 L_\odot$ it is $10^{-5} M_\odot/\text{yr}$. These values are close to the observed mass loss rates of massive O and B supergiants.

It is interesting to compare the kinetic energy loss of the wind, $E_w = \dot{M}v_\infty^2/2$, with the energy loss by stellar radiation, L . For the $10^6 L_\odot$ star mentioned above:

$$\frac{E_w^{\max}}{L} \simeq \frac{\dot{M}_{\max} v_\infty^2}{2L} \simeq \frac{v_\infty}{2c} \ll 1$$

Even if all photons from the star are absorbed and scattered in the wind, the wind carries away only a small fraction of the luminosity. The fact that the observed mass loss rates of luminous stars are close to the expected maximum values in case the winds are driven by radiation pressure, but the maximum observed stellar wind energy is very much smaller than the luminosity of the star, shows that these **winds are driven by the momentum of the stellar radiation and not by its energy.**

Remarks

- i. The first scattering (absorption + re-emission) of a photon that leaves the star is most efficient for transferring its outward directed momentum, because of its outward direction. The second or third scattering of the photon is less efficient in this respect, because it will come from a random direction.
- ii. In the estimates above we have assumed that the outward directed momentum of a stellar photon can be used only once. In reality, if there are many spectral lines, and the photons are scattered multiple times, the total momentum transfer can be increased by at most a factor of $\simeq 3$. So some hot stars have mass loss rates slightly higher than the value of \dot{M}_{\max} calculated above.

16.3.2 The lines that drive the winds of hot stars

Fig. 16.6 The wavelength distribution of the spectral lines that drive the winds of luminous hot stars. (ISW Fig 8.10)

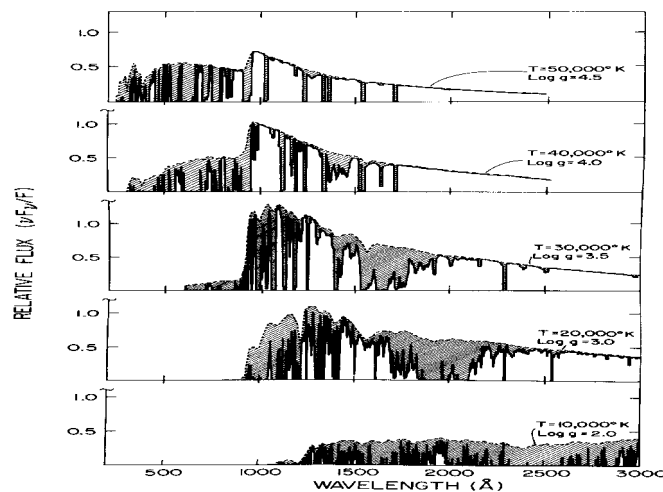


Fig 16.6 shows the fraction of the stellar radiation that is scattered or absorbed in the winds of stars of different T_{eff} .

Notice the enormous numbers of spectral lines that can be used for momentum transfer. At $T_{\text{eff}} < 30\,000\text{K}$ the driving is mainly done by absorption lines of Fe-group elements (Fe, Ni, Co). At $T_{\text{eff}} > 30\,000\text{K}$ the ions of C, N and O are mainly responsible for the mass loss.

16.3.3 Mass loss rates and wind velocities of line driven winds

The winds from massive stars are due to radiation pressure onto the outer atmospheres of stars due to a multitude ($\sim 10^5$) of optically thick and thin spectral lines in the UV. Both observations and theory show that the mass loss can be described by a formula of the type

$$\log(\dot{M}v_{\infty}R_*^{1/2}) = A + B \log(L/L_{\odot}) + C \log(Z/Z_{\odot})$$

with the left side in units of [$M_{\odot}/\text{yr} \times 1000 \text{ km/s} \times \sqrt{R_{\odot}}$]

where	$A = -6.74$	and	$v_{\infty} \sim 2.6 v_{\text{esc}}$	if	$T_{\text{eff}} > 21000\text{K}$
	$B = +1.51$		$v_{\infty} \sim 1.3 v_{\text{esc}}$	if	$10000 < T_{\text{eff}} < 20000\text{K}$
	$C = +0.85$		$v_{\infty} \sim 0.7 v_{\text{esc}}$	if	$8000 < T_{\text{eff}} < 10000\text{K}$

(A more elaborate and more accurate description is given in Sect. 16.4). Fig. 16.7 shows the observed terminal velocities of the winds of early type supergiants. Notice that the ratio $v_{\infty}/v_{\text{esc}}$ is different for different stellar temperatures ranges. The transitions between these regimes are called **bi-stability jumps**.

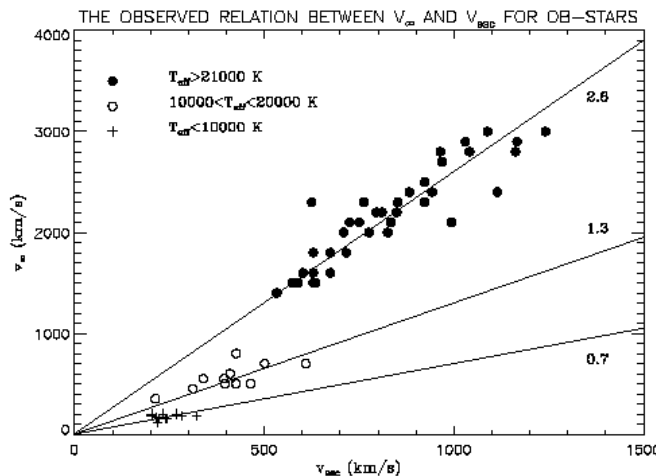


Fig 16.7: The observed relation between v_{∞} and v_{esc} for the line driven winds of hot luminous stars. (ISW Fig 2.20, after Lamers et al. 1995)

The physical reasons for this expression comes from the theory of line driven winds as first described by Castor, Abbott and Klein (1975, ApJ, 195, 157), called **CAK theory**, which predicts (ISW 8.7.1)

$$\dot{M} \sim L^{\frac{1}{\alpha}} M_{\text{eff}}^{\frac{\alpha-1}{\alpha}} \quad \text{with} \quad M_{\text{eff}} = M_*(1 - \Gamma_e) \quad \text{and} \quad \Gamma_e = \sigma_e L_* / 4\pi c GM$$

where Γ_e is the Eddington factor (see Sect 8.3) that corrects the stellar mass for radiation pressure by electron scattering, and

$$v_\infty \simeq 2v_{\text{esc}} \sim (M_{\text{eff}}/R_*)^{1/2}$$

where α is a factor, $0 < \alpha < 1$, that describes the ratio between the contribution by strong (optically thick) spectral lines and weak (optically thin) spectral lines to the line radiation pressure.

So the momentum loss of the wind is

$$\dot{M}v_\infty \sim L^{1/\alpha} R_*^{-1/2} M_{\text{eff}}^{1-\frac{1}{\alpha}+1/2}$$

It turns out that $\alpha \simeq 2/3$ so $1 - \frac{1}{\alpha} + \frac{1}{2} \simeq 0$ so the mass drops out of the expression for the wind momentum. This is nice because the mass of a star is usually much less well known than L , \dot{M} , or v_∞ . So we can expect

$D_{\text{obs}} \equiv \dot{M}v_\infty R_*^{\frac{1}{2}} \sim L^{1/\alpha}$

where D is called “**modified Wind momentum**” (Kudrtizki et al 1995). Observations show that this relation is so tight, that it can be used to derive luminosities of massive stars, if the mass loss rates and wind velocities are derived from spectra. Stars with known distance and luminosities can be used to determine the proportionality constant.

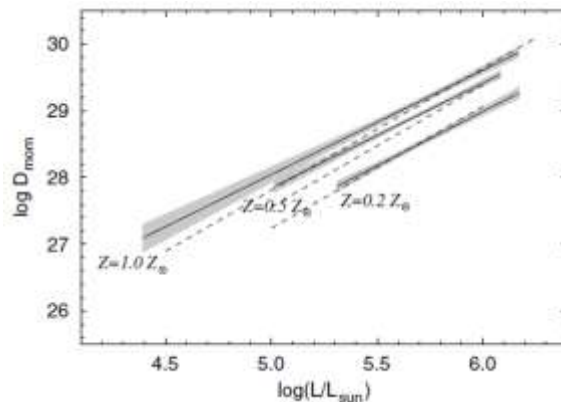


Fig 16.8
The observed modified wind momentum versus L relation. Grey bands are observations of Galactic, LMC and SMC stars by Mokiem et al. (2007). Dashed lines show the predictions by Vink et al. (2001), discussed in Sect 16.4.

16.3.4 Mass loss rates of massive main sequence stars

M	30	50	80	100
log L/L ₀	5.15	5.58	5.97	6.16
log \dot{M}	-6.51	-5.86	-5.27	-4.99

A few typical values for main sequence stars. These rates are so high that massive stars lose about 10 to 20% of their initial mass during the MS phase!

Q? Check this!

16.4 Mass loss formulae used for stellar evolution

16.4.1 Massive O, B, A stars

Vink et al. (2001, AA 369, 572) predicted mass loss rates of luminous hot stars of $L > 3 \cdot 10^4 L_{\text{sun}}$, based on the line driven wind theory, using Monte Carlo simulations to follow the track of a large number ($> 10^5$) of photons in the wind and derive their momentum transfer from photons to the gas. These predictions fit the observations very well. They derived formula of the type:

$$\log \dot{M} = A + B \log(L/10^5 L_{\text{sun}}) + C \log(M/30 M_{\text{sun}}) + D \log(0.5 v_{\infty}/v_{\text{esc}}) \\ + E \log(T_{\text{eff}}/T_{\text{ref}}) + F (\log(T_{\text{eff}}/T_{\text{ref}}))^2 + G \log(Z/Z_{\text{sun}})$$

with \dot{M} in M_{sun}/yr , $Z_{\text{sun}}=0.02$ and $v_{\infty}/v_{\text{esc}}$ as described in sect 16.3.3.

For the temperature ranges of $27500 < T_{\text{eff}} < 50000$ and $12500 < T_{\text{eff}} < 22500$ the constants are respectively

A = -6.697	-6.688
B = +2.194	+2.210
C = -1.313	-1.339
D = -1.226	-1.601
T _{ref} = 40 000	20 000
E = + 0.933	+1.07
F = -10.92	0
G = +0.85	+0.85

These formulae are now used in most stellar evolution codes.

Fig 16.8 shows a comparison between these predictions and observations for luminous hot stars in the Galaxy, the LMC and the SMC.

16.4.2 Wolf-Rayet stars

Wolf-Rayet stars are late stages of massive stars that have almost completely lost their H-rich envelope. (They will be discussed later)

Nugis and Lamers (2000, AA 360, 227) derived an expression for the mass loss of Wolf-Rayet stars from the observations of 64 C-rich and N-rich (WN) stars.

$$\dot{M} \simeq 2.8 \cdot 10^{-5} \left(\frac{L}{10^5} \right)^{1.29} Y^{1.7} Z^{0.5} \quad \text{where } Y \text{ is the Helium mass fraction}$$

16.4.3 Non-pulsating Red supergiants: the Reimers-relation

Reimers (1975, Mem. Soc Roy Sci Liege 6° Serie 8, 369) derived mass loss rates of 6 red giants and supergiants with $4 < M < 18 M_{\odot}$, $10^3 < L < 10^5 L_{\odot}$, $40 < R < 600 R_{\odot}$ and $3500 < T_{\text{eff}} < 5000$ K. He derived the empirical relation

$$\boxed{\dot{M} = -4 \times 10^{-13} \eta_R \frac{L}{L_{\odot}} \frac{R}{R_{\odot}} \frac{M_{\odot}}{M} \quad M_{\odot}/\text{yr}}$$

where η_R is a correction factor that was later added to adjust this to more observations and different types of late type stars. This is the famous **Reimers relation**, which is often used in evolution codes to describe the mass loss rates of cool stars.

- Q?** What would η_R be if the Reimers relation was used to predict \dot{M} of the Sun?
Notice that this empirical relation implies that

$$\dot{M}M/R \sim \dot{M}(GM/R) \sim \dot{M}v_{\text{esc}}^2 \sim L .$$

Winds of cool supergiants and AGB stars have $v_{\infty} \ll v_{\text{esc}}$. So **the Reimers relation implies that for these stars a fixed fraction of the stellar luminosity is used to provide the potential energy of the winds, that allows the gas to escape the gravity of the star.** (This is different from the case of the hot stars where the *momentum* of the wind scaled with the *momentum* of the radiation).

16.4.4 Pulsating Miras and AGB stars

Vassiliadis and Wood (1993, ApJ 413, 641) derived empirically from the infrared of dusty winds (see Fig 16.4)

$$\begin{aligned} \log \dot{M} &= -11.4 + 0.0123 \quad P(\text{days}) && \text{if } P < 600 \text{ days and } M < 2.5 M_{\odot} \\ \log \dot{M} &= -11.4 + 0.0123 \quad \left\{ P(\text{days}) - 100 \left(\frac{M}{M_{\odot}} - 2.5 \right) \right\} && \text{if } P < 600 \text{ days and } M > 2.5 M_{\odot} \\ \log \dot{M} &= -4.0 && \text{if } P > 600 \text{ days} \end{aligned}$$

all with

$$\log P_{(\text{days})} = -2.07 + 1.94 \log(R_*/R_\odot) - 0.9 \log(M/M_\odot)$$

The terminal velocity of these winds is about 5 to 20 km/s.

H16.1. Homework

- a. Calculate the mass loss rate at the ZAMS and TAMS of stars of 20, 40, 60, 120 M_{sun} , and solar metallicity, using Schallers (1992, AA Sup 96, 269) stellar data and Vink's equations.
Hint: The TAMS is the point in the models where X is “almost” 0 in the center, and the star makes a short left loop in the HRD.
Take the mean value and estimate the fraction of mass that is lost from these stars during the Main Sequence.
Compare this with the mass that is lost in Schallers models and realize that Schaller calculated his models before Vink made his predictions.
- b. Do the same for 60 M_{sun} models of LMC and SMC metallicity and compare it with the solar metallicity.
- c. Calculate the mass loss rates of non-pulsating red giants (H-shell burning) of 1, 2 and 5 $M_\odot L_{\text{sun}}$ at (a) the end of the MS phase = beginning of the red sub-giant branch, (b) when the star reaches the Hayashi limit and (c) when the star has reached the tip of the RGB. Use Reimers formula $\eta=1$
Use the duration of the sub-giant phase and the RGB in Table F for solar metallicity to estimate the total amount of mass that is lost during H-shell fusion.
- d. Calculate the mass loss rates of pulsating cool stars of 1, 2 and 5 M_\odot using the data for AGB stars from Appendix F.

H16.2 Homework

Calculate the mass loss rates for a variety of O, B and A stars with $L > 3 \cdot 10^4 L_{\text{sun}}$, for which the Vink et al. (2001) predictions apply, using stellar data from Appendix B1 to B3.

Show that these predictions support the empirical statement that $D \sim L^{1/\alpha}$ and derive the empirical value of α .

17. Mass ranges of Post-MS Evolution

For describing the evolution of stars it is useful to separate **five ranges** of their initial mass

- a. **$M_i < 0.08 M_\odot$** : these stars do not reach H-fusion and are brown dwarfs.
- b. **$0.08 < M_i < 0.8 M_\odot$** : these stars go through H-fusion, but will not reach He-fusion, so they end as He-rich white dwarfs.
The evolution of these stars is not discussed in these lectures because their MS lifetime is longer than the Hubble time.
(He-rich WDs can be formed in close binaries with mass transfer or mass stripping if the stars were initially $M \gtrsim 0.8 M_\odot$.)
- c. **$0.8 < M_i \lesssim 2 M_\odot$** : in these stars the fusion of Helium is ignited in a degenerate core so the stars go through a Helium flash and end as CO-rich white dwarfs.
- d. **$2 \lesssim M_i \lesssim 8 M_\odot$** : in these stars the Helium fusion is ignited in a non-degenerate core so they go through a Helium flash, but they do not make it to C-fusion because of insufficient core mass or due to severe mass loss in the AGB phase.
- e. **$M_i \gtrsim 8 M_\odot$** : these stars can go through all evolution phases and end their lives as supernovae.

The mass limits between these regions have been derived from stellar evolution models compared with observations. The mass limits between the regions are not very strict because they depend on metallicity, mass loss and overshooting. For instance, more overshooting will give more massive cores; and lower mass loss rates on the AGB will allow stars initially less massive than $8 M_\odot$ to reach C-fusion.

In addition, the evolution of close binaries may involve mass transfer (accretion or stripping) or severe mass loss (non-conservative mass transfer) or even merging. All of these effects may drastically change the evolution of a star.

18. H-Shell Fusion and the Red Giant Branch

18.1 The start of the H-shell fusion

When H is exhausted in the core, the core contracts. The layers around it also contract and their temperature increases to above $T > 10^7 \text{ K}$, i.e. hot enough for shell H-fusion.

In the stars of $M \gtrsim 1.2 M_\odot$, which had a convective core during the MS-phase, the whole star contracts before H-shell fusion starts. This is because the whole core is out of H at the same time due to the equalization of the abundances by convection. This produces a shrinking of the stellar radius and produces a small leftward motion in the HRD (see tracks in Fig 14.1 and Appendix E).

(N.B. There is no shell mirror-action in this phase because the shell is not yet ignited.) This shrinking of the radius ends when the H-fusion is ignited in the shell.

In stars of $M \lesssim 1.2 M_\odot$ the H-fusion in the shell starts gradually because the chemical profile is gradual. So as the core contracts, the regions around it where fusion is going on at a slower pace gradually become hotter and denser. So the transition from H-core fusion to H-shell fusion is smooth. So the envelope of these stars does not contract and the evolution tracks do not show the small leftward loop (see tracks in Appendix E)

18.2 The H-shell fusion phase of a star of $1 M_\odot$

We first describe the evolution of a $1 M_\odot$ star as an example of the evolution of a star with $0.8 \lesssim M \lesssim 2 M_\odot$.

In presenting the evolution of the stars we will use the combination of their tracks in the HRD combined with their **Kippenhahn-diagram** (Kippenhahn, 1965). These diagrams show the changes in the interior structure as a function of time (horizontal axis) and mass fraction (vertical axis), with various colours and shadings to indicate regions of different fusion phases, convection and composition changes. The combination of the Kippenhahn diagram with the HRD provides very good insight into stellar evolution.

The figure below shows the evolution in two ways:

1. The evolution track in the HRD.
2. The Kippenhahn diagram (KD) with the letters corresponds to the location in the HRD at that time. The fusion regions are indicated by hatched areas with thick and thin hatching for efficient and inefficient fusion.

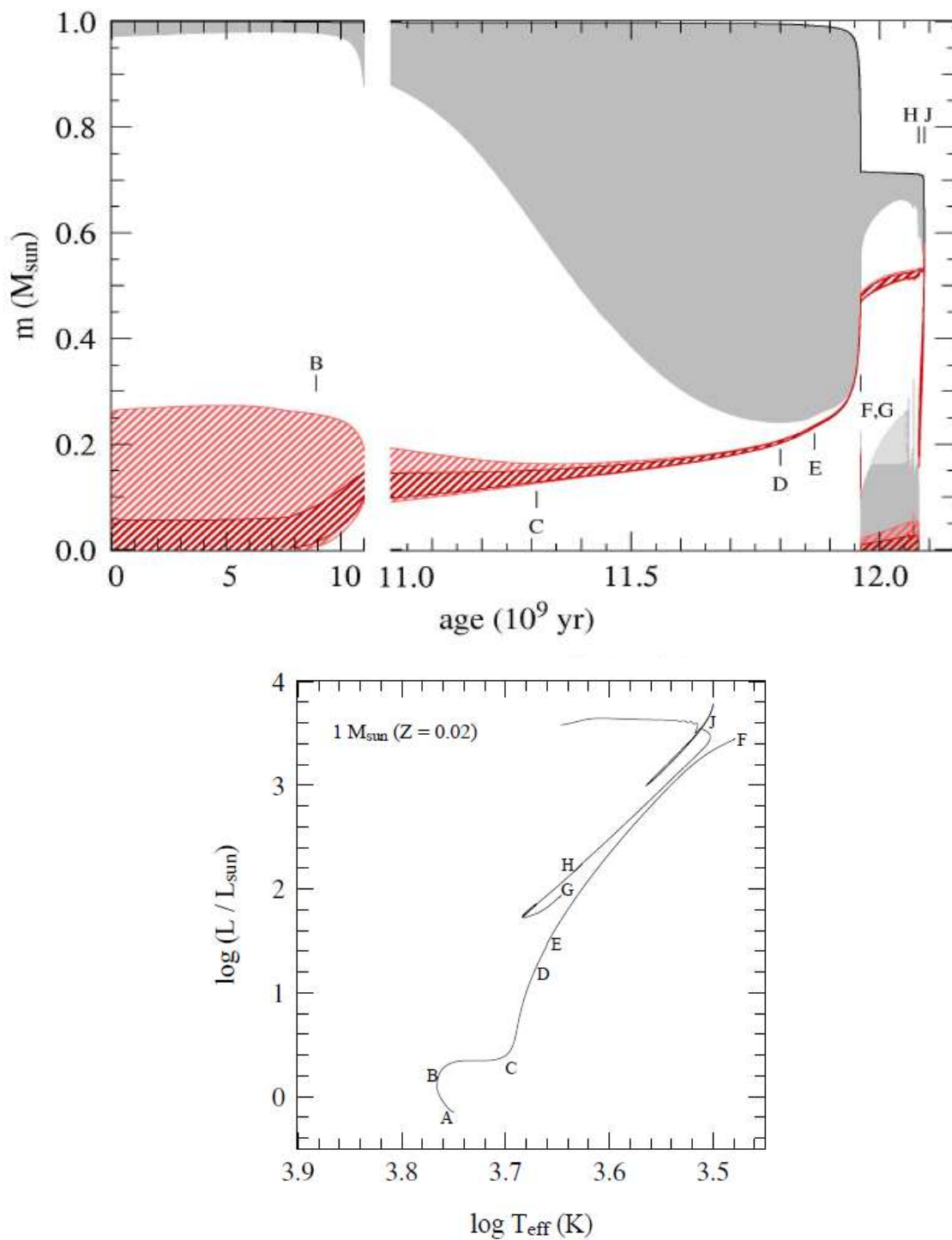


Fig 18.1 The Kippenhahn diagram and the HR-diagram showing the evolution of a star of $1 M_{\odot}$. Hatched areas indicate fusion regions. Dark hatched for efficient fusion ($\epsilon > 5 L/M$) and light hatched for inefficient fusion ($\epsilon < 5 L/M$). Grey regions indicate convection. The light grey area indicates semiconvection. (See Pols, Fig. 9.5, for a colour version.)

A-B: The main sequence phase of H-fusion in the core.

B: H becomes exhausted in the center ($X < 10^{-3}$) at point B. At that point H-shell fusion starts. Because of the mirror effect of the shell, the outer layers expand as the core contracts and the star moves to the right in the HRD. Meanwhile an increasingly fraction of the stellar mass becomes convective. The phase B-C lasts about 2 Gyrs. The star is now on the “**sub-giant branch**.”

C: At this point about half of the stellar mass is convective and the star is so large that it reaches the **Hayashi line**. From now on it is a “**red giant**”. Around that time the **He-core has become degenerate!**

C-D: The H-shell fusion keeps adding mass to the degenerate core, which therefore contracts. (Degenerates cores shrink as mass is added). Because of the mirror-action of the H-fusion shell, the envelope expands. The star is on the Hayashi line, so its T_{eff} hardly changes, which implies that the expansion results in an increasing luminosity. (The star climbs the Hayashi line in the HRD during the “**red giant branch**” phase). As the **core contracts** the density in the shell increases because it is directly on top of the degenerate core, and so the shell-fusion becomes more efficient. This produces the increasing luminosity required by H.E. and T.E. for stars on the Hayashi track! Notice that the mass in the fusion shell gets smaller (narrower in the KD) because less mass is needed for the higher fusion-efficiency.

The star climbs the red giant branch for about 0.5 Gyr.

D: Near point D the outer convection reaches so deep into the star (to $m(r) = 0.25$), that the products of H-fusion from the main sequence are mixed to the surface. The surface abundance may now start to show evidence of a slight enrichment by He (difficult to detect in spectra of cool stars) and change in N abundance (from 0.0013 to 0.0020) and a decrease of C and O.

This is called “**the first dredge-up**.”

Q?

Check this with the Schaller models (1992).

D-E-F: As the degenerate core gets more massive, it keeps shrinking and so the star keeps expanding and the luminosity increases. The H-shell fusion reaches hotter layers and becomes more efficient, producing the required luminosity. This results in a faster and faster growing of the core and an even more rapid increase in luminosity, etc. This acceleration of the evolution can clearly be seen in the KD, by the **fast growth of the core mass**. The increase in efficiency of the shell fusion can also been seen in this diagram, because the mass of the shell decreases whereas its energy output (luminosity) increases.

E: At this point the shell has reached a mass zone, $m(r) = 0.3 M_{\odot}$, which was earlier reached by the deepest extent of the convective envelope. The convection has mixed fresh H from the outer layers down to this depth. (Although the main H-fusion occurred in deeper layers, there had been some

depletion of H due to inefficient fusion during the MS phase. This can be seen in the Fig 14.4: at the end of the MS phase X was reduced to about 90% of its initial value.) So at phase E, the H-fusion shell finds itself in a layer with a higher H content and a lower mean atomic weight than before. As a consequence, it starts burning at a slightly lower rate. In fact, its luminosity temporarily decreases (because L_H depends on μ) and the star moves slightly down the Hayashi track as it shrinks a little. This produces a “loop” in the track, that is shown in Fig. 18.2. The star spends about 20% of its RGB time near this loop. **This produces the observed red clump** in the luminosity distribution of RGB stars.

(Note: the luminosity of the red clump depends very sensitive on the stellar parameters such as metallicity and adopted overshooting)

Q? Why is it so sensitive to these parameters?

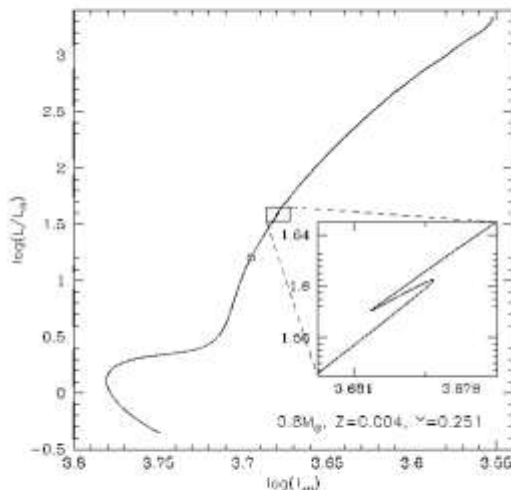


Fig 18.2 The loop in the RGB evolution of a star of $0.8 M_{\text{sun}}$ occurs when the H-fusion shells finds itself in a layer where the H-abundance is larger because envelope convection. This loop causes the red clump in the observed luminosity distributions. (Fig 5.16 from SC)

E-F: During this phase the shell is burning in a region of higher H-abundance, so the fusion can be slower and still produce the required luminosity. Therefore the phase from E-F lasts longer than the phase D-E, although the luminosity is higher.

Q? Check this on the KD and the HRD.

F: At this point the degenerate core has reached a mass of about $0.45 M_{\odot}$. The contraction of the core has resulted in a temperature high enough for igniting He-fusion in the degenerate core. The star leaves the Red Giant Branch.

18.3 The H-shell fusion phase of stars of $1-2 M_{\odot}$

The H-shell fusion of stars in the mass range of up to $2 M_{\odot}$ is qualitatively similar to the one described above. The main difference is that the cores of stars with $M > 1 M_{\odot}$ become degenerate at a slightly later age on the RGB. Once they have a degenerate core, the evolution of the cores is similar for all stars with $1 < M < 2 M_{\odot}$ because the shell fusion is then set by the mass of the core and the pressure of the shell directly on top of it.

18.4 The H-shell fusion phase of stars of $2-8 M_{\odot}$

The H-shell fusion evolution of stars more massive than $M > 2 M_{\odot}$ is similar to that of the lower mass stars, except that the core does not become degenerate during this phase.

Fig 18.3 shows the HRD and KD diagrams of a star of $5 M_{\odot}$ as a typical example. It also shows the evolution of the different Lagrangian radii.

A-B-C: This part of the evolution is the similar as for the lower mass stars. Because the star had a convective core during the MS phase, the transition from H-core fusion to H-shell fusion is more abrupt than in a star of $1 M_{\odot}$. The star briefly contracts as a whole, which results in the short leftward motion (B-C) in the HRD (compare tracks in Fig 18.1 and 18.3). The H-shell fusion starts at C.

C-D: When the H-fusion in the shell starts the mass of the He core is $0.4 M_{\odot}$, which is below the Schonberg-Chandrasekhar limit for stable isothermal cores. This means that the core does not have to shrink, so the star remains in thermal equilibrium. The core is not very dense, so the pressure and density in the shell is not very high. This means that a relatively large fraction of the stellar mass is in the H-shell (larger than for a $1 M_{\odot}$ star). This is called **thick shell fusion**. As more Helium is added to the core, it is on its way to reach the S-C limit so it slowly contracts. The H-shell layer then comes in a region of higher-density where the fusion is more efficient, so a smaller mass fraction is needed for the production of the luminosity by H-fusion: the mass fraction of the shell decreases. This is called **thin shell fusion**.

Because of the mirror-action of the H-fusion shell, the envelope expands and becomes more and more convective. At D the star is almost fully convective and has arrived on the Hayashi line for **red giants**.

Q? Check this in the KD and the HRD.

The figure shows that the luminosity in phase C-D is decreasing. Because the outer convection zone grows very deep into the star in a short time, (less than 2 Myr from $t = 81$ to $t = 83$ Myr) the expansion also occurs on a short timescale.

Part of the energy produced in the shell is then used for expansion of the envelope, from about $5 R_\odot$ in C to $50 R_\odot$ in D. Hence the slight decrease in L.

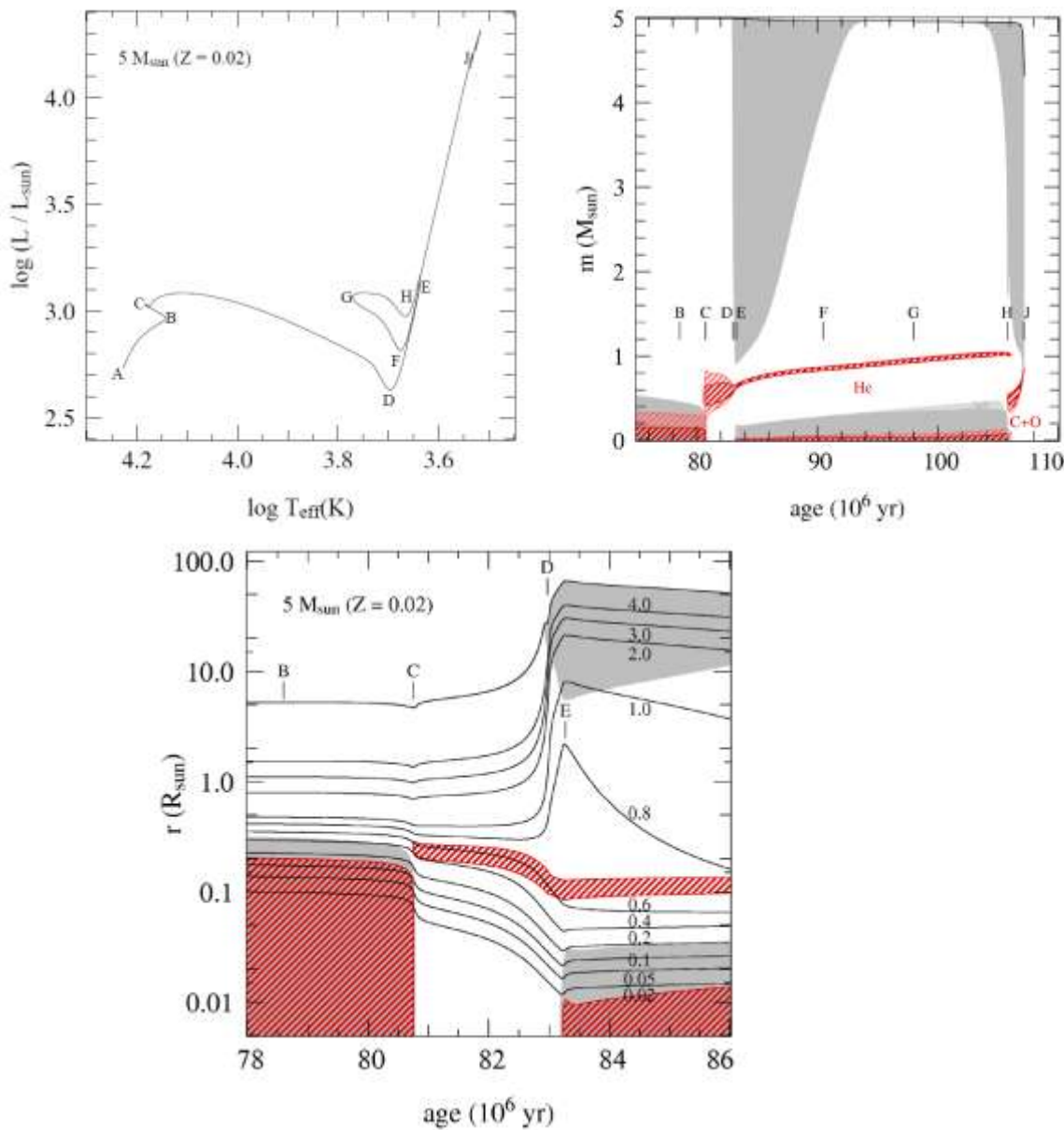


Fig 18.3 The post-MS evolution of a star of $5 M_\odot$ shown in the HRD (fig a), the KD (fig b) and the expansion and contraction of the different Lagrangian layers (fig c). Thick shaded regions indicate efficient fusion (H or He fusion) and thin shaded regions indicate inefficient fusion. The gray regions indicate convection zones (Pols: figs 9.2, 9.3, 9.4. see Pols for colour versions)

D-E: The mass of the He core exceeds that of the S-C limit, so the core contracts and pulls the H-fusion with it. The contraction of the core occurs on

the Kelvin-Helmholtz timescale which is only about a Myr: the evolution from D to E is fast.

E: The convection reaches its maximum depth close to E. The convection has then reached the layers where the composition has been changed due to the former H-core fusion. Products of this fusion are then brought to the surface. This is the **first dredge-up** phase.

F: Helium fusion starts in a non-degenerate core.

18.5 The core mass –luminosity relation for RGB stars

Stars with $M_i \lesssim 2 M_\odot$ have a degenerate helium core when they are on the RGB. In these stars the density contrast between the core and the envelope is so large that they are practically decoupled. This implies that the efficiency of the shell fusion is completely determined by the core-mass and not by the envelope. Detailed evolutionary models have shown that there is a strong and steep **relation between L and the core mass for stars with a degenerate He-core**.

$$L/L_\odot \simeq 2.3 \times 10^5 (M_c/M_\odot)^6$$

Notice the strong dependence!

The luminosity is independent of the *total mass* of the star. Therefore, all evolutionary tracks of stars of different mass converge onto the Hayashi line of the RGB. In other words, from the location of a star on the RGB one can easily derive the core-mass, but the total mass is more difficult.

18.6 Metallicity dependence of the RGB

We have seen that fully convective stars are on the Hayashi line, which gives the coolest T_{eff} that any star with a given luminosity can get. We derived this location by setting the pressure in the atmosphere at $\tau \simeq 1$ equal to the pressure of a polytropic star ($n = 1.5$) at that same density. However, the opacities of stellar atmospheres depend on metallicity (even if H^- is the dominant opacity source) because the metals provide the electrons for H^- . A higher metallicity provides more free electrons and a higher opacity. A higher opacity means that $\tau \simeq 1$ is reached at a lower density, i.e. further outward. So the Hayashi line for metal rich stars is at slightly lower T_{eff} (further to the right), than that of metal poor stars.

This is the reason that the metallicity of globular clusters can easily be derived from the location of the RGB in the HRD (no spectra are needed).

This is shown in Fig. 18.4 which shows the CMD of the cluster M54, which is the center of the Sagittarius Dwarf Elliptical Galaxy. Therefore it had multiple star formation periods with different metallicities due to infalling gas.

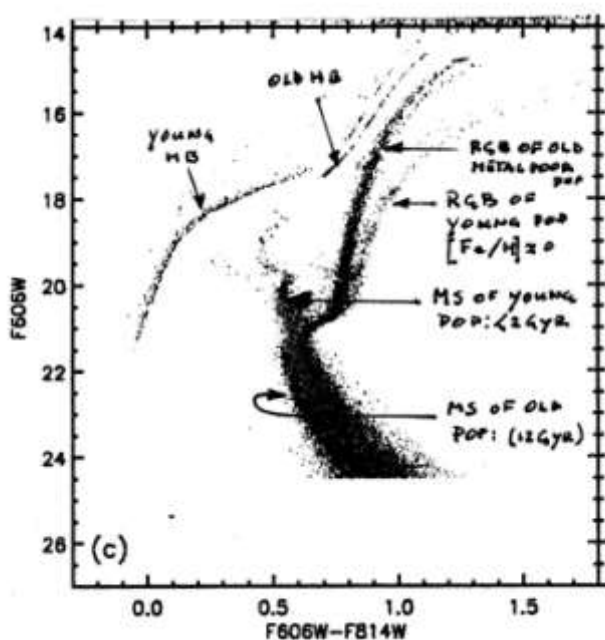


Fig. 18.4
HRD of the cluster M54, which is the center of the Sagittarius dwarf elliptical galaxy. The left (most populated) RGB is from old stars with $[Fe/H] = -1.8$. The right RGB is from stars with $[Fe/H] \approx 0$. Notice also the multiple horizontal branches.
(from Siegel et al. 2007, ApJL 667, L57)

18.7 Mass loss on the RGB

During the RGB stars are losing mass by means of a stellar wind. For low luminosity RGB stars the wind is possibly driven by gas pressure in a chromosphere, although radiation pressure on molecules has also been proposed. For stars higher up on the RGB, the pulsating Miras, the winds are driven by a combination of stellar pulsation and radiation pressure on dust.

In many stellar evolution calculations the Reimers relation (Sect 16.4.3) is adopted with a free efficiency factor $\eta_R \approx 0.25$ to 0.5, which seems to give reasonably good evolution predictions.

Adopting this description, a star of $1 M_\odot$ loses about $0.3 M_\odot$ on the RGB and a star of $5 M_\odot$ loses between 0.5 and $1 M_\odot$ during the RGB phase. This is shown in the KDs of Figs 18.1 for a $1 M_\odot$ star and in Fig 18.3 for a $5 M_\odot$ star by the decrease in the mass.

19. Ignition of Helium Fusion in Low Mass Stars: from the tip of the RGB to the Horizontal Branch

We have seen that stars with $M_i \lesssim 2 M_\odot$ have a **degenerate helium core** at the end of their RG phase (tip of the RGB is point F in Fig 18.1).

On the other hand, stars with $M_i \gtrsim 2 M_\odot$ have a **non-degenerate helium core** at the tip of RGB (point E in Fig 18.3)

19.1 The He-flash in degenerate cores of stars of $M \lesssim 2 M_\odot$

When the mass of the degenerate He-core reaches a value of about $0.45 M_\odot$, (independent of the total stellar mass !) the core has contracted so much that it reaches the ignition T of He-fusion at $T_c \sim 10^8$ K. Ignition in a degenerate core results in an *explosive* start of the fusion: the predicted “**Helium flash**.”

The reason is the following:

When He is ignited, the produced energy leads to a T-increase.

- In a *non-degenerate core*, such a T-rise would result in an increase in P and the core would expand (because P would become larger than required for hydrostatic equilibrium). Due to the expansion, T and p decrease, and this would reduce the fusion efficiency. The energy production drops and the core shrinks until it reaches hydrostatic equilibrium again. So in this case gravity acts like a regulator: the fusion does not run out of hand.
- In a *degenerate core* the ignition of He-fusion produces a T-rise, but this does *not* result in an increased P, because in a degenerate core P is independent of T! So T rises, but the core does not expand so the density does not change, the energy production ϵ increases drastically (remember that $\epsilon \sim T^{30}$ for He-fusion!). This leads to more efficient fusion, still higher T, ...etc. A degenerate core that is ignited acts like a bomb!

As the temperature shoots up and reaches a value of a few 10^8 K, the degeneracy is lifted. This is because the limit between degenerate and ideal gas is set by $T_c \sim \rho_c^{2/3}$ (Figs 15.1) and so for any density there is a T where the gas is no longer degenerate. The density of the degenerate He core is about 10^6 g/cm³, so degeneracy is lifted when $T_c \approx 3 \cdot 10^8$ K.

From then on the pressure increases when T-rises, so the core expands very quickly, the density drops and the degeneracy is lifted. The star then settles into a normal (non degenerate) He-core fusion in hydrostatic equilibrium.

The star is now on the “**Horizontal Branch**” in the HRD = point G in Fig 18.1

The luminosity produced in the core during the He-flash is very high, and of order $10^{10} L_\odot$ (!), but it lasts very short. The Helium flash has never been observed! The energy of the flash is used to expand the originally degenerate core by a factor 10^2 in volume (from a degeneracy density of order 10^6 to non-degeneracy at 10^4 g/cm^3). Neutrinos also remove a substantial fraction of the fusion energy.

During the ignition of the Helium fusion by a Helium flash the star is clearly out of hydrostatic and thermal equilibrium. Therefore we cannot plot a track in the HRD between point F and G! The evolution track just jumps from F to G in Fig. 18.1.

19.2 The start of the Helium core fusion in stars of $M \gtrsim 2 M_\odot$

When the mass of a Helium core reaches a mass of about $0.45 M_\odot$, Helium is ignited. The ignition of the Helium core fusion in a star of $M_i \gtrsim 2 M_\odot$ occurs in a non-degenerate core. This means that the gravity regulates the start of the fusion as described above. These stars are also found on the Horizontal Branch when the Helium core fusion has started. During the slow transition from the top of the RGB to the HB, the evolutionary track can be followed: see the loop from phase E to F (when helium fusion is ignited to F) in Fig. 18.3

NB: In both the low mass stars with degenerate cores and the intermediate mass stars with non-degenerate cores the helium fusion is ignited when the helium core has reached the same mass of $0.45 M_\odot$! This turns out to be important for the Horizontal Branch morphology.

20. Helium fusion in the core: the Horizontal Branch

When He-fusion has started in the core, the star settles into a new equilibrium and we find the stars on the Horizontal Branch (HB) in the HRD.

This is shown in the evolution track of a $1 M_{\odot}$ star (Fig 18.1) as the instantaneous transition from point F (= He-flash) to point G (= start of He-fusion in the core).

The He-fusion (G-H) occurs at $L \approx 10^2 L_{\odot}$, with a core mass of $\sim 0.5 M_{\odot}$.

The track of $5 M_{\odot}$ shows a more gradual transition from H-shell to He-core fusion (D-E). The fusion (F-G-H) occurs at $L \approx 10^3 L_{\odot}$, with a core mass of $0.9 M_{\odot}$.

HB stars consist from inside out of:

- **Core with He-fusion:** $\text{He} \rightarrow \text{C}$.
Due to the strong T-dependence of the 3α -process the inner $\sim 1/3$ of the core is convective.
- **Inert He-region** around it without fusion.
- **H-fusion shell**
- **H-rich envelope.** This envelope is mainly radiative equilibrium, but with a convective outside (check the KDs!).

HB-stars have a smaller radius (\rightarrow higher T_{eff}) than Red Giants. This is because of the Virial Theorem and the resulting “mirror effect” of the H-fusion shell: as the core expands (because degeneracy is lifted), the envelope shrinks \rightarrow smaller R_* , higher T_{eff} . This is shown by the loop F-G-H in the evolution track of a $5 M_{\odot}$ star, whose T_{eff} increases to about 6000K, and to a smaller extent also in track of the $1 M_{\odot}$ star which reaches 5000K at its smallest radius.

The duration of the HB-phase of a $1 M_{\odot}$ star is about 0.1 Gyr and that of a $5 M_{\odot}$ star is 22 Myr. This is longer than the expected nuclear lifetime of star with a luminosity of about $10^2 L_{\odot}$ (for $1 M_{\odot}$) or $10^3 L_{\odot}$ (for $5 M_{\odot}$), considering the high luminosity and the small mass deficiency for Helium fusion (0.0007). This is due to the large contribution of the energy production by the H-shell fusion. (see Homework 20.1 and 20.2)

The Helium fusion occurs originally by the 3α -process ($3 \text{He} \rightarrow \text{C}$), but as the Helium abundance decreases and the C abundance increases, the reaction $\text{H} + \text{C} \rightarrow \text{O}$ becomes more important. So at this point the C abundance starts to decrease again but the O-abundance increases in the core.

H20.1. Homework

Study the Kippenhahn diagrams for stars of $1 M_{\odot}$.

- a. *Derive the amount of Helium that is fused during the Horizontal Branch phase (F-H) and calculate the total amount of generated energy.*
- b. *Derive the amount of energy generated by the H-shell fusion during the same period*
- c. *Which fraction of the energy is due to the H-shell and which fraction is due to the Helium core?*
- d. *Compare your results with the luminosity and the duration of the HB phase.*

H20.2 Homework

Do the same for the $5 M_{\odot}$ model.

20.1 The evolution on the Horizontal Branch

Because the He-fusion phase lasts only a fraction of the H-fusion phase, all HB stars in a cluster at any time come from a small range in initial masses. This implies that they all have about the same core mass and therefore also about the same luminosity at the beginning of the He-fusion.

So the **HB is approximately horizontal in log L or M_{bol}** , but bends down at high T_{eff} if plotted in V magnitude.

Q?

Why?
From the evolution tracks of 1 and $5 M_{\odot}$ we can see that a cluster of 12 Gyr has a HB at $10^2 L_{\odot}$, and a cluster of 0.1 Gyr has a HB at $10^3 L_{\odot}$.

The radius of the HB-stars, and hence their T_{eff} (location in HRD) depends on the depth of the convection in the H-envelope: the deeper the H-convection zone → the larger R_* → the cooler the star. The tracks of 1 and $5 M_{\odot}$ stars show that the depth of the convection decreases during the He-fusion, but at the end it increases again. This explains why HB stars make a leftward-loop in the HRD during core-Helium fusion and then move back to the Hayashi line. When the convection zone reaches its minimum depth, that star has the maximum T_{eff} .

The He-fusion on the HB and the H-fusion phase on the MS differ in two ways:
(a) by the mirror action of the H-fusion shell in the HB phase and
(b) the evolution is determined by the properties of the *core*, and the envelope follows.

Compare the radius evolution of a HB star, with that of a MS star. During the MS phase the star expands (rightward motion in HRD), and at the end of the MS phase the star contracts (short leftward loop). Because of the mirror

principle, a star in the HB phase does exactly the opposite: contraction of the outer layers during He-fusion in the center, when the core expands, and expansion of the outer layers near the end of the He-fusion, when the core shrinks. The expansion and contraction of the star is produced by the increasing and decreasing depth of the outer convection zone.

The thickness of the convection layer (and therefore the hottest T_{eff} that a star can reach on the HB) depends on the envelope mass at the time the core-He fusion starts. This is demonstrated in Fig. 20.1 which shows the location in the HRD of low mass stars with $Z=0.001$ (charactic of old globular clusters) at the start of the He-fusion phase.

The smaller the envelope mass, the bluer the star during the HB phase.

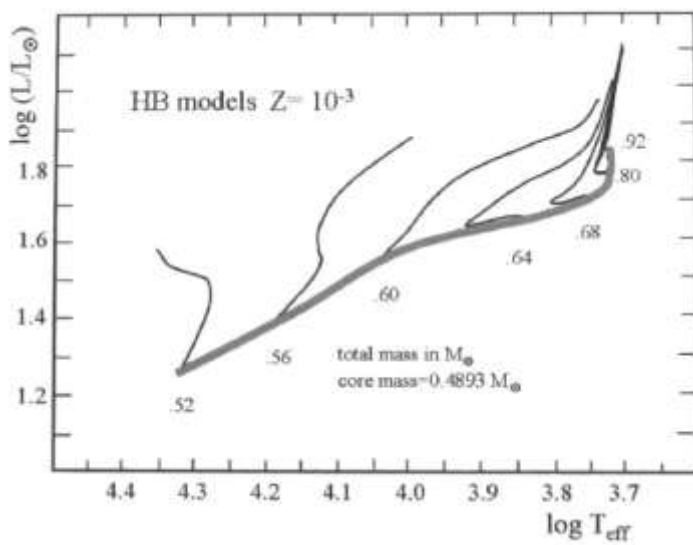


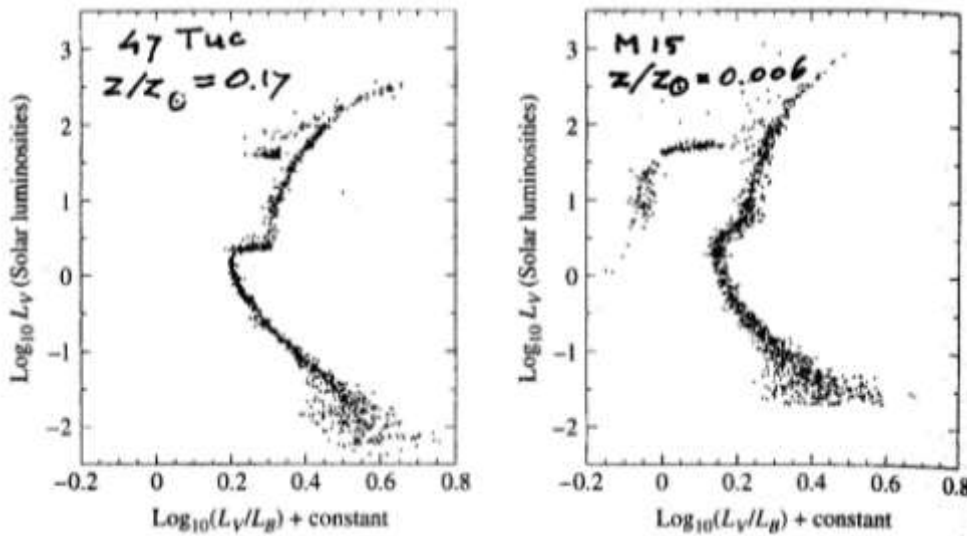
Fig 20.1
The wide grey line shows the location of stars with the same Helium core mass ($0.49 M_{\odot}$) at the beginning of the He-core fusion, for different total masses ranging from 0.52 to $0.92 M_{\odot}$, and so for envelope masses from 0.03 to $0.43 M_{\odot}$. The full lines show the evolution tracks during the core-He fusion. The location depends on the envelope mass.
(Pols, Fig 9.8, from Maeder)

20.2 The observed HB in globular clusters

HB-stars in a clusters have about the same L , but the range in T_{eff} reflects the different amounts of H-envelope mass at the onset of the He-fusion. So to first order approximation, the blue-extent of the HB depends on the amount of H outside the H-shell fusion after the He-flash.

Observations show that metal poor cluster have in general an extended Blue HB and metal rich clusters have in general a short Red HB.

This is shown in Fig 20.2 which shows the colour magnitude diagrams of a metal rich globular cluster, 47 Tuc with $Z=0.17 Z_{\text{sun}}$, and a metal poor cluster, M15 with $Z=0.006 Z_{\text{sun}}$.

*Fig. 20.2*

CMDs of two GCs of different metallicities. The HB of the cluster with the lowest Z extends much bluer (higher Teff) than the high metallicity cluster. (CO Fig. 13.20)

The immediate conclusion to be drawn from the comparison with the figure above is that stars in more metal rich clusters have a larger envelope mass when they arrive at the HB than those in metal poor clusters. This would imply that stars with higher Z have lost less mass during the RGB phase.

However, this is opposite to expectations because the RGB mass loss is (probably) increasing with metallicity (more dust and more molecules to produce radiation pressure).

Models suggest that the extent of the HB is also sensitive to the initial He abundance as shown in Fig. 20.3.

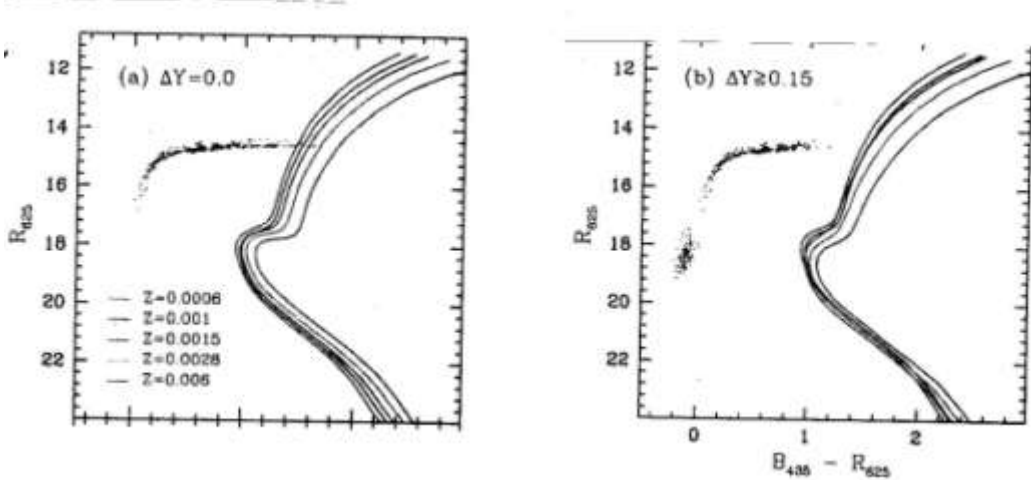


Fig 20.3 The effect of different Helium and metal abundances on the extent of the HB. A higher initial He abundance results in a wider HB.

(Fig from Lee et al. 2005, ApJ 621, L57. See their figure 1 in colour.)

However, some globular clusters have a Blue HB or Red HB *although their metallicity is the same!* This suggests there must be another mechanism (apart from RGB mass loss and metallicity) affecting the extent of the convective envelope and the T_{eff} of the HB stars. This problem is called **the second parameter problem.**

Some of the solutions that have been suggested involve:

- The stars in some clusters may be faster rotating than in other clusters. This would produce extra mixing (we will discuss the effects of rotation later).
- Convective overshooting may have played a role. This would result in a larger core and a different chemical profile.

These effects could result in a different core-mass for stars of the same age and metallicity and in a different depth of the convection zone on the HB.

Multiple stellar populations in clusters.

It is possible that second parameter problem is related to the problem of the multiple stellar populations that have been observed in many massive GCs. These clusters show multiple main sequences and different abundance ratios within the cluster, clearly indicating that not all stars in a GC had the same initial abundances.

Two types of solutions have been proposed:

1. Multiple star formation episodes, where the mass loss products of massive stars are gathered in the center of the cluster until enough enriched gas has been collected for a second burst of starformation. These second generation stars will be more metal rich and more He-rich. (D'Erocle et al. 2008, MNRAS 391, 825). Most of the first generation stars have to be expelled from the cluster to explain that it contains about 50 % second generation stars.
2. The ejected enriched gas from massive star winds have been captured by the accretion disks of low mass stars, which are forming much more slower. The accreted enriched gas ends up in low mass stars as these cross the central regions of the cluster where the gas resides. This produces a fraction of the low mass stars to be metal rich and He rich. (Bastian et al. 2013, MNRAS 436, 2398).

21. The Asymptotic Giant Branch phase for stars of $1 < M < 8 M_{\odot}$.

At the end of the HB phase, when He is exhausted in the core, the core is without energy source, so it will contract. Because the star still has a H-burning shell (with mirror-action), the core contraction results in an envelope expansion. So the star moves to the right in HRD. Because the expanding envelope absorbs part of the energy, the luminosity actually decreases a bit during the expansion. (This is seen in the track of the $5 M_{\odot}$ star, Fig 18.3, at point H)

The core contracts until He starts to burn in a shell. In stars with an initial mass in the range of $2 < M < 8 M_{\odot}$ **the CO core will become degenerate**.

The star is now at the bottom of the ***Asymptotic Giant Branch (AGB)***. This corresponds to phase H in the evolution track of a $5 M_{\odot}$ star (Fig. 18.3).

An AGB star consists from inside out of:
degenerate C/O core,
He-burning shell : $\text{He} \rightarrow \text{C} \rightarrow \text{O}$
He-rich intershell zone,
H-fusion shell; $\text{H} \rightarrow \text{He}$
convective H-rich envelope.

The internal structure of an initially $5 M_{\odot}$ star is shown in the figure below. The star has a radius of $44 R_{\odot}$. Notice that the core, including the H-fusion shell, is very small: $0.0056 R_{\odot}$. The core contains only 2×10^{-7} of the volume of the star, but 1/5 of the stellar mass.

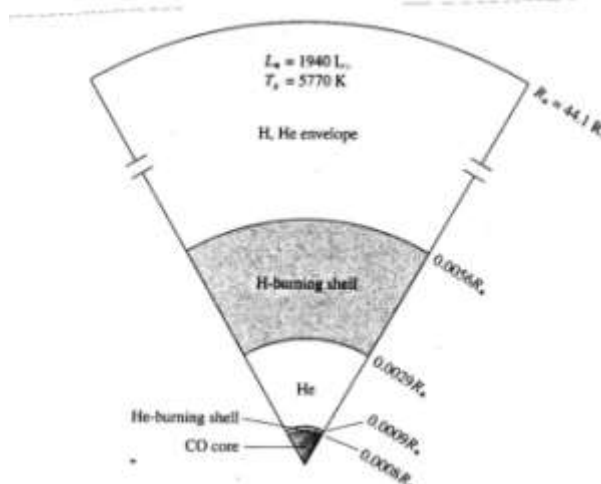


Fig 21.1 The internal structure of a $5 M_{\odot}$ star at the start of the AGB phase. This shows the distribution of the different layers in terms of extent. The distribution in mass is very different! (CO Fig. 13.8)

In terms of mass, the distribution of this star is (see Fig 18.3 point H):
CO-core $0.40 M_{\text{sun}}$, He-burning shell $0.10 M_{\text{sun}}$, He intershell zone $0.50 M_{\text{sun}}$,
H-burning shell $0.05 M_{\text{sun}}$, H and He envelope $3.25 M_{\text{sun}}$.
Total mass $4.30 M_{\text{sun}}$.

The AGB phase is one of the most fascinating evolutionary phases because several interesting physical processes are happening in that phase.

- A. The C/O core becomes degenerate. For stars with a shell fusion around a degenerate core the luminosity is set by the core-mass (we have seen this already for RGB and HB stars). A star with a C/O core of $0.6 M_{\odot}$ has $L \sim 5 \times 10^3 L_{\odot}$ no matter if the mass of its H-envelope is $0.4 M_{\odot}$ or $4 M_{\odot}$!
- B. The two shell burning phases alternate in producing the luminosity of the star, with a periodicity of about 10^3 years, with the changes triggered by shell-flashes. These are called **thermal pulses**.
- C. The very deep convection can bring the products of the He-fusion (i.e. C) to the surface. These are called **second and third dredge-up**. This can create a sudden flip in surface composition from a C/O-ratio < 1 to > 1 . This has dramatic effect on the dust around these stars. Even s-process elements, produced in the thermal pulses are dredged to the surface.
- D. The stars have very high mass loss rate due to the combination of pulsation and radiation pressure on dust. The mass loss rate increases from about $10^{-7} M_{\odot}/\text{yr}$ at the bottom of AGB to 10^{-5} or $10^{-4} M_{\odot}/\text{yr}$ at the tip of AGB.
- E. The end of the AGB phase and the final fate of low mass stars is completely dominated by this mass loss. The mass of White Dwarfs is set by the mass loss on the AGB.

21.1 The Core-Mass \leftrightarrow Luminosity Relation of AGB stars

The C/O cores of the AGB stars are degenerate, so there is a fixed core-mass \leftrightarrow core radius relation. This implies that the pressure of the shells is mainly set by the mass of the C/O core, and so is their energy production. (This differs from normal, i.e. non-degenerate stars, in radiative equilibrium, where L is usually depends on the *total mass*.)

Paczynski (1971, Acta Astron. 21, 271) has shown that this results in a relation between the luminosity and the *core-mass*: usually called the Paczynski-relation. (An analogous relation exists for the RGB, when the H-burning shell is on top of the degenerate He-core.)

For AGB-stars the Paczynski-relation is: (for solar metallicity)

$$\left[\frac{L}{L_{\odot}} \approx 5.9 \times 10^4 \left(\frac{M_c}{M_{\odot}} - 0.52 \right) \right]$$

Some values:

M_c/M_{\odot}	L/L_{\odot}
0.537	10^3
0.689	10^4
1.000	$3 \cdot 10^4$

This relation has interesting consequences:

- If we know L of an AGB star we know its core mass, but not the envelope mass or total mass.
- For a given luminosity we know the rate at which fusion occurs. This fusion adds mass to the core, so we know the growth of the core mass and the increase of L . So we can easily calculate the “speed” with which these stars will climb the AGB. (We will do this later).
- With the core growth, strong mass loss is reducing the mass of the envelope and finally stopping its ascent on the AGB.

21.2 The second dredge-up at the beginning of the AGB phase

The internal structure of a star during the early AGB phase is shown in Fig 21.2. This is the KD of a star of initially $5 M_{\odot}$, of which the evolution track and the KD of the earlier evolution were shown in Fig. 18.3.

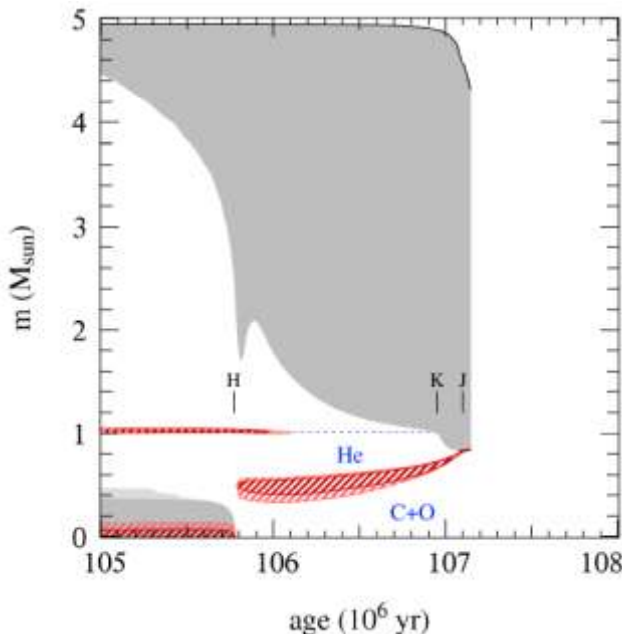


Fig 21.2
Kippenhahn Diagram of the start of the AGB phase of a $5 M_{\odot}$ star. The letters refer to the evolution track in Fig. 18.3. Note the second dredge up at point K when the convection zone reaches the He-rich intershell zone. (OP Fig. 9.4)

Shortly after the He-shell burning starts, the H-shell burning is switched off, at point H in the evolution track. The increasing core mass results in an increasing luminosity, up to point J in the evolution track, which implies an increasing radius, because the star is at the Hayashi T_{eff} lower limit. This increase in radius is achieved by the deepening of the convection zone. (Outer convection zones bloat the stars: the deeper the outer convection the larger the stars)

When the convection zone reaches the He-rich intershell zone it mixes the products of H-fusion (CNO-cycle) with the outer envelope and brings it to the surface. The inter shell zone had no more H, a very low abundance of C and O, but a high abundance of N. The amount of the abundance change at the surface depends on the ratio between the mass of the intershell zone and the mass of the envelope.

This is called the second dredge up.

The second dredge up is similar to the first dredge-up during the RGB phase, but stronger.

21.3 Thermal Pulses and the third dredge-up of AGB stars

When the star climbs the AGB the star goes through a series of He-flashes that are called “*thermal pulses*” at time intervals of $\sim 10^3$ yr to 10^4 yr. (Do not confuse the thermal pulses with the He-flash that started the He-core burning).

The basic reason for the occurrence of pulses is the unequal burning rate of the the H-burning shell and the He-burning shell. The H-shell leaves more He behind than the He-shell can fuse, so the region between the two shells, the intershell region (ISR), grows in mass until it becomes unstable. See Fig 21.3.

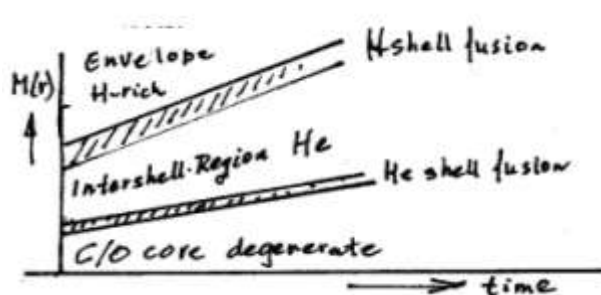


*Fig 21.3
Sketch of the
mass evolution of the
He-burning shell and
the H-burning shell
and the He-rich intershell
region during the
AGB phase.*

This results in the two fusion shells (H-shell and He-shell) being alternatively active. (See Fig. 21.4). Many pulses occur during the AGB phase.

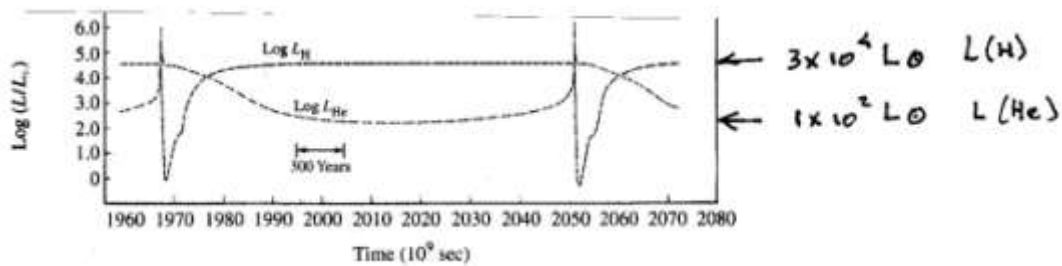


Fig 21.4 This figure shows the alternating activity of the two shells of an AGB star of $M_i = 7 M_\odot$ since the beginning of the AGB-phase. The figure covers a period of 3000 yrs. Many of such pulses occur during the AGB phase. (from Iben 1975, ApJ 196, 525)

During thermal pulses, interesting mixing processes occur. For understanding the time sequence, follow the description in Fig. 12.5 (from Pols section 10.1.1).

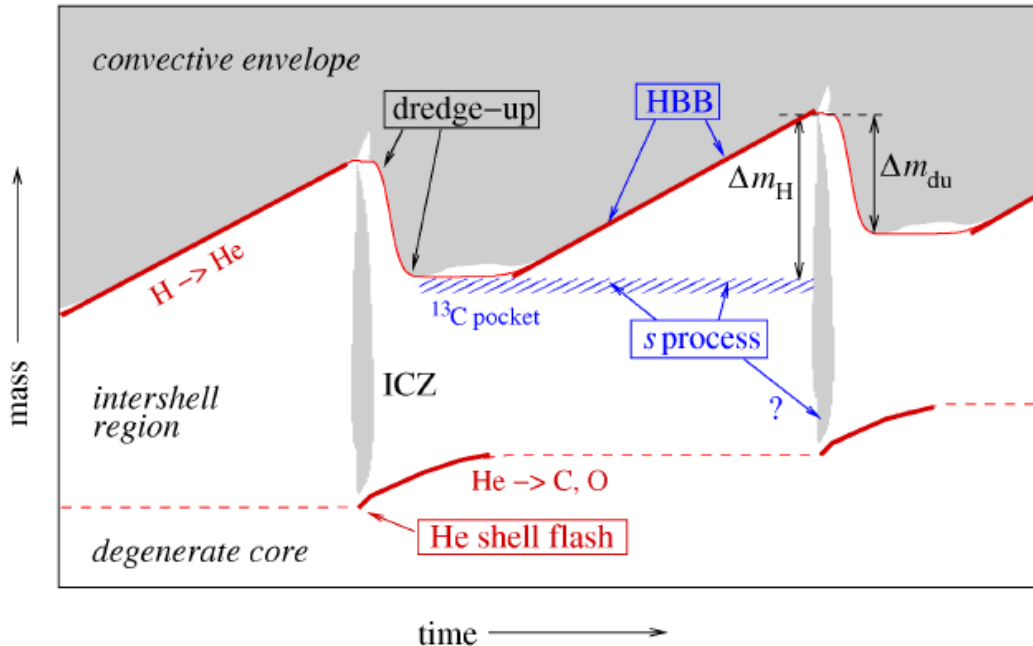


Fig. 21.5 The internal evolution of an AGB star during two thermal pulses described in the text. (see OP Fig. 10.3 for a colour version).

1. Most of the time the H-burning shell produces almost all luminosity and the He-shell is inactive. So in mass, $M(r)$, the H-shell moves out faster than the He-shell. This implies that the He-layer increases in mass.

2. As the intershell region (ISR), that consists of Helium, grows in mass, the pressure at the bottom of that region steadily increases because more and more Helium is piled on top of the degenerate C/O. When the pressure reaches a critical value, helium is ignited in a thin shell.
3. Ignition in a **thin shell** leads to a thermal instability of the same type as the ignition in a degenerate core, although the gas is not degenerate! The reason is the following: When the fusion is ignited, the gas is heated and it expands. However, if the shell is very thin (thinner than about 0.25 times its radius) the expansion is not enough to bring down the temperature so the fusion keeps going at a faster rate until the layer has time to expand and then the shell burning is stable. So it looks like a flash in degenerate gas, but the reason is different. (See Pols section 6.5.2 for details.)
4. As the He-shell fusion starts, it produces so much energy (up to $10^8 L_\odot$) that the ISR becomes convective and expands. The H-shell is pushed upwards where the pressure drops to a value that cannot keep the H-fusion going. So as the He-shell fusion goes on, the H-shell fusion is extinguished. This lasts for about 10^2 years.
5. When the He-shell fusion is active, the ISR becomes convective (due to the large energy flux that cannot be transported by radiation). This convection in the ISR distributes the products of the Helium-fusion (mainly C) over the ISR. The intershell convective zone (ICZ) is shown in the figure.
6. When the He-shell fusion is active and moves outward in mass into the ISR, the degenerate C/O core contracts.

Q:

Why?

As the core contracts, and the He-shell is active, the envelope expands. As the star is on the Hayashi line, it can only expand by deepening its envelope convection region. So the outer convection now moves into the ISR which is now enriched with He-fusion products and brings these to the surface. This is called the "**third dredge-up**."

It brings C to the surface, but also s-process elements that are formed during the thermal pulse!

7. After the dredge-up, the H-shell becomes active again and the He-shell becomes inactive. As the H-shell moves outward in mass, the ISR grows in mass again until the pressure at the bottom of the ISR is again so high that the He-shell is ignited again and then the cycle is repeated.
8. The duration of the active He-shell is typically about 10^2 yrs, and that of the active H-shell (i.e. the time in between two thermal pulses) is about 10^3 years for the more massive AGB stars of $M > 4 M_\odot$, and 10^4 years for the lower mass AGB stars.

9. The phase of the repeating thermal pulses is called “the **TP-AGB phase**.” Each cycle brings more and more C to the surface, so that eventually the massive AGB stars near the tip of the AGB phase have a photosphere with a C/O ratio > 1 , instead of the classical case of O/C > 1 . These stars are easily distinguished because instead of O-rich molecules and dust (i.e. silicates) they have C-rich molecules and dust (carbonaceous-grains). The flip from an O-rich to C-rich atmosphere is drastic because the CO-molecule is the most abundant and strongly-bound molecule. So when O/C > 1 all C is in CO and the remaining O forms OH-molecules etc. and silicate dust. On the other hand if C/O > 1 , then all O is locked in CO-molecules and the remaining C can form molecules such as CH etc. and carbon-dust.
10. In the most massive TP-AGB stars the H-shell is active at such a high temperature that the H-fusion occurs via the CNO-cycle and not via the PP-chain. This implies that C (that was transported by convection of the ISR during the time when the He-shell was active) is converted into N. This process is called “**hot-bottom burning**” and it may prevent TP-AGB stars to become very C-rich and become instead N-rich at the surface.

Hot bottom burning also produces nuclei like ^7Li , ^{23}Na , ^{25}Mg and ^{26}Mg , which are found to be overabundant in globular clusters with a second generation of star formation.

21.5 Summary of the dredge-up phases

The dredge-up phases of stars of $M_i < 8 M_\odot$ are shown below.

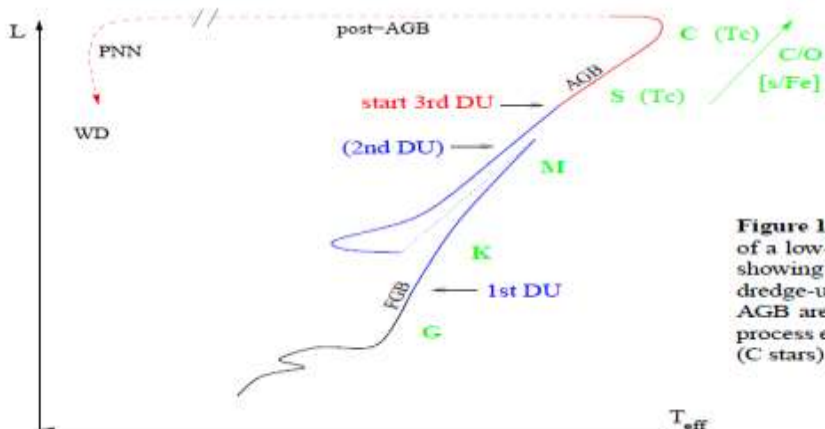


Figure 11.5. Schematic evolution track of a low-mass star in the H-R diagram, showing the occurrence of the various dredge-up episodes. Stars on the upper AGB are observed to be enriched in s-process elements (S stars) and in carbon (C stars).

Fig 21.6 The dredge-up phases during the late evolution of low mass stars. The changes in surface compositions are written next to the track.
(OP fig. 11.5)

1. The **first dredge-up** occurs when the star is on the RGB and the envelope convection reaches the depth where He was enriched during the MS phase. This results in a small increase of He at the surface.
2. The **second dredge-up** occurred in the early AGB phase for stars of $M_i > 4 M_\odot$ when the star expands after the HB phase. This expansion is produced by the growing of the convective envelope. It reaches even below the depth (in mass) of the H-shell during the HB phase. So it reaches into the He-layer! It brings He, and N-rich and C-poor and O-poor gas, mixed with the original envelope mass to the surface. So the photospheres become enriched in N.

Q: Is N enriched by the same factor as C is depleted?

3. The **third dredge-up** (or rather dredge-ups) occurs during the later AGB phase when the envelope convection after the thermal pulses reach into the ISR which does not contain H but mainly He and products of the He-fusion, such as C. The surface gradually becomes C-richer. This also brings s-process elements, such as technetium (Tc) to the surface. These are the **S-stars**.

For the most massive AGB stars the C/O ratio may even change from < 1 to > 1 . These are the **C-stars**.

All of the envelope mass of AGB stars is expelled by mass loss during the late AGB phase. **AGB stars are the main producers of C, N and s-process elements in the Universe**

21.6 The Evolution Speed During the AGB phase

Because the luminosity during the AGB phase is set by the coremass, but the growth of the coremass is set by the luminosity, there is a simple way to estimate the speed with which a star ascends the AGB-branch.

The luminosity of AGB stars is related to their core mass by the Paczynski-relation.

$$\frac{L}{L_\odot} = 5.9 \times 10^4 \left(\frac{M_c}{M_\odot} - 0.52 \right)$$

On the other hand, the core mass grows due to nuclear fusion. About 90% of the time the fusion is dominated by H-shell and 10% by He-fusion.

$$\begin{aligned} \text{The energy production of H-fusion is } 6 \times 10^{18} \text{ ergs/g} \\ \text{The energy production of He-fusion is } 6 \times 10^{17} \text{ ergs/g} \end{aligned} \quad \overline{\epsilon} = 5.5 \times 10^{18} \text{ ergs/g}$$

$$\frac{dM_c/M_\odot}{dt} = \frac{L}{\overline{\epsilon}} = \frac{5.9 \times 10^4}{5.5 \times 10^{18}} \left(\frac{M_c}{M_\odot} - 0.52 \right) = 1.1 \times 10^{-14} \left(\frac{M_c}{M_\odot} - 0.52 \right) \text{ per sec}$$

$$\frac{d \ln(M_c/M_\odot - 0.52)}{dt} = 2.1 \times 10^{-14} \text{ sec}^{-1} = 1/1.4 \text{ Myr}$$

This yields

$$\frac{M_c}{M_\odot} - 0.52 = \left(\frac{M_c}{M_\odot} - 0.52 \right)_{t=0} \cdot e^{t/1.4 \text{ Myr}}$$

$$\text{Now substitute } M_c/M_\odot - 0.52 = (5.9 \times 10^4)^{-1} L/L_\odot$$

$$L(t) = L(t=0) \cdot e^{+t/1.4 \text{ Myr}} \quad \rightarrow \quad \text{e-folding time only } \sim 1.4 \times 10^6 \text{ yrs}$$

where $t = 0$ is defined as the time when the star enters the AGB with a luminosity $L = 10^3 L_\odot$.

Suppose a star enters the AGB at $L \sim 10^3 L_\odot$ (see fig 18.3) then it will reach

$$\begin{aligned} L &\sim 5 \times 10^3 L_\odot & \text{at } t \sim 2.3 \times 10^6 \text{ yrs} & \text{with } M_c = 0.60 M_\odot \\ L &\sim 3 \times 10^4 L_\odot & \text{at } t \sim 4.8 \times 10^6 \text{ yrs} & \text{with } M_c \sim 1.0 M_\odot \end{aligned}$$

- So 1. AGB stars ascend the AGB fast = exponentially in few 10^6 yrs
- 2. During that time the core mass increases to $\sim 0.6 M_\odot$ or larger.

21.7 Mass Loss and the End of the AGB Evolution

Observations of White Dwarfs in clusters show that stars with initial mass up to about 6 or 8 M_{\odot} end their lives as white dwarfs with $M \sim 0.6 M_{\odot}$. So obviously, most stars must terminate their AGB phase with $M_c \sim 0.6 M_{\odot}$ or $L \sim 5 \times 10^3 L_{\odot}$. More massive WD with $M \sim 1 M_{\odot}$ must have reached $L \sim 3 \times 10^4 L_{\odot}$ at the AGB-tip.

We have seen before that stars climb the AGB in an exponential function of time, so the mass of the core also increases exponentially with time. What could stop this growing of the core? Mass loss!

Observations show that all AGB stars suffer mass loss at a rate that increases from $10^{-7} M_{\odot}/\text{yr}$ at the bottom of the AGB to very high values of $\sim 10^{-5} M_{\odot}/\text{yr}$ at the tip of the AGB. We have seen before that the high mass loss rates of AGB stars are due to pulsation and dust driven mass loss.

We now describe a simple method to estimate the effect of mass loss on the AGB and to predict the mass of the resulting white dwarfs.

Suppose we can describe the mass loss rate M_{wind} as a function of L , then we can also describe it as a function of t (because $L = f(t)$).

Let $M_{\text{env}}(t = 0)$ be the envelope mass when the star enters the AGB. The envelope mass decreases due to:

- | | |
|----------|--|
| Inside: | 1. Nuclear fusion: $(dM_{\text{env}}/dt) = -dM_c/dt$ |
| Outside: | 2. Mass loss by the stellar wind $= (dM_{\text{env}}/dt)_w = -M_{\text{wind}}$ |

$$\text{So } \frac{dM_{\text{env}}}{dt} = -\frac{dM_c}{dt} - \dot{M}_{\text{wind}}$$

Throughout most of the AGB phase mass loss by the wind is more efficient in reducing the envelope mass than the growth of the core. In that case

$$\dot{M}_{\text{env}} \simeq -\dot{M}_{\text{wind}} \rightarrow \Delta M_{\text{env}} \simeq \int \dot{M}_{\text{wind}} dt$$

We want to estimate how long it takes to remove (almost) the full envelope mass.

For simplicity, let us adopt the well-known “*Reimers-relation*” (sect 16.4.3), with $\eta_R = 2$ although it is not the most accurate one for AGB stars.

$$\dot{M}_w \sim 4 \times 10^{-13} \eta_R \cdot \frac{(L/L_{\odot})(R/R_{\odot})}{(M/M_{\odot})} \quad \text{in } M_{\odot}/\text{yr}$$

Using $L(t)$ derived before and $R = (L/4\pi\sigma T_{\text{eff}}^4)^{1/2}$ for constant $T_{\text{eff}} \simeq 2500\text{K}$ gives $R/R_{\odot} \simeq 5.2(L/L_{\odot})^{1/2}$. Now, with $M_* = M_c + M_{\text{env}}$, we can solve the decrease of envelope mass as a function of time.

Let us make a *simple estimate* for a star that enters the AGB phase with $M = 3 M_{\odot}$, consisting of a core of $M_c = 0.54 M_{\odot}$ and an envelope of $M_{\text{env}} = 2.46 M_{\odot}$ at $t = 0$. The Paczynski relation predicts that $L_* = 1.2 \times 10^3 L_{\odot}$ at $t = 0$.

Since L is the dominant variable in the Reimers relation for M , we take $T_{\text{eff}} \sim 2500\text{K}$ is constant and adopt a mean $\langle M_* \rangle \simeq 2M_{\odot}$ during the AGB phase of this star.

In that case

$$\dot{M}_w \simeq 2.0 \times 10^{-12} (L/L_{\odot})^{\frac{3}{2}} = 2.0 \times 10^{-12} (1.2 \times 10^3)^{3/2} \cdot e^{\frac{1.5t}{1.4\text{Myr}}} \quad M_{\text{sun}}/\text{yr}$$

$$\dot{M}_w \simeq 8.3 \times 10^{-2} \exp(t/0.95\text{Myr}) \quad M_{\text{sun}}/\text{Myr} (!)$$

Integration gives

$$\Delta M_{\text{env}} = \int_0^t -\dot{M}_w dt = 8.0 \times 10^{-2} e^{t/0.95\text{Myr}} \quad M_{\odot}$$

This shows that the total mass of the envelope, $2.46 M_{\odot}$, is removed by the wind after 3.2×10^6 yrs! At that time $L = 1.2 \times 10^4 L_{\odot}$ and $M_c = 0.72 M_{\odot}$.

Compare this with:

- a. the observed maximum L of AGB stars in the Glob Cluster M3 (fig 1.3)
- b. the derived mass of the White Dwarfs $\langle M_{\text{WD}} \rangle \sim 0.6 M_{\odot}$

So we see that:

1. *The AGB terminates because mass loss has stripped (almost) the full envelope.*
2. *The final mass of the WD is determined by \dot{M} (AGB)*
3. *The maximum luminosity of the AGB stars is set by \dot{M} (AGB)*
4. *The mass loss of the AGB prevents that stars in the mass range of about 2 to $8 M_{\odot}$ become supernovae.*
(If it was not for this mass loss, the SN-rate would be much higher!)
5. *We see from this simple estimate that we can expect the AGB lasts about 3 Myrs and that it ends at $L \sim 10^4 L_{\odot}$ with a degenerate core mass and $\sim 0.6 M_{\odot}$!*

We have used the Reimers' relation for \dot{M} (AGB). Observations show that the mass loss on the AGB increases more drastically near the tip of the AGB and reaches a value of a few $10^{-5} M_{\odot}/\text{yr}$ during a short **superwind phase**. This is important for the formation of Planetary Nebulae (to be discussed later).

H21.1 Homework

Calculate the evolution of two AGB-stars that start the AGB with

$$M_* = 2.0 M_\odot \quad \text{and} \quad M_c = 0.522 M_\odot$$

$$M_* = 5.0 M_\odot \quad \text{and} \quad M_c = 0.55 M_\odot$$

Use the mass loss rate derived from IR-flux of OH/IR stars (= AGB stars), and its relation with the period of pulsation (sect 16.4.4), or the Reimers relation with $\eta=2$ (whichever is the larger of the two).

Assume the relation between T_{eff} and L from the track in Fig 18.3.

1. *Write the differential equations that describe $L(t)$, $M_c(t)$, $M_{\text{env}}(t)$. Solve them by computer. Assume that the AGB evolution ends when the envelope mass is smaller than $0.01 M_\odot$.*
 2. *Calculate $L(t)$, $M_c(t)$, $M_{\text{env}}(t)$ and indicate where pulsation driven mass loss dominates.*
 3. *What is the core mass M_c and L at the tip of the AGB? How long does the AGB phase last for these stars?*
-

22. The Post-AGB Evolution and Planetary Nebulae

22.1 The Post-AGB Phase

Evolutionary calculations show that a star will leave the AGB when the mass in the H-envelope has decreased to only about 10^{-2} to $10^{-3} M_{\odot}$, depending on the core mass. At that time, this little amount of H-envelope mass cannot keep a fully developed convection zone. The convective envelope now slowly shrinks and part of it becomes non-convective, but radiative. This is first in the deepest layer of the envelope, where κ is smallest.

The star still has double-shell fusion around the degenerate core and its luminosity is still given by the Paczynski-relation of the AGB-phase.

This post-AGB phase is short, about 10^3 to 10^4 years, so the core mass does not increase much during that time. This means that the star moves *horizontally* to the left in the HRD.

The post-AGB evolution track of a star with a degenerate core of $0.6 M_{\odot}$ that leaves the AGB with an envelope mass of $0.003 M_{\odot}$ is shown in Fig 22.1

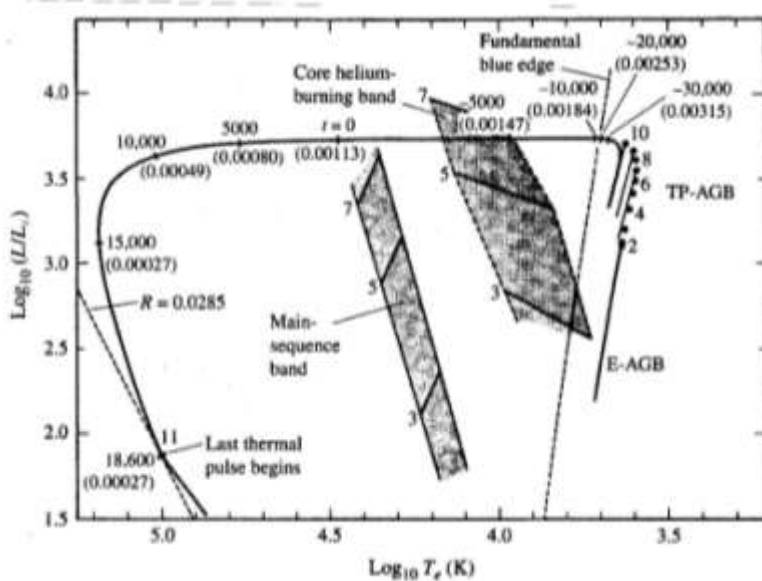


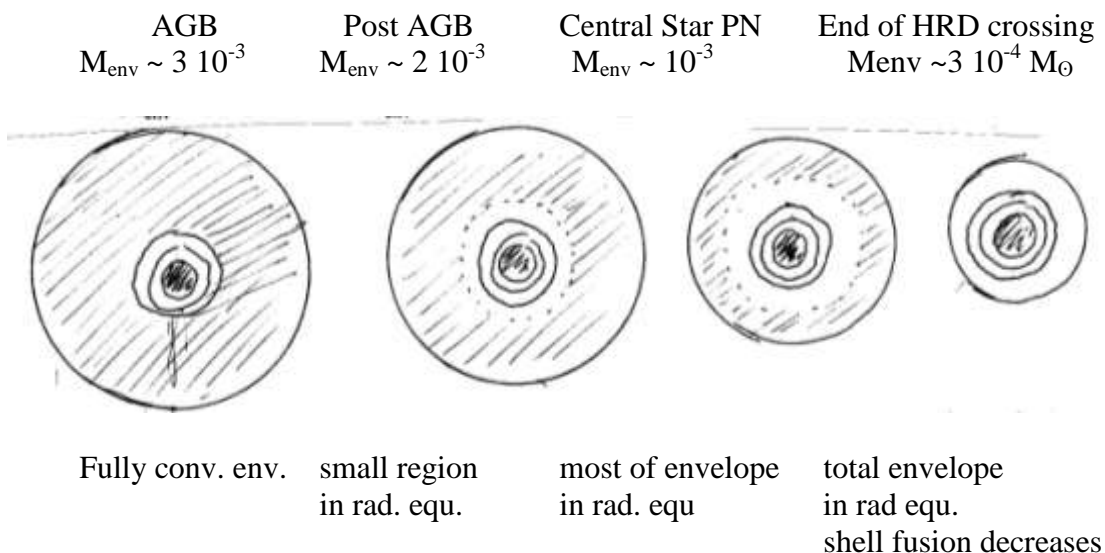
Fig 22.1 The post-AGB evolution track of a star of $M_c=0.60$ and $M_{env}=0.003 M_{\odot}$. The numbers in parentheses indicate the decreasing envelope mass. The other values are the times, in years, compared to the moment when $Teff=30000K$. At that time it is the central star of a planetary nebula (CSPN). The full crossing takes $3 \cdot 10^4$ years. Notice the 10 thermal pulses on the AGB and the decrease in L when $M_{env} < 0.0005 M_{\odot}$. (Fig from CO fig 13.3, based on Iben 1982).

The location of the star during the horizontal crossing in the HRD, i.e. its T_{eff} and R , depends on the mass of the envelope. As long as $M_{\text{env}} \sim 10^{-2} M_{\odot}$ for a high luminosity AGB, or $10^{-3} M_{\odot}$ for a low luminosity AGB, the star remains close to the AGB. But as the shells keep fusing, the envelope loses mass to the core, so the envelope mass decreases steadily. This forces the envelope to contract, as it has less and less mass to keep the envelope extended by convection. The star keeps moving to the left in the HRD.

When $T_{\text{eff}} \approx 30000\text{K}$ and the radius has decreased from $2000 R_{\text{sun}}$ to $3 R_{\text{sun}}$, the star is the central star of a Planetary Nebula (CSPN) as we will show later. At that temperature the star develops a line driven stellar wind, the same we discussed before for the hot luminous stars, with a mass loss rate of order 10^{-6} to $10^{-8} M_{\odot}/\text{yr}$ or so (strongly dependent on luminosity as $M \sim L^{1.6}$) and a terminal wind-velocity of about 1000 to 4000 km/s. So now the envelope loses mass even faster: not only to the core but also to the wind, and so the crossing of the HRD goes even faster. The speed of the crossing is determined by the continuing mass loss from the envelope! The crossing time is of order 10^3 to 10^4 years.

When the envelope mass has decreased to as much as about $\sim 3 \cdot 10^{-4}$ or $3 \cdot 10^{-5} M_{\odot}$ (depending on L) the star is on the left of the HRD with a small radius of about $0.25 R_{\text{sun}}$ and $T_{\text{eff}} \simeq 10^5 \text{K}$. Soon after that the fusion stops completely because the envelope does not produce sufficient pressure anymore for the fusion to continue.

Fig 22.2 Schematic description of star during crossing of HRD



During the first part of the post-AGB track, the star is invisible, because it is hidden in the dust that was ejected at the end of the AGB-phase, during the so-called “superwind phase” when the mass loss rate was as high as $10^{-4} M_{\odot}/\text{yr}$.

At $T_{\text{eff}} \sim 30,000$ K, two effects start to happen at about the same time:

- the star is so hot that it develops a radiation-driven wind (driven by UV lines)
- the high UV flux starts to (1) destroys the dust grains of the late AGB wind,
(2) dissociates the molecules, (3) ionizes the ejected material.

So part of the circumstellar material (AGB wind and star wind) becomes ionized → H II region → Planetary Nebula (to be discussed later).

22.2 Born-Again AGB stars

In some cases, a star experiences a last thermal pulse while it is moving to the left of the HRD. This is possible because we have seen that the time between two thermal pulses is on the order of 10^3 to 10^4 yr and the HRD-crossing time is also of that same order. It is estimated that about $\frac{1}{4}$ of all the AGB stars will have a late thermal pulse when they have already left the AGB.

The two most famous examples are **Sakurai's object** (discovered in 1996 by a Japanese amateur astronomer) and **FG Sagittae** (FG Sge).

FG Sge was discovered to be variable in 1943. In 1955 its spectrum suggested that it was a blue B-type star that was slowly getting redder. In 1991 it was a yellow F star and then kept going to the red where it ended as a K-star.

The star was the central star of a PN. This means that it had been an AGB star before and had already crossed the HRD to the left and produced a PN a few thousand years ago. When it was a hot star, the last thermal pulse produced so much energy that the thin envelope expanded again which resulted in an increasing radius and a decreasing T_{eff} : its return to the right of the HRD.

22.3 Planetary Nebulae

For a long time PN were explained in terms of the central star ionizing the previous AGB wind. The problem with this idea was that the expansion speed of the PNe is typically $v_{\text{exp}} \sim 50$ km/s, but the AGB winds are ejected with $v_{\text{AGB}} \sim 10\text{-}15$ km/s. How could the AGB material have been accelerated?

At about 1975 it became clear that central stars of PN (CSPN) have a stellar wind with mass loss rates ranging from 10^{-8} to $10^{-6} M_{\odot}/\text{yr}$, with the higher values reached at $T_{\text{eff}} \sim 30$ to 40 kK, i.e. when the star is halfway its crossing over in the HRD. The wind velocities are about 1000 to 4000 km/s, scaling approximately as $v_{\text{wind}} = 4 v_{\text{esc}}$.

Based on these new discoveries Kwok (1975 and 1978) proposed a completely different scenario for the formation of PN.

Planetary Nebulae are the result of the interaction between the slow AGB wind and the fast CSPN wind!

(See Lamers & Cassinelli ISW section 12.5 for a detailed description of theory.)

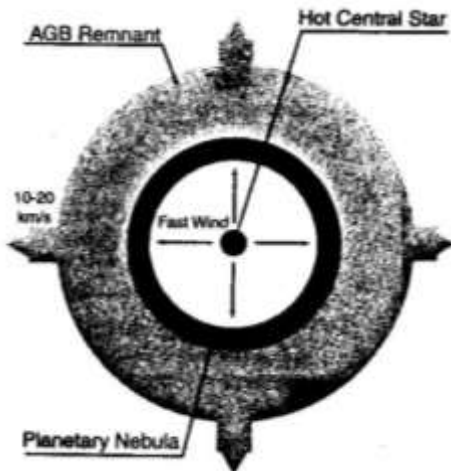


Fig 22.3

A model for the formation of Planetary Nebulae: the fast wind from the central star runs into the slow wind ejected during the AGB phase. The interaction region (black) is shock heated and ionized, producing the nebula. Outside the nebula is the un-shocked cold AGB wind. (ISW Fig 12.8)

It is easy to show (ISW 12.5) that the velocity of the interaction region between the slow AGB-wind and the fast CSPN wind is

$$V_{PN}(t) \simeq V_{AGB} \left\{ 1 + \sqrt{\frac{\dot{M}_{CS} V_{CS}}{\dot{M}_{AGB} V_{AGB}}} \right\}$$

Adopting mean values of $\dot{M}_{CS} \approx 10^{-7}$ and $\dot{M}_{AGB} \approx 10^{-4}$ M_{sun}/yr and $V_{CS} = 2000$ and $V_{AGB} = 20$ km/s, we find that $V_{PN} \approx 40$ km/s, in agreement with the observations.

The mass of the interaction region, part AGB wind and part CSPN wind, is

$$M_{PN}(t) \simeq t \times \dot{M}_{CS} \sqrt{\frac{\dot{M}_{AGB}/V_{AGB}}{\dot{M}_{CS} V_{CS}}}$$

where t is the time since the wind of the CSPN has reached the AGB wind.

Q?

Explain why the expansion velocity of a PN depends on the ratio $\dot{M}_{CS} V_{CS} / \dot{M}_{AGB} V_{AGB}$

The Table below (ISW Table 12.1) shows the results of calculations.

Notice that:

- The mass of the interacting zone (i.e. the PN) after 10^4 years is of order $0.2 M_\odot$, which is only a small fraction of the mass ejected on the AGB.
- The expansion velocity is of order $30 - 50$ km/s which is much faster than the AGB wind and much slower than the CSPN wind.
- The size of the PN after 10^4 yrs is about 0.2 to 0.5 pc.

Table 12.1 Planetary nebulae gas shell parameters from the interacting wind model

\dot{M}_{cs}	\dot{M}_{rg}	v_{cs}	v_{rg}	$V_s(t)$	$\frac{M_s(t)}{t}$	$\frac{R_s(t)}{t}$	$\frac{\Delta R_s(t)}{R_s(t)}$
$\frac{M_\odot}{\text{yr}}$	$\frac{M_\odot}{\text{yr}}$	$\frac{\text{km}}{\text{s}}$	$\frac{\text{km}}{\text{s}}$	$\frac{\text{km}}{\text{s}}$	$\frac{M_\odot}{10^3 \text{ yr}}$	$\frac{\text{pc}}{10^3 \text{ yr}}$	
3×10^{-7}	1×10^{-5}	1000	10	27	0.017	0.027	0.31
3×10^{-7}	3×10^{-6}	1000	10	40	0.009	0.041	0.12
1×10^{-6}	3×10^{-6}	1000	5	44	0.024	0.045	0.08

The subscript “s” refers to the shocked interaction region, which is the PN.
The mass and the expansion velocity of the PN refer to 1000 yrs after the onset of the fast wind.

Note: Most PN have complex morphologies that require additional effects to be taken into account such as:

- rotation and non-spherical winds of AGB stars
- binarity
- magnetic fields.

(see Balick and Frank, 2002, ARAA; and July 2004 Scientific American)

23. White Dwarfs

23.1 The Evolution of White Dwarfs

When $M_{\text{env}} < 10^{-4}$ to $10^{-6} M_{\odot}$ (depending on L) the shell fusion stops, the luminosity decreases and the radius decreases. The star moves into the WD-cooling track (see Fig 22.1). All stars with initial mass $M_i < 8 M_{\odot}$ end their lives as WDs.

White dwarfs are stars that are electron non-relativistic degenerate, so their EoS is $P \sim \rho^{5/3}$. This means that they are polytropes with $\gamma = 5/3$ or $n = 1.5$.

Combining this EoS with hydrostatic equilibrium gives the mass radius relation for WDs.

$$P_c \sim GM^2/R^4 \sim (\rho/\mu)^{5/3} \sim M^{5/3} / \mu^{5/3} R^{5/3}$$

so

$$R \sim M^{-1/3} \text{ or } M \sim \text{Vol}^{-1}$$

Numerically:

H - WD	A/Z = 1	$R = 3.2 \times 10^4 (M_{WD}/0.5M_{\odot})^{-1/3}$ km
He or C/O WD	A/Z = 2	$R = 1.0 \times 10^4 (M_{WD}/0.5M_{\odot})^{-1/3}$ km

Since the mass remains constant, the radius remains constant. So an evolution track (cooling track) of a WD is along a line of constant R!

The luminosity of WD comes from the cooling.

The electrons cannot cool ! because they are degenerate, so their energy distribution is set by the density (which does not change) and not by the temperature. Only the ions can cool and they contain almost all of the mass of the WD. The loss of thermal energy is converted into radiation at the photosphere.

Initially the ions had a temperature of order 10^8 K, which was the temperature of the Helium-fusion shell and also that of the isothermal core. Such young very hot WD cool down fast and so their luminosity is relatively high ($\sim 10^{-1} L_{\odot}$). However, as the ions cool, the luminosity decreases and so the cooling slows down even more and the luminosity decreases over time.

(For the derivation of the cooling time: see Pols 10.2.1)

Cooling time:

$$\tau_{\text{cool}} \simeq \frac{4.5 \times 10^7}{\mu_{\text{ion}}} \cdot \left(\frac{L/L_{\odot}}{M/M_{\odot}} \right)^{-5/7} \text{ in yrs} \quad \mu_{\text{ion}} = 2 \text{ for He and C,O}$$

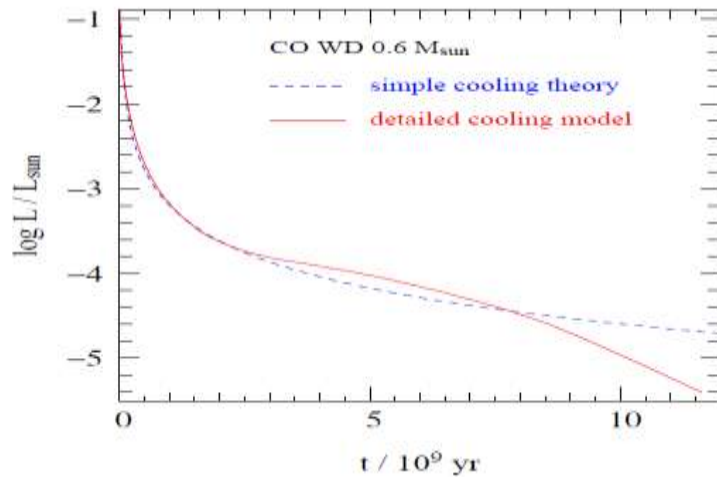


Fig. 23.1 The cooling curve of a CO-WD of 0.6 Msun. Dotted line: simplified model (Mestel 1952). Full line: taking into account crystallization (Winget 1982) (OP fig 10.8)

To go from PN ($L \sim 10^4 L_\odot$) to $10^{-2} L_\odot$ (average $\sim 1 L_\odot$) takes few 10^7 yrs.

To cool down a WD from $10^{-2} L_\odot$ to $10^{-4} L_\odot$ takes few 10^9 years.

To cool down a WD from $10^{-4} L_\odot$ to $10^{-5} L_\odot$ takes 10^{10} years.

White dwarfs come in two groups:

1. with a spectrum dominated by H-lines = DA
2. with a spectrum dominated by He-lines = DB

This distinction is based on the spectrum. But that does not give information on the internal composition! The gravity at the surface of a WD is high ($\sim 10^8$ cm/s²) and the atmosphere is so stable that gravitational diffusion made the Helium settle below the (often extremely thin) H-atmosphere. WD that really consist of H (instead of He or C-O) can be distinguished on the basis of their mass radius relation!

23.2 The Chandrasekhar Mass-Limit for White Dwarfs

The Mass-Radius relation for WD shows that R will decrease as M increases. However, as M/R^3 increases with increasing mass, the density may become so high that the electrons become relativistic degenerate. If the WD is completely relativistic degenerate the EoS is $P \sim \rho^{4/3} \rightarrow n = 1/(\gamma - 1) = 3$.

Combining this with the H.E. condition gives

$$P_c \sim GM^2/R^4 \sim (\rho/\mu_e)^{4/3} \sim M^{4/3}/R^4$$

so

M = constant for relativistic degenerate white dwarfs.

This shows that relativistic degenerate stars can only exist for one specific value of the mass. This is the **Chandrasekhar mass limit**

$$M_{ch} = 1.46 (2/\mu_e)^2 M_\odot \quad \text{with} \quad \begin{aligned} \mu_e &= 1 \text{ for H} \\ \mu_e &= 2 \text{ for He, C, O} \end{aligned}$$

In reality this implies that stars with $M > M_{ch}$ cannot exist. They will collapse as a **Supernova of type Ia** (no H lines) = collapse of a C/O white dwarf.

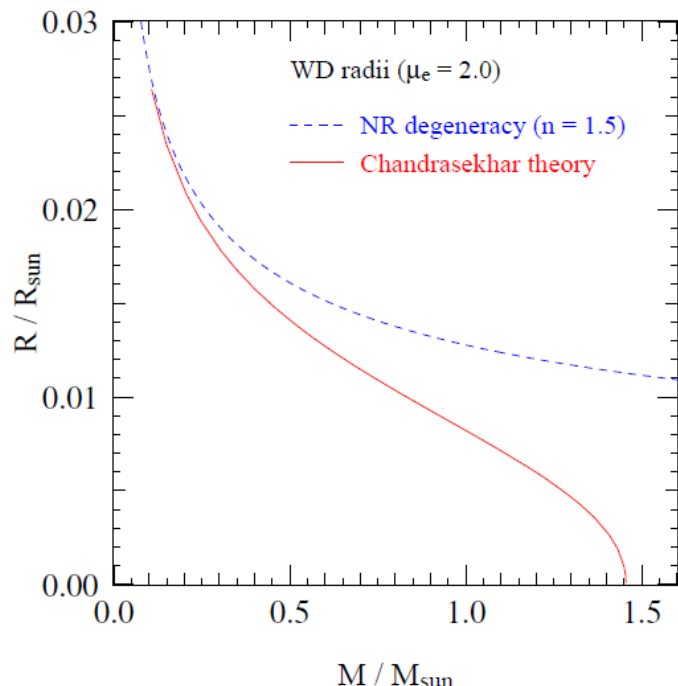


Fig 23.2 The mass radius relation of a helium or CO white dwarf.

Dotted line: the $R \sim M^{1/3}$ or $V \sim M^1$ relation for non-relativistic degenerate WDs.

As the mass increases and the radius decreases a larger and larger fraction of the WD becomes relativistic degenerate. This is shown by the dotted line. The radius goes to zero at the Chandrasekhar limit of $1.46 M_{\text{sun}}$. (OP fig. 10.6)

24. Stellar Pulsation

24.1 The instability strip in the HRD: RR Lyrae stars, Cepheids and δ Scuti stars.

There is a strip in the HRD where stars pulsate when their evolution track passes through it : **the instability strip**

- *Low mass metal poor stars* cross this strip during core-He fusion on the Horizontal Branch, where they are
RR Lyrae stars of spectral type A5 to A7 during maximum and F1 to F3 during minimum, with periods of 0.05 to 1 day, and $L \sim 10^2$ to $10^3 L_{\text{sun}}$.
- *Massive metal rich stars* cross the instability strip when they describe a loop HRD during the core-He burning phase, where they are
Delta Cepheids or simply **Cepheids** of spectral type F5 to F8 during maximum with periods of 1 to 50 days and $L \sim 3 \cdot 10^2$ to $3 \cdot 10^4 L_{\text{sun}}$.
WW Virginis stars are the metal-poor (Pop II) equivalents of Cepheids.
- There is even an extension of the instability strip down to the *main sequence*, where they pulsate as
Delta Scuti stars of spectral type ~F3 with periods of 0.1 to 0.2 days.

Both the low mass and the high mass stars also cross the instability strip when the move from the MS to the Hayashi track during the H-shell fusion phase. However this transition is so fast that the number of observed variables is much smaller than in the longer phase of He-core fusion

All these stars pulsate in the fundamental mode and so their period scales with the dynamical timescale:

$$P = C \tau_{\text{dyn}} = \frac{C}{\sqrt{G\rho}} \quad \text{with } C \text{ of order unity.}$$

The pulsation is in fact a standing pressure wave, driven in the ionization zone, and travelling between the stellar center and the open outside. Because the temperature structure in the different types of stars is not the same, and so the sound speed crossing time depends on the evolutionary phase, the constant C is different for the different types of variables.

24.2 The κ-Mechanism

RR Lyrae stars, Cepheids and δ Scutis are variable because of the κ-mechanism in the H and He-ionization zone. (κ = absorption coefficient)

The κ-mechanism works in layers which is partly ionized, because in ionization zones the degree of ionization and the opacity can change during compression and expansion.

To explain this: let us first look at the working of a normal combustion motor (e.g. in a car). For an engine to work, it needs heat input in the cylinder at the right moment, i.e. when the gas is compressed. This is done by producing a spark in the fuel during compression. This spark results in heated gas which expands and drives the cylinder upwards. It is crucial that the gas is heated when it is compressed! (If you would ignite the spark at the moment of minimum compression, i.e. when the cylinder is at its highest position, the motor would not work.)

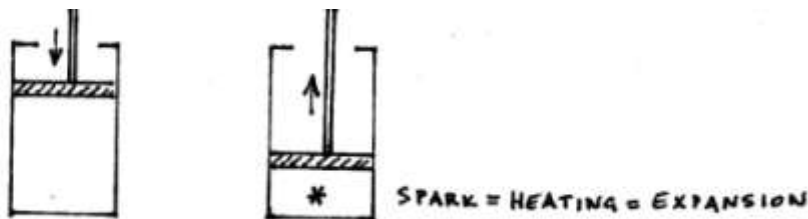


Fig 24.1 The working of a combustion motor. The spark ignites the fuel gas when the gas is compressed. This heats the gas so its expands.

Compare that with the energy of an ionization zone in a star, i.e. at $2 - 4 \cdot 10^4$ K. In a normal, fully ionized = non-pulsating layer:

Compression $\rightarrow \rho \uparrow, \rho T \uparrow, \kappa \downarrow$ (because $\kappa \sim \rho T^{-7/2}$)

and so: radiation escapes more easily if a layer is compressed.

In a partly ionized = pulsating layer:

Compression $\rightarrow \rho \uparrow$ but T rises marginally because the heat goes into ionizing the gas

$\rightarrow \kappa \uparrow$ and so radiation flow is blocked (trapped)

\rightarrow heat input during compression!

Expansion $\rightarrow \rho \downarrow, T$ about constant because gas recombines and releases energy, $\kappa \downarrow$ = energy escapes.

This works like a motor because the **ionization layer stores energy during compression and releases it during expansion**.

This effect can also be explained in terms of γ_{ad} (e.g. CO ch 14, OP ch 10.4). A layer is pulsational unstable if $\gamma_{ad} < 4/3$. We have seen in Section 5.8 that this happens in partly ionized zones. This is basically the same explanation because it also describes how T changes during compression.

In principle this could work in the partial ionization zone of *any* star, but it only produces an efficient pulsation if:

- the ionization = pulsating layer is **not too deep**, otherwise the layers above it will damp the pulsation. This occurs for very cool stars. **Q:** why?
- the ionization = pulsation layer is **not too close** to the surface, otherwise there is no mass to push up and down. This occurs for the hot stars.

So: stars only pulsate via the κ -mechanism if the partial ionization zone has the right depth, i.e. the star has the right surface temperature. That is the reason why there is an instability strip of RR Lyrae and Cepheids in the HRD.

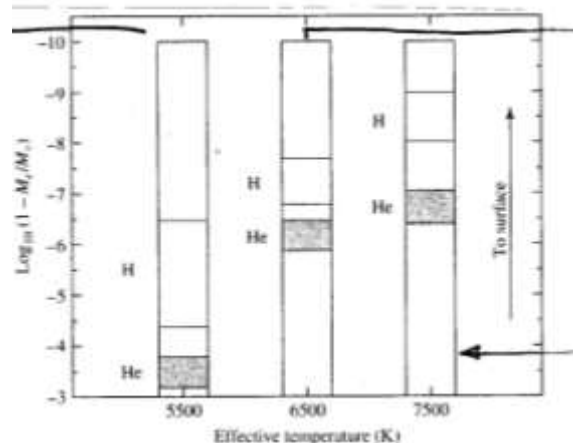


Fig 24.2 The depth of the Helium-ionization zone in stars of different T_{eff} . In the left model, the star is too cool and the He ionization zone is too deep: and the layers above it damp the pulsation inside the star. In the right hand model, the star is too hot and the ionization zone it not deep enough: there is not enough mass above the ionization zone to push the ionization zone layer the middle model the ionization zone is at the right depth for pulsation.

24.3 Pulsating stars in the HRD (C+O p. 547)

Notice that stars with radial pulsation (Cepheids, RR Lyrae, δ Scuti) are all in a narrow T-strip in HRD. This is the strip where the He-ionization zone has the right depth. (The H-ionization zone is usually not very efficient: it is too close to the surface with not enough material above it).

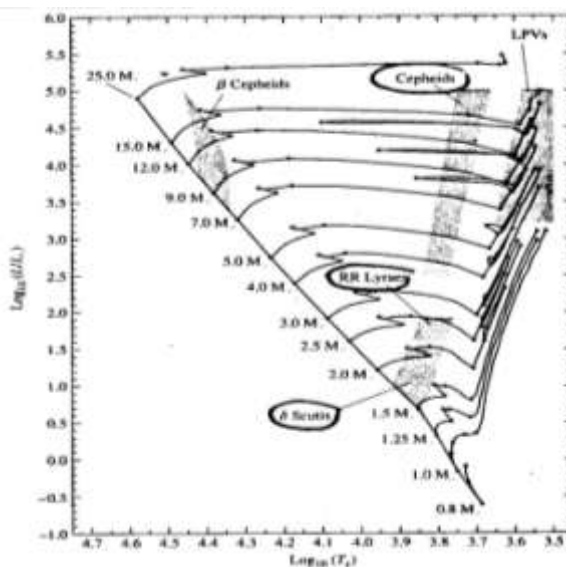


Fig 24.3
For stars pulsating in the fundamental mode, Cepheids, RR Lyr, and δ Scuti, the period scales with the dynamical time $P \sim 1/\sqrt{G\rho}$
For narrow instability strip this translates into a **P-L relation**
 $P = f(L)$

Stars can also pulsate in other ways:

- **radial pulsation in higher n modes**, i.e. overtones
- **non-radial pulsation modes**, in which the star changes shape, e.g. like Bessel harmonic functions.

Non-radial pulsations can be due to

- **gravity modes, (g-modes)** in which gravity is the restoring force, or
- **pressure modes, (p-modes)** in which pressure is the restoring force.

An overview of the different types of variables is shown in Fig 24.4.

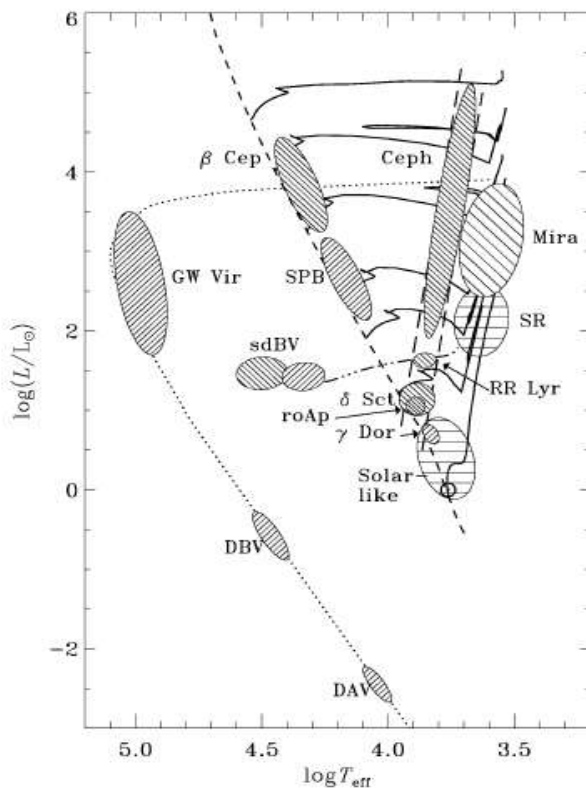


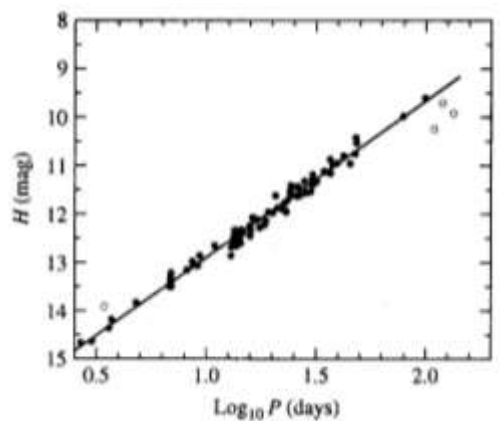
Figure 10.11. Occurrence of various classes of pulsating stars in the H-R diagram, overlaid on stellar evolution tracks (solid lines). Cepheid variables are indicated with ‘Ceph’, they lie within the pulsational instability strip in the HRD (long-dashed lines). Their equivalents are the RR Lyrae variables among HB stars (the horizontal branch is shown as a dash-dotted line), and the δ Scuti stars (δ Sct) among main-sequence stars. Pulsational instability is also found among luminous red giants (Mira variables), among massive main-sequence stars – β Cep variables and slowly pulsating B (SPB) stars, among extreme HB stars known as subdwarf B stars (sdBV) and among white dwarfs. Figure from Christensen-Dalsgaard (2004).

Fig 24.4 An overview of all types of variable stars and their location in the HRD. Notice the main instability strip for radial pulsation that covers the Cepheids, RR Lyrae and δ Scuti stars.

24.4 Radial pulsations

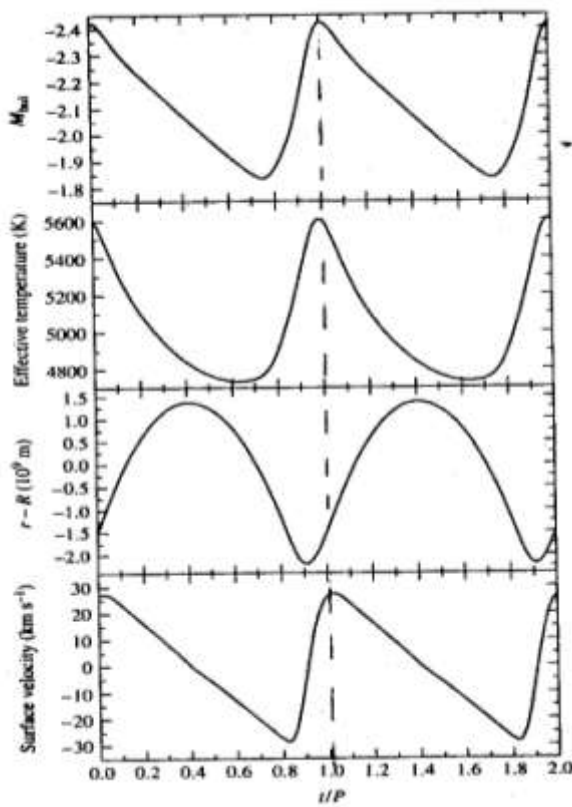
Radial pulsators have periods that strictly follow Period-Luminosity relations, which are due to the fact that pulsations are standing waves with a sound speed crossing time that is proportional to $p^{-0.5}$.

The most accurate P-L relations are those in the infrared, because the IR is in the Rayleigh-Jeans part of the spectrum, where the magnitudes are less sensitive to the details of the changes in spectral type.



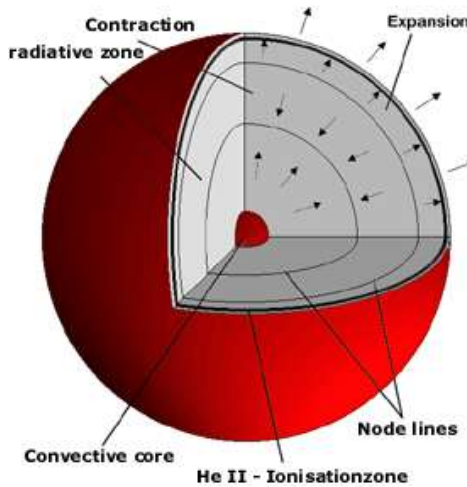
*Fig 24.5
The P versus H -magnitude
relation of Cepheids in the LMC.
(Fig CO)*

Fig 24.6 shows the variations in L , T_{eff} , R and v_{rad} of an RR Lyrae star. Notice that the velocity curve and M_{bol} have a sawtooth shape, with maximum luminosity corresponding to maximum outward velocity. This agrees with the explanation of the κ -mechanism, which requires that the radiation that is trapped in the ionization zone is released during expansion ! T_{eff} and R are almost anticorrelated, showing that minimum radius occurs just before maximum T_{eff} .



*Fig 24.6
Variation in M_{bol} , T_{eff} , R
and v during the pulsation
of an RR Lyrae star.
Notice that T_{eff} and R vary
almost opposite and that
maximum L coincides
with maximum expansion
velocity.
(Fig CO)*

Most radial pulsators pulsate in the fundamental, $n=1$ mode, in which case there is only one node. Stars can also pulsate in overtones, $n>1$. In that case there are more (viz n) nodes. An example of a Cepheid with $n=2$ pulsation is shown in Fig. 24.6.



*Fig 24.6
Schematic picture of a Cepheid pulsating in the $n=2$ mode.
(Figure from Zima 1999, Master thesis)*

24.5 Non-radial pulsations (NRP)

The pulsation pattern of NRPs is characterized by two quantum numbers (m,l):

- **m describes the number of meridional nodes.**
 $m=0$ is symmetric around the rotation axis.
 $m=1$ is two opposite moving (east-west) hemispheres, where one half is moving upward when the other half is moving downward.
- **$l-m$ is the number of nodes in the latitude direction.**
if $l=m$ there are no latitude nodes.

Fig. 24.7 shows the modes for $l=3$ and different m modes.

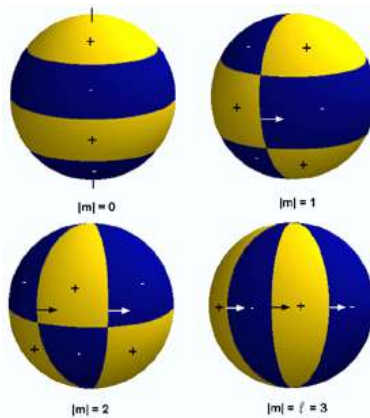


*Fig 24.7
The topology of NRP for $l=3$ modes
and different m modes.
From upper left to lower right:
 $(m, l-m) = (0,3), (1,2), (2,1), (3,0)$*

*Notice: $m = \text{nr of longitudinal zones}$
 $l-m = \text{nr of latitudinal zones}$*

(Figure from Zima 1999, Master thesis)

25. The Evolution of Massive Stars

We have seen that massive stars ($M > 8 M_{\odot}$) can go through all phases of nuclear fusion, up to the Fe-core. So the *internal evolution* goes by a series of successive fusion-phases, ending with a shell like structure, consisting of shells of different compositions.

25.1 Main characteristics of massive star evolution

- 1 The *external evolution* of massive stars proceeds mostly along horizontal lines in the HRD, i.e. about constant luminosity, because the star does not develop a degenerate core and most of the mass is in radiative equilibrium.
- 2 The luminosity increases slightly during the MS phase (due to the μ -effect) and when the star briefly reaches the Hayashi limit.
- 3 **The evolution of massive stars is strongly influenced by mass loss.**
Stars above $30 M_{\odot}$ typically lose about 15 percent of their mass during the main sequence phase so the products of nuclear fusion appear at the surface right after the MS phase.

The evolution proceeds differently in three distinct mass ranges

- (1) The stars with $8 < M_i < 25 M_{\odot}$ become **red supergiants** (RSG) in their H-shell fusion phase. (This is similar to the RGB of lower mass stars, but their He core is not degenerate.) During their He-core fusion phase they make a leftward loop in the HRD and temporarily become **yellow supergiants**. (This is similar to the HB of low mass stars). The later fusion phases are all spent as a RSG (Hayashi limit). In the end these RSGs explode as SN. So their evolution track in the HRD is quite similar to those of stars of $M > 4 M_{\odot}$ but they never develop a degenerate core.
- (2) The stars with $25 < M_i \lesssim 50 M_{\odot}$ also become **RSG**, but their mass loss rate is so high that after a short time at the Hayashi limit they have lost most of their envelope and move to the left of the HRD. (This is similar to the post AGB evolution of lower mass stars, but they do not become WDs). When they are in the left of the HRD they have a very high mass loss rate and their atmospheres are dominated by He, N and C. These are **Wolf-Rayet stars** (WR-stars). They explode as SN in the WR phase.
- (3) Stars with $M_i \gtrsim 50 M_{\odot}$ become instable due to radiation pressure in their envelope immediately after the MS, because they are very close to the photospheric Eddington limit. They become **Luminous Blue Variables** with high mass loss rates and occasional eruptions. They stay on the blue side in the HRD where they become **Wolf-Rayet stars** and explode as SN.

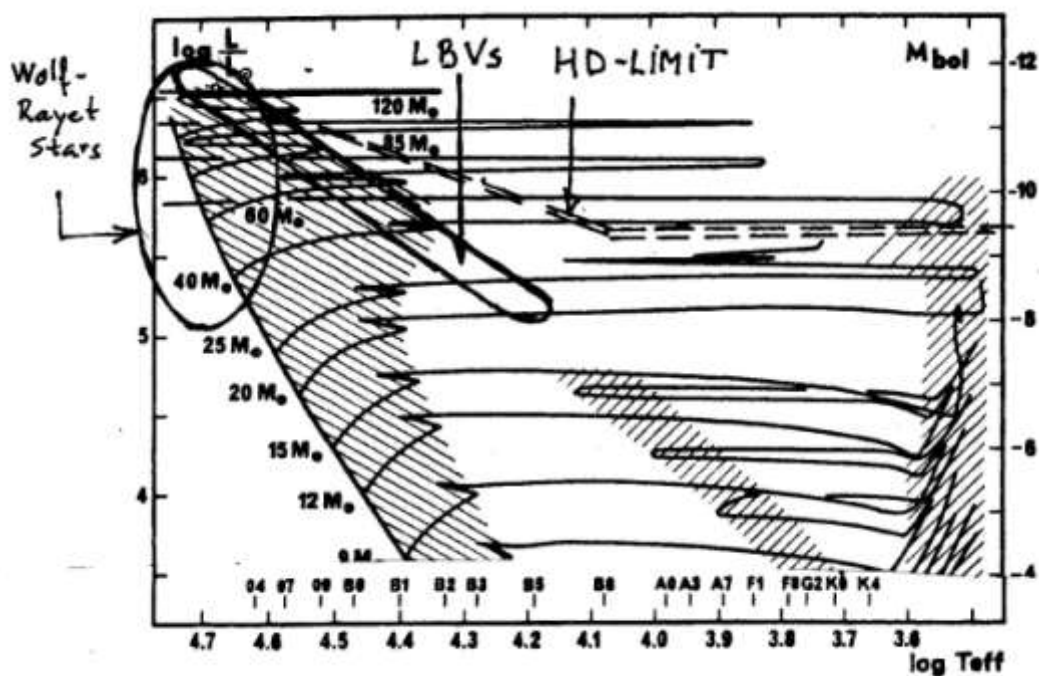


Fig 25.1 Predicted evolutionary tracks of massive stars with mass loss and overshooting are shown in the Appendix E (from Maeder 2009). The figure shows the top part with several phases indicated. Left-slanted dashed areas indicate H-core fusion. Right-slanted dashed areas indicate later fusion phases. The leftward loops occur during He-core fusion (equivalent to the HB of lower mass stars). The location of the Wolf-Rayet stars and the Luminous Blue Variables are indicated. The Humphreys-Davidson limit (HD-limit) is the observed upperlimit of stars in the HRD.

25.2 The effect of mass loss during the MS phase

The evolution of massive stars is dominated by mass loss.

Fig. 25.2 shows the first calculations of the mass loss on the evolution of massive stars.

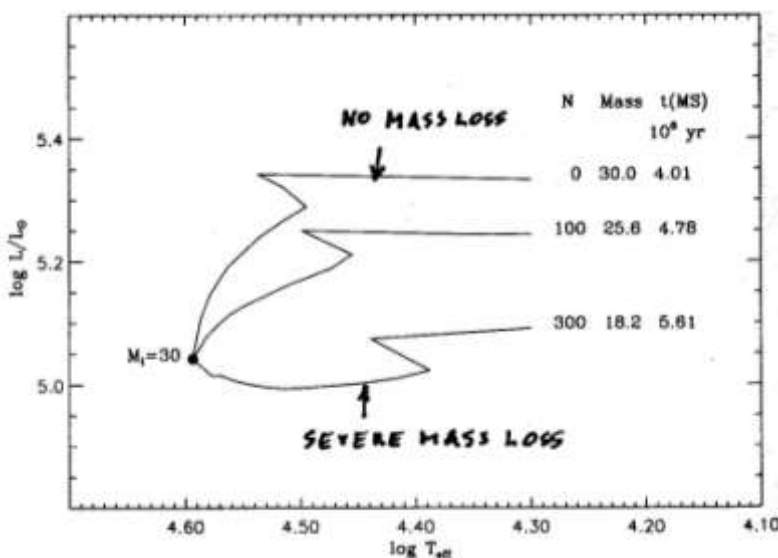


Fig 25.2 The effect of mass loss during the MS phase of a $30 M_{\odot}$ star. The mass loss is specified as $dM/dt = N L/c^2$ with $N=0$, 100 ($= 7 \cdot 10^{-7} M_{\odot}/\text{yr}$ on the ZAMS) and 300 ($= 2 \cdot 10^{-6} M_{\odot}/\text{yr}$ on the ZAMS). Remember that L/c^2 is the mass loss rate produced by one strong absorption line in the wind. The table gives the remaining mass at the end of the MS (TAMS) and the MS lifetime. (Fig ISW, from Lamers and de Loore 1978)

The figure below shows the first calculations of the effect of mass loss on the evolution of massive stars. Evolution without mass loss is “conservative” evolution. We call the initial mass M_i and the final mass M_f . For conservative evolution $M_f = M_i$.

Notice that:

- The luminosity increases less than in conservative evolution. This is because the total mass decreases and also the size of the convective core is less than in conservative evolution. As a consequence, μ increases less.
- At the end of the MS the star is less luminous than for conservative mass loss, but more luminous than expected on the basis of its *actual* mass, M_f . This is because the star has a more massive He core than a star that started with a mass M_f and evolved conservatively.
- The MS phase lasts longer due to the lower L .

- At the end of the MS phase the N-abundance increases at the surface: it is an **ON-star** (O for spectral type O, and N for nitrogen). This is because the core with convective overshooting has brought N into the *radiative* envelope, up to the point where $M(r) \sim 0.9 M_*$. When the star is peeled off by mass loss during the mainsequence to this depth during, the enriched layers appear at the surface. (This is different from the dredge-ups of low mass stars, where the enriched matter is brought all the way to the surface by envelope convection).

25.3 The predicted Photospheric Eddington Limit and the observed Humphreys-Davidson upperlimit.

The photospheric Eddington Limit (Eddington dip)

Massive stars have such a high luminosity that they are close to their Eddington limit for radiative pressure. We have seen that for massive stars with electron scattering opacity in their interior, the Eddington limit

$L_E = 4\pi c G M / \sigma_e \approx 3 \text{ to } 4 \cdot 10^6 L_{\text{sun}}$ with $M \approx 150 \text{ to } 200 M_{\text{sun}}$. (Sect 8.3). However in the upper envelope and the photosphere the absorption coefficient is higher than σ_e . See the peak in κ at $T < 10^6 \text{ K}$ for $\rho < 10^{-8}$ in Fig. 6.1 (p 34). At photospheric densities of order 10^{-10} the opacity has a peak around 10 to 20 kK. A peak in κ implies a drop in the photospheric Eddington Limit $L_E(\text{phot})$ because $L_E \sim 1/\kappa$.

Lamers and Fitzpatrick (1988) argued that this results in a limit in the HRD that has a minimum L_E around $T_{\text{eff}} \approx 10\,000 \text{ K}$. Stars that reach that limit when they evolve to the right in the HRD after the MS phase will become unstable and suffer severe mass loss. The situation is sketched in Fig 25.3.

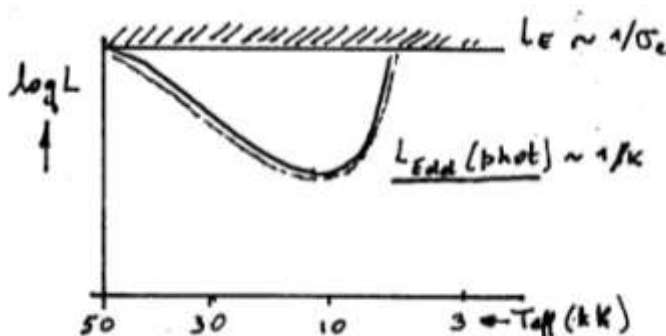


Fig 25.3
The effect of a bump in the absorption coefficient in photospheres of $T_{\text{eff}} \approx 10\,000 \text{ K}$ results in a dip in the photosphere Eddington limit, compared to the standard (interior) L_E .

The empirical Humphreys-Davidson limit (HD-limit)

The observed distribution of massive stars shows a conspicuous absence of star above $M_{\text{bol}} = -9.5$, corresponding to $L=5 \cdot 10^5 L_{\text{sun}}$. This same limit was found for the Milky Way, the LMC and SMC. (Humphreys and Davidson 1994, PASP 1026, 1025). On first sight this is strange, because more luminous main sequence stars exist, and their evolution tracks are supposed to be horizontal in the HRD. This shows that stars more massive than about $50 M_{\text{sun}}$ do not evolve to the right of the HRD and do not become red supergiants.

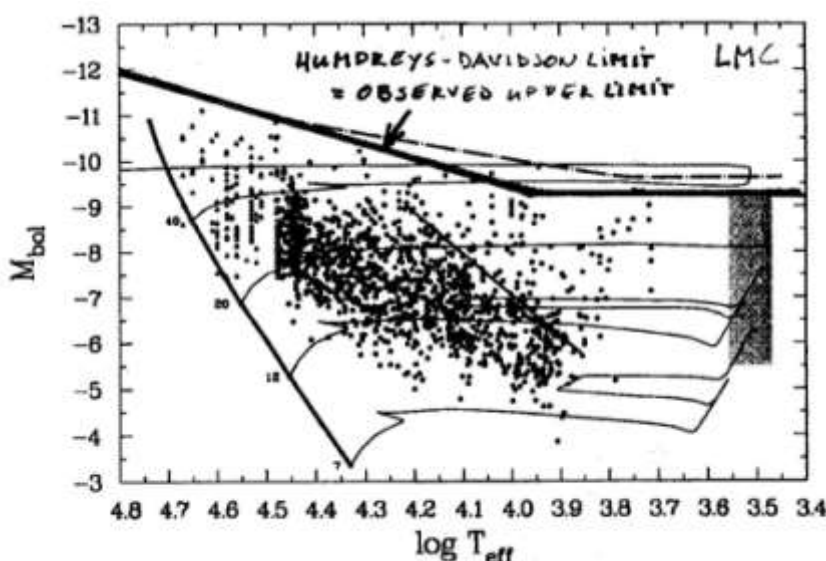


Fig 25.5

*The Humphreys-Davidson limit (observed luminosity upper limit) in the HRD of the LMC
(Fig. Massey 2003, ARAA 41, 15)*

The observed HD-limit can be explained by the photospheric Eddington dip. When stars more massive than about $50 M_{\text{sun}}$, ($M_{\text{bol}} < -9.5$) leave the MS and expand during the H-shell burning phase, they will hit the down-sloping hot side of the photospheric Eddington dip and their envelope will become unstable. This is the **Luminous Blue Variable** phase. The stars lose a large amount of mass in that phase, until the envelope is no longer massive enough to let the star evolve to the right of the HRD. Remember that post MS stars evolve to the right, i.e. increase their radius, because their envelopes becomes largely convective. The star then shrinks at constant luminosity and becomes **Wolf-Rayet star**.

25.4 Luminous Blue Variables (LBVs)

Luminous Blue Variables (LBVs) are very luminous blue supergiants with $L/L_\odot > 3 \cdot 10^5$ that show large and irregular variations in their V-magnitude. The variations occur on timescales from weeks to years, with occasional large eruptions

- every year or decade they change their radius: $30 R_\odot \rightarrow 100 R_\odot$.
After a few to ~ 10 years the radius goes back to normal.
- every few 10^2 to 10^3 years they have a “large eruption” (ala Eta Carina in 1860 and P Cygni in 1600) and eject $\sim 1 M_\odot$ of gas.

These stars are found near the HD-limit, indicating that they are marginally stable against radiation pressure. LBVs are rare: there are only a handful known in our Galaxy.

Fig. 25.6 shows the variations in V of 2 LBVs: S Dor (Gal) and R127 (LMC). Notice the large variations up to 1 or 2 magn over a period of about 10 years.
From: “LBVs: Astrophysical Geysers” (Humphreys and Davidson, 1994, PASP 106, 1025).

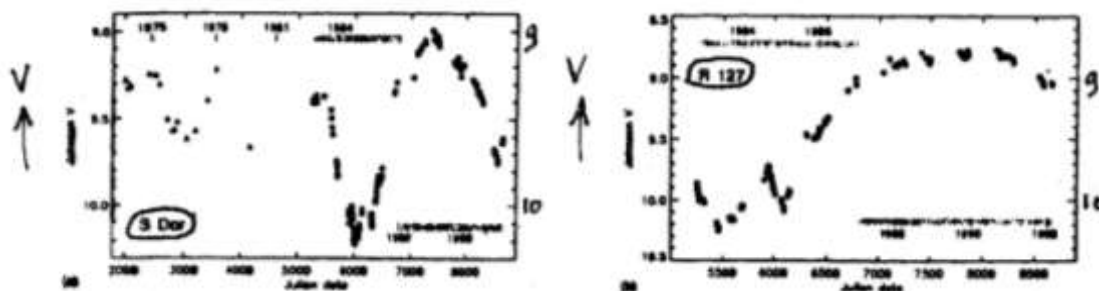


*Fig. 25.6 Lightcurves of two LBVs:
Left : S Dor (Galactic) from JD 2000-9000 (1973-1990).
Right: R 127 (LMC) from JD 5000-9000 (1983-1990).
Notice the strong but irregular variations of $\Delta V = 1.5$ to 2.0 magn. on timescales of years. (Fig from Spoon et al. 1994, A&AS 106, 141)*

Observations over the full spectrum have shown that the luminosity of the LBV remains approximately constant during these variations! This means that the variations are due to changes in T_{eff} and in the resulting bolometric corrections. **So the variability of LBVs is due to large radius variations, up to a factor 8.**

Figure 25.7 shows the locations of LBVs in the HRD and their variability. When the stars are faint, they are hot ($T_{\text{eff}} > 15000$ K) and most of their energy is in the UV. When they are bright, they are cool ($T_{\text{eff}} \sim 8000 - 9000$ K) and most of their energy is in the visual.

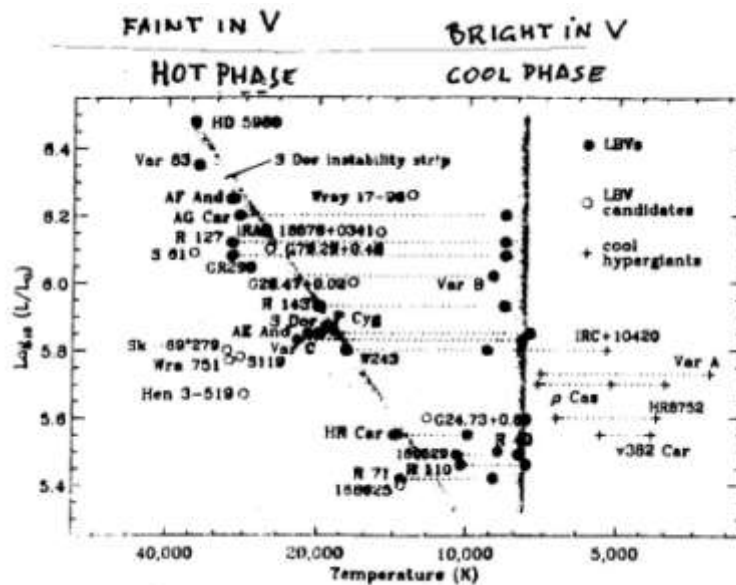


Fig 25.7 The locations of LBVs in the HRD. Each LBV makes horizontal excursions from the visual faint (high Teff and small R) to the visual bright (low Teff and large R) regions. (Fig from Humphreys and Davidson, 1994, PASP 106, 1025 “LBVs: astrophysical Geysers”)

Notice than in the “hot” phase (visual minimum) the stars are very close to the Humphreys-Davidson limit and to the photospheric Eddington Limit! In the hot phase they are to the left of the Eddington-dip and in the cool phase to the right. So the instability of these stars is somehow related to the fact that their envelopes and photospheres are only loosely bound, but the real reason or the mechanism is still not known.

25.5 Wolf-Rayet Stars (WR)

WR stars are luminous stars ($L > 10^5 L_\odot$) that have such a high mass loss rate (few $10^{-5} M_\odot/\text{yr}$), that one does not see the photosphere but only the wind: the spectrum is dominated by very broad emission lines formed in the wind with velocities of $V \sim 2000 - 4000 \text{ km/s}$. Their mass loss rates are high: 2 to $4 \cdot 10^{-5} M_\odot/\text{yr}$. (Nugis & Lamers, 2000, A&A 360, 227).

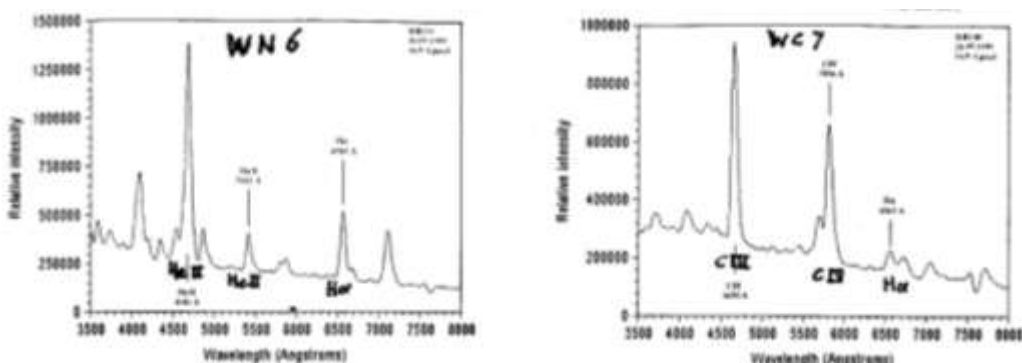


fig 25.8 Optical spectra of a WN star and a WC star. The WN star shows strong emission lines of H, HeII and NIII and NIV. The WC star has strong emission lines of HeII and CIV. The width of the lines indicates outflow velocities of ~ 2000 to $\sim 3000 \text{ km/s}$. The numbers in the classification 6 and 7 refer to an T_{eff} scale that goes from 3 (very hot) to 8 (hot) (Fig from ISW)

WR stars are end stages (= peeled-off) of massive stars.

They are located to the left of the MS at $30\,000 \text{ K} < T_{\text{eff}} < 50\,000 \text{ K}$ and $10^5 < L/L_\odot < 10^6$.

There are three types. In order of age or stage of peeling:

WNL = late WN = WR star with strong N-lines and “late” spectral type,
 $T_{\text{eff}} \approx 30\,000$ to $40\,000 \text{ K}$.

Some H left, He-enriched, N-rich

These are very massive stars near end of MS

WNE = early WN = N-rich WR stars of early spectral type $T_{\text{eff}} \gtrsim 40\,000 \text{ K}$.
No More H, He-rich, N-rich, C-poor (= products of CNO-fusion)

WC = C-rich WR star

$T_{\text{eff}} > 40\,000 \text{ K}$.

No more H; He-rich, C-rich, (= products of He-fusion)

WC stars are peeled-off further than WN stars.

(There is also a third class WO = O-rich, but that is not an abundance effect but a high temperature effect, when the O IV lines become stronger than the C IV lines.)

25.6 An example of a $60 M_{\odot}$ Star with Mass Loss

As an example of the evolution of a massive star with mass loss, we show the evolution track and the Kippenhahn diagram of a star of $60 M_{\odot}$, calculated by Maeder & Meynet (1989, AA 210, 155), tabulated in (1989, AA Supl 76, 411)

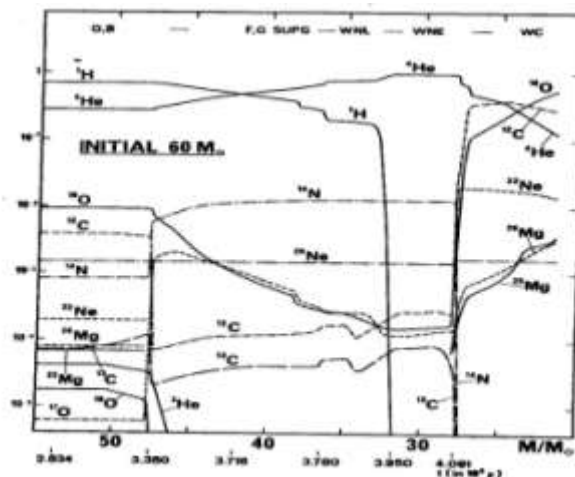
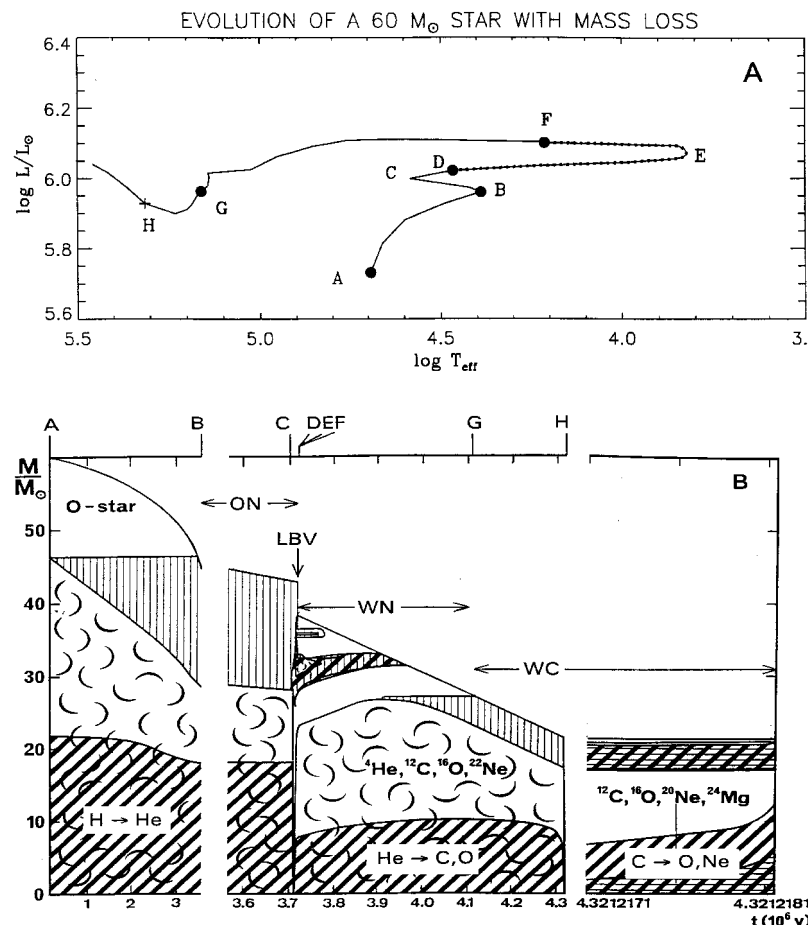


Fig 25.9.
The evolutionary track, the Kippenhahn diagram and the surface abundance during the evolution of a star of $60 M_{\odot}$. Hatched areas indicate fusion layers. Curls indicate convective zones. Vertical striped regions indicate modified abundances. (Figs Maeder & Meynet 1989)

Notice:

- The upper limit in the lower graph shows the mass that remains. (timescale is broken in three sections)
- The mass of He-core after H-fusion is larger than the Schonberg - Chandrasekhar limit. So the core immediately contracts after the MS and He-fusion starts in the core almost right after the MS. (see the KD). (This is different from low mass stars which have a phase of H-shell fusion: the RGB phase).
- In the very short time between the end of the H-core fusion and the He-fusion, the H-shell is the only energy source, so the H-shell fusion is in a thick layer. As soon as He-core fusion starts, the H-shell becomes less massive.
- Steep mass decrease at 3.7 Myr is due to LBV eruptions.
- Changes in *surface composition* in various stages as function of remaining mass are shown below. Correlate these with the tracks and try to explain them.

25.7 Evolution life times of massive stars

The table below gives the lifetimes (in Myrs) of H-fusion, and He-fusion for a grid of non-rotating massive stars (from Maeder & Meynet 1989 A&A 210, 155)

Table 2. Lifetimes in nuclear phases (in unit of 10^6 yr)

Initial mass	H-burning phase	He-burning phase	C-burning phase
$120 M_\odot$	2.9379	0.5132	0.001050
85	3.3236	0.5007	0.001840
60	3.7135	0.6058	0.001940
40	4.7902	0.6405	0.004798
25	7.0894	1.1711	0.007103
20	8.8068	1.2570	0.008789
15	12.1149	1.6232	0.015516
12	17.4571	2.6948	0.024600
9	28.7123	4.5948	0.058900
7	47.3028	9.6774	0.25 :
5	98.8419	27.1461	—
4	173.993	42.0780	—
3	398.803	128.956	—
2.5	733.586	234.196	—
2	1679.88	326.690	—

25.8 Summary of the Evolution of Massive Stars: the Conti Scenario

Before 1970 there were categories of massive stars with strange properties, e.g. the N-rich ON stars, the Of stars with many emission lines, the N-rich Wolf-Rayet stars (WN), the C-rich Wolf-Rayet stars (WC), the Luminous Blue Variables, etc. The evolutionary connection of these stars was totally unknown!

When mass loss from massive stars was discovered in the mid-late 1970s, Conti (1976) suggested a scheme for the evolution of massive stars, based partly on observations and partly on predictions that connected these different types in evolutionary sequences. (Conti 1976, Mem. Soc. Royale des Sciences de Liege, 9, 193; see also Maeder & Conti 1994, ARAA, 32, 277)

Conti-scenario
For $M \gtrsim 50 M_{\odot}$ (always blue) O-star – Of-star – BSG – LBV – WN – WC – (WO) – SN
For $25 M_{\odot} < M \lesssim 50 M_{\odot}$ (blue-red-blue) O-star – BSG – YSG – RSG – WN – (WC) – SN (high mass loss) – WN – SN (low mass loss)
For $M < 25 M_{\odot}$ (blue-red) O-star – BSG – RSG – YSG (and Cepheid) – RSG – SN

The different types of stars in this scenario are:

- O = O-stars without emission lines (low $\dot{M}, < 10^{-6} M_{\odot}/\text{yr}$)
- Of = O-stars with emission lines (high $\dot{M}, > 10^{-6} M_{\odot}/\text{yr}$)
- BSG = Blue Supergiants (O, B, A)
- YSG = Yellow Supergiant (F, G)
- RSG = Red Supergiant (K, M)
- LBV = Luminous Blue Variable (with Eruptions)
- WN = WR star with N-rich wind, He-rich, some H (high $\dot{M}, > 10^{-5} M_{\odot}/\text{yr}$)
- WC = WR star with C-rich wind, He-rich, no H (high $\dot{M}, > 10^{-5} M_{\odot}/\text{yr}$)

NB: The limit of $50 M_{\odot}$ is somewhat uncertain. It is between 40 and $60 M_{\odot}$.

26. The Effect of Rotation on Stars

Massive stars are in general rapid rotators, at least on the Main Sequence. Rotation affects the evolution of stars in several ways.

- i. A rapidly rotating star is not spherical but oblate, with a higher temperature at the poles than at the equator.
- ii. Rapid rotation in a star produces mediational circulation which can lead to severe mixing and to the transport of angular momentum to the envelope. This slows down the core and speeds up the outer layers.
- iii. The winds of rapidly rotating stars are not spherical: it may be enhanced at the equator (due to lower effective gravity) or at the poles due to the higher radiative flux. This depends on the effective temperature of the star.
- iv. Very rapidly rotating stars of high luminosity may become unstable by the combination of the large radiation pressure (Γ -effect) and centrifugal force (Ω -effect). This results in an $\Omega\Gamma$ -limit in the HRD, which is at lower luminosity than the classical Eddington Γ_e -limit.

26.1 The Von Zeipel Effect

Lines of constant effective gravity, $g_{\text{eff}} = g_{\text{grav}} - g_{\text{centr}}$, in rapidly rotating stars are not spheres but become oblate, by the centrifugal acceleration, g_{centr} . The **critical velocity**, v_{crit} , is the equatorial rotation velocity where $g_{\text{eff}} = 0$ at the equator.

$$\frac{v_{\text{crit}}^2}{R_{\text{eq}}} = \frac{GM_{\text{eff}}}{R_{\text{eq}}^2} \rightarrow v_{\text{crit}} = \sqrt{\frac{GM_{\text{eff}}}{R_{\text{eq}}}} = \sqrt{\frac{GM_*(1-\Gamma_e)}{R_{\text{eq}}}}$$

where we have used $M_{\text{eff}} = M_*(1 - \Gamma_e)$ with $\Gamma_e = \sigma_e L / 4\pi c GM$ to correct for radiation pressure by electron scattering (Sect 8.3). Using $v_{\text{rot}} = \Omega R_{\text{eq}}$ we can express this in terms of a **critical angular velocity**

$$\Omega_{\text{crit}} = \sqrt{GM_*(1 - \Gamma_e)/R_{\text{eq}}^3}$$

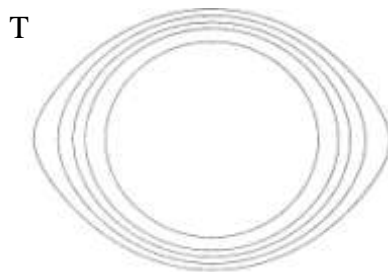


Fig 26.1

The figure shows the lines of constant g_{eff} for a rigidly rotating star, rotating at about half the critical rotation speed. (Fig from ISW)

Lines of constant g_{eff} are also iso-potential lines and iso-pressure and iso-thermal lines. Close to the pole the iso-thermal lines are closer together than at the equator. This implies that the T-gradient and hence the radiative flux (local T_{eff}) is higher at the pole than at the equator!

The Von Zeipel Theorem:
The local radiative flux is proportional to the local effective gravity

$$F_{\text{rad}}(\Omega, \Theta) = \sigma T_{\text{eff}}^4(\Omega, \Theta) = \frac{L}{4\pi GM_*} \cdot g_{\text{eff}}(\Omega, \Theta) \rightarrow T_{\text{eff}}(\Omega, \Theta) \sim g_{\text{eff}}(\Omega, \Theta)^{1/4}$$

where Ω is the angular velocity and Θ is the latitude ($\Theta=0$ and π at the poles). The total luminosity is

$$L_* = 4\pi \int_0^{\pi/2} R^2(\Theta) F(\Theta) \cdot \sin(\Theta) d\Theta$$

As a result, the **T_{eff} and spectral type at the poles are hotter than at the equator**. This implies that the spectral type and the luminosity derived from observations will depend on the orientation of the rotation axis compared to the line of sight! Part of the widening of the MS of globular clusters could be due to this effect (de Mink and Bastian, 2010).

The table below gives the mean values for main sequence stars (half way between the ZAMS and TAMS) of to $120 M_{\odot}$ (from Maeder)

Table 4.1 Initial masses, actual masses, log luminosities, log T_{eff} , radii, Eddington factor Γ , critical velocities $v_{\text{crit},1}$, spectral types and observed average rotational velocities for MS stars at the middle of MS evolution when the central H content $X_c = 0.30$. The masses, luminosities and radii are in solar units, the velocities in km s^{-1} . The average observed rotational velocities \bar{v} are obtained from the observed $v \sin i$ [139, 463, 519] multiplied by $4/\pi$ to correct for random orientation effects. See Table 14.2 for Γ at the end of the MS phase

Initial M	Actual M	Log L	Log T_{eff}	R	Γ	$v_{\text{crit},1}$	SP	\bar{v}
120	98.96	6.316	4.642	24.91	0.544	711	O3	—
85	77.61	6.114	4.603	23.63	0.436	646	O5	220
60	57.07	5.876	4.594	18.72	0.343	623	O6	220
40	38.74	5.551	4.571	14.32	0.239	586	O7.5	220
25	24.39	5.105	4.521	10.79	0.136	536	O9	220
20	19.60	4.867	4.490	9.46	0.098	513	B0	280
15	14.84	4.533	4.444	7.96	0.060	487	B0.5	290
12	11.95	4.252	4.402	6.99	0.039	466	B1	310
9	8.99	3.857	4.339	5.93	0.021	439	B2	255
7	7.00	3.485	4.277	5.14	1.14×10^{-2}	416	B3	240
5	5.00	2.956	4.184	4.29	4.70×10^{-3}	385	B5	290
4	4.00	2.588	4.117	3.82	2.52×10^{-3}	365	B7	320
3	3.00	2.090	4.026	3.28	1.06×10^{-3}	342	B9	260
2.5	2.50	1.759	3.968	2.92	5.98×10^{-4}	330	A1	—
2	2.00	1.353	3.897	2.54	2.93×10^{-4}	316	A7	160
1.7	1.70	1.055	3.846	2.28	1.74×10^{-4}	308	F1	110
1.5	1.50	0.825	3.821	1.96	1.16×10^{-4}	312	F3	75
1.25	1.25	0.488	3.795	1.50	6.41×10^{-5}	325	F7	35
1	1.00	-0.003	3.765	0.98	2.58×10^{-5}	360	G2	<10

Notice that MS stars with $M_i > 2 M_{\odot}$ rotate at about half the critical velocity.

26.2 Meridional Circulation

Rapid rotation induces meridional circulation due to shear-forces between layers of different rotation speed. This effect is strong on the main-sequence. The figures below show the circulation pattern in a MS star of $20 M_{\odot}$ (from Maeder, Section 11).

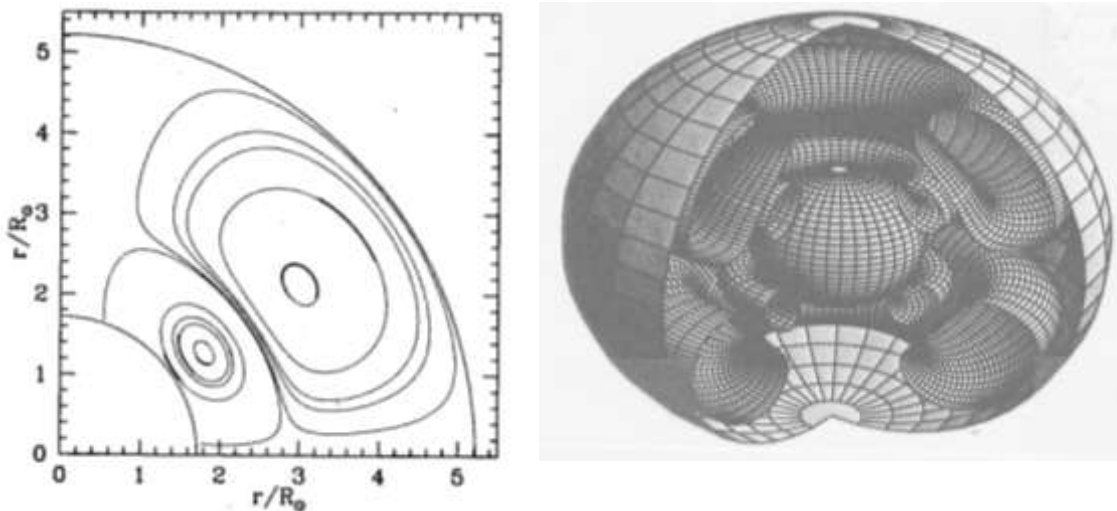


Fig 26.2 Two representations of the meridional circulation currents in a $20 M_{\odot}$ MS star, halfway between the ZAMS and TAMS. The initial rotation velocity is 300 km/s.

Left: schematic. Right: 3-D demonstration of the same pattern.

The inner sphere is the convective core. The inner circulation cell is rising toward the pole and descending along the equator. The outer circulation is rising along the equator and descending along the poles. (see Maeder Fig 11.2 for a colour version)

Meridional circulation is very **efficient for mixing**. In general, massive stars only have convective mixing and overshooting in their cores. But rapid rotation can produce mixing all the way up to the surface during the MS phase. This explains the observed correlation between $V \sin i$ and the N/C abundance ratio on and near the end of the MS (Brot et al. 2011).

In the most extreme case, with very fast rotation, the mixing is so severe that the star remains chemically homogenous. In that case a massive star evolves to the left and upward in the HRD during its H-fusion phase, and evolves gradually from the ZAMS for H-stars to the MS for Helium stars, which is to the left and higher of the MS for H-stars (remember Homework 2.2).

26.3 Non-Spherical Mass Loss of Rotation Stars

The winds from hot stars are driven by radiation pressure. Rapidly rotating stars are more luminous at the pole, so they will have a **higher mass loss rate from the pole than from the equator**. At the same time, the wind velocity V_∞ will also be higher at the pole than at the equator, because $V_\infty \sim V_{\text{esc}}$.

However, observations of massive stars often show that the **wind density is concentrated in the equatorial plane**. For instance, **Be stars** (B main sequence stars with optical emission lines) and **B[e] supergiants** (B-type supergiants with forbidden emission line) have equatorial outflowing disks. So in these stars the wind is concentrated along the equator and not along the poles.

This can be explained by two effects:

- The **density** of the wind scales as $\rho_w \sim \dot{M}/4\pi r^2 v_w$. So even if \dot{M} is higher at the pole, the density of the wind may be higher at the equator because V_∞ is smaller at the equator.
- The wind changes its characteristics (\dot{M} and V_∞) around $T_{\text{eff}} \sim 21000\text{K}$. This is called the **bi-stability jump**. We have seen this already in Sect 16.3.3 and Fig 16.7 which showed that the wind velocity changes drastically from $2.6 v_{\text{esc}}$ at $T_{\text{eff}} > 21000\text{ K}$ to $1.3 v_{\text{esc}}$ at $T_{\text{eff}} < 21000\text{ K}$. At $T_{\text{eff}} > 21000\text{K}$ the wind is mainly derived by Fe IV lines and at $T_{\text{eff}} < 21000\text{K}$ it is driven by lower ionization lines (Fe III etc). This explains the jump in V_∞/V_{esc} from 2.6 at $T_{\text{eff}} > 21000\text{K}$ to 1.3 at $T_{\text{eff}} < 21000\text{K}$.

A rapidly rotating star with $T_{\text{eff}} > 21000\text{K}$ at the poles may have $T_{\text{eff}} < 21000\text{K}$ at the equator. At some inclination angle between the pole and the equator, the structure of the wind may change due to the bi-stability effect, where the mass loss increases and V_∞ decreases towards the equator. So ρ_{wind} increases strongly toward the equator. This produces **rotation-induced-bistability** disks of B[e] supergiants and possibly also the Be main sequence stars (Pelupessy et al. 2000)

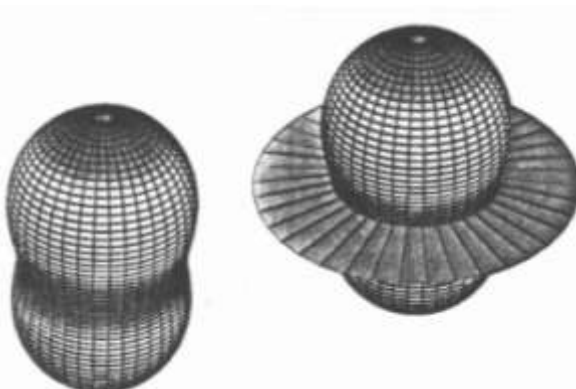


Fig 26.3

Left: Mass flux from a rotating star of $100 M_{\text{sun}}$ and $L=3 \cdot 10^6 L_{\text{sun}}$ with a rotational velocity of 80% of the critical velocity and assuming $T_{\text{eff}}=30\,000\text{K}$ at the pole. Right: the same star with $T_{\text{eff}}=25\,000\text{ K}$ at the pole. This star has a rotation induced bistability disk . (Fig Maeder)

27. Late Evolution Stages of Massive Stars

27.1 Fusion phases

The late evolution phases of stars more massive than about $M_i \sim 8 M_\odot$ proceed at an increasing speed. This is mainly due to the loss of energy by neutrinos. For a star to remain in equilibrium its energy production has to be $L_{\text{tot}} = L_{\text{rad}} + L_\nu$ with L_{rad} required to maintain hydrostatic and thermal equilibrium and L_ν is the neutrino loss. The timescale of each phase is approximately

$$t = M_{\text{nuc}} \times \left(\frac{\Delta m}{m}\right) \cdot c^2 / (L_{\text{rad}} + L_\nu)$$

where M_{nuc} is the mass of the nuclear material available for fusion.

The table in Sect 25.7 gives the timescales of the H, He and C fusion phases for stars of different masses. Notice the very short time of the C-fusion phase, less than 10^4 yr for stars initially more massive than $15 M_\odot$. The later evolution phases go even faster.

The Table below gives the timescales of the different fusion phases for a star of **$15 M_\odot$** . The Ne-fusion and O-fusion lasts about a year, whereas the Si-fusion lasts only a few weeks. (from Wooley et al. 2006, ARAA 44, 507)

burning stage	$T (10^9 \text{ K})$	$\rho (\text{g/cm}^3)$	fuel	main products	timescale
hydrogen	0.035	5.8	H	He	$1.1 \times 10^7 \text{ yr}$
helium	0.18	1.4×10^3	He	C, O	$2.0 \times 10^6 \text{ yr}$
carbon	0.83	2.4×10^5	C	O, Ne	$2.0 \times 10^3 \text{ yr}$
neon	1.6	7.2×10^6	Ne	O, Mg	0.7 yr
oxygen	1.9	6.7×10^6	O, Mg	Si, S	2.6 yr
silicon	3.3	4.3×10^7	Si, S	Fe, Ni	18 d

The table below (from Hirschi et al. 2004 AA 425, 649) gives the lifetimes of the different fusion phases for a range of masses. It also shows the mass of the different chemical elements at the end of the stable Si-fusion. The last two lines give the total mass of Si and Fe when the core collapses. These are slightly higher than at the end of the Si-fusion.

Notice the effect of stellar rotation on the evolution. Fast rotating stars have more mixing and higher mass loss rate.

	Initial model properties									
M_{ZAMS}	15	15	20	20	25	25	40	40	60	60
v_{ZAMS}	0	300	0	300	0	300	0	300	0	300
Lifetime of burning stages										
τ_{H}	1.13 (7)	1.43 (7)	7.95 (6)	1.01 (7)	6.55 (6)	7.97 (6)	4.56 (6)	5.53 (6)	3.62 (6)	4.30 (6)
τ_{He}	1.34 (6)	1.13 (6)	8.75 (5)	7.98 (5)	6.85 (5)	6.20 (5)	4.83 (5)	4.24 (5)	3.85 (5)	3.71 (5)
τ_{C}	3.92 (3)	1.56 (3)	9.56 (2)	2.82 (2)	3.17 (2)	1.73 (2)	4.17 (1)	8.53 (1)	5.19 (1)	5.32 (1)
τ_{Ne}	3.08	0.359	0.193	8.81 (-2)	0.882	0.441	4.45 (-2)	6.74 (-2)	4.04 (-2)	4.15 (-2)
τ_{O}	2.43	0.957	0.476	0.132	0.318	0.244	5.98 (-2)	0.176	5.71 (-2)	7.74 (-2)
τ_{Si}	2.14 (-2)	8.74 (-3)	9.52 (-3)	2.73 (-3)	3.34 (-3)	2.15 (-3)	1.93 (-3)	2.08 (-3)	1.95 (-3)	2.42 (-3)
End of central silicon burning										
M_{total}	13.232	10.316	15.694	8.763	16.002	10.042	13.967	12.646	14.524	14.574
M_{α}^{75}	4.211	5.677	6.265	8.654	8.498	10.042	13.967	12.646	14.524	14.574
$M_{\text{CO}}^{\text{int}}$	2.441	3.756	4.134	6.590	6.272	8.630	12.699	11.989	13.891	13.955
M_{CO}^{01}	2.302	3.325	3.840	5.864	5.834	7.339	10.763	9.453	11.411	11.506
M_{Si}^{50}	1.561	2.036	1.622	2.245	1.986	2.345	2.594	2.212	2.580	2.448
M_{Fe}^{50}	1.105	1.290	1.110	1.266	1.271	1.407	1.464	1.284	1.458	1.409
Last model										
M_{Si}^{50}	1.842	2.050	2.002	2.244	2.577	2.894	2.595	2.868	2.580	2.448
M_{Fe}^{50}	1.514	1.300	1.752	1.260	1.985	1.405	2.586	1.286	2.440	1.409

Fig 27.1 shows the evolution of the centers of stars in the T_c - ρ_c diagram for stars of 15, 25 and 35 M_{\odot} . We have argued in Sect 10.11 that the core is expected to evolve as $T_c \sim M_c^{2/3} \rho_c^{1/3}$.

The figure shows a slower increase: i.e. $\rho_c^{0.24}$. This is due to the fact that the mass of the core for every next fusion phase is smaller than the previous one.

The figure shows that the star settles into a new equilibrium (little wiggles) every time the next fusion phase occurs. In terms of time, the evolution of the core in this diagram speeds up enormously when it reaches higher temperatures. For instance, see the times given in the table for a 15 M_{\odot} star.

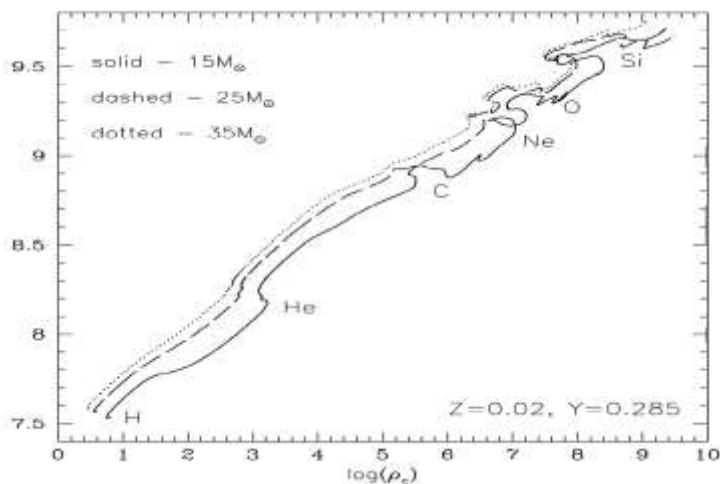


*Fig 27.1
The evolution of the cores
of stars of 15, 25 and 35
 M_{\odot} . in a T_c - ρ_c diagram.
(Fig 7.13 from SC)*

Fig 27.2 gives the corresponding Kippenhahn diagram of the inner $15 M_{\odot}$ as a function of time until collapse. (During all these phases the star is a red supergiant with $L \sim 5 \times 10^4 L_{\odot}$.) The hatched regions are the convective zones. Most of these are the core-fusion regions, and fusion shells with the reactions indicated. Notice the extremely short duration of the phases.

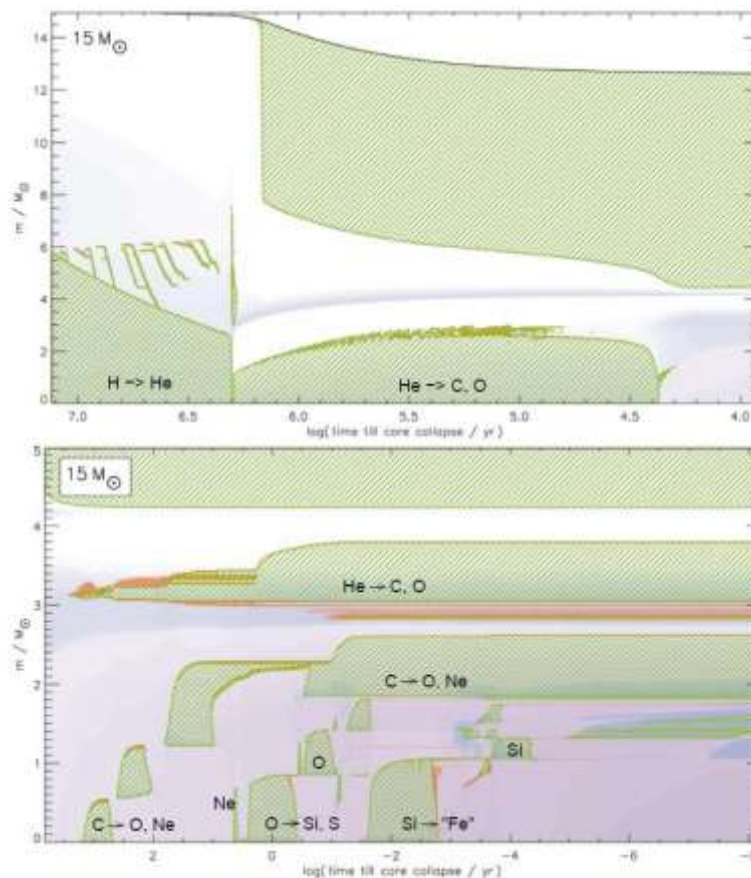


*Fig 27.2
The Kippenhahn
Diagram of the
late evolution
phases of a star
of $15 M_{\odot}$,
expressed as a
function of time
until core-
collapse.
(Fig OP 12.7, from
Woosley et al.
2002)*

27.2 Pre-Supernovae

Just before a massive star ends as a supernova, it has an onion-skin chemical structure with successive layers of fusion products.

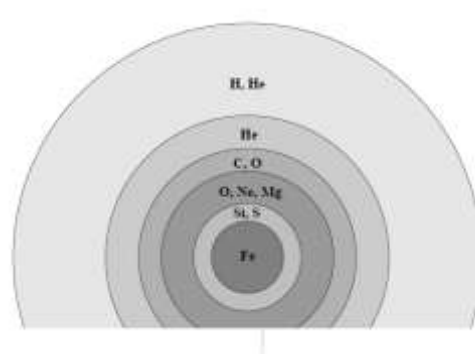


*Fig 27.3
The onion skin model of a massive
star just before the supernova
collapse. (OP Fig 15.1)*

The masses of the different cores during the various fusion phases are given in the table below, for stars of different initial masses, and initial rotation, $V_{\text{ini}} = 0$, and $V_{\text{ini}} = 300 \text{ km/s}$. (From Hirschi et al. 2004)

M_i is the initial mass, M_{final} is the final mass before the star explodes, $M_i - M_{\text{final}}$ is the mass that is lost during the evolution.

M_α is the mass of the Helium core after the H-fusion phase,

M_{CO} is the mass of the CO core after the He-fusion phase,

M_{Fe} is the mass of the Fe core after the Si-fusion phase.

M_{remn} is the remnant mass after the SN has exploded.

M_{ini}/M_\odot	$v_{\text{ini}} [\text{km s}^{-1}]$	M_{final}	M_α	M_{CO}	M_{Fe}	M_{remn}
9	0	8.663	2.185	0.920	-	0.920
9	300	8.375	2.547	1.413	-	1.239
12	0	11.524	3.141	1.803	-	1.342
12	300	10.199	3.877	2.258	-	1.462
15	0	13.232	4.211	2.441	1.561	1.510
15	300	10.316	5.677	3.756	2.036	1.849
20	0	15.694	6.265	4.134	1.622	1.945
20	300	8.763	8.654	6.590	2.245	2.566
25	0	16.002	8.498	6.272	1.986	2.486
25	300	10.042	10.042	8.630	2.345	3.058
40	0	13.967	13.967	12.699	2.594	4.021
40	300A	12.646	12.646	11.989	2.212	3.853
60	0	14.524	14.524	13.891	2.580	4.303
60	300A	14.574	14.574	13.955	2.448	4.323
85	0	17.236	17.236	16.564	-	5.115
85	300A	12.314	12.314	11.666	-	3.776
120	0	16.254	16.254	15.591	-	4.819
120	300A	11.270	11.270	10.663	-	3.539

Stars with $M_i < 25 M_\odot$ (depending on v_{ini}) still have substantial amount of H when they explode. They end their life as Red Supergiants and produce H-rich SNe.

Stars with $M_i > 25 M_\odot$ (depending on v_{ini}) have $M_{\text{final}} = M_{\text{He}}$. So all of the H has been lost. They end their life without H. These are the WR stars that produce H-poor SNe.

Notice that the remnant mass of stars of $M > 40 M_\odot$ is about the mass of the Fe-core plus the Si-shell. For $M < 20 M_\odot$ the remnant mainly contains the mass of the Fe-core. The mass of the Si-shell is ejected.

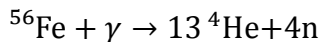
28 Supernovae

28.1 Core Collapse

After the star has developed an Fe-core it runs out of nuclear energy. At that time the core has a temperature of $T \sim 4 \times 10^9$ K and a density of $\rho > 10^9$ g/cm³ (see Fig 27.1) so the core is relativistic degenerate (see Fig 5.5, left), with $M > M_{\text{chandra}} \sim 1.3 M_{\odot}$ for stars of $M_i > 12 M_{\odot}$ (see Table in section 27.2). This cannot be stable so the core collapses.

Stars of $8 < M_i < 12 M_{\odot}$ do not reach Si-fusion so they do not produce an Fe-core. They can still go into core-collapse when at high-densities the electrons are captured by heavy nuclei. This reduces the pressure produced by electrons and the core collapses.

As the core collapses its temperature becomes so high, $T > 10^{10}$ K that the photons are energetic enough to break up heavy nuclei into lighter ones



Since this is an endothermic reaction that costs energy, rather than produces it, the core quickly cools and the collapse accelerates.

28.2 The SN Explosion

As the core collapses, and eventually is halted when it is a neutron star, the envelope is ejected in the SN-explosion. There are several processes that occur at the same time, but the three major effects for the ejection of the outer layers are:

- a. **Bouncing shock** at the surface of the neutron star. The matter that falls onto the very compact neutron star experiences a shock. The bounce of this shock is so strong and so energetic that it runs outward against the infalling material and eventually ejects it.

- b. During the infall the temperature is so high that the photons create neutrinos
Photo-neutrino production $\gamma + e^- \rightarrow e^- + \nu_e + \bar{\nu}_e$

$$\text{Pair-annihilation} \quad \gamma + \gamma \rightarrow \nu_e + \bar{\nu}_e$$

In the layers just above the neutron star, the density is so high ($\rho \sim 10^{11}$ g/cm³) that the neutrinos can be captured by the infalling gas. This is the case in the layers where the optical depth for neutrinos is $\tau_v > 1$.

(The layer where $\tau_v \sim 1$ is called the neutrino photosphere.)

The capture of the neutrinos by photons, neutrons and heavier particles just above the neutrino photosphere suddenly heats up the infalling layers so

strongly that the infall stops and is converted into an explosion with mass ejection.

- c. The fusion in the infalling fusion shells suddenly becomes very efficient, due to the increase in T and ρ . This creates a large amount of energy, that heats the infalling layers and produce so much gas-pressure that the explode.

These mechanisms work together to eject the layers outside the neutron star. If the neutron star captures more mass than about $2 M_\odot$, it collapses into a black hole.

28.3 Energetics of Supernovae

The **energy released** during the core collapse when its radius decreases from R_{ci} to R_{cf} is

$$E_{\text{collapse}} \simeq -\frac{GM_c^2}{R_{ci}} + \frac{GM_c^2}{R_{cf}} \simeq \frac{GM_c^2}{R_{cf}} \sim 3 \times 10^{53} \text{ erg}$$

Assuming that the core collapses from a WD ($M_c \sim 1.4 M_\odot$ and $R_{ci} \sim R_{wd} \sim 10^4$ km) to a neutron star with $R_{cf} \sim 20$ km we find that $E \sim 3 \times 10^{53}$ ergs.

The **potential energy necessary to expel the envelope** with mass $M_{\text{env}} = M - M_c$ is

$$E_{\text{env}}^{\text{pot}} = \int_{M_c}^{M_*} \frac{Gm}{r} dm \ll \int_{M_c}^{M_*} \frac{Gm}{R_{ci}} dm \simeq \frac{GM^2}{R_{ci}} \sim 3 \times 10^{52} \text{ erg}$$

Where we have used $M > M_c \sim 10 M_\odot$ and $R_{\text{env}} \gg R_{ci} = R_{wd} = 10^4$ km. This is a severe overestimate because we used $R_{\text{env}} \sim R_{ci}$. A more realistic model for the envelope gives $E_{\text{env}}^{\text{pot}} \sim 10^{50}$ erg.

The **kinetic energy** of the envelope is

$$E_{\text{env}}^{\text{kin}} = \frac{1}{2} M_{\text{env}} V^2 \sim 6 \times 10^{51} \text{ erg} \quad \text{if } M_{\text{env}} \sim 6 M_\odot \text{ and } V \sim 10^4 \text{ km/s.}$$

The peak luminosity of the SN is typically 10^8 to $10^9 L_\odot$ during about 60 days. So the **radiative energy** of the SN is about $E \sim 10^{48} - 10^{49}$ erg.

We see that $E_{\text{env}}^{\text{pot}} + E_{\text{env}}^{\text{kin}} + E_{\text{rad}} \ll E_{\text{collapse}}$

Only a small fraction of the energy released in the core collapse is used for ejecting the envelope and emitting light.

Most of the energy comes out in the form of neutrinos!

28.4 Types of Supernovae

The types of SN and their origin is shown in the figure below.

There are four major types

Type I = no H in spectrum

Ia = collapsing WD (from low mass binary system)

Ib = iron core collapse no H (from WR star)

Ic = iron core collapse , no H, no He (from WC star)

Type II = iron core collapse, with H (from Red Supergiant)

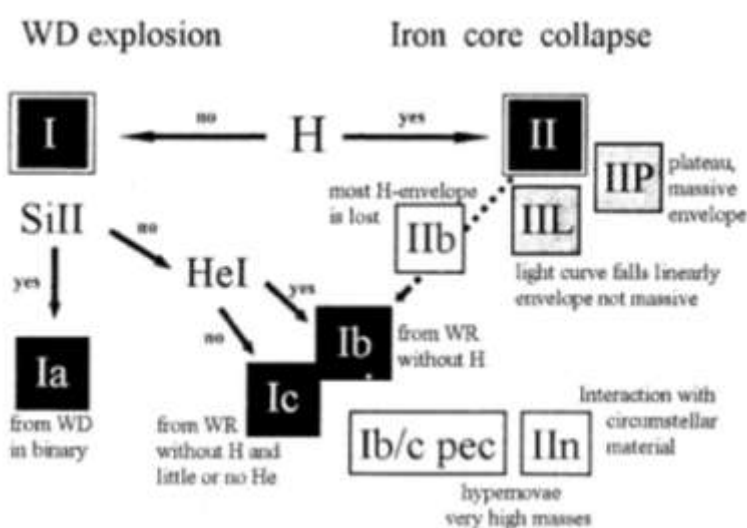


Fig 28.1
Different types of SN and
their progenitors (M fig
28.9)

28.5 The Remnants of Stellar Evolution

Fig 28.2 shows the types of SN and remnants as a function of M_i for $Z = 0.02$.

- The upper curve shows the mass after He-core fusion.
- The mass of H-rich material expelled (light grey)
- M_a is the mass of He that is expelled (middle grey)
- M_{co} is the mass of C and O that is expelled (dark grey)
- The mass of the remnants (black)

The fate of stars with $M_i > 50 M_\odot$ is uncertain. The final fate of stars also depends not only on their initial mass but also on metallicity and initial rotation velocity.

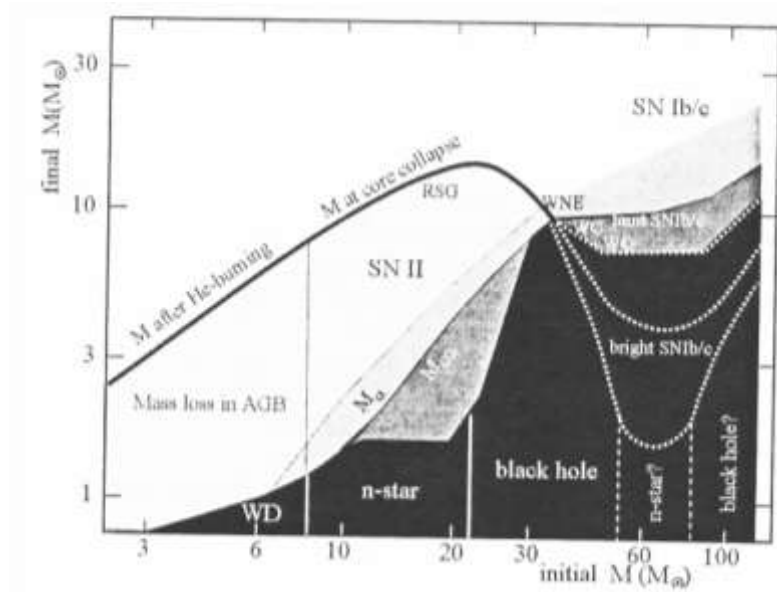


Fig 28.2

The remnants of stellar evolution.

(Mfig 28.13)

29. Stellar Yields of Single Stars.

Stellar yields describe the amount of gas and its composition that is returned to the ISM during the stellar life cycle. Yields can be calculated for each stellar mass. The **total yield** is the yield per star, multiplied by the relative number of the stars, i.e. by the Stellar Initial Mass Function.

Fig 29.1 shows the stellar yields for massive stars in the range of 8 to 120 M_{\odot} . It shows how much mass is ejected at each phase. (O=O-star, BA = A or B supergiant, RSG=red supergiant)

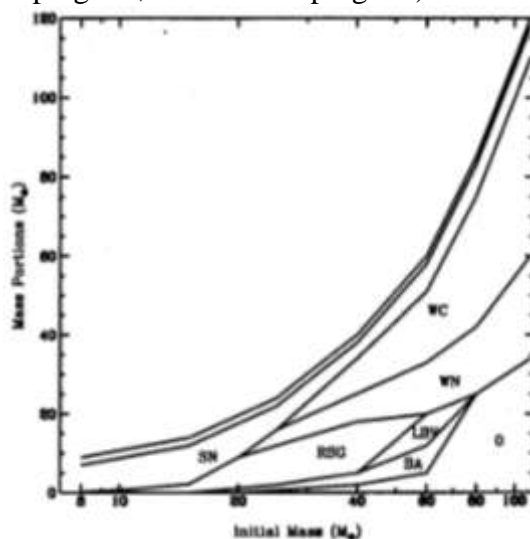


Fig. 29.1

The fraction of the matter that is returned to the ISM during various phases, as a function of M_i .
The narrow strip at the top is the mass that remains in the remnant.
(ISW Fig 12.9)

Fig 29.2 shows the total yield, i.e. the same as above but now weighted with a Salpeter IMF: $N(M) \sim M^{-2.35}$.

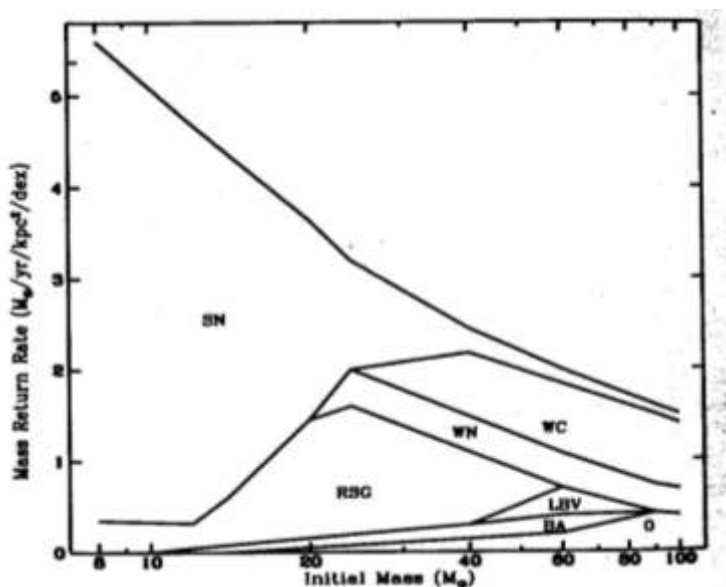


Fig 29.2

The total yield=
the mass that is returned to the
ISM by stellar evolution,
weighted with the number of
stars from the IMF
 $N(M) \sim M^{-2.35}$
(ISW Fig 12.10)

The effective yields is the mass fraction of the *new* heavy elements ejected into the ISM by winds and SN from massive stars.

Fig 29.3 shows the effective yields of massive stars separated by chemical elements.

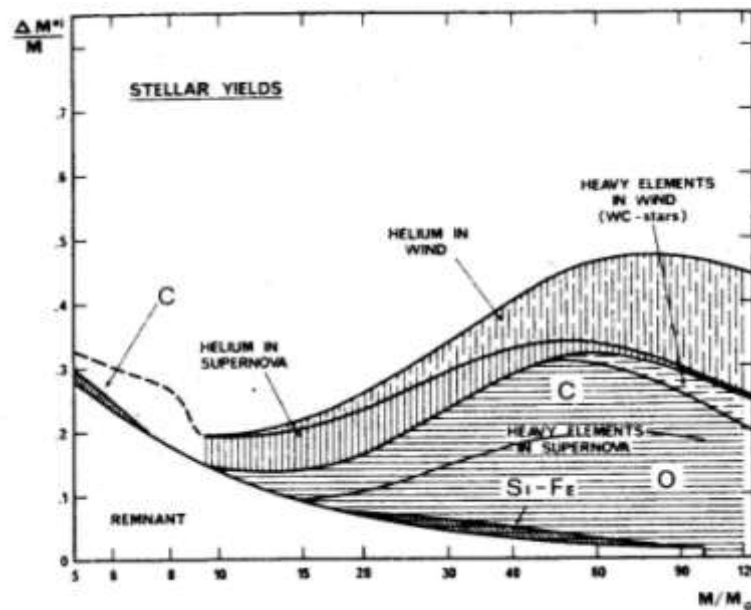


Fig 29.3

The effective yields: the mass fraction of *new* He and *new* heavy elements ejected as a function of the stellar mass. The contributions by winds and SN are separated. (Fig from Chiosi & Maeder 1986, ARAA 24, 329).

Notice:

- He:**
 - the most massive stars ($M = 20 - 120 M_{\odot}$) eject He by their winds.
 - the lower mass stars eject most of their He in SNe
 - although the lower mass stars ($M < 10 M_{\odot}$) eject a smaller fraction of their mass in the form of He than the massive stars. The overwhelming number of low mass stars implies that most of the enrichment of He comes from low mass stars.
- C:**
 - the most massive stars ($M > 60 M_{\odot}$) eject C in their winds (as WC stars)
 - the stars in the range of $10 - 120 M_{\odot}$ also eject a large fraction of their mass in the form of C by SNe.
 - the low mass stars ($M < 8 M_{\odot}$) also eject C in the form of C-rich AGB winds. The overwhelming number of low mass stars implies that most of the C-enrichment is these winds of low mass stars.
- O:**
 - most of the O-enrichment is by SN of massive stars ($M > 10 M_{\odot}$)
 - the most massive stars ($M > 40 M_{\odot}$) also lose O in the form of winds from WC stars.
- Fe-Si:** the enrichment of these elements is due to SN from massive stars ($M > 15 M_{\odot}$)

30 Binary evolution (see O.Pols 2014: Binary Evolution)

30.1 Potential surfaces of binaries

In this last chapter we will briefly consider the evolution of interacting binary stars. These are stars whose evolution is affected by the close presence of a companion.

Fig. 30.1 shows the equipotential surfaces of a binary system with a mass ratio of $M_1/M_2=2$.

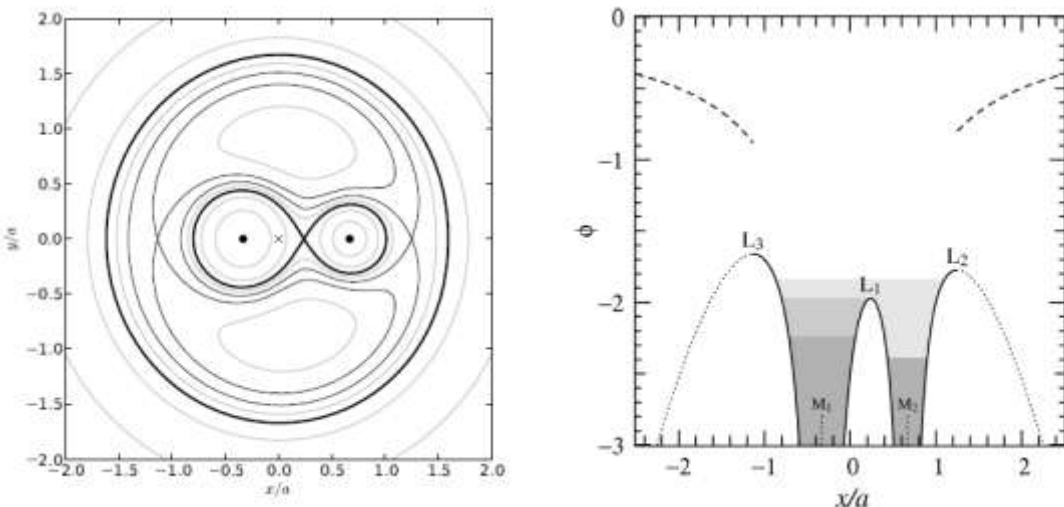


Fig 30.1 Left: the equipotential surfaces of a binary system with $M_1/M_2=2$, as seen from the orbital pole. The thick inner 8-shaped figure is the Roche lobe. Right: the depth of the potential wells of this binary system as a function of distance x/a from the center of gravity, where a is the separation. Star 1 is the heavier one, so it is closer to the zero point and the potential well is twice as deep as for M_2 . The location of the Lagrange points L_1 , L_2 and L_3 are indicated. The gray scales indicate three possible stable configurations: dark gray = detached systems, light gray = semi-detached systems where one of the components just fills its Roche lobe. Light gray = contact systems. (Pols 2014, figs 14.1 and 14.2)

Matter outside L_2 and L_3 is still bound to the binary, but it cannot maintain co-rotation.

30.2 Contact Phases

Binaries start to interact when the size of one of the two components reaches or overflows the Roche lobe. This depends on their separation and their radius. The radius of a star increases during several evolutionary phases:

- A. during the main sequence phase
- B. during the H-shell fusion phase when the star expands:
(evolution towards the RGB for low mass stars and
towards the RSG for massive stars)
- C. during the rise along the Hayashi line with fully convective envelope
(AGB phase for low mass stars, increasing L for RSG)

The evolution of interacting binaries is classified in three cases accordingly.:

Case A: when the first contact occurs during the MS phase

Case B: when the first contact occurs during H-shell fusion

Case C: when the first contact occurs when the star is on the Hayashi track.

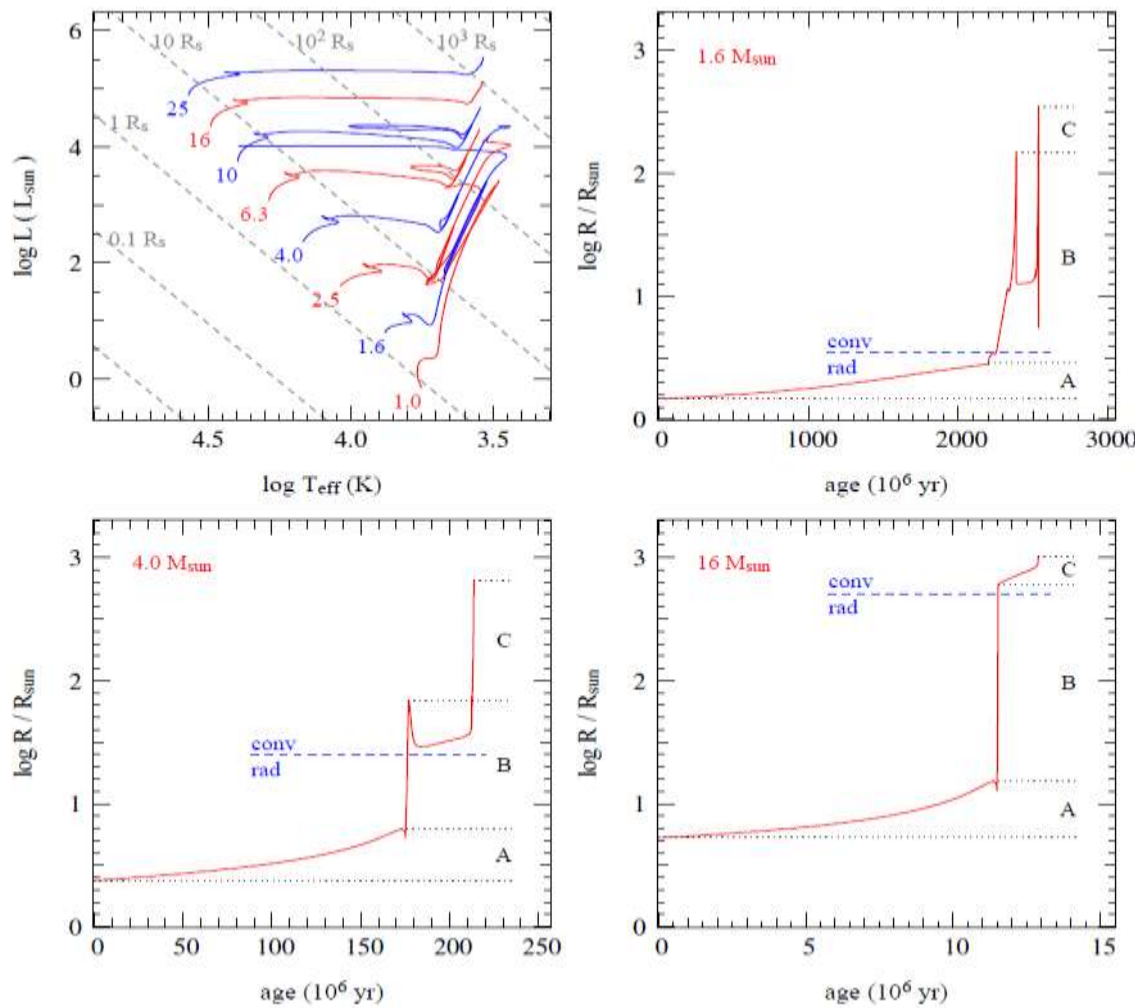


Fig 30.2 The HRD with the evolution tracks of stars between 1 and $25 M_{\odot}$ and the radius evolution of three stars of 1.6 , 4.0 and $16 M_{\odot}$. The ranges of radii for evolution in case A (MS), base B (H-shell fusion) and case C (climbing the Hayashi track) are indicated by dotted lines. The dashed lines indicate the separation between the times when the outer envelope is radiative and when it is convective. (Fig 14.3 of O.Pols 2014).

The larger the increase in radius at some phase, the more likely it is that the binary reaches contact at that phase.

30.3 Changes in period and separation during mass transfer

When one of the binary stars reaches its Rochelobe, matter may overflow to its companion. In the early lifetime of binaries the more massive star is the one to reach Rochelobe overflow first, because it evolves on a shorter timescale. In that case the **donor (d)** is the more massive star and the **accretor (a)** is the less massive one. However in later phases the less massive star might be the donor that transfers mass to the more massive one. For instance, in the case of a low mass red giant with a more massive neutron star companion.

Mass transfer can be **conservative** (no mass is lost) or **non-conservative** (mass is lost from the system: not all mass lost by the donor reaches the companion).

Mass transfer changes the period and the separation of a binary system. For conservative mass transfer of a binaries in a circular orbits the change in separation is (Pols sect 16.1.1).

$$\frac{da/dt}{a} = 2 \left(\frac{M_d}{M_a} - 1 \right) \frac{dM_d/dt}{M_d}$$

This shows that **the separation reaches a minimum if $M_d=M_a$** , i.e. when the masses become equal. The changes in separation and periods due to conservative mass transfer are

$$\frac{a}{a_i} = \left(\frac{M_{di}}{M_d} \cdot \frac{M_{ai}}{M_a} \right)^2 \quad \text{and} \quad \frac{P}{P_i} = \left(\frac{M_{di}}{M_d} \cdot \frac{M_{ai}}{M_a} \right)^3$$

where the subscript i indicates the initial value.

30.4 Stable and run-away mass transfer.

Mass transfer occurs when one of the two components fills its Rochelobe. When mass is transferred from a donor to an accretor three properties have to be considered: the change in radius of the donor, the change in separation and in Rochelobe size, the change in radius of the accretor.

Stable mass transfer occurs when the radius of the donor decreases due to mass transfer faster than the size of the Rochelobe. In this case the transfer of an amount of mass leads to a shrinking of the donor radius and it moves back within its Rochelobe. Stellar evolution of the donor will then let the radius expand again until it fills its Rochelobe and again transfers mass. This results in stable mass transfer on the **timescale of the evolution of the donor**. This is the case for **case A** transfer.

Run-away mass transfer = dynamically unstable mass transfer occurs when the transfer of the mass results in a shrinking of the Rochelobe whereas the donor radius does not shrink fast enough or even keeps expanding . In that case the mass transfer is so fast that the donor is out of hydrostatic equilibrium. Run-away mass loss occurs in stars with deep convection zones, i.e if the donor is on the Hayashi track : this happens in **case C mass transfer**.

The reason that interacting binaries on the Hayashi track will suffer dynamically unstable mass loss is because their luminosity is set by the core mass and their T_{eff} is almost constant. This mean that their radius is independent of the mass of envelope. So as an AGB star transfers mass to a lower mass companion, their separation decreases which decreases the Rochelobe volume, so more of the envelope mass of the AGB star will be transferred. etc. This will end when the star has lost almost all of its envelope and contracts on its way to become a WD, or a WR-star if it is massive.

Unstable mass transfer on thermal timescale is in between these two extremes. In that case the donor is out of thermal equilibrium (energy balance), but the mass transfer is slow enough for the donor to remain in hydrostatic equilibrium. (The time scale for mass transfer is slower than the dynamical timescale). Readjustment to thermal equilibrium occurs on a Kelvin Helmholtz timescale, so in this case the mass transfer is self-regulating and the timescale is **the Kelvin-Helmholtz timescale**. This happens in stars with radiative envelopes, i.e. in **case B transfer of massive stars** that are expanding after the MS but do not yet have reached the Hayashi track.

30.5 Case A transfer = Algol systems.

We discuss one typical example of case A mass transfer: an Algol binary

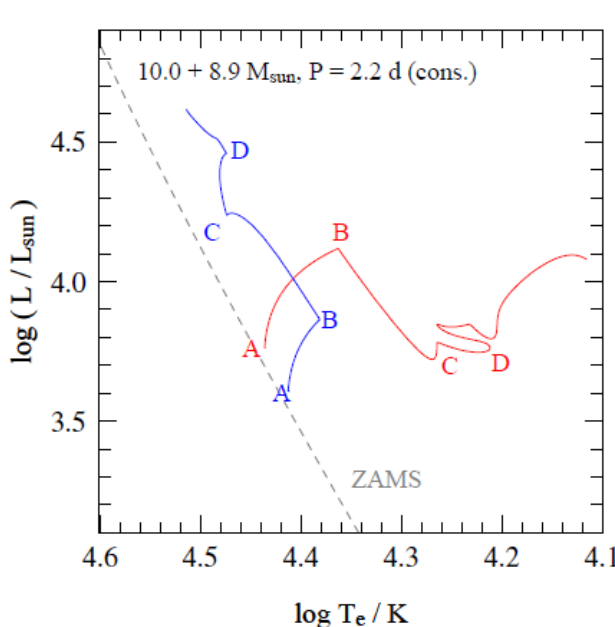


*Fig 30.3
The evolution tracks of the two components of a binary of $10 + 8.9 M_{\text{sun}}$ with $P=2.2$ days initially.
(O.Pols, 2014 Fig 17.2)*

Between point B and C (the star is still on the MS) the primary transfers mass to the secondary. The primary loses mass and gets fainter. At C it has lost 4 M_{sun} and so $M_1=6 \text{ M}_{\text{sun}}$ and $M_2=12.9 \text{ M}_{\text{sun}}$. After C it evolves more or less as a normal star of lower mass (HB and AGB). The secondary gains mass between B and C while it is still on the MS and so it moves up along the MS. When the mass of such a star exceeds that of the turn-off point of a cluster, it is a **blue straggler**.

30.6 Case B transfer = massive interacting binaries

When massive stars cross the Hertzsprung gap, i.e. when they move in the HRD from the MS to the Hayashi track, their radius may reach the Roche lobe and the star transfers mass. In this phase the expansion of the donor is on the Kelvin–Helmholtz timescale and so as the orbit shrinks, the mass transfer rate is much higher than in case A transfer.

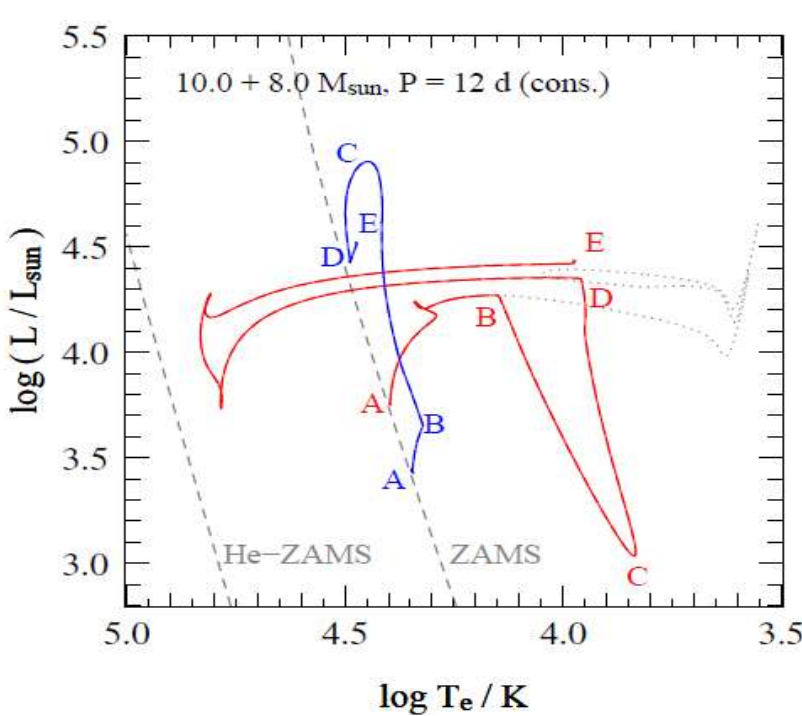


*Fig 30.4
Case-B mass transfer
of a binary of $10 + 8$
 M_{sun} with an initial
period of 12 days. The
evolution tracks of both
stars are shown.
(O.Pols 2014, Fig
17.3)*

The transfer starts at point B, when the primary is crossing the Hertzsprung gap and continues to point D. The low L at point C corresponds to the maximum transfer rate because the star is out of thermal equilibrium. The star has the tendency to shrink due to mass loss (because the envelope is still mainly in radiative equilibrium) but at the same time its internal evolution forces it to expand. A considerable fraction of the energy from the H-shell fusion is used for the continuing expansion of the envelope.

The mass transfer keeps going until the stars have reached equal mass and the separation reaches its minimum value. However as the donor keeps expanding the mass transfer continues on the Kelvin-Helmholtz timescale of the donor.

At point D Helium is ignited in the core and so the star makes a blue loop in the HRD. The accretor is still on the MS and becomes more massive and more luminous.

30.7 Case C = Unstable mass loss

If mass transfer occurs when the donor is on the Hayashi line, the mass transfer will be unstable. This will lead to a rapid shrinking of the orbital separation. The result will be a **common-envelope star**.

When stars are on the Hayashi line, their radius can reach such high values that case-C mass transfer may occur for a large range of initial periods and separations. Therefore, common envelope evolution is not a rare fate of binaries.

30.8 The evolution of high mass X-binaries

The evolution of a high mass binary system, leading to the formation of a high mass X-binary, like LMC-X3, is shown in Fig. 30.5

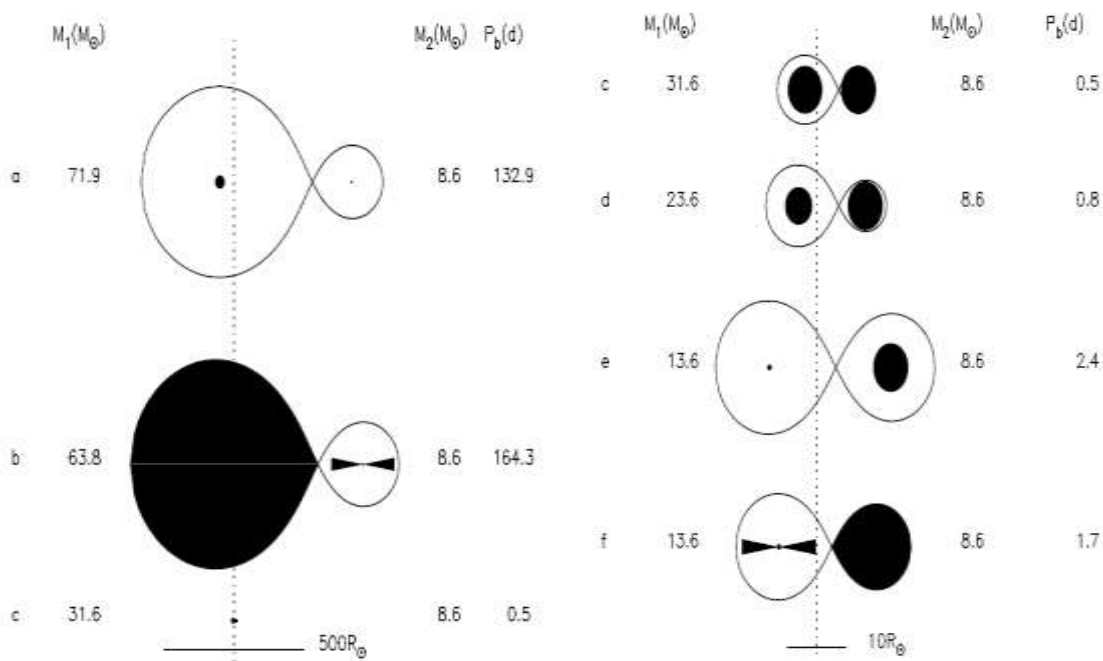


Fig 30.5. The evolution of a close binary of $71.9 + 8.6 M_{\text{sun}}$ with a period of 132.9 days. Notice the different sizes of the first (left) and later (right) phases. The disk like structure indicates that spin-up has occurred, and that the secondary cannot accept the mass lost by the primary. It is lost in a wind and goes into a circum-binary disk.

a: initial configuration. **b:** the primary fills its Rochelobe as a red supergiant which results in run-away mass loss. The star goes through a common envelope phase with spiral-in.

c: at the end of the common envelope phase, the primary has lost almost half of its mass, from 63.8 to $31.6 M_{\text{sun}}$, and the orbit has been shrinking from about $500 R_{\text{sun}}$ ($P=164.3$ days) to less than $10 R_{\text{sun}}$ ($P=0.5$ days)! **d:** the primary explodes as a supernova, leaving a remnant black hole of $13.6 M_{\text{sun}}$. **e:** the secondary fills its Rochelobe and transfers mass to the BH via an accretion disk. (Pols 2014, Fig 20.2)

30.9 The formation of low mass X-binaries.

Fig. 30.6 shows the evolution of system of system of $10 + 1 M_{\text{sun}}$ with a period of 300 days, that leads to the formation of a low mass X-binary system.

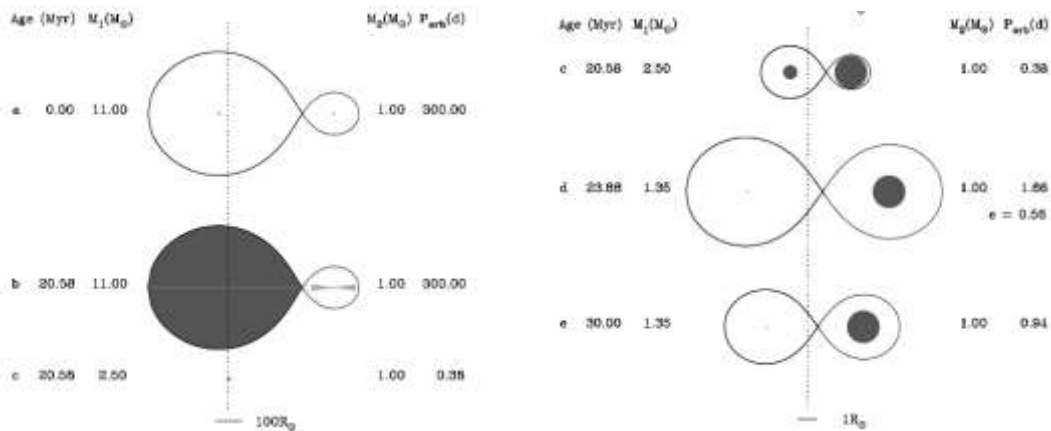


Fig 30.6 Notice the different size scales between the first (left) and the later (right) phases.
b: The primary fills its Rochelobe when it has a He core of $2.5 M_{\text{sun}}$ on the red giant branch. **c:** the primary has lost $8.5 M_{\text{sun}}$ and the friction has lead to a significant spiral-in of the orbit, from about $300 R_{\text{sun}}$ to about $3 R_{\text{sun}}$. The primary is now a Helium star. **d:** the Helium star explodes as a SN, leaving behind a neutron star of $1.35 M_{\text{sun}}$ and a main sequence star. **e:** Due to tidal interaction, the orbit circularizes resulting in a $1 M_{\text{sun}}$ MS star and a neutron star in a tight orbit. (Pols 2014, fig 20.3)

THE END

I hope you enjoyed this class
(I did) and that what you
learned is useful for you.

Good luck with your research and your
career in astronomy!

Henny Lamers

Seattle June 4, 2014

h.j.g.l.m.lamers@uu.nl

PS1: If you have questions, contact me by email

PS2: in case you wondered: H.J.G.L.M. =
Hermanus Johannes Gerardus Lambertus Maria

Appendix A

Physical and Astronomical Constants

Listed below are some useful physical and astronomical constants derived from various sources. The prime reference for the physical constants is Cohen, E.R., and Taylor, B.N. 1987, *Rev. Mod. Phys.*, **59**, 1121 (who use MKS units). In some cases we have rounded the values.

speed of light in vacuum: $c = 2.99792458 \times 10^{10} \text{ cm s}^{-1}$

Newtonian constant of gravitation: $G = 6.6726 \times 10^{-8} \text{ g}^{-1} \text{ cm}^3 \text{ s}^{-2}$

Planck's constant: $\hbar = 2\pi\hbar = 6.6260755 \times 10^{-27} \text{ erg s}$

elementary charge: $e = 4.8032068 \times 10^{-10} \text{ e.s.u.}$

electron mass: $m_e = 9.1093898 \times 10^{-28} \text{ g}$, $5.4858 \times 10^{-4} \text{ amu}$,
 $0.5109991 \text{ MeV c}^{-2}$

proton mass: $m_p = 1.6726231 \times 10^{-24} \text{ g}$, 1.00727647 amu ,
 $938.27231 \text{ MeV c}^{-2}$

neutron mass: $m_n = 1.6749286 \times 10^{-24} \text{ g}$, 1.0086649 amu ,
 $939.56563 \text{ MeV c}^{-2}$

Avogadro's constant: $N_A = 6.0221367 \times 10^{23} \text{ mole}^{-1}$

Boltzmann's constant: $k = 1.380658 \times 10^{-16} \text{ erg K}^{-1}$,
 $8.617386 \times 10^{-5} \text{ eV K}^{-1}$

gas constant: $R_{\text{gas}} = N_A k = 8.314511 \times 10^7 \text{ erg K}^{-1} \text{ mole}^{-1}$

Stefan-Boltzmann constant: $\sigma = 5.67051 \times 10^{-5} \text{ erg cm}^{-2} \text{ K}^{-4} \text{ s}^{-1}$

radiation density constant: $a = 4\sigma/c = 7.56591 \times 10^{-15} \text{ erg cm}^{-3} \text{ K}^{-4}$

eV to erg conversion: $1 \text{ eV} = 1.60217733 \times 10^{-12} \text{ erg}$

amu to gram conversion: $1 \text{ amu} = 1.6605402 \times 10^{-24} \text{ g}$

solar luminosity: $L_\odot = (3.847 \pm 0.003) \times 10^{33} \text{ erg s}^{-1}$

solar mass: $M_\odot = (1.9891 \pm 0.0004) \times 10^{33} \text{ g}$

solar radius: $R_\odot = 6.96 \times 10^{10} \text{ cm}$

solar effective temperature: $T_{\text{eff}}(\odot) = 5780 \text{ K}$

parsec (pc): $1 \text{ pc} = 3.086 \times 10^{18} \text{ cm}$

astronomical unit (AU): $1 \text{ AU} = 1.496 \times 10^{13} \text{ cm}$

Appendix B1

Main-Sequence Stars (Luminosity Class V)									
Sp. Type	T_e (K)	L/L_\odot	R/R_\odot	M/M_\odot	M_{bol}	BC	M_V	$U - B$	$B - V$
O5	42000	499000	13.4	60	-9.51	-4.40	-5.1	-1.19	-0.33
O6	39500	324000	12.2	37	-9.04	-3.93	-5.1	-1.17	-0.33
O7	37500	216000	11.0	—	-8.60	-3.68	-4.9	-1.15	-0.32
O8	35800	147000	10.0	23	-8.18	-3.54	-4.6	-1.14	-0.32
B0	30000	32500	6.7	17.5	-6.54	-3.16	-3.4	-1.08	-0.30
B1	25400	9950	5.2	—	-5.26	-2.70	-2.6	-0.95	-0.26
B2	20900	2920	4.1	—	-3.92	-2.35	-1.6	-0.84	-0.24
B3	18800	1580	3.8	7.6	-3.26	-1.94	-1.3	-0.71	-0.20
B5	15200	480	3.2	5.9	-1.96	-1.46	-0.5	-0.58	-0.17
B6	13700	272	2.9	—	-1.35	-1.21	-0.1	-0.50	-0.15
B7	12500	160	2.7	—	-0.77	-1.02	+0.3	-0.43	-0.13
B8	11400	96.7	2.5	3.8	-0.22	-0.80	+0.6	-0.34	-0.11
B9	10500	60.7	2.3	—	+0.28	-0.51	+0.8	-0.20	-0.07
A0	9800	39.4	2.2	2.9	+0.75	-0.30	+1.1	-0.02	-0.02
A1	9400	30.3	2.1	—	+1.04	-0.23	+1.3	+0.02	+0.01
A2	9020	23.6	2.0	—	+1.31	-0.20	+1.5	+0.05	+0.05
A5	8190	12.3	1.8	2.0	+2.02	-0.15	+2.2	+0.10	+0.15
A8	7600	7.13	1.5	—	+2.61	-0.10	+2.7	+0.09	+0.25
F0	7300	5.21	1.4	1.6	+2.95	-0.09	+3.0	+0.03	+0.30
F2	7050	3.89	1.3	—	+3.27	-0.11	+3.4	+0.00	+0.35
F5	6650	2.56	1.2	1.4	+3.72	-0.14	+3.9	-0.02	+0.44
F8	6250	1.68	1.1	—	+4.18	-0.16	+4.3	+0.02	+0.52
Sp. Type	T_e (K)	L/L_\odot	R/R_\odot	M/M_\odot	M_{bol}	BC	M_V	$U - B$	$B - V$
G0	5940	1.25	1.06	1.05	+4.50	-0.18	+4.7	+0.06	+0.58
G2	5790	1.07	1.03	—	+4.66	-0.20	+4.9	+0.12	+0.63
Sun ^a	5777	1.00	1.00	1.00	+4.74	-0.08	+4.82	+0.195	+0.650
G8	5310	0.656	0.96	—	+5.20	-0.40	+5.6	+0.30	+0.74
K0	5150	0.552	0.93	0.79	+5.39	-0.31	+5.7	+0.45	+0.81
K1	4990	0.461	0.91	—	+5.58	-0.37	+6.0	+0.54	+0.86
K3	4690	0.318	0.86	—	+5.98	-0.50	+6.5	+0.80	+0.96
K4	4540	0.263	0.83	—	+6.19	-0.55	+6.7	—	+1.05
K5	4410	0.216	0.80	0.67	+6.40	-0.72	+7.1	+0.98	+1.15
K7	4150	0.145	0.74	—	+6.84	-1.01	+7.8	+1.21	+1.33
M0	3840	0.077	0.63	0.51	+7.52	-1.38	+8.9	+1.22	+1.40
M1	3660	0.050	0.56	—	+7.99	-1.62	+9.6	+1.21	+1.46
M2	3520	0.032	0.48	0.40	+8.47	-1.89	+10.4	+1.18	+1.49
M3	3400	0.020	0.41	—	+8.97	-2.15	+11.1	+1.16	+1.51
M4	3290	0.013	0.35	—	+9.49	-2.38	+11.9	+1.15	+1.54
M5	3170	0.0076	0.29	0.21	+10.1	-2.73	+12.8	+1.24	+1.64
M6	3030	0.0044	0.24	—	+10.6	-3.21	+13.8	+1.32	+1.73
M7	2860	0.0025	0.20	—	+11.3	-3.46	+14.7	+1.40	+1.80

^aValues adopted in this text.

Appendix B2

Appendix G Stellar Data

Giant Stars (Luminosity Class III)									
Sp. Type	T_e (K)	L/L_\odot	R/R_\odot	M/M_\odot	M_{bol}	BC	M_V	$U - B$	$B - V$
O5	39400	741000	18.5	—	-9.94	-4.05	-5.9	-1.18	-0.32
O6	37800	519000	16.8	—	-9.55	-3.80	-5.7	-1.17	-0.32
O7	36500	375000	15.4	—	-9.20	-3.58	-5.6	-1.14	-0.32
O8	35000	277000	14.3	—	-8.87	-3.39	-5.5	-1.13	-0.31
B0	29200	84700	11.4	20	-7.58	-2.88	-4.7	-1.08	-0.29
B1	24500	32200	10.0	—	-6.53	-2.43	-4.1	-0.97	-0.26
B2	20200	11100	8.6	—	-5.38	-2.02	-3.4	-0.91	-0.24
B3	18300	6400	8.0	—	-4.78	-1.60	-3.2	-0.74	-0.20
B5	15100	2080	6.7	7	-3.56	-1.30	-2.3	-0.58	-0.17
B6	13800	1200	6.1	—	-2.96	-1.13	-1.8	-0.51	-0.15
B7	12700	710	5.5	—	-2.38	-0.97	-1.4	-0.44	-0.13
B8	11700	425	5.0	—	-1.83	-0.82	-1.0	-0.37	-0.11
B9	10900	263	4.5	—	-1.31	-0.71	-0.6	-0.20	-0.07
A0	10200	169	4.1	4	-0.83	-0.42	-0.4	-0.07	-0.03
A1	9820	129	3.9	—	-0.53	-0.29	-0.2	+0.07	+0.01
A2	9460	100	3.7	—	-0.26	-0.20	-0.1	+0.06	+0.05
A5	8550	52	3.3	—	+0.44	-0.14	+0.6	+0.11	+0.15
A8	7830	33	3.1	—	+0.95	-0.10	+1.0	+0.10	+0.25
F0	7400	27	3.2	—	+1.17	-0.11	+1.3	+0.08	+0.30
F2	7000	24	3.3	—	+1.31	-0.11	+1.4	+0.08	+0.35
F5	6410	22	3.8	—	+1.37	-0.14	+1.5	+0.09	+0.43
G0	5470	29	6.0	1.0	+1.10	-0.20	+1.3	+0.21	+0.65
G2	5300	31	6.7	—	+1.00	-0.27	+1.3	+0.39	+0.77
G8	4800	44	9.6	—	+0.63	-0.42	+1.0	+0.70	+0.94
K0	4660	50	10.9	1.1	+0.48	-0.50	+1.0	+0.84	+1.00
K1	4510	58	12.5	—	+0.32	-0.55	+0.9	+1.01	+1.07
K3	4260	79	16.4	—	-0.01	-0.76	+0.8	+1.39	+1.27
K4	4150	93	18.7	—	-0.18	-0.94	+0.8	—	+1.38
K5	4050	110	21.4	1.2	-0.36	-1.02	+0.7	+1.81	+1.50
K7	3870	154	27.6	—	-0.73	-1.17	+0.4	+1.83	+1.53
M0	3690	256	39.3	1.2	-1.28	-1.25	+0.0	+1.87	+1.56
M1	3600	355	48.6	—	-1.64	-1.44	-0.2	+1.88	+1.58
M2	3540	483	58.5	1.3	-1.97	-1.62	-0.4	+1.89	+1.60
M3	3480	643	69.7	—	-2.28	-1.87	-0.4	+1.88	+1.61
M4	3440	841	82.0	—	-2.57	-2.22	-0.4	+1.73	+1.62
M5	3380	1100	96.7	—	-2.86	-2.48	-0.4	+1.58	+1.63
M6	3330	1470	116	—	-3.18	-2.73	-0.4	+1.16	+1.52

Appendix B3

Appendix G Stellar Data

Supergiant Stars (Luminosity Class Approximately Iab)									
Sp. Type	T_e (K)	L/L_\odot	R/R_\odot	M/M_\odot	M_{bol}	BC	M_V	$U - B$	$B - V$
O5	40900	1140000	21.2	70	-10.40	-3.87	-6.5	-1.17	-0.31
O6	38500	998000	22.4	40	-10.26	-3.74	-6.5	-1.16	-0.31
O7	36200	877000	23.8	—	-10.12	-3.48	-6.6	-1.14	-0.31
O8	34000	769000	25.3	28	-9.98	-3.35	-6.6	-1.13	-0.29
B0	26200	429000	31.7	25	-9.34	-2.49	-6.9	-1.06	-0.23
B1	21400	261000	37.3	—	-8.80	-1.87	-6.9	-1.00	-0.19
B2	17600	157000	42.8	—	-8.25	-1.58	-6.7	-0.94	-0.17
B3	16000	123000	45.8	—	-7.99	-1.26	-6.7	-0.83	-0.13
B5	13600	79100	51.1	20	-7.51	-0.95	-6.6	-0.72	-0.10
B6	12600	65200	53.8	—	-7.30	-0.88	-6.4	-0.69	-0.08
B7	11800	54800	56.4	—	-7.11	-0.78	-6.3	-0.64	-0.05
B8	11100	47200	58.9	—	-6.95	-0.66	-6.3	-0.56	-0.03
B9	10500	41600	61.8	—	-6.81	-0.52	-6.3	-0.50	-0.02
A0	9980	37500	64.9	16	-6.70	-0.41	-6.3	-0.38	-0.01
A1	9660	35400	67.3	—	-6.63	-0.32	-6.3	-0.29	+0.02
A2	9380	33700	69.7	—	-6.58	-0.28	-6.3	-0.25	+0.03
A5	8610	30500	78.6	13	-6.47	-0.13	-6.3	-0.07	+0.09
A8	7910	29100	91.1	—	-6.42	-0.03	-6.4	+0.11	+0.14
F0	7460	28800	102	12	-6.41	-0.01	-6.4	+0.15	+0.17
F2	7030	28700	114	—	-6.41	0.00	-6.4	+0.18	+0.23
F5	6370	29100	140	10	-6.42	-0.03	-6.4	+0.27	+0.32
F8	5750	29700	174	—	-6.44	-0.09	-6.4	+0.41	+0.56
G0	5370	30300	202	10	-6.47	-0.15	-6.3	+0.52	+0.76
G2	5190	30800	218	—	-6.48	-0.21	-6.3	+0.63	+0.87
G8	4700	32400	272	—	-6.54	-0.42	-6.1	+1.07	+1.15
K0	4550	33100	293	13	-6.56	-0.50	-6.1	+1.17	+1.24
K1	4430	34000	314	—	-6.59	-0.56	-6.0	+1.28	+1.30
K3	4190	36100	362	—	-6.66	-0.75	-5.9	+1.60	+1.46
K4	4090	37500	386	—	-6.70	-0.90	-5.8	—	+1.53
K5	3990	39200	415	13	-6.74	-1.01	-5.7	+1.80	+1.60
K7	3830	43200	473	—	-6.85	-1.20	-5.6	+1.84	+1.63
M0	3620	51900	579	13	-7.05	-1.29	-5.8	+1.90	+1.67
M1	3490	60300	672	—	-7.21	-1.38	-5.8	+1.90	+1.69
M2	3370	72100	791	19	-7.41	-1.62	-5.8	+1.95	+1.71
M3	3210	89500	967	—	-7.64	-2.13	-5.5	+1.95	+1.69
M4	3060	117000	1220	—	-7.93	-2.75	-5.2	+2.00	+1.76
M5	2880	165000	1640	24	-8.31	-3.47	-4.8	+1.60	+1.80
M6	2710	264000	2340	—	-8.82	-3.90	-4.9	—	—

Appendix C1

TABLE 2.1. Zero age main sequence models

No.	M/M_{\odot}	(X, Y)	$\log L/L_{\odot}$	$\log T_{\text{eff}}$	R_{10}	ref.
1	60	(0.74, 0.24)	5.701	4.683	70.96	(1)
2	40	(0.74, 0.24)	5.345	4.642	56.89	(1)
3	30	(0.74, 0.24)	5.066	4.606	48.53	(1)
4	20	(0.74, 0.24)	4.631	4.547	38.73	(1)
5	15	(0.74, 0.24)	4.292	4.498	32.89	(1)
6	10	(0.74, 0.24)	3.772	4.419	25.94	(1)
7	7	(0.74, 0.24)	3.275	4.341	20.99	(1)
8	5	(0.74, 0.24)	2.773	4.259	17.18	(1)
9	3	(0.74, 0.24)	1.951	4.118	12.76	(1)
10	2	(0.74, 0.24)	1.262	3.992	10.30	(1)
11	1.75	(0.74, 0.24)	1.031	3.948	9.683	(1)
12	1.50	(0.74, 0.24)	0.759	3.892	9.141	(1)
13	1.30	(0.74, 0.24)	0.496	3.834	8.831	(1)
14	1.20	(0.74, 0.24)	0.340	3.800	8.650	(1)
15	1.10	(0.74, 0.24)	0.160	3.771	8.035	(1)
16	1.00	(0.74, 0.24)	-0.042	3.752	6.934	(1)
17	0.90	(0.74, 0.24)	-0.262	3.732	5.902	(1)
18	0.75	(0.73, 0.25)	-0.728	3.659	4.834	(2)
19	0.60	(0.73, 0.25)	-1.172	3.594	3.908	(2)
20	0.50	(0.70, 0.28)	-1.419	3.553	3.553	(3)
21	0.40	(0.70, 0.28)	-1.723	3.542	2.640	(3)
22	0.30	(0.70, 0.28)	-1.957	3.538	2.054	(3)
23	0.20	(0.70, 0.28)	-2.238	3.533	1.519	(3)
24	0.10	(0.70, 0.28)	-3.023	3.475	0.805	(3)
25	0.08	(0.70, 0.28)	-3.803	3.327	0.650	(3)

TABLE 2.2. ZAMS models (continued)

No.	M/M_{\odot}	$T_{\text{c},6}$	ρ_c	$\log P_c$	q_c	q_{env}
1	60	60	39.28	1.93	16.22	0.73
2	40	40	37.59	2.49	16.26	0.64
3	30	30	36.28	3.05	16.29	0.56
4	20	20	34.27	4.21	16.37	0.46
5	15	15	32.75	5.48	16.44	0.40
6	10	10	30.48	8.33	16.57	0.33
7	7	7	28.41	12.6	16.71	0.27
8	5	5	26.43	19.0	16.84	0.23
9	3	3	23.47	35.8	17.06	0.18
10	2	2	21.09	47.0	17.21	0.13
11	1.75	11	1.75	20.22	66.5	17.25
12	1.50	12	1.50	19.05	76.7	17.28
13	1.30	13	1.30	17.66	84.1	17.28
14	1.20	14	1.20	16.67	85.7	17.26
15	1.10	15	1.10	15.57	84.9	17.22
16	1.00	16	1.00	14.42	82.2	17.17
17	0.90	17	0.90	13.29	78.5	17.11
18	0.75	18	0.75	10.74	81.5	10^{-7}
19	0.60	19	0.60	9.31	79.1	5×10^{-5}
20	0.50	20	0.50	9.04	100	17.10
21	0.40	21	0.40	8.15	104	17.04
22	0.30	22	0.30	7.59	107	17.05
23	0.20	23	0.20	6.53	180	17.24
24	0.10	24	0.10	4.51	545	17.68
25	0.08	25	0.08	3.30	775	17.83

EXTERNAL PROPERTIES

INTERNAL PROPERTIES

Appendix C2

ZERO-AGE MAIN SEQUENCE MODELS

Stellar parameters on the zero-age sequence for models of composition $X = 0.68$, $Y = 0.30$ and $Z = 0.02$ [120, 513]

M/M_{\odot}	$\log L/L_{\odot}$	$\log T_{\text{eff}}$	$\log g$	R/R_{\odot}	q_c	$\bar{\rho}$	$\log \rho_c$	$\log T_c$
120	6.252	4.727	4.126	15.683	0.867	0.0438	0.171	7.638
85	6.006	4.705	4.134	13.075	0.822	0.0536	0.233	7.621
60	5.728	4.683	4.173	10.506	0.746	0.0729	0.332	7.611
40	5.373	4.640	4.180	8.510	0.664	0.0914	0.429	7.589
25	4.897	4.579	4.208	6.515	0.555	0.1273	0.577	7.564
20	4.650	4.544	4.218	5.760	0.508	0.1474	0.653	7.550
15	4.303	4.492	4.232	4.908	0.446	0.1787	0.762	7.529
12	4.013	4.448	4.249	4.305	0.408	0.2118	0.858	7.513
9	3.617	4.383	4.260	3.681	0.367	0.2542	0.988	7.488
7	3.257	4.321	4.263	3.235	0.342	0.2912	1.104	7.464
5	2.740	4.235	4.290	2.651	0.314	0.3780	1.290	7.433
4	2.385	4.173	4.300	2.344	0.294	0.4375	1.412	7.410
3	1.909	4.088	4.311	2.004	0.262	0.5250	1.570	7.377
2.50	1.600	4.031	4.313	1.826	0.235	0.5783	1.669	7.355
2.00	1.209	3.958	4.315	1.629	0.208	0.6516	1.780	7.323
1.70	0.916	3.901	4.309	1.512	0.186	0.6927	1.851	7.295
1.50	0.676	3.852	4.299	1.437	0.173	0.7119	1.881	7.265
1.25	0.325	3.808	4.395	1.175	0.031	1.085	1.928	7.213
1.00	-0.163	3.751	4.558	0.871	0.000	2.133	1.891	7.134
0.90	-0.313	3.729	4.574	0.811	0.000	2.378	1.917	7.108
0.80	-0.554	3.694	4.624	0.722	0.000	2.996	1.905	7.070
0.70	-0.821	3.654	4.673	0.638	0.000	3.793	1.893	7.030
0.60	-1.090	3.623	4.751	0.540	0.000	5.367	1.880	6.990
0.50	-1.370	3.595	4.840	0.445	0.000	7.986	1.869	6.953
0.40	-1.640	3.572	4.921	0.363	0.000	11.817	1.885	6.926

MAEDER 2005

q_c = mass fraction in convective core

Physics, FORMATION AND

EVOLUTION OF ROTATING STARS

MAIN SEQUENCE LIFE TIMES

The MS-lifetimes t_H as a function of mass for $X = 0.68$ and $Z = 0.02$ with mass loss and an overshooting of $0.2 H_P$ [513]

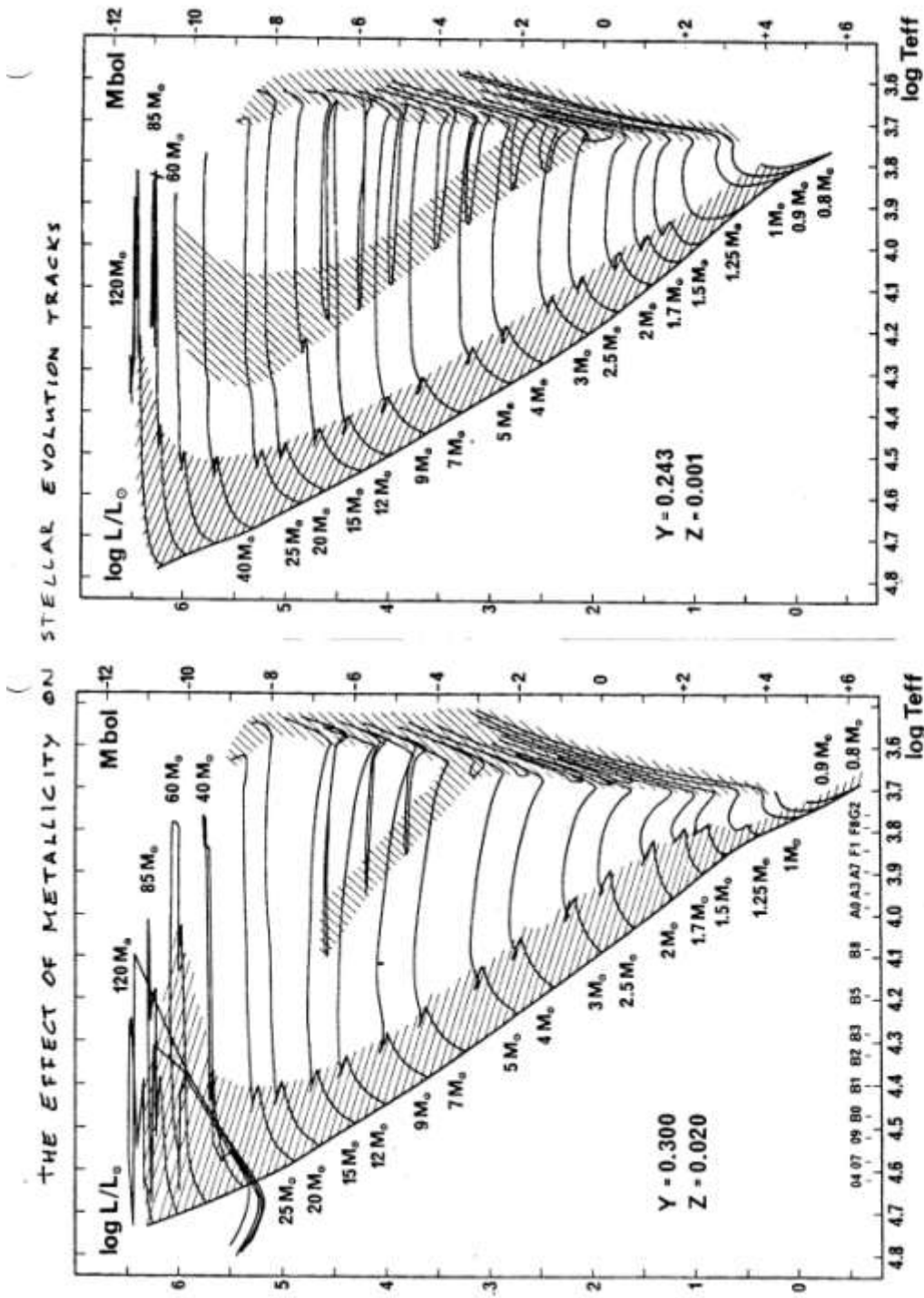
Mass (M_{\odot})	t_H (yr)	Mass (M_{\odot})	t_H (yr)
120	2.561×10^6	4	1.647×10^8
85	2.823×10^6	3	3.525×10^8
60	3.447×10^6	2.5	5.849×10^8
40	4.303×10^6	2	1.116×10^9
25	6.408×10^6	1.7	1.827×10^9
20	8.141×10^6	1.5	2.695×10^9
15	1.158×10^7	1.25	3.948×10^9
12	1.600×10^7	1.00	9.845×10^9
9	2.639×10^7	0.90	1.550×10^{10}
7	4.319×10^7	0.80	2.503×10^{10}
5	9.446×10^7		

Appendix D

Table 2.4. A model of the present Sun ($Z+n$ means $Z \times 10^n$)

m/m_\odot	r/r_\odot	P [Pa]	T [K]	ρ [kg/m ³]	L/L_\odot	X	μ
1.0000	1.0000	1.16+04	5.778+3	3.03-4	1.000	.727	1.251
1.0000	.9999	2.22+04	8.871+3	3.71-4	1.000	.727	1.234
1.0000	.9996	4.23+04	1.107+4	5.34-4	1.000	.727	1.162
1.0000	.9993	8.05+04	1.251+4	8.48-4	1.000	.727	1.093
1.0000	.9990	1.53+05	1.378+4	1.39-3	1.000	.727	1.035
1.0000	.9986	2.92+05	1.506+4	2.32-3	1.000	.727	.985
1.0000	.9981	5.57+05	1.642+4	3.88-3	1.000	.727	.942
1.0000	.9976	1.06+06	1.793+4	6.52-3	1.000	.727	.903
1.0000	.9970	2.02+06	1.966+4	1.09-2	1.000	.727	.867
1.0000	.9964	3.85+06	2.167+4	1.83-2	1.000	.727	.833
1.0000	.9956	7.34+06	2.408+4	3.03-2	1.000	.727	.800
1.0000	.9947	1.40+07	2.702+4	4.98-2	1.000	.727	.769
1.0000	.9937	2.67+07	3.067+4	8.10-2	1.000	.727	.740
1.0000	.9925	5.08+07	3.526+4	1.30-1	1.000	.727	.713
1.0000	.9911	9.68+07	4.119+4	2.06-1	1.000	.727	.689
1.0000	.9894	1.85+08	4.914+4	3.20-1	1.000	.727	.669
1.0000	.9873	3.52+08	6.010+4	4.86-1	1.000	.727	.654
1.0000	.9846	6.70+08	7.489+4	7.29-1	1.000	.727	.644
1.0000	.9812	1.28+09	9.363+4	1.09+0	1.000	.727	.637
1.0000	.9769	2.43+09	1.166+5	1.65+0	1.000	.727	.629
.9999	.9715	4.63+09	1.457+5	2.47+0	1.000	.727	.621
.9999	.9648	8.83+09	1.843+5	3.67+0	1.000	.727	.616
.9998	.9563	1.68+10	2.352+5	5.43+0	1.000	.727	.612
.9997	.9454	3.21+10	3.019+5	8.00+0	1.000	.727	.611
.9994	.9318	6.11+10	3.885+5	1.18+1	1.000	.727	.610
.9990	.9147	1.16+11	5.007+5	1.73+1	1.000	.727	.609
.9980	.8885	2.52+11	6.801+5	2.75+1	1.000	.727	.608
.9945	.8343	8.24+11	1.088+6	5.59+1	1.000	.727	.608
.9872	.7664	2.44+12	1.675+6	1.07+2	1.000	.727	.608
.9730	.6833	7.08+12	2.384+6	2.17+2	1.000	.727	.605
.9448	.5881	2.26+13	3.079+6	5.36+2	1.000	.727	.605
.8922	.4921	7.66+13	3.919+6	1.43+3	1.000	.727	.605
.8340	.4285	1.80+14	4.621+6	2.86+3	1.000	.727	.605
.7795	.3860	3.25+14	5.188+6	4.60+3	1.000	.727	.605
.7071	.3425	6.04+14	5.870+6	7.54+3	1.000	.726	.605
.6460	.3127	9.28+14	6.410+6	1.06+4	.999	.725	.605
.5808	.2850	1.38+15	6.987+6	1.45+4	.998	.723	.606
.5307	.2658	1.82+15	7.437+6	1.79+4	.994	.722	.607
.4747	.2456	2.41+15	7.949+6	2.22+4	.986	.719	.608
.4120	.2242	3.23+15	8.540+6	2.78+4	.971	.715	.610
.3398	.2002	4.43+15	9.254+6	3.54+4	.939	.706	.614
.2798	.1802	5.70+15	9.896+6	4.30+4	.895	.693	.620
.2312	.1636	6.98+15	1.047+7	5.03+4	.841	.679	.627
.1794	.1449	8.66+15	1.116+7	5.96+4	.756	.655	.639
.1240	.1228	1.10+16	1.201+7	7.23+4	.620	.617	.659
.0673	.0952	1.44+16	1.309+7	9.13+4	.410	.555	.695
.0168	.0562	1.95+16	1.445+7	1.23+5	.127	.453	.762
.0027	.0295	2.24+16	1.511+7	1.43+5	.022	.395	.807
.0000	.0000	2.37+16	1.540+7	1.53+5	.000	.368	.829

Appendix E



Tracks in the HR diagram of models calculated with an overshooting parameter $d_{\text{over}}/H_P = 0.20$. At $1.25 M_\odot$, a model without overshooting is used. The hatched areas indicate the slow phases of nuclear H burning (main sequence) and He burning (giants). Spectral types are indicated. The parts of the tracks descending to the left of the ZAMS for the most massive stars correspond to WR stars without hydrogen of types WNE and WC (Sect. 27.5). From MATTEI 2009

Appendix F

PROPERTIES OF AGB STARS

M_f (M_\odot)	Z	$M_{\text{bol}}^{\text{max}}$ (EAGB)	$M_{\text{bol}}^{\text{min}}$ (TPAGB)	$M_{\text{bol}}^{\text{max}}$ (TPAGB)	$M_{\text{EAGB}}^{\text{min}}$ (M_\odot)	M_f (M_\odot)	P_{max} (days)	t_{opt} (yr)	t_{wind} (yr)	$t_{\text{wind}}/t_{\text{opt}}$
1.0	0.016	-3.61	-3.12	-4.03	1.000	0.568	740	4.34E+05	6.1E+04	0.141
1.5	0.016	-3.73	-3.29	-4.52	1.500	0.600	1180	7.29E+04	9.8E+04	0.135
2.0	0.016	-3.78	-3.32	-4.90	2.000	0.633	1510	1.06E+06	1.2E+05	0.114
2.5	0.016	-3.65	-3.02	-5.14	2.500	0.666	1850	2.07E+06	1.1E+05	0.053
3.5	0.016	-5.17	-4.72	-5.65	3.500	0.751	2370	2.97E+05	1.3E+05	0.438
5.0	0.016	-5.91	-5.67	-6.22	5.000	0.891	2800	1.42E+05	1.2E+05	0.843
0.945	0.008	-3.32	-2.90	-3.92	0.722	0.553	375	5.48E+05	2.2E+04	0.040
1.0	0.008	-3.62	-3.07	-4.22	1.000	0.578	620	5.94E+05	5.6E+04	0.094
1.5	0.008	-3.96	-3.29	-4.76	1.500	0.619	970	8.60E+05	7.8E+04	0.091
2.0	0.008	-4.05	-3.37	-5.07	2.000	0.667	1210	1.25E+06	9.1E+04	0.073
2.5	0.008	-3.97	-3.38	-5.32	2.500	0.678	1420	1.72E+06	1.1E+05	0.064
3.5	0.008	-5.44	-5.09	-5.84	3.500	0.794	1900	2.41E+05	1.1E+05	0.457
5.0	0.008	-5.95	-5.75	-6.39	5.000	0.910	2000	2.50E+05	1.1E+05	0.440
0.89	0.004	-3.22	-2.85	-3.98	0.691	0.558	310	7.55E+05	1.6E+04	0.021
1.0	0.004	-3.72	-3.09	-4.46	1.000	0.592	510	8.25E+05	4.3E+04	0.052
1.5	0.004	-3.99	-3.41	-4.91	1.500	0.639	700	9.09E+05	5.8E+04	0.064
2.0	0.004	-3.89	-3.41	-5.24	2.000	0.672	870	1.48E+06	7.6E+04	0.051
2.5	0.004	-4.54	-4.03	-5.46	2.500	0.691	1290	1.15E+06	9.5E+04	0.082
3.5	0.004	-5.70	-5.44	-6.03	3.500	0.853	1100	1.63E+05	8.9E+04	0.545
5.0	0.004	-6.00	-5.86	-6.46	5.000	0.941	1600	2.15E+05	9.7E+04	0.451
1.0	0.001	-3.41	-3.10	-4.68	1.000	0.623	310	1.33E+06	2.7E+04	0.020
1.5	0.001	-3.94	-3.55	-5.05	1.500	0.663	320	1.08E+06	4.7E+04	0.044

LIFETIMES OF MAJOR EVOLUTIONARY PHASES

M (M_\odot)	Z	τ_{MS}	$\tau_{\text{PGB-C}}$	τ_{PGB}	τ_{HeB}	τ_{EAGB}	τ_{TPAGB}	τ_{AGB}	$\tau_{\text{FGB-C}}$	τ_{AGB}	τ_{TPAGB}	τ_{AGB}
		(yr)	(yr)	(yr)	(yr)	(yr)	(yr)	(yr)	τ_{MS}	$\tau_{\text{FGB-C}}$	τ_{EAGB}	τ_{TPAGB}
1.0	0.016	1.125E+10	5.786E+07	3.563E+09	1.416E+08	1.209E+07	4.946E+05	1.258E+07	0.409	0.218	0.041	0.089
1.5	0.016	2.742E+09	5.197E+07	7.570E+08	1.359E+08	9.191E+06	8.266E+05	1.002E+07	0.373	0.193	0.090	0.038
2.0	0.016	1.236E+09	5.454E+07	1.648E+08	1.509E+08	7.933E+06	1.175E+06	9.108E+06	0.361	0.167	0.148	0.060
2.5	0.016	6.192E+08	1.429E+08	4.283E+07	2.805E+08	1.084E+07	2.184E+06	1.303E+07	0.051	0.911	0.201	0.046
3.5	0.016	2.307E+08	1.669E+06	1.110E+07	9.142E+07	2.793E+06	4.270E+05	3.220E+06	0.018	1.929	0.153	0.035
5.0	0.016	9.560E+07	3.638E+05	2.578E+06	2.353E+07	1.145E+06	2.624E+05	1.408E+06	0.015	3.869	0.229	0.060
0.945	0.008	1.052E+10	6.094E+07	3.038E+09	1.356E+08	1.057E+07	5.704E+05	1.114E+07	0.449	0.183	0.054	0.082
1.0	0.008	8.129E+09	4.860E+07	2.776E+09	1.336E+08	9.600E+06	6.502E+05	1.025E+07	0.364	0.211	0.068	0.077
1.5	0.008	2.461E+09	3.450E+07	5.140E+08	1.304E+08	7.783E+06	9.385E+06	8.721E+06	0.265	0.253	0.121	0.067
2.0	0.008	1.018E+09	4.458E+07	1.286E+08	1.520E+08	1.340E+07	1.339E+06	1.474E+07	0.293	0.331	0.100	0.097
2.5	0.008	5.170E+08	9.028E+06	3.355E+07	2.209E+08	1.035E+07	1.827E+06	1.217E+07	0.041	1.349	0.177	0.055
3.5	0.008	2.009E+08	1.100E+06	9.042E+06	6.388E+07	3.032E+06	3.509E+05	3.383E+06	0.017	3.075	0.116	0.053
5.0	0.008	8.567E+07	2.496E+05	2.426E+06	2.161E+07	8.036E+05	3.601E+05	1.150E+06	0.012	4.662	0.448	0.053
0.89	0.004	1.096E+10	6.276E+07	2.617E+09	1.294E+08	1.127E+07	7.711E+05	1.204E+07	0.485	0.192	0.068	0.093
1.0	0.004	6.650E+09	5.872E+07	2.111E+09	1.279E+08	8.008E+06	8.684E+05	8.875E+06	0.459	0.151	0.108	0.069
1.5	0.004	2.088E+09	3.650E+07	4.202E+08	1.268E+08	6.302E+06	9.667E+05	7.269E+06	0.288	0.199	0.153	0.057
2.0	0.004	8.930E+08	3.693E+07	1.082E+08	1.539E+08	6.705E+06	1.559E+06	8.264E+06	0.240	0.224	0.233	0.054
2.5	0.004	4.604E+08	5.953E+06	2.745E+07	1.669E+08	5.149E+06	1.248E+06	6.397E+06	0.036	1.075	0.242	0.038
3.5	0.004	1.844E+08	7.070E+05	6.868E+06	5.355E+07	2.150E+06	2.524E+05	2.402E+06	0.013	3.398	0.117	0.045
5.0	0.004	8.058E+07	1.759E+05	2.180E+06	1.864E+07	5.924E+05	3.123E+05	9.205E+05	0.009	5.143	0.527	0.049
1.0	0.001	5.737E+09	3.436E+07	1.344E+09	1.211E+08	7.737E+06	1.357E+06	9.094E+06	0.284	0.265	0.175	0.075
1.5	0.001	1.603E+09	3.633E+07	3.606E+08	1.222E+08	4.962E+06	1.127E+06	6.088E+06	0.297	0.168	0.227	0.050